University of Nottingham
UK | CHINA | MALAYSIA

Faculty of Engineering
Manufacturing & Process Technology
Advanced Manufacturing Technology

PH.D. THESIS

This thesis is submitted to the University of Nottingham for the degree of Doctor of Philosophy (Ph.D.)

The Application of Stochastic Design Strategies to Primitive and Complex Shapes

---

Author: Jan-Hendrik Groth
Date of Birth: 08.05.1991

Main Supervisor: Prof. Dr. Adam Clare

Co-Supervisor: Prof. Dr. Christopher Tuck
Co-Supervisor: Prof. Dr. Mirco Magnini
Submission Date: 14.07.2023

Nottingham, October 18, 2023

Included publications

Included Journal Papers:

- Groth, J.H., Anderson, C., Magnini, M., Tuck, C. and Clare, A., 2022. Five simple tools for stochastic lattice creation. Additive Manufacturing, Volume 49, 102488.
- Groth, J.H., Magnini, M., Tuck,C. and Clare, A., 2022. Stochastic design for additive manufacture of true biomimetic populations. Additive Manufacturing, Volume 55, 102739.

Included unpublished publications:

- Groth, J.H., Magnini, M., Tuck, C. and Clare, A., 2023, Mimicking nature's variance for superior engineering performance. Target journal: Royal Society Open Science
- Groth, J.H., Al-Ketan, O., Magnini, M., Tuck, C. and Clare, A., 2023, Five simple tools for stochastic triply periodic minimal surface-based lattice creation. Target journal: Additive Manufacturing
- Groth, J.H., Al-Ketan, O., Yu, B., Magnini, M., Clare, A., 2023, Aperiodic architected structures by additive manufacturing: A review of the literature and practical guide for their creation. Target journal: Additive Manufacturing

Published Patents:

- Clare, A., Groth, J.-H., Magnini, M., Tuck, C, 2021. Stochastic structures (International Publication Number WO 2023/041402 A1 - Patent pending)

Acknowledgments

A Ph.D. is an extraordinary journey to learn in-depth about a topic. I am very thankful for having had this opportunity and want to thank everyone who accompanied me through this journey.

First of all, a special thanks to my supervisors Adam Clare, Mirco Magnini, and Christopher Tuck who made this Ph.D. possible through their support and valuable experience. Also, I am very grateful for the opportunity Adam Clare gave me to visit him at the University of British Columbia to gain a new experience abroad. I also want to acknowledge their help in reading the publications and this manuscript to improve it.

Likewise, I would like to thank my family for supporting me. Mainly, I want to thank my parents, my Mom, Beate, and my Dad Michael, for being such great parents and for the support they gave me throughout my life to make me the 'man' I am today. I also want to thank my brother Christopher, my sister Michelle, her husband Alex, and their always smiling son, Lias.

Furthermore, I would like to thank my grandparents, Ursula Groth, Käthe and Gerhard Nehls, who unfortunately cannot see this accomplishment.

I would like to thank Caelan Anderson for helping to implement the stochastic design strategies for strut-based lattices.

I would like to thank Sam Connors for exploring the creation of a graphical user interface in MATLAB for the different stochastic design strategies for strut-based lattices.

I would like to thank Luke Stansfield for conducting a topology optimisation study on beams with included disordered ellipsoids.

I would like to thank Alexander Apps for exploring different interpolation strategies and for showing the influence of stochasticity on the mean curvature of a triply periodic minimal surface cellular material.

I would also like to thank Mark East and Adam Whitbread for Additively Manufacturing the strut-based cellular material samples.

A special thanks also goes to Alexander Jackson-Crisps for assisting to assemble the flow channel test apparatus and for manufacturing the pin fin samples.

I would also like to thank Alistair Speidel for taking the time to read parts of this Thesis and teaching me how to use the Alicona G4 measurement system.

I would also like to thank André Thieme for the many discussions around software development, which gave me many insights into how to choose the right programming tools.

I also thank Siemens Energy Industrial Turbomachinery Ltd. for funding this PhD. A special thanks goes to Roger Wells for discussing the progress of the Ph.D. regularly and allowing me to develop Stochastic Design tools. Additionally, I want to thank John Maltson and Eddie Wright from Siemens Energy Industrial Turbomachinery Ltd. for the insightful discussions around heat transfer.

Furthermore, I thank Oraib Al-Ketan for additive manufacturing the coloured TPMS cellular materials and providing images. I also want to thank him and Bosco Yu for their comments and editing of the literature review paper.

Finally, I dedicate this Ph.D. to my grandfather Gerhard Nehls, the greatest inspiration for my life and beyond.

Abstract

Corporations and research institutes increasingly adopt Additive Manufacturing (AM) as a complementary manufacturing process, which enables them to manufacture parts or components that either cannot be manufactured from Traditional Manufacturing (TM) processes or the cost is significantly lower. This adoption process involves rethinking design strategies to leverage the full potential of AM, namely the design of highly complex and customised parts. Inevitably, intelligent design strategies will lead to increased part or equipment performance. This raises competitiveness over companies that do not efficiently apply these design strategies. One of these design strategies is cellular material design, which is an essential part of this thesis and will be explained. Cellular material design is considered a design strategy of Biomimicry. Biomimicry assumes that natural designs provide an acceptable solution for applications such as thermal devices, body armour, etc.

Typical elements that can be found in nature are surface or volume elements. Prominent examples of surface elements are shark denticles or surface pedestals on lotus leaves. Well-known volume elements are cellular materials such as sponges or bee's honeycomb structures. These structures are attractive for fluid dynamic and mechanical applications and have found a broad research community over the years.

An important detail is missing when the natural designs are translated from the natural world to the engineering world. This detail is the variation that can be observed in their natural counterparts. Moreover, this variation is not the same; it is instead a range. This range is mainly designed and explored in Voronoi-based cellular materials and least in other cellular materials and surface elements because only a few design software and design strategies are available.

This thesis addresses this by developing design rules and design strategies for surface elements and cellular materials by using a pseudo-random number generator (RNG) that samples a Gaussian distribution, which allows for designing different levels of stochasticity.

To design a stochastic array, it is necessary to consider the range of stochasticity to produce a feasible design. These design rules include designing structures with stochastic levels that must be larger than the manufacturing tolerance but lower than a specific stochastic level at which the structure's performance is reduced. Moreover,

rules are explained that help to determine the maximum level of stochasticity by preventing invalid volumes or overlaps.

Five design strategies are implemented for strut-based and sheet-based cellular materials, and four for surface elements. The first design strategy is Isotropic Randomness, where the stochastic level is the same for a set of parameters such as the spatial coordinates x, y, and z. The second design strategy is Anisotropic Randomness, which enables selecting different levels of stochasticity for each parameter of a parameter set. The third strategy involves the spatial variation of the level of stochasticity along a defined direction for a parameter or a parameter set, termed Graded Randomness. Fourth, Layered Randomness is demonstrated, which allows the creation of layers in 3D and bands in 2D (surface elements). Fifth, Stochastic Surface Roughness is introduced, which can modulate the surface roughness of cellular materials.

For these design strategies and elements, a Blender Plug-In provides five distinct stochastic design strategies for cellular materials and four for surface elements. The cellular materials include strut-based and sheet-based cellular materials. These are Cubic, Body Centred Cubic (BCC), a standard and modified Face Centred Cubic structure (FCC) and three Triply Periodic Minimal Surfaces (TPMS). The surface elements include shark denticles, spheres, cubes, cylinders, and cone structures.

The developed software tools and the design rules will enable other researchers to explore the influence of different levels of stochasticity on surface elements and cellular materials on the thermohydraulic performance, mechanical properties, or their ability to promote osseointegration in implants.

Contents

Nomenclature **1**

1 Introduction **6**
1.1 Aim and objectives . . . 12
1.2 Thesis outline . . . 13

2 Literature Review **15**
2.1 Introduction . . . 15
2.2 Aperiodic Cellular Materials . . . 15
2.2.1 Definition and Classification of Cellular Materials . . . 16
2.2.2 Cellular Material Design . . . 19
2.2.3 Classification of Stochastic Design Processes . . . 29
2.2.4 The Influence of Randomness on Cellular Material Properties . . . 35
2.2.5 Combined design strategies utilising stochasticity . . . 48
2.2.6 Software Tools . . . 49
2.2.7 Applications . . . 58
2.3 Research Gaps . . . 63

3 Materials and Methods **65**
3.1 Introduction . . . 65
3.2 Software . . . 65
3.3 Shapes . . . 67
3.3.1 Primitive Shapes . . . 67
3.3.2 Shark skin shape . . . 68
3.3.3 Primitive-based cellular material shapes . . . 70
3.3.4 TPMS Shapes . . . 71
3.4 Equations . . . 74
3.4.1 Gaussian Distribution . . . 74
3.4.2 Weibull Distribution . . . 76
3.4.3 Graded Randomness . . . 77
3.4.4 Layered Randomness . . . 79
3.4.5 Binary surface roughness . . . 79
3.4.6 Perlin Noise surface roughness . . . 80
3.4.7 Parametrising Stochasticity . . . 80
3.5 Algorithms . . . 81
3.5.1 Procedure to create a generic surface element-based array . . . 81

3.5.2 Procedure to create a cellular material from a primitive structure . . 83
3.5.3 Procedure to create Stochastic TPMS Structures 84
3.5.4 Procedure to create a stochastic array 86
3.6 Shapiro-Wilk test 88
3.7 Hardware 89
3.7.1 Stereolithography 90
3.7.2 Selective laser sintering 91
3.7.3 Material jetting 92
3.8 Materials 93
3.8.1 Stereolithography resin 94
3.8.2 Selective laser sintering powder 94
3.8.3 Material jetting resin 94
3.9 Pin characterisation method 94

4 Stochastic design for strut-based cellular materials 97
4.1 Introduction 97
4.2 Results 98
4.2.1 Validating the Gaussian Distribution from an RNG using the Shapiro-Wilk Test 98
4.2.2 A Comparison of the Manufacturing Tolerance and the introduced Level of Stochasticity 99
4.2.3 Isotropic Randomness 100
4.2.4 Anisotropic Randomness 102
4.2.5 Graded Randomness 103
4.2.6 Layered Randomness 104
4.2.7 Surface Roughness 105
4.2.8 Example Application 106
4.3 Conclusions 107

5 Stochastic design for sheet-based cellular materials 109
5.1 Introduction 109
5.2 Results 110
5.2.1 Isotropic Randomness 110
5.2.2 Anisotropic Randomness 113
5.2.3 Graded Randomness 116
5.2.4 Radial Randomness 117
5.2.5 Layered Randomness 118
5.2.6 Surface Roughness 119
5.2.7 Example Application 122
5.3 Conclusions 122

6 Stochastic design **124**
6.1 Introduction . . . 124
6.2 Results . . . 125
6.2.1 Stochastic design level consideration . . . 125
6.2.2 Concept of isotropic and anisotropic randomness . . . 126
6.2.3 Application of different stochastic design levels to shark skin . . . 127
6.2.4 Designing a shark skin with nature-like variation . . . 132
6.2.5 Application of different probabilistic functions . . . 133
6.3 Conclusions . . . 134

7 Stochastic design Plug-In for Blender **137**
7.1 Introduction . . . 137
7.2 Stochastic design toolbox for lattices . . . 138
7.2.1 User interface . . . 138
7.2.2 Design workflow . . . 139
7.2.3 Possible Applications . . . 144
7.3 Stochastic design toolbox for surface elements . . . 146
7.3.1 User interface . . . 146
7.3.2 Design workflow . . . 148
7.3.3 Possible Applications . . . 152
7.4 Conclusions . . . 154

8 Thesis Conclusions **156**

9 Future work **159**

Acronyms **161**

References **163**

List of Figures **185**

List of Tables **192**

A Parameters to create cellular materials **194**
A.1 Parameters to design stochastic TPMS-based structures . . . 194

B Stochastic design parameters **197**
B.1 Stochastic cellular structure design parameters . . . 197
B.2 Stochastic surface elements design parameters . . . 199

Nomenclature

Number sets

$\mathbb{R}$	Real number	[-]

Other symbols

α, β, γ	Angle	[°]
ΔR	Applied roughness	[-]
δ	Stochasticity parameter	[%]
ϵ	Strain	[-]
ϵ_D	Densification strain	[-]
λ	Weibul scaling factor	[-]
μ	Mean value	[-]
ν	Poisson's ratio	[-]
ϕ	Scalar field	[-]
ϕ_{CM}	Cellular material scalar field	[-]
ϕ_c	Scalar field with offset	[-]
$\phi_{ellipsoid}$	Ellipsoid scalar field	[-]
ϕ_{hyb}	Hybrid scalar field	[-]
ϕ_{PN}	Perlin noise scalar field	[-]
ψ	Kernel	[-]
ρ_{rel}	Relative Density	[-]
σ	Standard deviation	[-]
σ_{max}	Maximum standard deviation	[-]

σ_{min}	Minimum standard deviation	[-]
σ_N	Stress	[N /m^2]
σ_{pl}	Plateau stress	[N /m^2]
θ	Polar coordinate angle	[-]
ξ	Polar coordinate angle	[-]
A	Surface area	[mm^2]
a_B	Number to divide a beam	[-]
a_s	Shark riblet angle	[°]
ADP	Average distance parameter	[-]
b_M	Beams in Maxwell criterion	[-]
b_s	Shark riblet angle	[°]
c	Offset parameter	[-]
C_1, C_2	Sphere caps 1 and 2	[-]
C_S	Scaling law constant	[-]
CP	Chemical potential	[J /kg]
CV	Covariance	[-]
D	Diameter	[mm]
d	Distance	[mm]
D_F	Diffusion constant	[-]
d_{min}	Minimum distance	[mm]
d_x, d_y, d_z	Discretiser	[mm]
E	Elastic Modulus	[N /m^2]
FDP	Fixed distance parameter	[-]
G	Shear Modulus	[N /m^2]

Nomenclature

H	Height	[mm]
$hr0, -hr2$	Ridge height	[mm]
$hr0y, -hr2y$	Ridge y position	[mm]
i, j, N	Counting variables	[-]
K	Concentration	[kg /m^3]
k_1, k_2	Curvatures in the principle directions	1 /m
K_B	Bulk modulus	[N /m^2]
k_{PN}	Perlin noise transformation constant	[-]
k_S	Sigmoid shape factor	[-]
k_w	Weibull shape factor	[-]
L	Lacunarity	[-]
l_0	Length at x=0	[mm]
l_B	Beam length	[mm]
l_x	Length at x	[mm]
$level1 - level5$	Height levels	[-]
$lr0 - lr2$	Ridge length	[mm]
LY	Layers	[-]
M	Matrix	[-]
m_M	System degree of freedom in Maxwell criterion	[-]
m_{PN}	Perlin noise transformation slope	[-]
M_{rot}	Rotation Matrix	[-]
MC	Mean Curvature	[1 /m]
MDP	Minimum distance parameter	[-]
MR	Mesh resolution	[mm]

MW	Maxwell Criterion	[-]
n_c	Offset exponent	[-]
n_M	Joint degree of freedom in Maxwell criterion	[-]
n_s	Scaling law exponent	[-]
n_x, n_y, n_z	Number of unit cells in one direction	[-]
P	Persistence	[-]
p	Significance level	[-]
p^*	Structural property	[-]
p_e	Period	[-]
p_S	Material specific property	[-]
p_x, p_y, p_z	Period, Period scaling	[-]
q_l	Weighting function denominator	[-]
q_u	Weighting function nominator	[-]
r_x, r_y, r_z	x, y, z Radius	[-]
$rh2 - rh5$	Scaling ratio	[-]
S	Seed	[-]
SDP	Standard deviation parameter	[-]
$SP1, SP2$	Sphere 1 and 2	[-]
t	Time	[s]
t_S	Sine curve thickness	[mm]
tot	Total	[-]
U	Energy Absorption	[kJ /kg]
u_c, u_x, u_y, u_z	Unit cell size	[mm]
V_{Box}	Box volume	[mm^3]

V_{cap}	Cap volume	[mm^3]
V_{CM}	Cellular material volume	[mm^3]
V_{mean}	Average volume	[mm^3]
V_{sphere}	Sphere volume	[mm^3]
W	Shapiro-Wilk parameter	[-]
w	Weight	[-]
w_s	Shark denticle width	[mm]
X, Y, Z	Modified coordinates	[mm]
x, y, z	Coordinates	[mm]
x_c, y_c, z_c	Centre coordinates	[mm]
$X_{rot}, Y_{rot}, Z_{rot}$	Rotation matrices	[-]
x_{sg}, y_{sg}	x and y spacing	[mm]
ym	Amplitude	[mm]

Physics constants

π	Pi constant	[3.14159]
e	Euler's number	[2.71828]

Subscripts

Box	Box	[-]
CM	Cellular material	[-]
rel	Relative	[-]

Chapter 1

Introduction

Additive Manufacturing (AM) is a process where a material is deposited layer-by-layer on a substrate to form a designed shape [1]. It emerged in the 1980s when Kodama [2] published the description of a manufacturing process where a resin was selectively polymerised layer-by-layer using a laser. This process is termed VAT polymerisation or Stereolithography (SL).

To effectively design parts for AM, these parts need to be either more cost-effective or provide functionality that Traditional Manufacturing (TM) cannot reach. Currently, Design for AM (DfAM) focuses on different design strategies, which were discussed by Diegel et al. [1]: These involve the design of highly complex shapes (part complexity), the combination of a multitude of parts into one (part consolidation), and to design objects that are made to fit uniquely to one person or machine (mass customisation).

Under the umbrella of all three design strategies, the design strategy of Biomimicry can be placed. Biomimicry involves using nature as a template to create a solution for a specific part because evolution took billions of years to balance all requirements to produce a design good enough to survive in a niche [3, 4].

The design strategies to arrive at a biomimetic design are outlined in du Plessis et al.'s review [3]. These strategies involve, for example, the utilisation of cellular materials for a myriad of purposes, the direct copying of nature's design elements (replication) or the use of Topology Optimisation (TO), where TO designs have an irregular structure, which is similar to that which can be found in nature.

Some prominent structures that can be observed in nature are surface elements and volume elements. Here, most probably, the shark skin or the lotus surface are known to the biomimetic engineer as having drag reduction [5, 6] and water repellent properties [7]. It is claimed that shark skin surfaces placed on aircraft can

lower drag by approximately 1%, which positively influences fuel consumption [8]. Shark-like surfaces were also proposed for thermal devices [9], and their thermo-hydraulic rating indicates that they possibly have an advantage in this field. Popular volume elements are cellular materials, which can be found in nature [10] and can be combined with even more sophisticated design strategies such as relative density grading [11] or hierarchical design [12]. These gradients and hierarchical structures, among others, are commonly occurring natural design strategies [10].

These cellular materials are often termed differently, and the following names can be found throughout the literature: lattices, architectured materials, cellular solids, meta-materials, foams, etc. In this work, the term cellular material will be predominantly used. The terminology unit cell, isotropic, and anisotropic are often used, too. In this work, the term unit cell is used to describe 2D or 3D building blocks such as a square (2D), a hexagon (2D), or a cube (3D) (See Fig. 1.1 a-c) that can be filled with any geometry or lattice configuration and periodically occurs in space [13]. In materials science, the terms isotropic or anisotropic refer to direction-dependent mechanical properties such as the elastic modulus or strength. Hence, isotropic elastic modulus means that the elastic modulus is the same in the coordinate directions, while an anisotropic elastic modulus refers to different elastic moduli in the coordinate directions. This work extends this terminology to stochastic properties such as the standard deviation of a Gaussian Random Number Generator. Isotropic Randomness refers to the same standard deviation in the coordinate directions, and Anisotropic Randomness means not the same standard deviation in the coordinate direction. The coordinate directions are x, y, and z.

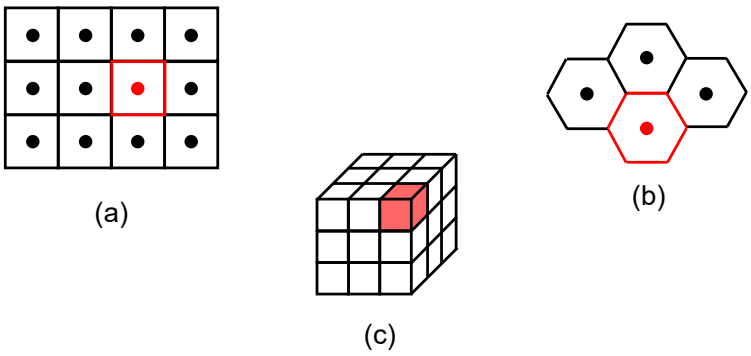

Figure 1.1: Unit cell. a) Squared unit cells. b) Hexagon unit cells. c) Cubic unit cells.

Cellular material research has been conducted over a hundred years, as presented in Fig. 1.2. Starting from the mid 1800s with the description of the Triply Periodic Minimal Surfaces (TPMS), alias the Schwarz-Diamond and the Schwarz-Primitive

surface [14]. His student Neovius [15] discovered the Neovius surface in the 1880s. However, manufacturing these at scale could be considered tedious, if not impossible, at that time. At the beginning of the 20th century, Voronoi [16, 17] described a partitioning algorithm for creating all types of Voronoi structures or diagrams. During the First World War, Hugo Junkers, a German aerospace engineer, patented honeycomb structures for his newly designed all-metal aircraft to provide high-specific stiffness aero-structures [18]. The honeycomb structures were also proposed as a core between two plates [19], which is nowadays widely used, for example, in cardboard to protect goods. Approximately one decade later, the French inventor Meller patented a metal foaming process, which allowed him to create foams in many different shapes [20]. In the 60s, the Spinodal decomposition process was described by Cahn [21], which currently helps to design the spinodal structures. Alan Shoen experimented in the 70s with soap bubbles and discovered the Gyroid and other structures presented in his NASA report [22]. However, it was still a time-consuming process to create these structures, but with the beginning of the 80s, the first VAT polymerisation process/ SL process [2], Fused Deposition Modelling [23] and the now commonly used Polymer Powder Bed Fusion (PBF) process Selective Laser Sintering (SLS) [24] emerged. Ten years later, the metal PBF process selective laser melting (SLM) followed [25]. The published work by Gibson et al. [26] and Ashby et al. [27] helped new academics get into cellular materials. The increasing use of computers and the advancement in AM helped to progress the research on cellular materials. With the ongoing adoption of computers, more Computer-Aided Design (CAD) software emerged that also started to include cellular materials between 2010 and 2020. Currently, Artificial Intelligence (AI) has become more important in many sectors, where complex inverse design processes for creating bone-like imitations for implants were made possible using neural networks (NN) [28]. However, the complete implications of AI on future design processes remain unknown.

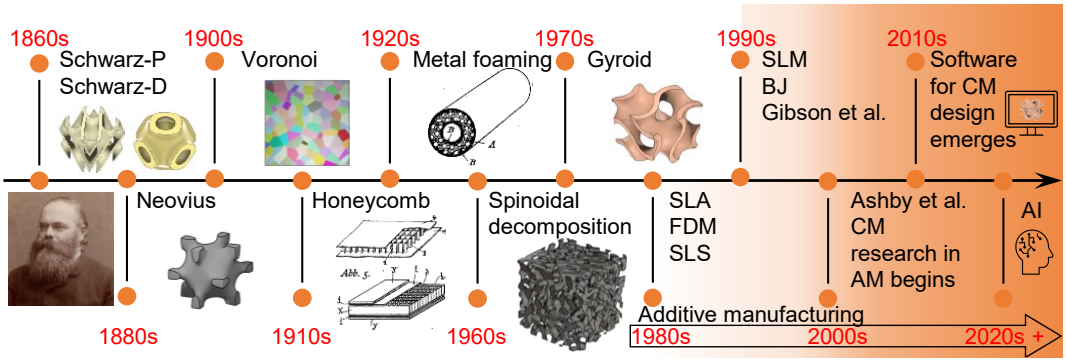

Figure 1.2: Cellular Material timeline. 1860s: portrait adapted from [29]. The 1910s: image adapted from [18] and [19]. 1920s: image adopted from [20]. The 1960s: Spinodal structure created with Gibbon [30].

These cellular materials were the subject of a multitude of reviews, which mainly examined the use of periodic cellular materials for lightweight applications [31], their use for energy absorption applications [32], their fatigue response [33], their use for thermal devices [34], the design process and research around TPMS structures [35], or the evaluation of properties and application fields [36, 37]. These reviews do not provide many insights into the stochastic design for cellular materials, even though variation can be observed in nature. This was already known to Sir Francis Galton in the late 19th century [38], who invented the so-called Galton board, which shows that a population's variation can be described with a distribution. But the question is from where the distribution in nature's designs originate and why it could be useful to incorporate them into a design. The designs found in nature evolved over a long period through evolution. The evolutionary process works as follows. Starting from a set of designs, which vary from each other, only those survive over time that can cope with the various external conditions such as temperature changes, food supply changes, attacks from predators, and others. The designs that cannot cope vanish, while the others can reproduce with variation, which causes them to cope better or worse with external conditions. This process repeats (natural selection), which makes the design more robust. While this means that designs become better or adapt over time [39], it does not necessarily imply an optimal design is reached at any given point [4]. Compared to that, an engineering design process involves an iterative design process to arrive at an optimum for a given set of boundary conditions. Therefore, why should a nature-inspired design process be used rather than a traditional one?

One way to use a nature-inspired design process is when a defined problem exists, and the responsible engineer finds a similar solution in nature and then adopts the complex natural design [3]. This will allow the engineer to adapt the shape to fit the boundary conditions and arrive at a suitable solution. Thus, the engineer would most likely end up with a regular solution because arriving at a 'simple' stable design is more time-effective than an irregular design using, for example, TO. However, most of the natural designs show irregularity.

The irregularity within a natural structure is likely caused by the many different boundary conditions that changed during the growing process and for which the structure adapted. Once the growing process stopped, these irregularities were embedded in the structure and should not change dramatically. A competent engineer who uses a design approach based on regular structures is limited to a few design parameters, such as the radius of a cylinder and its spatial distance to other cylinders in the x and y direction to create an array. This potentially limits the reachable

performance within these three parameters, see the red dotted line in Fig. 1.3. While all possible solutions could be accessed through randomisation, black dashed line, it is not necessarily efficient because it involves guessing all solutions. Here, the nature-inspired process of mutation comes into place, where controlled stochasticity (for example, a random displacement within a specific range) is added to the regular array, which limits the solution space to performances near the regular solution and changes the performance characteristics either to the good or to the bad. By examining the performance characteristics of the newly designed arrays with controlled randomness, only those with increased performance are selected, and potential design rules are established while those arriving at lower performance are rejected. Evidence from the literature shows that there is a potential to improve the compression strength by approximately 20% [40], or increase osseointegration rates [41] when stochasticity is applied to a regular cellular material structure.

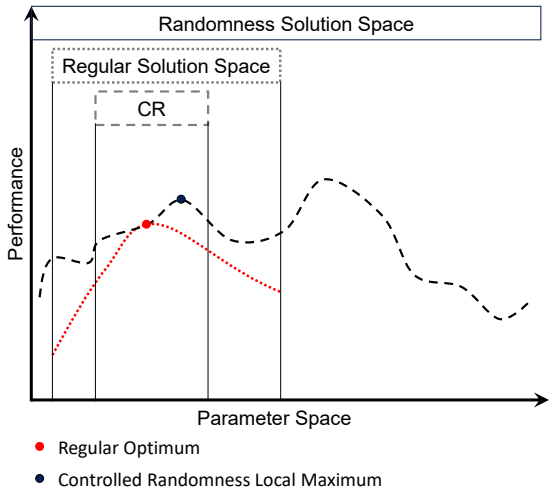

Figure 1.3: Performance example of a regular and stochastic design approach.

If it comes to variation, one interesting observation can be made from the data and observations presented by van Egmond et al. [42]. Their data enhanced with data from trees [43] and shark skin [44] is presented in Fig. 1.4 a), where a regular structure is indicated by 0% and levels greater than 0% indicate an increase in variation. The chart presents that manufactured cellular materials predominantly exhibit a low level of stochasticity $< 1\%$ or a high level of stochasticity $> 7\%$ as represented by metal foaming processes. However, natural surface elements, tree components, and natural cellular materials show a wide range of stochastic levels ranging from more or less regular bee honeycombs (Fig. 1.4 a) to approximately 9%

stochasticity in vertebrae. However, this important detail of a range of stochasticity levels is often overlooked when Biomimetic design strategies are used, such as designing hexagon structures based on bee honeycombs, Fig. 1.4 b-c), or designing Gyroid structures, which can also be found in the wings of a Callophrys Rubi butterfly [45], see Fig. 1.4 d-e).

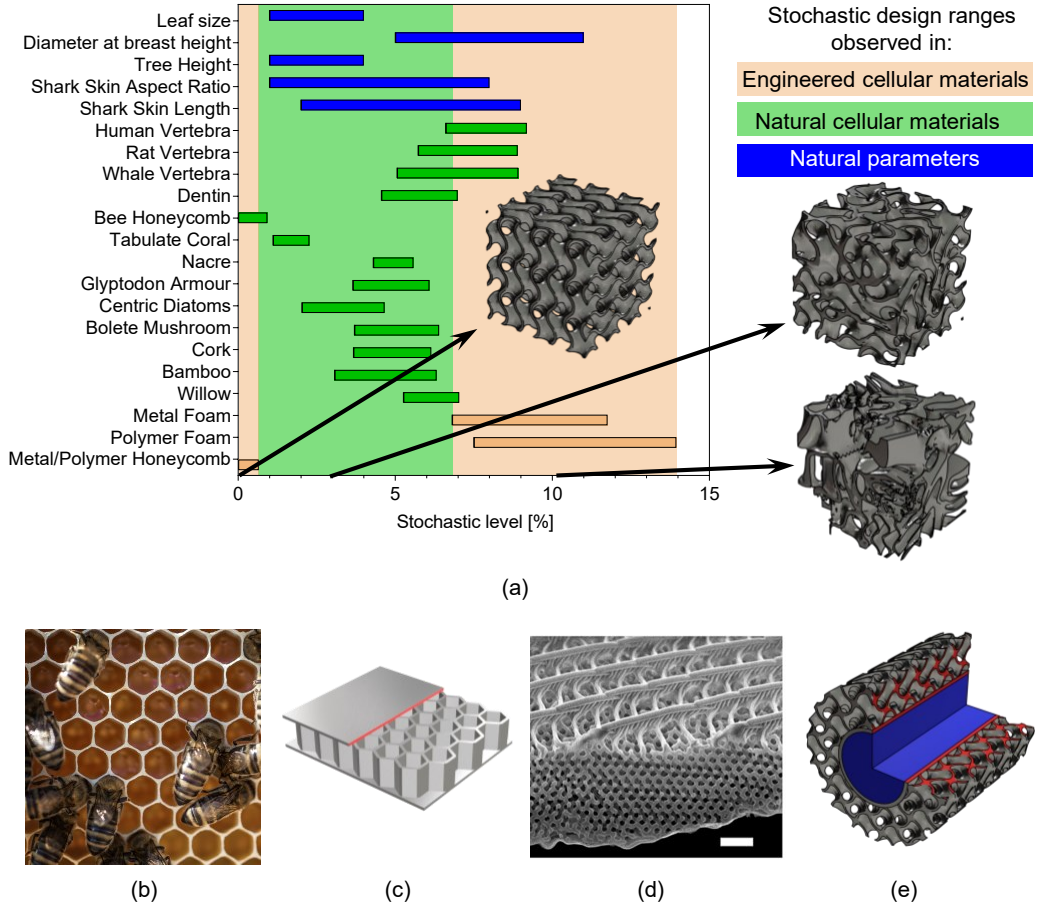

Figure 1.4: Commonly observed stochastic ranges and examples of natural and artificial cellular materials. a) Ranges of stochasticity observed in artificial and natural biological entities adapted from [42] (max and min values) and extra values computed from [44] and [43]. b) Honeycomb cells created from bees (image adapted from David Halbützel from Pixabay [46]. c) Sandwich panel utilising a honeycomb structure d) Butterfly wing where the scale is $1\mu m$, adapted from Corkery et al. [45]. e) A pipe surrounded by Gyroid fins for cooling.

The question is now, why does nature use this span of stochasticity, which implies that there are some benefits to using different levels of stochasticity. Some studies suggest that stochasticity might have the ability to increase osseointegration [47, 41], improve energy absorption during cracking [42], increase heat transfer [48, 49] and could potentially allow for a design of the mechanical response through combining different design strategies [50]. Variation can also be used to manipulate

light, as demonstrated in the review by Yu et al. [51]. However, more research is necessary, and currently, no software tools allow for designing different levels of stochasticity for TPMS structures, primitive element-based cellular materials, and surface elements (See Table 2.2).

To solve this problem and enable other researchers to investigate the influence of stochasticity for different surface-based elements and cellular materials in various research fields, design strategies and rules will be developed for surface-based elements, strut- and sheet-based cellular materials, which will be combined in a single design tool.

1.1 Aim and objectives

Controlled stochasticity has been mainly applied to beam- and Voronoi-based cellular materials and very little to primitive and complex shapes. Moreover, design strategies that change the level of stochasticity spatially of cellular materials are not used. This thesis aims to apply controlled stochasticity to primitive and complex shapes. The methodology to apply stochastic design strategies to primitive and complex shapes is developed and integrated into a design tool to enable the investigation of controlled stochasticity in the future. To achieve this aim, the following objectives are identified:

1. Combining the stochastic design frameworks of moving vertices in strut-based and Voronoi-based cellular materials to create controlled stochasticity primitive-based cellular materials and enhance this design framework with stochastic design strategies. The used Gaussian RNG will be validated by a Shapiro-Wilk test, and a manufactured sample array will be used to validate that stochasticity can be manufactured through AM. This is necessary to provide further unit cells and design strategies for controlled stochasticity and its exploration.
2. Enhancement of the design framework to create stochastic TPMS-based cellular materials to allow the introduction of controlled stochasticity to each unit cell starting from a regular discretiser grid. This gives full control over the cellular material structure to implement advanced stochastic design strategies, which include Graded Randomness, Layered Randomness, and Stochastic Surface Roughness. This will provide a framework for using controlled stochasticity and stochastic design strategies in stochastic TPMS-based cellular materials, enabling their exploration.

3. Enhancement of existing stochastic design frameworks to create stochastic surface elements by including overlap prevention and the establishment of design rules for the Gaussian distribution-based random number generation. This is necessary to create surface element arrays without overlaps and reduce the time to set up any stochastic design array.
4. Combining the enhanced design frameworks into a single Python library for cellular materials and surface elements that can be readily accessed through a Blender Plug-In. This is necessary to ensure that further unit cells can be added and that the included structures use the same design framework for a fair comparison in the future.

By working through these objectives, this thesis will contribute a user-friendly software tool that enables researchers to use five stochastic design strategies for cellular materials and four for surface-based elements. This builds the foundation for other researchers to investigate the influence of different stochastic design levels and strategies on these novel structures' mechanical, thermohydraulic, and biomechanical performance.

1.2 Thesis outline

After the Introduction (Chapter 1), eight Chapters will be structured the following way. First, the Literature Review will provide the necessary information on the creation of cellular materials and the state-of-the-art stochastic design processes and their implications for mechanical properties and knowledge gaps are identified. Second, the "Materials and Methods" (Chapter 3) will provide the methodologies used across several Chapters. The Result Chapters are shown in Fig. 1.5. The first Result Chapter, "Stochastic design for strut-based cellular materials" (Chapter 4), will apply five design strategies to primitive-based strut-based cellular materials: Isotropic, Anisotropic, Graded, Layered Randomness, and Stochastic Surface Roughness. This gives in total five stochastic design templates, which are essential for the designer to, for example, guide the cellular material collapse process (Layered Randomness) or help to improve heat transfer by adding Stochastic Surface Roughness. However, strut-based cellular materials are only one type. Another equally crucial cellular material type are TPMS structures. The design methods are developed for TPMS structures to apply the five stochastic design strategies. The design capabilities of this method are outlined in the second Result Chapter (Chapter 5). The third Result Chapter, "Stochastic design" (Chapter 6), will introduce stochastic design strategies

and rules applied to a complex shape. The rules will guide designers to easily set up a stochastic system using a Gaussian Distribution. The fourth Result Chapter, "Stochastic design Plug-In for Blender" (Chapter 7), will integrate the previously established stochastic design strategies into one design tool for surface-based and cellular material-based geometries. This will make the design tools available for inexperienced users in script-based design techniques. After presenting the Result Chapters, a thesis conclusion (Chapter 8) and future work (Chapter 9) follow.

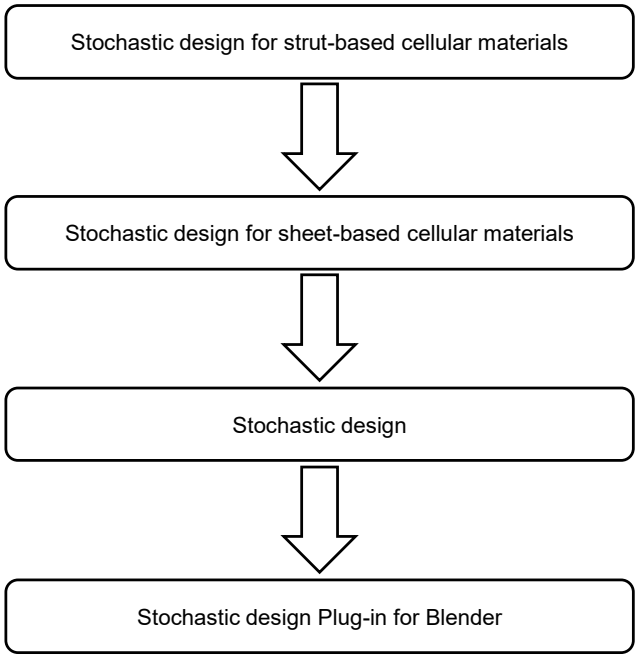

Figure 1.5: Result Chapter outline.

Chapter 2

Literature Review

2.1 Introduction

The literature review is separated into two sections to provide background information for this thesis. Aperiodic cellular material design is reviewed to provide a broad foundation of the design of cellular materials concerning AM and stochastic design. Finally, the literature is summarised, and research gaps are outlined.

Further information: The literature review is based on the review paper "Aperiodic architected structures by additive manufacturing: A review of the literature and practical guide for their creation". In this review, the author of this thesis is the first author.

2.2 Aperiodic Cellular Materials

This section describes the background knowledge of aperiodic cellular materials. First, a classification of cellular materials will provide a guide as to how different design strategies can be combined and which cellular material design criteria exist. Second, the different cellular material categories are introduced, and how they are designed is described. Third, a classification for stochastic design strategies is presented with examples from the literature. Fourth, stochastic design impacts cellular material properties and as such, the impact of stochastic design on mechanical properties is reviewed. Fifth, the combination of different design strategies for cellular materials is explained. Sixth, a selection of typical CAD design software and their capability in creating stochastic designs is demonstrated. Finally, applications for stochastic design strategies are discussed.

2.2.1 Definition and Classification of Cellular Materials

Currently, the number of unit cells that can form a cellular material and are known to the research community exceeds 17,000 [52]. As a consequence, it is important to classify cellular materials which are intended to be used for research or engineering applications. Gibson et al. [26] mainly described a cellular material broadly by the connectivity and elements it is made of. The connectivity of a cellular material can be described by vertices, edges, and faces (Fig. 2.1), [53]. Edges are lines that connect two vertices, and faces consist of at least three vertices and three edges. The edges can be formed through elements such as beams or faces and can be represented by surfaces [53]. By forming the cellular material through connected beams of different size and shape, the cellular material has a volume V_{CM} that is smaller than the volume of the bounding box V_{Box} of that cellular material. As such the relative density ρ_{rel} of the cellular material can be described by Eq. 2.1, [26, 27].

$$\rho_{rel} = \frac{V_{CM}}{V_{Box}} \tag{2.1}$$

2D and 3D cellular materials can be formed from the connectivity paired with the elements. Gibson et al. [26] termed these Honeycombs and foams, respectively. This terminology is broad for a classification , and this classification was improved. Recently, a more accurate classification of cellular materials was proposed, which is demonstrated in Fig. 2.1, and which is a combination of the classification proposed by Bhate et al. [53] and Ramirez-Chavez et al. [54]. Bhate et al. describe a cellular material by its connectivity, elements and tessellation. The tessellation describes the distribution of unit cells in space and how they relate. The tessellation is either periodic, aperiodic or hierarchical. The classification of periodic and hierarchical goes back to Bhate et al., while the aperiodic classification is based on Ramirez-Chavez et al.

Periodic cellular materials [53] are structures where at least one type of unit cell (unary) is repeatedly used in the design domain. The unit cell can be arranged edge-to-edge, shifted (non-edge-to-edge), or exhibit a certain degree of overlap. The unit cells can also be arranged hierarchically [53]. Overlayed, branched, and nested structures can be observed in hierarchical structures. Overlayed means that extra beams are used inside the unit cell to increase the connectivity. Branching means that a beam branches out beginning at a starting point. Nested means that smaller

unit cells are sampled within the macro unit cell.

Aperiodic structures are either made from hybridisation, grading, or perturbation as described by [54]. Hybridisation means that at least two different types of cellular materials are merged (Allocation), at least two different cellular materials interpenetrate (Interpenetration), or unit cells or parts of a unit cell of the parent structure were removed (Deletion). Grading means that a parameter such as the unit cell size varies according to a set pattern. Finally, aperiodic structures can be created by applying perturbation (stochasticity). This can be done by using random fields or algorithms. Commonly used algorithms are, for example, the Voronoi or the Possoin Disc Sampling algorithm [54].

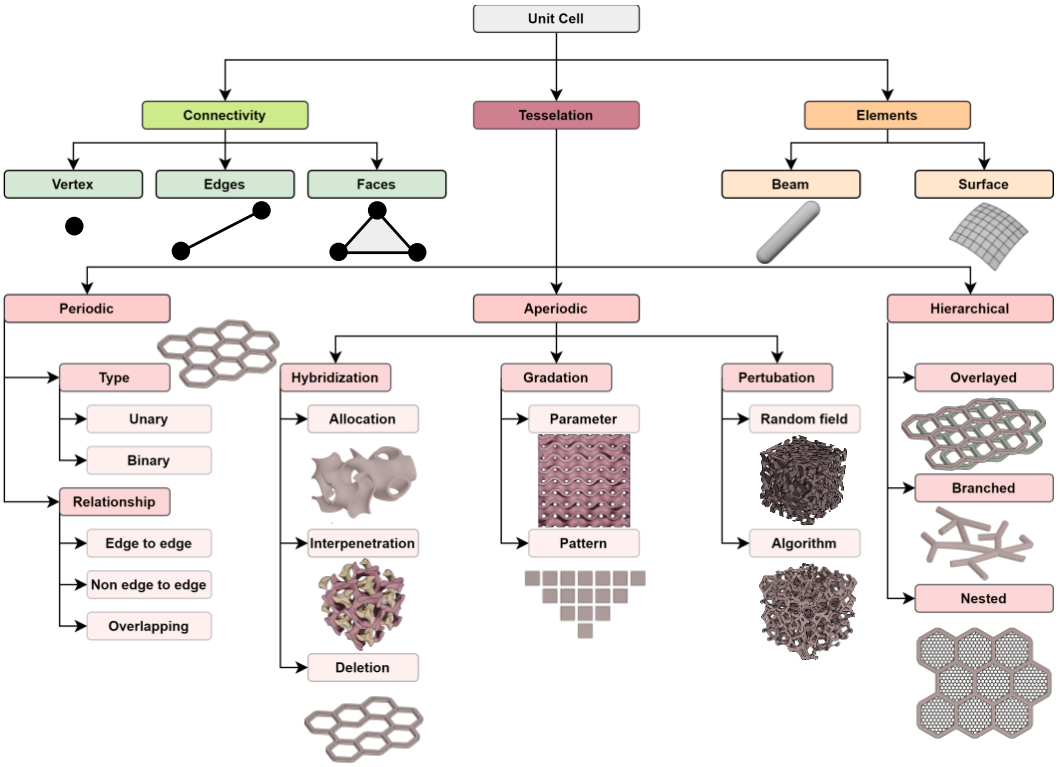

Figure 2.1: Classification of cellular materials. Graph adapted, simplified and merged from Bhate et al. [53] and Ramirez-Chavez et al. [54].

The cellular materials that can be described by the discussed classification can be further divided into stretch and bending-dominated cellular materials [55]. The response can be determined by the Maxwell criterion [55, 56] MW (Eq. 2.2), which can be used to describe the degree of freedom of a mechanism. A mechanism comprises beams b_M, which are connected through joints J. The joints have a rotational degree of freedom of n_M and the mechanism a degree of freedom of m_M.

In 2D $n_M = 2$ and $m_M = 3$ and in 3D $n_M = 3$ and $m_M = 6$. The Maxwell criterion can describe three cases [55], an over-constrained $MW > 0$, an under-constrained $MW < 0$, and determined $MW = 0$ case. A determined system and over-constrained mechanism cannot move and is rigid, which is characteristic of a stretch-dominated cellular material [55] (Fig. 2.2 a). On the contrary, an under-constrained mechanism is compliant and therefore has $MW < 0$ [55], for example, a bending-dominated cellular material (Fig. 2.2 b).

$$MW = b_M - n_M \cdot J + m_M \tag{2.2}$$

Both the stretch and bending-dominated cellular material exhibit a characteristic stress-strain curve as shown in Fig. 2.2, a) and b), respectively. The main difference between the stretch-dominated and the bending-dominated cellular material is that the fist is stiffer than the second [26]. However, bending-dominated structures show a more or less constant plateau stress after yielding, which makes them ideal candidates for energy absorption applications [26].

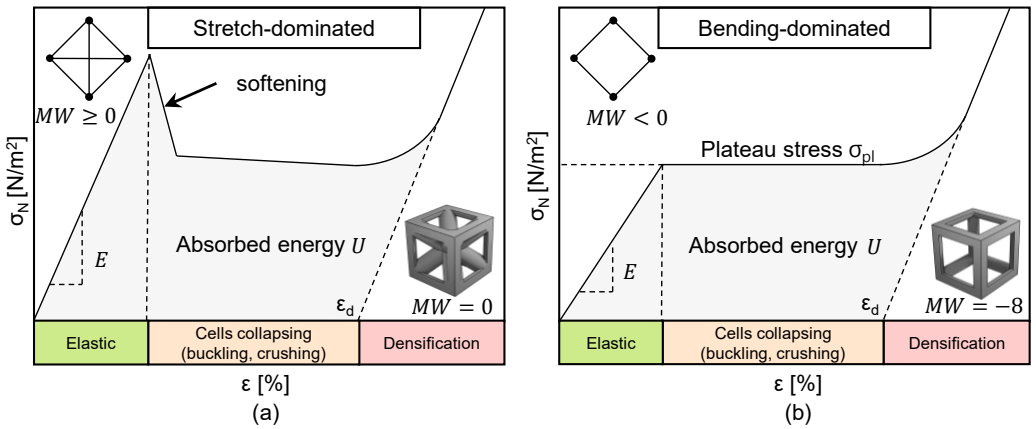

Figure 2.2: Characteristic stress-strain curves of cellular materials. a) Stress-strain curve of a stretch-dominated cellular material that meets the Maxwell stability criterion of $MW \geq 0$ such as the BCC structure [55]. The stretch-dominated structure exhibits an elastic region prior to yielding, after yielding the structure either buckles or crushes in the collapsing zone, after the collapsing zone, it enters the densification zone. b) The stress-strain curve of a bending-dominated cellular material is characterised by a Maxwell criterion of $MW < 0$ and forms a typical stress plateau [55]. A cellular material that has this characteristic is a cubic cellular material. E is the elastic modulus, U is the energy absorption, ϵ_d is the densification stress. σ_N is the stress and ϵ is the strain. Images adapted from [55]

The properties of cellular materials can be evaluated according to scaling laws found in [27] or [26]. The general approach to describe a property of cellular materials is

to use a scaling law and link the relative density (Eq. 2.1) to the specific material property p_s and the structural property p^*. Here, C_s and n_s are both constants.

$$\frac{p^*}{p_s} = C_S \cdot \rho_{rel}^n s \tag{2.3}$$

2.2.2 Cellular Material Design

This section discusses the design of the basic cellular materials, such as the cellular materials based on struts, TPMS unit cells, Spinodal decomposition, and Voronoi cells. After understanding the basic design theory of cellular materials, different design strategies are discussed to help the reader understand the wide range of cellular material design strategies and unit cells. In aperiodic design, the idea is to create heterogeneous structures, and as such, interpolation methods are described to transition between different unit cells. Subsequently, the stochastic design process is discussed.

Strut-based design

A strut-based cellular material is a structure where connections (vertices) are spatially distributed to form a crystal lattice configuration [26]. Thus, a list of vertices and edges defines the strut-based cellular material. The edges can be explicitly designed by using CAD through 'sweep' tools and sketches. This can be a tedious process. A simpler process is to compute the signed distance field (SDF) [57, 58, 59] of each edge and perform a Boolean union of the created edges. An SDF [57, 58] represents an object's surface, where in a grid, each grid-point represents the shortest distance to the surface. A positive value indicates a positive offset from the surface, and a negative value indicates a negative offset. From this SDF, an isosurface can be evaluated at the surface or a distance away from the surface to visualise the object. To evaluate the isosurface, a marching cube algorithm can be used [60]. Another way of designing strut-based cellular materials is to use a line representation of the struts and slice the structure so that the strut thickness is controlled by the energy of the laser beam that melts the metallic powder in an SLM machine [61].

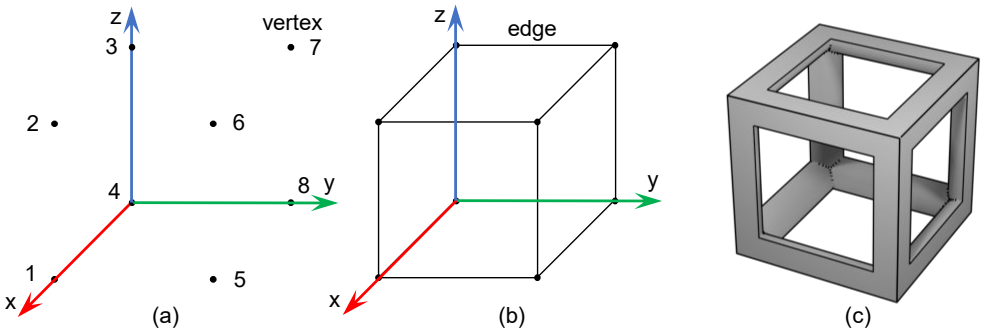

Figure 2.3: Strut-based cellular material design process. a) Definition of vertices for a cubic unit cell. b) Connection of the vertices through edges in the correct order. c) Rendering of the final cubic cellular material unit cell.

Triply periodic minimal surface design

A TPMS is a cellular material that continuously expands in all three directions of the Cartesian coordinate system. It is characterised as a minimal surface, meaning it has the smallest possible surface area within a given boundary [62]. An example of a minimal surface, a hand drawing, and a rendered Neovius TPMS is shown in Fig. 2.4 a) and b). A minimal surface is mathematically defined by a surface exhibiting a mean curvature MC (Eq. 2.4) of zero at every evaluated node of said surface [62]. MC is determined by calculating the average of the curvatures k_1 and k_2 in the principal direction (See Fig. 2.4 b).

$$MC = \frac{k_1 + k_2}{2} \tag{2.4}$$

Commonly used TPMS structures are the Schwarz-D and Schwarz-P structures, described in the 1860s by Schwarz [14]. Other common TPMS structures are the Neovius structure [15] (Fig. 2.4 a, b) and Schoen's [22] Gyroid structure. These TPMS structures can be mathematically described by trigonometric equations, which were reported by von Schnering et al. [63].

The design process of TPMS structures is described in several publications, such as by Yoo et al. [64], Al-Ketan et al. [65] and Maskery et al. [66]. To design a TPMS structure, a trigonometric equation of a TPMS structure is chosen such as Eq. 2.5. This equation represents the Schwarz-P unit cell [63]. X, Y and Z define the expansion and period of the unit cell, where for a periodic cellular material $X = 2\pi x/u_c$ (For Y and Z, replace X. x, y and z are the grid coordinates). u_c

describes the unit cell size.

$$\phi = cos(X) + cos(Y) + cos(Z) \tag{2.5}$$

To then realise either a network or a sheet-based TPMSstructure, the scalar field ϕ needs to be offset by a parameter c. To create a network TPMS structure, the exponent n_c must be one and two for a sheet-based TPMS [66].

$$\phi_c = \phi_c^n - c_c^n \tag{2.6}$$

A marching cube algorithm [60] can then evaluate the scalar field of the TPMS structure to find the isosurface that represents the required network or sheet-based TPMS structure.

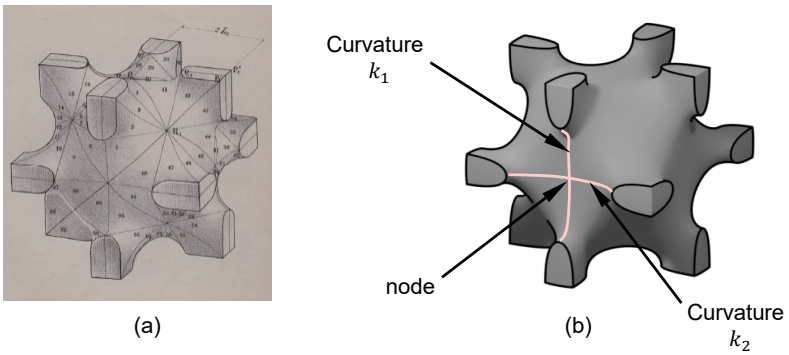

Figure 2.4: Neovius surfaces. a) A hand drawing of the Neovius surface, reproduced from [15]. b) A modern rendering of the Neovius surface.

Spinodal design

Spinodal decomposition refers to a process where two more or less mixed components separate over time and space [21]. This process can be described by the Cahn-Hilliard equation 2.7 [21]. The original equation by Cahn Hilliard can also be written as Eq. 2.7, [67]. Here, K is the concentration, t is the time, D_F is the diffusion coefficient and CP is the chemical potential. This decomposition process results in a scalar field where the boundary between the two phases can be visualised through an isosurface. This boundary (Fig. 2.5 a) to d) can be then used as a representation of a cellular material.

$$\frac{\partial K}{\partial t} = -\nabla(D_F \nabla CP) \tag{2.7}$$

A sum of trigonometric cosine functions can also represent a spinodal structure often referred to as a Gaussian Radial Field [68, 69], where each cosine equation is sampled randomly. From the domain of random samples situated on a unit sphere, only those

directions are chosen that full fill predefined angle criteria in the direction of the x, y and z axis [68, 69]. Depending on these predefined criteria, the resulting spinodal structure is either lamellar, columnar, cubic, or isotropic and can be designed as demonstrated in Fig. 2.5 e-h).

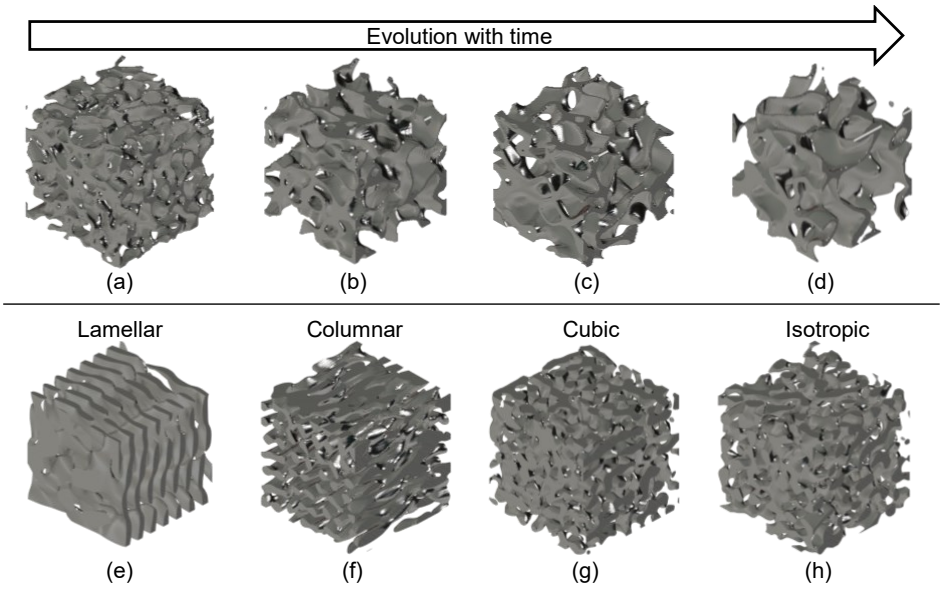

Figure 2.5: Spinodal decomposition. a) Boundary representation of two randomly mixed phases (50 time steps). Decomposition after 100 b), 150 c), and 200 d) time steps. (Code created with ChatGPT). e) Lamellar, f) columnar, g) cubic and h) isotropic spinodal structures (Created with Gibbon [30]).

Voronoi design

An in-depth description of Voronoi structures can be found by Aurenhammer who gives a broad review of the techniques for the creation of Voronoi structures [17]. A Voronoi cellular material is a structure composed of seeds S_i, either created through a stochastic sampling process or offsetting a uniform array with random values. The Voronoi cells can be constructed by identifying the nearest seed points S_j to every S_i. A line perpendicular to $\overline{S_i S_j}$ situated equidistant to S_i and S_j then forms an edge of the Voronoi cell. If this line intersects another line created similarly, the intersection forms a Voronoi vertice v_i. Repeating this process, polygon cells are formed in the 2D space and polyhedra in the 3D space. An exemplar structure of creating a cellular material with the Voronoi algorithm is shown in Fig. 2.6. a) presents a uniform cellular material composed of a Kelvin unit cell. In b) and c) Voronoi cellular materials are shown that include stochasticity of 10% and 20%, respectively.

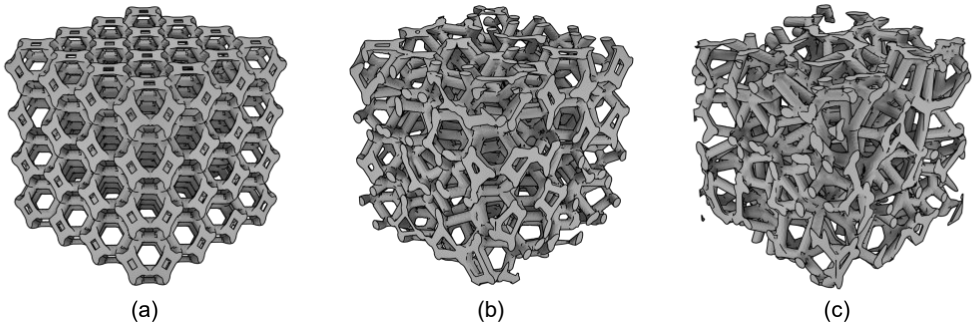

Figure 2.6: Three dimensional Voronoi structure with different levels of stochasticity. a) Uniform structure. b) Stochasticity level 10%. c) Stochasticity level 20%.

Efforts were also made to increase the design capabilities for Voronoi structures, such as spatially varying seed positions and relative density [70, 71] or to design cells that smoothly follow property maps [72, 73, 74]. Designing these highly aperiodic Voronoi structures help to better facsimile biological structures [75].

Architected material design strategies

Cellular materials offer a wide range of design flexibility where the experienced designer needs to balance the material and structural properties to achieve the required properties for a specified design. This section will give a brief overview of the most relevant design practices used for cellular material design. Examples of authors who used these design methods are given. For more details, please refer to Ramirez-Chavez et al. [54]. The authors provide in-depth categorisations of the design classifications that are only briefly touched on here. The most simplistic way to design a cellular material is to keep the geometrical properties constant throughout the design. One such example of a periodic BCC cellular material manufactured from AlSi10Mg and subsequently heat-treated is shown in Fig. 2.7 a) [11]. Depending on the design intent, this cellular structure can be modified. One of such modification is to use a graded design approach where at least one geometrical parameter is graded alongside at least one direction, as shown in Fig. 2.7 b) [11], where the relative density is graded from the top to the bottom from a low to a high level of relative density. This design process changes the deformation process from the formation of an unpredictable shear band in the uniform cellular structure a) to a designed so-called “layer-by-layer” deformation procedure [11], which is beneficial for engineering requirements where managing the energy absorption behaviour plays an important role. Other grading strategies involve radial grading [76], grading according to a trigonometric equation [77], or cell size grading [76, 78], among

others. The design strategy where at least two different unit cells transition from one to another is termed hybridisation or multi-morphology design [79, 80]. One such additively manufactured cellular structure demonstrates the transition from a sheet-based Schwarz-Diamond to a sheet-based Gyroid cellular structure is shown in Fig. 2.7 c) [78]. Characteristic for the hybrid designs made of network-TPMS is to deform first at the transitional zone [77] due to a low relative density, which can be corrected [77, 81]. If this transitional zone is oriented perpendicular to the introduced force, a layer-by-layer failure can be observed in sheet-based TPMS structures [78], while a shear band can occur if the applied force is parallel to the transitional zone. Furthermore, a cellular material is normally designed in a control volume where the solid material forms a network in most cases and is surrounded by a void as shown in Fig. 2.7. This void can be either filled with another cellular material separated from the first, which is a so-called interpenetrating cellular material [82] (Fig. 2.7 d) or the void can be filled by a compliant material to form an interpenetrating phase composite (IPC) [83] (Fig. 2.7 e). The interpenetrating cellular materials, as described by White et al. [82] offer a plurality of cellular material combinations that broaden the application spectrum to build highly integrated filtering, electrical, or mechanical devices by combining the properties of at least two different cellular materials. The IPC cellular materials on the contrary to interpenetrating cellular materials form a structure where two or more phases are in contact [83]. The TPMS-based IPCs investigated by [83] showed a bending-dominated compression behaviour and the additional compliant phase prevents the stiffer TPMS phase from fracturing, thus making IPCs good candidates where impact energy should be dissipated, or vibrations should be reduced. Hierarchical design strategies have been applied to cellular materials in AM. Some examples show Honeycomb structures, where another hexagon is placed at nodes where the edges intersect [84, 85], and network-based [86] and sheet-based TPMS [12] cellular materials are shown where the solid material of the initial TPMS unit cell is replaced with a smaller unit cell. An example of such a sheet-based TPMS structure that is a hierarchical design is presented in Fig. 2.7 f). Out-of-plane impact compression tests on hierarchical honeycomb structures manufactured from AlSi10Mg suggests an elevated energy absorption at a relative density of approximately 20%, while for increasing relative density levels, the difference diminishes [85]. Sheet-based hierarchical TPMS structures showed, in general, a lower elastic modulus and strength across different relative density levels [12], however at relative density levels lower than 2% some hierarchical configurations could achieve a higher strength.

Additionally, the deformation process [87], or cracking path [88] in cellular materials can be altered by introducing defects by removing edges, which changes the adjacency of the cellular material locally. This is also called beam deletion by some authors [89, 90], an example of such structure is shown in Fig. 2.7 g). It was shown that changing the adjacency in honeycomb structures locally can be beneficial to achieve an elevation in energy absorption - if correctly designed and optimised - [87, 88, 89] when compared to periodic structures.

Several stochastic design processes can be found in the literature, discussed later. Here, an example of a stochastic TPMS structure, which was created by [91], is shown in Fig. 2.7 h). The design of stochastic TPMS structures normally involve separating the control volume into subdomains, which are then filled with randomly oriented cellular materials [92, 93]. Several authors have shown that computer tomographic (CT) scans can be translated to relative density values, thus allowing the design of cellular materials with a relative density distribution similar to their bone counterpart [94, 95]. An example of a cellular material slice with adjusted relative density according to a CT image is shown in Fig. 2.7 i). Apart from designing cellular materials in cuboids and merging them with geometries of arbitrary shape, cellular materials can follow the shape of a geometry. These design strategies where the cellular materials unit cells follow the shape of the outer contour is called conformal design, which was applied by [59], see Fig. 2.7 j). Cellular materials are well suited for TO, where an ideal mass distribution is sought to fulfil a given set of boundary conditions [96, 97]. An example of a TO structure where a scalar field representing relative density values is filled with a strut-based cellular material is shown in Fig.2.7 k) [98]. TO was also demonstrated utilising sheet-based cellular material geometries [99].

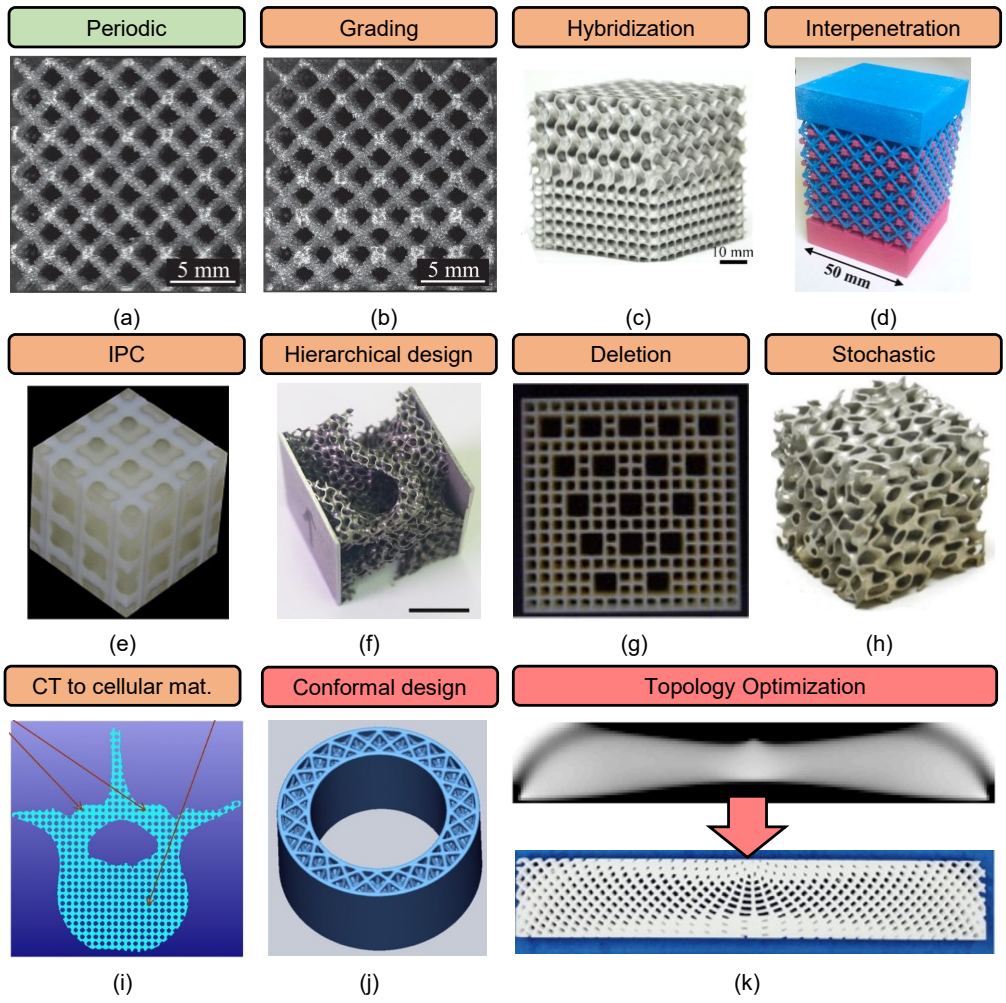

Figure 2.7: Main design strategies applied to cellular materials. a) Uniform, reproduced from [11]. b) Relative density grading, reproduced from [11]. c) Hybridisation, reproduced from [78]. d) Interpenetration, reproduced from [82]. e) Interpenetrating Phase Composites (IPC), reproduced from [83]. f) Hierarchical design, reproduced from [12]. g) Beam deletion, reproduced from [90]. h) Stochastic design, reproduced from [91]. i) CT-based design, reproduced from [94]. j) Conformal design, reproduced from [59]. k) Topology Optimisation, reproduced from [98].

These design strategies can be applied to the different unit cells constituting a cellular material. As previously mentioned, the number of known cellular materials is over 17,000 [52]. Hence, only a selection of unit cells can be presented here. A selection of two- and three-dimensional unit cells is shown in Fig. 2.8. Cellular structures that are often used are the sheet-based a) and network-based b) TPMS structures. More of these can be found in [63]. The well-known honeycomb structure [26], a hexagon, is shown in c). Several strut-based unit cells are presented in d). For more information on different strut-based cellular materials, the interested reader is referred to [52, 100].

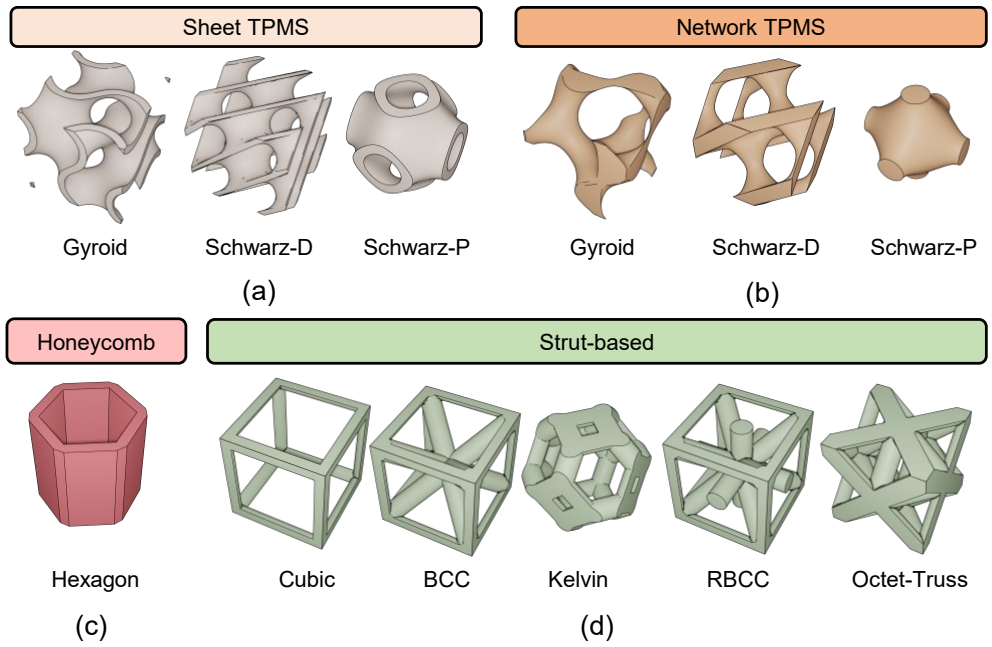

Figure 2.8: A selection of cellular material unit-cells. a) and b) present sheet- and strut-based TPMS structures, respectively. c) shows the famous honeycomb unit cell, which is a hexagon. d) several different strut-based cellular material unit cells. [26, 52, 100]

Interpolation methods

Interpolation methods are important when designing cellular materials, especially when the design methods become complex. This can be when different cellular materials (Keyword hybridisation) or differently oriented cellular materials should be stitched together. To do so, interpolation strategies were applied by various authors. The utilised interpolation strategies are mainly derivatives of the so-called Radial Basis Function (RBF) [101]. Here, ϕ_i is the i-th cellular material domain, and w_i are the weights that describe where to turn the domain in the space on and off. ψ is a Kernel that needs to be chosen and d_{ist} is a distance field $|x - x_i|$, see Eq. 2.8.

$$\phi_i = \sum_{i=0}^{N} \cdot w_i \cdot \psi(d) \tag{2.8}$$

Typical Kernels that were used for the creation of cellular materials were the thin-plate-spline [94], the Gaussian kernel [102] or the compactly supported radial basis function [103]. To then create the overall hybrid structure ϕ_{hyb}, each cellular material

ϕ_i has to then be multiplied by each domain's weight w_i, see Eq. 2.9.

$$\phi_{hyb} = \sum_{i=0}^{N} \cdot w_i \cdot \phi_i \tag{2.9}$$

This results in two steps that have to be solved, first the weight vector w_i has to be solved for a given set of distance fields established from a Kernel $\psi(d_{ist})$ which results in a computational effort of $O(N^3)$ [101] and an additional effort of $O(N)$ for creating the structure ϕ_{hyb} [101]. Thus, a more efficient approach that can be used is the Shepard Interpolation, which was proposed in the 60s by Shepard [104] and which is a derivative of the normalised RBF [101] function with a computational effort of $O(N)$. Shepard proposed an interpolation of the form shown in 2.10, which was used to create hybrid cellular materials ϕ_{hyb}, [79].

$$\phi_{hyb} = \frac{\sum_{i=0}^{N} \cdot w_i \cdot \phi_i}{\sum_{i=0}^{N} \cdot w_i} \tag{2.10}$$

The authors [65], [79] used this equation utilising a sigmoid function as the weight. Regarding the interpolation functions, it was observed that in the case of strut-based TPMS structures, the interface between domains did not comprise the desired relative densities; this can be corrected using the beta growth function [80], correcting the relative density with an algorithm [77] or with an improved weighting function [81]. Additionally, Eq. 2.9 can be simplified for the case of combining two different cellular materials as utilised by the authors [76], [79]. Here, w represents a map of values, either constructed using a sigmoid function as done by Yang et al. [79] as a weight or providing a map of values between 0 and 1 calculated from an RBF as done by Yoo et al. [76].

$$\phi_{hyb} = (1 - \psi)\phi_1 + (\psi)\phi_2 \tag{2.11}$$

Attempts were made to use a T-Spline interpolation [105], which gives adjustability at defined points within the cellular material domain.

Regarding the interpolation functions, it can be concluded that if calculation speed is a concern, the Shephard interpolation [104] should be preferred, while if controllability and precision are of significant concern the RBF or the T-Spline should be selected [101, 102, 105].

2.2.3 Classification of Stochastic Design Processes

This section describes the classification of stochastic design processes based on several authors. It provides a fundamental classification based on the literature on randomness, so-called Random Sets and Random Fields. Second, stochastic design methods that produce subsets of the fundamental classifications are explained. Third, methods are provided that could be used to describe the stochastic structure.

Stochastic design classification

Recently, several authors attempted to provide a classification for the different stochastic approaches that were used throughout the literature. Most notably, Ramirez-Chavez et al. [54] categorised aperiodic design strategies, among these stochastic design or as the authors termed it "perturbation", see Fig. 2.9 a). The authors split "perturbation" into two main classes: features and methods. The features are the elements that constitute a cellular material, such as a nucleus, nodes, and members. The methods are the Random Field and the algorithms. While it can be agreed that a Random Field is a stochastic design process, the Voronoi algorithm is not necessarily a stochastic design strategy; it is an algorithm for spatial separation that can work on every spatial data set [17]. Another classification for stochastic design methods was proposed by Feng et al. [106], and Kanwar et al. [107] provided examples and critiqued these design methods. Feng et al. [106] discusses the Random-Set method, and some methods that utilise Random Sets or Random Fields as a starting point to create stochastic cellular materials, which are maximum entropy, iterative non-linear transformation, and stochastic optimisation, see Fig. 2.9 b). As these optimisation methods result in a single solution, they are not further elaborated here. Groth et al. [108] focused more specifically on the utilisation of the random number generation itself and categorised the methods used by different authors in the random choice methods, sequential inhibition methods, adding an offset to periodic data and into field methods, see Fig. 2.9 c). These authors [54], [106], [107], and [108] have some methods in common, the Random Field method and methods that are derivates of the Random-Set method. As such, a synthesis of these classifications is proposed; see Fig. 2.9 d).

The fundamental core of any stochastic design strategy is the application of random values, which can be created using a Random Number Generator (RNG) implemented in common programming languages. Well established RNGs are for example

the Mersenne Twister [109] (Matlab [110]) and the PCG64 [111] (Python - Numpy [112]). These can not only produce uniformly distributed values but can also sample according to well-known distributions. The realisation of this is a topic on its own and is already implemented in many programming languages. Hence, it will not be discussed here. A brief explanation can be found in [113]. From these RNGs, the fundamental elements, a Random-Set or a Random Field, can be created [54, 106].

A Random-Set is understood as at least one array of randomly sampled numbers forming at least one solution of the infinite possible solutions in a random space [114]. This approach can create randomly distributed spatial values or random choices.

A Random Field combines at least two random values with Euclidean coordinates in the 2D or 3D space to either create a discrete Random Field where the values are not smoothly transitioning from one to another or a smooth Random Field where the random values transition from one to another [115, 116]. The next chapter will give examples and explanations for the different methods based on Random Fields and Random-Sets.

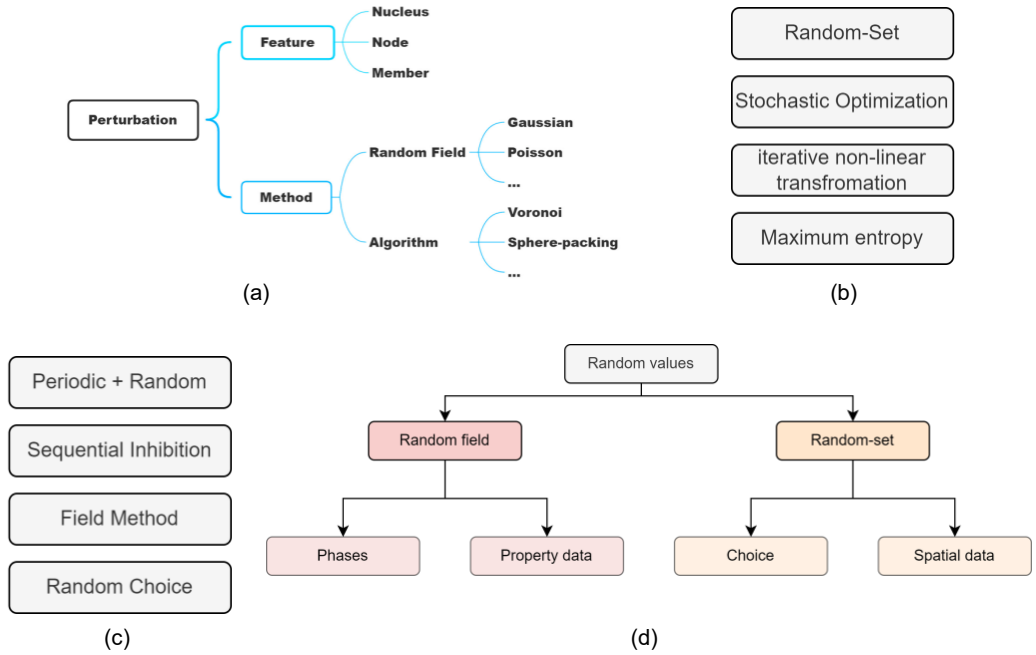

Figure 2.9: Stochastic design classes. a) Classification of stochastic design as proposed by Ramirez et al. [54], reproduced. b) Stochastic design methods as mentioned by Feng et al. [106]. c) Stochastic design categories based on Groth et al. [108]. d) Fundamental elements of stochastic design.

Stochastic design methods

As described in the previous section, the stochastic design methods are Random-Sets and Random Fields. Figure 2.10 a) shows the different design methods that form Random-Sets (yellow) and Random Fields (red). The methods resulting in Random-Sets or Random Fields are separated into ‘Single Stochasticity’ and ‘Double Stochasticity’, which refers to Baddeley et al. [117], who use the term "Doubly-stochastic processes" for processes that perform two different stochastic design methods in sequence. Six ‘Single Stochasticity’ approaches will be explained, and one ‘Double Stochasticity’ approach.

The first ‘Single Stochasticity’ approach is the so-called accept and reject (A-R) method which is a spatial variation process [113, 118]. Here, seeds are randomly sampled sequentially. After each sampling iteration, the distance between the new and previous seeds is checked. If the distance is outside a reject distance, it is accepted. In any other case, the seed is resampled. This process is commonly used to create stochastic Voronoi cellular materials, and can be found under the term Simple Sequential Inhibition (SSI) [42, 119, 120] or Poisson Disc sampling [70, 72,

121]. An example of a stochastic Voronoi structure based on SSI can be found in Fig. 2.10 b). The second stochastic design approach involves the creation of Random Fields. This is done by storing random values in a grid. Examples are the Gaussian field [122] (Fig. 2.10 c)) or random values [123] as a starting point for Spinodal decomposition, as presented in Fig. 2.10 d). However, if the Random Field creation process involves a subsequent interpolation between the random values, the result is a smooth transition [105, 116, 124]. A smooth transition was achieved using cubic T-splines as demonstrated by [105]. The same can also be achieved using Perlin Noise [116] or Simplex Noise [124]. The following two 'Single Stochasticity' approaches involve random positioning and movement. Random positioning creates a Random-Set of positional values to form, for example, sub-domains in cellular materials as demonstrated by [91, 92, 93, 125] and others, see Fig. 2.10 e). However, this Random-Set of values can also be added as an offset to periodic values to cause a random movement as demonstrated by [61, 108, 126, 127, 128, 129]. An example is shown in Fig. 2.10 f). Finally, apart from creating Random Fields to design geometrical parameters or producing some spatial variation, a stochastic cellular material can be created from choice, where a certain probability is linked to a specific unit cell [130], see Fig. 2.10 g).

As previously mentioned, "Doubly-stochastic processes" or 'Double Stochasticity' is when two different stochastic design procedures are applied sequentially [117]. As shown in Fig. 2.10 a), an A-R approach is coupled with manipulating the spatial variation after the sampling process. These "Doubly-stochastic processes" are implemented in the r library "spatstat" [117], and the usable methods are called Matern I, Matern II, the Thomas process, and the Neyman-Scott process. Interestingly, the 'Double Stochasticity' was not found to have been applied to cellular materials. This offers a potential research road.

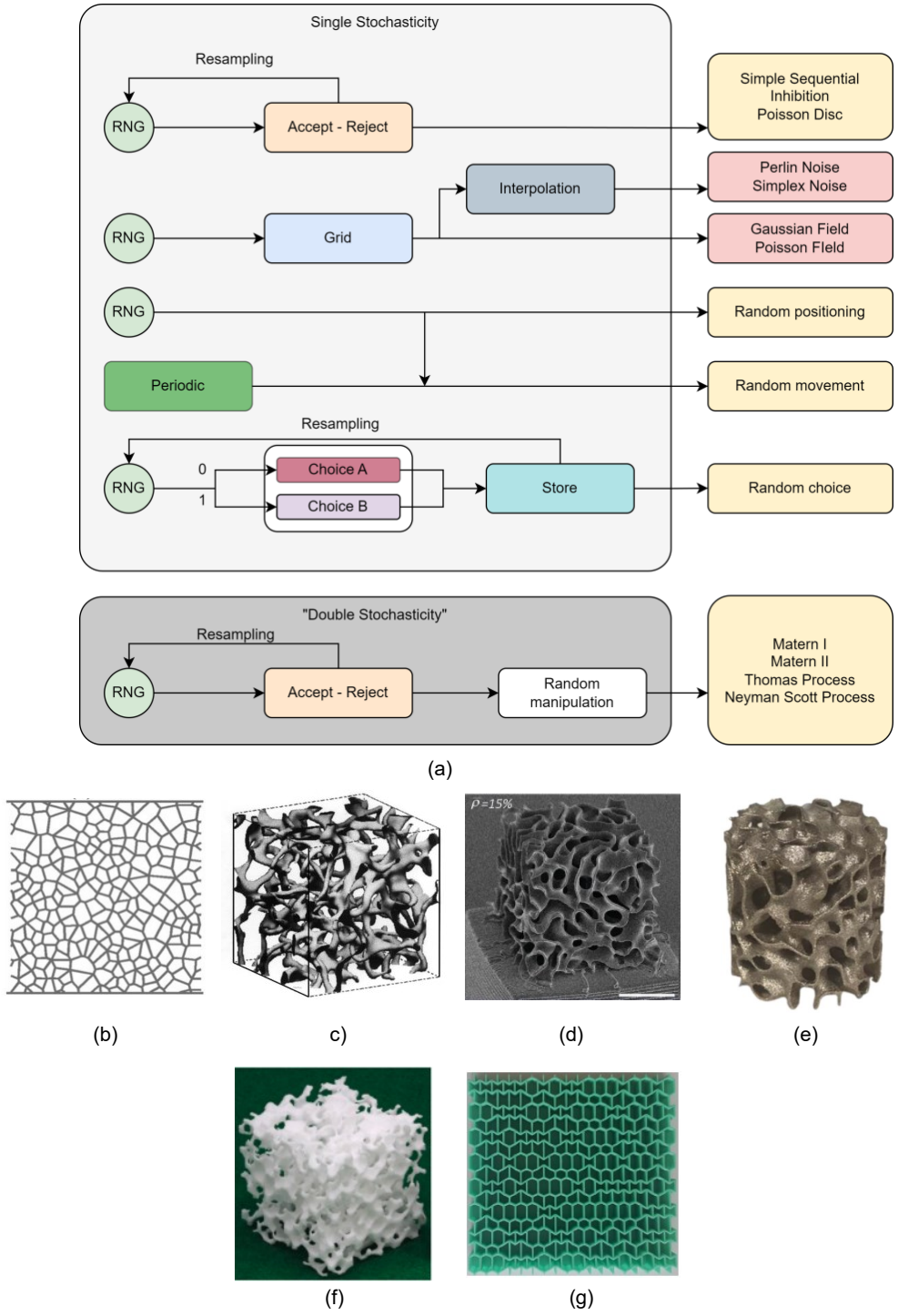

Figure 2.10: Fundamental stochastic design strategies and examples. a) Fundamental design strategies. Yellow = Random-Set, and red = Random Field. Examples of b) SSI, reproduced from [131] c) Gaussian noise, reproduced from [122], d) Spinodal structure, reproduced from [132], e) Random positioning and random field, reproduced from [125], f) Random offset and random field, reproduced from [108], and g) Random choice, reproduced from [130].

Describing disorder

To link relevant structural properties of a stochastic design to the introduced level of stochasticity, a parameter is needed. Firstly, global parameters are described, and then a local parameter is presented. It is essential to mention that the majority of these descriptors are simple. Thus, identified descriptors are presented and the author who used them. A global descriptor that is used to describe the level of stochasticity for Voronoi structures was proposed by Zhu et al. [121]. The parameter δ_{MDP} proposed by Zhu et al. considers the minimum distance d_{min} in a hexagonal or disordered array. It relates it to the distance of seed points d_0 of a regular hexagonal arrangement. This parameter varies from 0 to 1, where 1 describes the uniform array and values < 1 describe the system's stochasticity level. The 'MDP' in the equation stands for Minimum Distance Parameter.

$$\delta_{MDP} = \frac{d_{min}}{d_0} \tag{2.12}$$

Another global parameter δ_{SDP} to describe the level of stochasticity was used by Groth et al. [128], Okubo et al. [129] and Zhu et al. [133], to describe the level of stochasticity. The 'SDP' stands for Standard Deviation Parameter. μ describes the average value of the parameter intended to add stochasticity and the value σ, which drives the flatness of the Gaussian distribution. This parameter can range from 0 (uniform array) to ∞. Here, values > 0 describe stochasticity.

$$\delta_{SDP} = \frac{\sigma}{\mu} \tag{2.13}$$

Luxner et al. [134] used the parameter Eq.2.14 to describe the level of stochasticity, where l_B describes the length of the beam of a regular cellular material, and $a_B \in \mathbb{R} > 0$ is a number set by the user. This creates a distance offset δ_{FDP} that is a fraction of the beam length, which is added to the positional parameters of the cellular materials vertices. The term 'FDP' means fixed distance parameter.

$$\delta_{FDP} = \frac{l_B}{a_B} \tag{2.14}$$

Wang et al. [135] describes a stochastic level parameter δ_{ADP} based on the average distance between nuclei, where N is the number of nuclei, d_i the distance between one nuclei and its nearest neighbours, and d_0 is the distance between nuclei of a

regular cellular material. In this case, 'ADP' stands for Average Distance Parameter.

$$\delta_{ADP} = \frac{1}{N} \sum_{i=1}^{N} \frac{d_i}{d_0} \tag{2.15}$$

However, apart from the global parameters, it was suggested by Choukir et al. [119] to use an "Extracopularity coefficient" δ_{LVP} (Eq.2.16 that was introduced by Çamkiran et al. [136]. δ_{LVP} describes the binary logarithm of the number of pairs divided by the number of unique orientations m. The number of pairs is expressed by $(k^2 - k)/2$, where k is the number of links that a nucleus could form. The fraction in the bracket describes if there is a large number of variability at a node or not, thus this parameter could also be termed 'LDP': Local Variability Parameter.

$$\delta_{LVP} = log_2 \left[\frac{\text{No. of pairs}}{\text{No. of orientations}} \right] = log_2 \left[\frac{k^2 - k}{2m} \right] \tag{2.16}$$

A further parameter to describe the level of stochasticity was introduced by Okubo et al. [129]. This parameter is the coefficient of variation as shown in Eq. 2.17. CV describes the average normalised difference between the volume of each unit cell V_i and the average volume V_{mean} across all unit cells. N is the number of unit cells the structure is composed of.

$$CV = \sqrt{\frac{\sum_{i=1}^{N} (V_i - V_{mean})^2}{N \cdot V_{mean}^2}} \tag{2.17}$$

Six different parameters were shown that describe the disorder in cellular materials. The issue with these many parameters is that results are difficult to compare. Furthermore, it is difficult to determine if a rule to select a certain level of stochasticity. As such, there is a necessity to develop a design tool that focuses on using one stochastic design parameter for various structures to make structures comparable.

2.2.4 The Influence of Randomness on Cellular Material Properties

This section examines stochasticity's influence on cellular materials' mechanical properties. As the reader might expect, the properties are not only impacted by the level of stochasticity but also the geometry itself and how forces act on the geometry. As such, different unit cell types are described separately and grouped by compression or tension if relevant. The first group of stochastic cellular materials

are the honeycomb structures, followed by 3D cellular materials. Third, the group of TPMS cellular materials will be highlighted, and finally, Spinodal structures will be discussed. An overview of the impact on the mechanical properties linked to various authors can be found in Table 2.1

Table 2.1: Influence of the level of stochasticity on mechanical parameters during compression (simplified). V = Voronoi, TH = Theoretical, A-R = Accept or Reject method, RM = Random movement, σ is either plateau or peak stress. *Depending on the cellular unit cell and plane the force acts on. A shorter version of this table was presented by Duan et al. [137].

Source	Type	Method	E	G	K_B	ν	σ_N	U
[138]	2D-VS, FEM, TH	A-R	$\uparrow$	$\uparrow$	$\downarrow$	$\leftrightarrow$	-	-
[139]	2D-VS, FEM	A-R	-	-	-	-	$\downarrow$	-
[140]	2D-VS, FEM	A-R	$\uparrow$	-	-	-	$\downarrow$	-
[141]	2D-VS, FEM	A-R	$\leftrightarrow$	$\leftrightarrow$	-	$\leftrightarrow$	-	-
[142]	2D-VS, FEM	A-R	-	-	-	-	$\downarrow$	-
[42]	2D-VS, AM	A-R	$\downarrow$	-	-	-	$\downarrow$	$\downarrow$
[143]	2D-VS, FEM	RM	$\uparrow$	$\uparrow$	-	$\downarrow$	-	-
[144]	2D-VS, FEM	RM	-	-	-	-	$\downarrow$	$\downarrow$
[145]	3D-VO, FEM, TH	A-R	$\uparrow$	$\uparrow$	$\downarrow$	$\leftrightarrow$	-	-
[146]	3D-VO, FEM	A-R	$\uparrow$	-	-	$\leftrightarrow$	$\downarrow$	-
[120]	3D-VO, FEM	A-R	$\downarrow$	-	-	-	$\downarrow$	-
[129]	3D-VO, AM	RM	$\downarrow$	-	-	-	$\downarrow$	$\downarrow$
[147]	3D-VO, AM	RM	-	-	-	-	-	-
[134]	3D, FEM	RM	$\uparrow\downarrow$*	-	-	-	$\downarrow$	-
[148]	3D, FEM	RM	$\downarrow$	-	-	-	$\downarrow$	$\downarrow$
[149]	3D-VC, FEM	A-R	-	-	-	-	$\uparrow$	$\uparrow$
[150]	3D-VC, FEM	A-R	-	-	-	-	$\downarrow$	$\downarrow$
[137]	3D-VC, FEM, AM	A-R	$\downarrow$	-	-	-	$\downarrow$	$\downarrow$
[151]	3D-VC, FEM	A-R	-	-	-	-	$\downarrow$	-
[152]	3D-VC, FEM	A-R	$\downarrow$	-	-	-	$\downarrow$	-
[61]	3D-Strut, AM	RM	-	-	-	-	$\uparrow$	-

Honeycombs

Several authors studied the impact of introducing stochasticity to honeycomb cellular materials. Gibson et al. [26] dedicated two Subchapters to cellular materials, which include stochasticity in their seminal work from 1997. Since then, not only has AM become more widely used, but also computational power has increased, allowing for more sophisticated studies and new research into the field. First, studies that use

one level of stochasticity in 2D Voronoi cellular structures (VS) are explored, and second, research that utilises different levels of stochasticity is illustrated.

Silva et al. compared the compressive mechanical response of stochastic VS created from the A-R method with a regular Honeycomb design [141, 142]. The authors used FEM for their studies, where the VS were modelled using beams and a constant wall thickness throughout the cellular material. Their first study [141] contrasts the elastic modulus, Poisson's ratio, and the shear modulus of a stochastic VS against a regular Honeycomb cellular material, which did not reveal a large discrepancy. Nevertheless, their follow-up study [142] portrayed a 20 to 40% decreased strength for the stochastic VS compared to the regular Honeycomb structures at different relative densities.
Another study, conducted by Chen et al. [153] uses FEM to study the compressive yield strength (uniaxial and hydrostatic) and the elastic and bulk modulus. The authors presented that the mechanical response of VS created by random vertices sampled simultaneously differs from that created by the A-R method. The authors illustrated that both methods had a lower hydrostatic and uniaxial yield strength than the regular honeycomb structure. In contrast, the VS based on the random vertices was inferior in both when compared to the A-R VS. Interestingly, the VS created from the random vertices showed a similar elastic modulus as the regular structure. In contrast, the VS created from the A-R method had a higher elastic modulus. The bulk modulus of the A-R VS was comparable to the bulk modulus of the regular Honeycomb. In contrast, the bulk modulus of the VS with random vertices was decreased. It is important to mention that the two VS used by Chen et al. [153] are special cases; the VS based on random vertices, which were computed simultaneously, is a special case of the A-R method where every solution is allowed, which should give a higher variance.

As such, it is important to consider the influence of different levels of stochasticity. An image portraying the influence of different levels of stochasticity on a Honeycomb is shown in Fig. 2.11 a) [42] where 1.0 stands for a regular structure and 0.1 for a less restricted stochastic structure. It is evident that the variation increases from 1 to 0.1[1]. The change from a regular to a highly irregular structure dictates the behaviour of the elastic, bulk, and shear modulus and Poisson's ratio during

[1]For this whole section, the stochastic levels of authors will be translated to this definition. Thus, caution has to be applied when examining the original literature. This is done to prevent confusion in this work.

compression, as demonstrated by Zhu et al. [138]. The authors performed a FEM study on VS designed with different levels of stochasticity by applying the A-R method. An elevated stochastic level was observed to yield a higher elastic and shear modulus, while the bulk modulus decreases and the Poisson's ratio is more or less maintained. The elastic modulus was approximately 25% higher at a stochastic level of $\delta = 0$ when compared to the regular benchmark at $\delta = 1$, as shown in Fig.2.11 b). A similar trend was observed for stochastic VS by Sotomayor et al. [140], see Fig.2.11 b). Their FEM study of stochastic 2D VS revealed a more than 50% higher elastic modulus at $\delta = 0$, while the plateau stress plummeted by 25%, see Fig. 2.11 c). A lower stress plateau was also observed by [139]; the investigated range of δ was between 0 to 1. Their compression FEM study showed an almost 40% reduced stress plateau when the 2D VS of $\delta = 0$ is compared with the regular Honeycomb structure, see Fig. 2.11 c).

While the previous literature on 2D VS describes work on quasi-static compression analysis, Zheng et al. [154] demonstrated that the velocity with which an object hits a 2D VS is relevant. A FEM study exhibited that a higher level of stochasticity increases the plateau stress and that the velocity at which the compression takes place has to be considered. An ideal impact velocity exists for a specific stochastic 2D VS where the plateau stress is elevated by approximately 15 to 20%.

Although the previously discussed literature focused on compression tests analysed with FEM, van Egmond [42] explored the effect of stochastic levels on AM VAT Polymerisation specimens, performing tensile tests to quantify the elastic, peak stress, and energy absorption response to a range of stochasticity levels. A mode one tensile test was also conducted to specify the stochastic 2D Voronoi properties against fracture. The tensile test revealed the following. The elastic modulus showed a drop at $\delta = 0.3$ of approximately 10%. The maximum stress gradually decreases by 25% within a range of $\delta = 0.9$ to 0.3, and the energy absorption capacity decreases from $\delta = 0.8$ to 0.1 by 50%. However, the tensile mode one test revealed that beyond yielding, a stochastic level within $\delta = 0.5$ to 0.8 can elevate the energy absorption, prolonging the strain and yielding higher stress, thus influencing how cracks evolve through the whole structure.

Choukir et al. [119] investigated the tensile properties of a stochastic 2D VS comprising different levels of stochasticity, made from various materials, including

Alumina, Photopolymer and Aluminium. The authors conducted a numerical study and presented experimental data for uni-axial and mode one tensile tests. Generally, a downward trend can be observed for the maximum tensile strength as a function of stochasticity. The elastic moduli behave similarly, with the difference that it seems to flatten out after introducing stochasticity. The investigated critical stress intensity, fracture toughness, and critical crack mouth opening displacement exhibit a complex connection with the stochasticity parameter. However, at certain stochastic levels, the critical crack mouth opening displacement has the potential to be elevated by more than 50%.

Many studies were presented that describe the influence of stochasticity on mechanical properties such as the elastic modulus and the plateau stress, especially on Voronoi honeycomb structures. Interestingly, Alkhader et al. [131] compare the influence of the stochasticity parameter on the mechanical properties of different unit cells with different nodal connectivities. The authors studied Voronoi, honeycomb, triangular, and tetragonal unit cell-based 2D cellular materials and investigated their mechanical properties, such as the elastic modulus, peak, and plateau stress. This study demonstrates that the cellular materials on which stochasticity is introduced can show a different mechanical response if the nodal connectivity is different. For more information on the mechanics, please refer to Alkhader et al.

As shown by several authors, different stochastic levels can be applied to the spatial position of honeycomb structures. However, as Li et al. [143, 144] demonstrate stochasticity can be applied to both the spatial position and the wall thickness, which leads to different mechanical responses. While, for example, the elastic modulus and shear modulus can be elevated by increasing the level of stochasticity of the spatial position, properties like the Poisson's ratio follows a downward trend under quasi-static compression [143]. On the contrary, adding stochasticity to the wall thickness will lead to a downward trend of the elastic modulus, shear modulus, and an almost unaffected Poisson's ratio. In a dynamic compression scenario [144], adding stochasticity to the spatial coordinates and the wall thickness will lead to lower plateau stress and lower energy absorption.

Apart from designing and investigating stochastic Honeycomb structures based on A-R or RM approach, the random choice approach can also be used to design honeycomb structures. Mirzaali et al. [130] demonstrated by using a random choice

approach that changing the ratio with which two different auxetic cellular materials are tessellated in space, impacts the mechanical properties. This gives a cellular material designer the possibility to choose and design the Poison's ratio and the Young's modulus needed for a certain application.

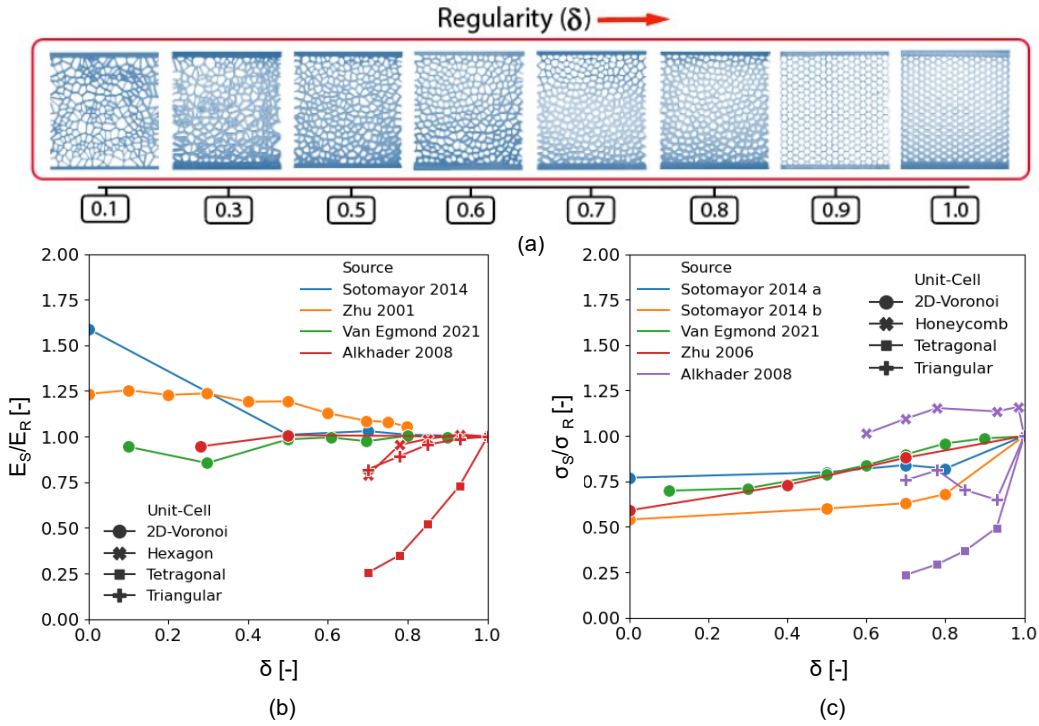

Figure 2.11: The influence of different levels of stochasticity on the geometry and mechanical parameters. a) Influence of the stochastic level on the geometry of a 2D Voronoi structure, taken from [42]. b) Affect of the stochastic level on the elastic modulus during compression [140, 138] and during tension [42]. c) Impact of the stochastic level on the plateau stress during compression [140, 120] and the maximum stress during tension [42].

Regarding 2D VS (see Table 2.1 and Fig. 2.11), it can be concluded that there is evidence that the elastic modulus and shear modulus can increase with applied stochasticity and that the plateau stress and energy absorption decreases in general. At the same time, the Poisson's ratio almost stays the same. However, the influence of the level of stochasticity on these mechanical properties also depends on the unit cell Fig. 2.11. Therefore, there is a lack of studying the effect of stochasticity on the mechanical properties of different unit cells while using the same stochastic design approach for additively manufactured samples. This would highlight the influence of the unit cell, the impact of the level of stochasticity, the influence of the material and the impact of the randomisation approach. Hence, a software tool that can design various shapes using the same randomisation strategies is necessary to compare the influence on properties.

3D cellular materials

In this section, the mechanical properties of open-cell Fig. 2.12 a) and closed-cell cellular Fig. 2.12 b) materials are presented. The general influence of different levels of stochasticity is shown in Table 2.1 and more specifically for different levels of stochasticity for the relative elastic modulus in Fig. 2.12 c) and for the relative plateau stress in Fig. 2.12 d).

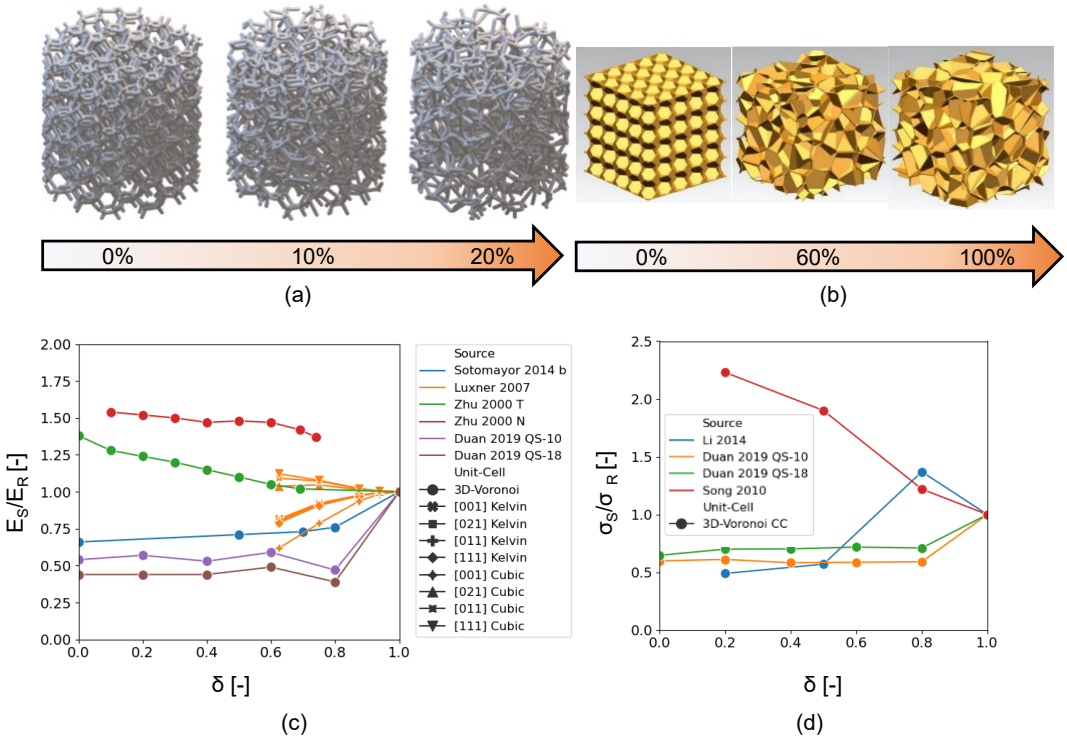

Figure 2.12: Open and closed-cell cellular materials and their mechanical properties Three 3D open-cell a) (adapted from [129]) and closed-cell b) (adapted from [137]) Voronoi cellular materials with different levels of stochasticity. c) Normalised elastic modulus and normalised plateau stress where 'S' stands for stochastic and 'R' for regular. Data from [134, 145, 150, 137, 120, 149]. Note that the stochastic parameters were adapted to suite the stochastic parameter δ_{MDP}.

Open-cell structures

The previous section explained the research conducted to understand the influence of stochasticity on the mechanical properties of 2D VS. These are essentially 2D structures, which can be extruded, so they differ from 3D VS. Therefore, the research on the influence of stochasticity on mechanical properties is presented here. In the early 2000s, Zhu et al. conducted several FEM studies to understand the impact of different stochastic levels on the elastic, shear, and bulk modulus, the Poisson's ratio [145] and the plateau stress [146] during quasi-static compression. Their first study

[145] revealed that the elastic and shear modulus is elevated with the increase of stochasticity. At the same time, the bulk modulus decreases, and the Poisson's ratio is not subject to a significant variation. However, upon investigating the stress plateau, Zhu et al.'s [146] data show that the plateau stress is significantly reduced. Although Zhu et al. [145] showed an increase in the elastic modulus during compression and with increasing stochasticity, this could not be shown by the FEM results collected by Sotomayor et al. [120]. Sotomayor et al. [120] demonstrated a drop of approximately 35% compared to an elevation of around 50% presented by [145], see Fig. 2.12 c). Nevertheless, Sotomayor et al. [120], too, confirms the trend that the plateau stress decreases with increasing levels of stochasticity, reaching an approximately 45% lower plateau stress as revealed in Fig. 2.12 d).

As these studies focused primarily on the Voronoi structures where, in the regular case, the constituent unit cell is a Kelvin cell, the directionality of the applied force plays a vital role [129, 134]. Therefore, the results gathered by Luxner et al. [134] present that the unit cell and the force's direction must be considered. Their FEM study with a force acting on four different planes of a Cubic and Kelvin unit cell on which different levels of stochasticity were superimposed revealed that if anisotropy is already low, the elastic modulus decreases. However, if a structure such as the Cubic structure has a higher anisotropy, the direction with the highest elastic modulus tends to decrease. In contrast, the direction with the lower elastic modulus tends to increase (See Fig. 2.12 c). This minimises anisotropy to some extent. Furthermore, Okubo et al. [129] investigated the mechanical response of PBF PA12 open-cell Voronoi structures (VO) with different levels of stochasticity under quasi-static compression. Several different orientations of the Voronoi structure were created to examine the directional dependence of the mechanical response. The authors demonstrated that the Voronoi structure shifts from an anisotropic to an isotropic mechanical response with increasing stochasticity. At a relative density of 10%, the authors showed that the effective elastic modulus peaks at roughly $CV = 0.1$ to 0.2, and the effective energy absorption, as well as the effective maximum stress, decreases. Du et al. [147] manufactured several different Voronoi structures of different levels of stochasticity using PBF and titanium. Results from compression tests were used to develop regression models to inversely design the global properties of an VO. Their evaluation of the statistical model indicates that the strength peaks at a stochastic level between 0.2 to 0.3. In contrast, at the same level of stochasticity, a minimum of the Young's modulus and porosity was observed.

The design can rely on quasi-static or dynamic compression tests for static applications or applications subject to impact. However, for more sophisticated applications where periodic or stochastically changing loading conditions occur, fatigue properties have to be taken into consideration. Zhu et al. [155] investigated the fatigue performance of VO manufactured from Ti6Al4V and PBF. The Voronoi structures exhibited a stochastic level of 0.4. Their study aimed to observe the impact of relative density and heat treatment on fatigue. Even though a Wöhler curve was not presented and the results not compared to a regular Voronoi structure, their findings suggest that the lower the relative density, the worse the fatigue performance, and a full annealing heat treatment positively impacts the fatigue compared to the as build or stress-relieved state. Raghavendra et al. also used the same material and a PBF AM process. [156] who investigated several different regular and stochastic cellular materials' fatigue performance. Their presented Wöhler curves reveal that the fatigue strength of stochastic cellular materials is generally inferior to their regular counterpart. The unit cell also plays a vital role in the quantitative difference between the regular and irregular unit cell's fatigue strength. Kechagias carried out a study on the fatigue of Titanium PBF stochastic cellular materials [157] and demonstrated that the connectivity of stochastic cellular materials plays an important role and allows modulating the fatigue performance response, where a higher connectivity is associated with a higher fatigue strength. Apart from studying the influence of different levels of stochasticity on the mechanical properties, other studies that focus on stochasticity only do not consider variation in the microstructure. In regards to energy absorption, Mueller et al. [148] numerically investigated the impact of Cubic, Kelvin, Octet-Truss, and RFCC unit cells and their orientation in space on energy absorption. The authors compared their energy absorption properties with stochastic cellular materials created with the same nodal connectivity. Their Ashby charts present the same typical trend, as found by other authors (see Table 2.1). The energy absorption, elastic modulus, and peak stress of stochastic cellular structures are, in general, lower with two exemptions: the Cubic unit cell-based structure showed a higher energy absorption and the Delaunay structure showed a similar elastic modulus when compared to their regular counterpart [148]. Another energy absorption study was conducted by Maliaris et al. [158] on PA11 VO manufactured from a proprietary PBF process. The authors compare the quasi-static and dynamic compression performance of Voronoi structures comprised of two relative densities and a variation of the strut number. The authors present that the ability of the stochastic structures to absorb energy depends on the relative density and the number of struts in the cellular material, which in return allows the informed designer to

create application-specific stochastic Voronoi structures. While the other studies mainly focus on the generation of stochastic structures from randomly sampled nodes combined with the Voronoi algorithm, Roberts et al. [122] presented scaling laws of a Voronoi structure, cellular materials with two different levels of connectivity and one structure created from a Gaussian Random Field. The authors analysed these structures utilising FEM and therefore were able to provide sufficient scaling laws for the Young's modulus of these.

The following can be concluded for the 3D VO according to Table. 2.1 and Fig. 2.12.

- ▷ The relative elastic modulus in VO, Kelvin and Cubic unit cells can decrease and increase, suggesting an influence of the unit cell.
- ▷ The plateau stress decreases for VO. However, Mullen et al. [40] demonstrated that the compression strength can also increase in octahedral cellular materials. This has to be investigated for further cellular material unit cells.
- ▷ The energy absorption was, in general, lower.

More research is necessary to collect more evidence for the influence of stochasticity on the mechanical properties of different types of unit cells and AM materials. To do that, a software tool is necessary that offers different types of unit cells and the same randomisation strategies to ensure comparability, as mentioned before. This could be the basis for future studies to perform mechanical tests to validate FEM studies.

Closed-cell structures

Previously, the mechanical properties of VO were presented as how stochasticity influences mechanical behaviour. Compared to the VO, closed-cell Voronoi structures (VC) are made up of sheets as visualised in Fig. 2.12 a) and b). Song et al. [149] is the only publication that presents an elevation of the plateau stress in response to a set of different levels of stochasticity introduced to VC (Fig. 2.12 d). The investigation was done using a numerical model. The different response of that study compared to the otherwise reported decrease of the plateau stress (Table 2.1) is due to the definition of the stochastic design parameter. The authors use the stochastic level in reverse order compared to their methodological description. Nevertheless, a later study of perhaps the same research group showed different results [150]. Li et al. [150] describe a numerical study on VC where mechanical properties such as densification strain and plateau stress were explored as a function of the stochasticity level under dynamic compression loading conditions. Their results generally indicate a downward trend of the plateau stress and the densification strain. However, it has to be noted that a maximum of the plateau stress was observed at a stochastic level

of 0.8. Thus implying a first increase of the plateau stress followed by a steep fall with flattening out beyond a stochastic level of 0.5 (Fig. 2.12 d) (Note: in this study, the stochastic parameter is defined differently; to fit the other description, it was presented in reverse order).
Duan et al. [137] used additively manufactured VC to explore the impact of different levels of stochasticity on the plateau stress, the collapse stress, and the energy absorption (Fig. 2.12 c) and d). The authors used numerical simulations to understand the structural behaviour for low levels of stochasticity better and presented that the use of stochasticity causes a lower plateau stress when compared to the regular structure and that the collapse stress drastically reduces between a stochastic level from 1 to 0.8. Past that, the influence of stochasticity on the plateau stress is nearly neglectable. Similarly to the previous authors, Tang et al. [151] demonstrated that the plateau stress of VC under quasi-static compression is lower than the regular benchmark case. However, the authors postulate that this decrease originates from the variation of the geometry rather than an effect of their cell size, backed up by FEM simulations carried out on 2D hexagons and 2D triangles rather than closed-cell 3D structures. However, one has to be careful in directly comparing these different results, and more in-depth research is required here to isolate the effects. Shi et al. conducted a more in-depth study on VC [152]. Their numerical and analytical results of closed-cell structures subjected to a range of stochastic levels confirmed the general trend that the plateau stress and elastic modulus tend to be beneath the properties of the regular unit cells.

Triply periodic minimal surfaces

Some publications created stochastic cellular materials based on TPMS unit cells. These can be divided into two broad categories: network or sheet-based TPMS unit cells. Al-Ketan et al. [91] designed a stochastic sheet-based TPMS structure based on Gyroid unit cells with varying subdomains. Each subdomain is based on a randomly placed seed, a random period, and the orientation of a sheet-based Gyroid. This cellular material is considered to have isotropic structural properties if composed of a minimum of nine subdomains. The reported mechanical properties of the stochastic structure were lower than the one of the periodic structure; this included the toughness, Young's modulus and plateau stress. However, there is some indication that the mechanical properties of the stochastic structure outpace the periodic ones at higher relative densities. Al-Ketan's [91] design approach is

based on methods explained by Yang et al. [92, 93] to create stochastic TPMS-based cellular materials. The shortfall of starting with randomly positioned descritisers is that the control over each unit cell is lost, and stochasticity is introduced in a less controlled manner. Hence, there is a need to start from a regularly placed discretiser set to a) provide control over the unit cell and b) make stochastic TPMS more comparable to other structures. The same critique can be applied to the subsequent work based on [91].

In a follow-up work by Novak et al. [125], the impact properties of an AM PBF SS316L stochastic sheet-based Gyroid TPMS structures with 15 subdomains investigated with randomness introduced to the rotation, period, and orientation. Quasi-static and dynamic compression tests and a numerical study were carried out on these parts. The authors presented that the specific energy absorption changes from around $8J/g$ to approximately $35J/g$ when the strain rate changes from low to high. A comparison of their stochastic cellular material with other unit cells made from different materials showed that the stochastic cellular material was among the better-performing structures.

Network-based Gyroid TPMS structures were investigated by Yang et al. [81] and Kanwar et al. [107]. Yang et al. performed a compression test on a network-based stochastic Gyroid made from PBF PA12. The stochastic Gyroid was composed of 125 randomly distributed subdomains, and the orientation of the Gyroid unit cell was randomly assigned. Compared to a periodic network-based Gyroid structure, the stochastic Gyroid structure showed a 40% lower stress level at 2.5% strain.

Kanwar et al. [107] investigated the in-vitro cell growth behaviour of a stochastic network-based Gyroid structure and its compression behaviour. The network-based Gyroid structure was composed of 15 subdomains, where the seed points were randomly distributed, and randomness was added to the period and orientation. The cellular structures were made from SS316L using a conventional PBF AM process. The authors showed that cell growth is possible on stochastic network-based Gyroid structures at porosities around 70%. However, no control study was performed against a periodic network-based Gyroid structure. Thus, no conclusion can be drawn if a stochastic TPMS shows better cell growth than a periodic structure. Kanwar et al. also showed that stochastic network structures exhibit a similar Young's modulus to bone, which is beneficial for implant design.

Singh et al. [159] designed IPC structures using an IWP sheet and network structure. Here, the sheet or the network structures were additively manufactured using VeroWhitePlus, while the complementary phase was made from TangoBlackPlus,

a compliant material. The results show that creating stochastic IPCs yields higher mechanical properties than non-IPC stochastic structures. An increase in energy absorption could be achieved with the elevation of the elastic modulus, the plateau stress, and the peak stress.

The work on stochastic TPMS structures did not study the influence of different levels of stochasticity. Hence, there to develop a design tool to control each unit cell of a stochastic TPMS and control more parameters than just the subdomain position [91, 92, 93], rotation [91], period [92, 93]. The relative density should also be randomisable. Additionally, stochastic design strategies are missing.

Spinodal structures

Spinodal structures formed through spinodal decomposition can be either a network or sheet-type cellular material [123] and can exhibit both isotropic or nonisotropic behaviour where the spinoid forms characteristic lamellar, cubic, or columnar structures [160]. This versatile design of spinodal structures led to their investigation. Hsieh et al. [123] investigated isotropic sheet and network-based spinodal cellular materials, which revealed isotropic mechanical properties and that the influence of defects on their properties is small. The energy absorption properties of nano-spinodal structures were investigated by Guell et al. [132], who discovered that isotropic sheet-based spinodal cellular materials exhibit an energy absorption rate approximately ten times higher than other nano-cellular materials. However, the definition of the densification strain used to compute the energy absorption is broad, thus rendering comparison with other publications complex, which is a limitation of this study. In contrast to [132], Portela et al. [161] reported a doubling of energy absorption, normalised strength, and normalised elastic modulus when comparing a columnar spinal structure against an octet structure under cyclic loading. This shows that it is crucial to determine which structure a cellular material is compared to for fair comparison. As already mentioned, the spinodal decomposition can also be manipulated by using an anisotropic Gaussian Random Field as the starting condition, resulting in anisotropic spinodal structures such as lamellar, cubic, or even columnar cellular materials as demonstrated by Vidyasagar et al. [160]. Through periodic homogenisation, the authors numerically investigated the elastic properties and the Poisson's ratio, where the highest anisotropy of the Poisson's ratio was observed in the lamellar structure. The authors showed that the specific Young's modulus of the lamellar and columnar spinodal cellular materials exhibit a larger directional difference than the cubic one.

While the previous studies mainly focused on nano-spinodal cellular materials, mesoscale cellular materials are interesting for many engineering designs. Zhang et al. [162] investigated interpenetrating spinodal phase composites. These composites comprise a network phase (usually a softer material) and a shell (normally stiffer). These spinodal designs were produced through a poly jet additive manufacturing process where the sheet part was made up of VeroWhitePlus, while the solid part was manufactured from Agilus30. Their numerical evaluation of spinodal cellular materials' energy absorption, stiffness, and yield strength and a Schwarz-P and Octet structure demonstrated that the mechanical parameters were similar. However, comparing the stochastic sheet spinodal structure to the periodic Schwarz-P and Octet structure, it was evident that it exhibited a more even stress distribution throughout the cellular material. It is also worth mentioning that spinodal cellular materials were used as an approximation of the inherent structure of nanoporous gold [163, 164], where scaling laws were provided for nanoporous gold [163] as well as for a combination of nanoporous gold and a polymer [165]. The use of spinodal structures recently gained attention in the field of acoustics [166]. However, this study is limited by its used material, PLA, and its manufacturing process, Fused Deposition Modelling. This study should be enhanced for applicable results for industrial use, using a material for an SLS or SLM AM manufacturing process.

In conclusion, spinodal structures show higher energy absorption capabilities than other cellular materials [132, 161]. However, these structures require a more in-depth investigation by using SLS or SLM to conduct a fair comparison with other stochastic cellular materials and ensure they are applicable for industrial applications.

2.2.5 Combined design strategies utilising stochasticity

Combining design strategies means combining the advantages of stochastic design with other design methods to achieve improved structural properties. One of these design strategies is to design the mechanical response as proposed by Pham et al. [50], which is to mimic hardening mechanisms found in metallic materials. The first design strategy refers to Grain Boundary Hardening, where cellular material domains are oriented to each other to force specific stress distributions, which allows the design of the failure mechanism. The second design strategy refers to Precipitation and Multi-Phase Hardening, where within a parent cellular material structure of one or more subdomains of either the same parent or a different unit cell are placed with a different relative density, which results in a higher compression strength. The third design strategy involves Hierarchical design, wherein the parent Voronoi

cell, the previously mentioned design strategies fill the daughter cells, where the daughter cells can be placed at random (orientation, relative density etc.). This gives considerable design freedom. The limitation of this work is that the design process is complex, and design tools are needed to make this design process more straightforward. Additionally, the authors do not mention that controlled randomness could be applied. In the hierarchical design, the transition between the subdomains is not clearly defined, which could lead to undesired mechanical behaviour and should be improved. Interestingly, stochastic gradients were not discussed and not applied. However, it was observed in the literature that stochastic design strategies were paired with relative density gradients [167, 107] and locally varying relative density [93]. Inspired by Pham et al. [50], Yu et al. [87] modified the adjacency in Honeycomb structures, allowing the authors to modulate the stress-strain response. These methods are influenced by nature, such as gradient or layered structures [10], and these combinations show great potential for improved mechanical designs [4]. These layers introduced as defects into structures have proven to change the deformation behaviour [168] or worked to design the pathway of a crack [88] through a structure to potentially increase the properties such as energy absorption. However, these nature-inspired design strategies were not combined with stochasticity. As such, there is a need to combine the design of gradients and layers with stochasticity to produce stochastic gradients and layers and integrate them into a design tool to make them accessible for exploration. To prevent the mismatch between unit cells, an interpolation function will be used to transition between unit cells to prevent the sharp transition that occurs in the work of Pham et al. [50].

2.2.6 Software Tools

There are several software tools available to design cellular materials. These can be categorised as commercial software, research software (open-source or not open-source), and open-source professional software tools. Each software tool is introduced, and Table 2.2 presents an overview of their capabilities.

The investigated commercial software include Fusion360, nTopology, Altair Inspire 2022.3, Altair Sulis 1.12, Metafold3D, General Lattice, Fabpilot, Siemens NX, Autodesk Within, Carbon Design Engine, and Ultrasim.

Fusion 360 (Version: 2.0.16985) [169] is a CAD software tool that offers parametric design, CAM, and several simulation tools such as FEM or Topology Optimisation. It offers the creation of cellular materials in a tool called “Volumetric Lattice”, which

allows creating strut and strut-based TPMS structures and 2D cellular materials. The cell size, rotation, and angle can be adjusted. The relative density can be either uniform or graded. The cellular material can be designed in an object. Fusion 360 can also design primitive elements such as cubes, cones, cylinders, etc., which can be patterned. However, Fusion 360 cannot introduce randomness to the cellular materials or the primitive elements. An API is also offered, allowing one to develop custom applications based on C++ or Python.

nTopology (Version: 4.9.3) [170] is a commercial software tool with a vast range of design capabilities and aids for AM. These include, for example, a package to design cellular materials, perform simulations, lightweighting, or set up an AM build job. The cellular material package offers strut-based, strut, and sheet-based TPMS cellular materials and stochastic cellular materials. The stochastic cellular material tab allows the designing of surface and volume-based Voronoi structures. Branched, Delaunay, and so-called "orthofoams" can also be designed. The "orthofoams" are created by stretching cellular material cells into a specific direction. Within nTopology, Surface Roughness can be applied to an object, and noise, such as "Simplex Noise" and "Cellular Noise", can also be applied to cellular materials. As nTopology is a field-driven design software, it also offers grading strategies. However, nTopology is limited by its stochastic design strategies; The stochasticity level cannot be controlled, and no stochastic design strategies can be applied.

Netfabb 2024 [171] by Autodesk is a software tool to set up AM build jobs. To set up a build job, objects are loaded into the software. Into these objects, cellular materials can be designed. In Netfabb, strut-based cellular materials and sheet-based TPMS structures can be created from level-set equations. Two stochastic cellular materials were identified from the set of strut-based cellular materials: the 'Trabecular' and 'Voronoi' type. In addition, grading can be applied to the relative density. However, the cellular material design in Netfabb is limited as the software does not seem to be primarily created to design cellular materials. As such, the stochasticity of the 'Trabecular' and 'Voronoi' cellular material cannot be manipulated, and stochastic design strategies do not exist.

Altair Inspire 2022.3 [172] is a CAD software package for AM, which offers print preparation tools, structural and fluid dynamic simulations, and the design of cellular materials. The cellular material tool uses strut-based cellular materials, including Cubic, FCC, BCC, and other cellular materials. However, the latticing tool is limited. The only parameters that can be changed in a strut-based cellular material are its cell

size and beam radius. Other design strategies, such as relative density grading or stochastic design strategies, are unavailable.

Altair Sulis 1.12 [173] is a commercial design software specialising in designing flow paths and cellular materials. The cellular material tool can create strut and sheet-based TPMS structures, strut-based structures, and stochastic cellular materials. The stochastic cellular material includes creating strut-based stochastic structures such as Voronoi structures based on Poisson Disc Sampling or Random Sampling. The Poisson Disk and Random Sampling methods can also be combined with defining the connectivity of a seed point with other seed points, which gives control over the number of beams per seed. Stochastic TPMS structures can be created by choosing control points (discretisers), which can be selected between 2 and 20; more control points can be added during the design process. The stochastic design of Altair Sulis is limited because the introduced level of stochasticity both for the strut and the TPMS cellular materials cannot be controlled. It is unclear to which parameters the stochasticity is added, and the sampling of the control points is also not controlled, which could lead to close control points. Additionally, a tool to create surface roughness was not identified.

Metafold3D [174] is a cloud-based cellular material design tool. Uploaded objects or primitive objects can be filled with a cellular material. The software has a repertoire of strut and sheet-based TPMS structures and strut-based cellular materials. Both of these cellular material classes can be graded. However, this software does not include stochastic cellular materials or stochastic design strategies.

General Lattice Frontier [175] is not a CAD tool. It is a cloud-based tool that allows the selection of an appropriate cellular material based on mechanical properties such as plateau stress, energy absorption, and Young's modulus. The tool suggests cellular materials, printing materials, and AM hardware based on selected mechanical properties. As of the beta version, it does not have any design capabilities.

Fabpilot [176] is a browser and cloud-based software tool by Sculpteo to manage the AM workflow. This includes part quotation, preparing files for printing, the set-up of builds for specific machines, and tracking build jobs. At the stage of file preparation for printing, the user can add infill cellular materials to a part. However, the cellular material capabilities are limited to one cellular material, and stochastic design strategies are unavailable.

Siemens NX [177] is a CAD software tool by Siemens. Primitive and more complex shapes can be designed with the included design functions. According to the documentation, cellular materials can be designed, and the documentation shows a node

editor [178], which can create Voronoi structures. The included cellular materials are strut-based structures such as a BCC or FCC and sheet-based TPMS structures [179]. However, the cellular material tool is not included in the student version. As specific stochastic design strategies were not mentioned, it can be concluded that Siemens NX does not include them.

Autodesk Within [180] is a software tool for the design of medical implants. It is stated that it can produce stochastic cellular materials and create stochastic surface roughness. However, how the stochastic cellular material design and the stochastic surface roughness work is not clearly stated.

The Carbon Design Engine [181] is a cloud-based cellular material design tool that aids design engineers by selecting an appropriate material and cellular material to design a part. Several cellular material types, such as Kagome, Kelvin, or a Voronoi structure, can be designed into a part. According to part specifications, the cellular materials can be designed uniform, conformal, or separated into zones to better accommodate external forces. This software could only be reviewed using the training material, as the software currently restricts the number of users. However, the tutorial did not mention stochastic design strategies. It mentioned Voronoi structures, but their approach to creating them was not explained.

The Ultrasim 3D Lattice Engine (Core Version 5.0) [182] is a software tool by BASF. An object can be loaded into the GUI, and if necessary, a relative density file can be loaded for the specific part to locally change the relative density. This software includes sheet-based TPMS structures and several strut-based cellular materials such as BCC and Kelvin. However, this software tool is limited. First, it is not a traditional CAD and focuses more on filling a structure with a cellular material. Second, no design strategy to create stochastic cellular materials is available.

FreeCad, Blender, and the Rhinoceros 3D Addon Crystallon are the professional open-source software tools presented.

FreeCad (Version 0.21) [183] is an open-source CAD software tool. The software tool is based on parametric design. It offers a wide range of first and third-party add-ons that enhance its capabilities, such as in CAM or simulation. Additionally, custom addons can be designed using the FreeCAD Python or C++-based API. A Lattice [184] Addon exits, but it cannot design cellular materials. Similarly, a Node Addon [185] makes it easier to combine functionalities, including a Voronoi tool to design Voronoi patterns on a surface or solid but does not include a cellular material tool for strut or TPMS-based shapes. Hence, FreeCAD is limited because it cannot create uniform or stochastic cellular materials based on strut or TPMS-based cellular

materials. Stochastic design strategies such as Isotropic, Anisotropic, Graded, or Layered Randomness and Surface Roughness are unavailable.

Another open-source software tool is Blender [186]. It is used to create non-parametric designs and perform realistic renderings and animations. It offers a wide range of Plug-Ins and the ability to use a Node-based design system. This allows the creation of Voronoi structures, and using the Addon Svershok-nodes [187, 188], even Minimal Surfaces can be created. Another Addon called Scaffolder [189] that can create cellular materials is discussed later. Stochastic design tools were not found.

Crystallon [190] is an open-source Plug-In for Rhinoceros 3D and works with Grasshopper. This tool offers the capability of designing strut-based, strut, and sheet-based TPMS cellular materials. Additionally, Voronoi cellular materials can be designed, too. Cellular materials can be designed into objects, and their relative density can be graded. The limitation of this Plug-In is that the node system can become complex and challenging to set up; another limitation is that apart from Voronoi structures, the already mentioned stochastic design strategies are not included. Stochastic surface roughness could be created through Rhinoceros 3D, but this also needs a complex node system to control the surface roughness.

The open-source and non-opensource software packages that are discussed are MSLattice, FlattPack, ASLI, Manipulator, Gibbon, The Porous Media Generator, MiniSurf, Scaffolder, Lattice _Karak and the TPMS Designer.

MSLattice [65] is a free research software tool based on MATLAB that can design uniform and relative density graded sheet and strut-based TPMS structures. The shapes can be designed into the shape of a sphere, cylinder, or cuboid. Additionally, the user can develop implicit functions that can be plotted and extracted, allowing for hybrid designs. This software is limited by a rough surface at the intersection boundary between the cylinder and sphere. Furthermore, it cannot use strut-based cellular materials or stochastic design strategies.

FlattPack [66] is also a MATLAB-based free research tool. It can design strut-based cellular materials and sheet and strut-based TPMS structures. The cellular materials can be designed in primitive shapes such as a sphere, cylinder, or cuboid or in an arbitrary shape that the user can choose. The relative density can be designed uniformly, functionally graded, or a predefined externally created relative density field can be used. FlattPack falls short in the design of stochastic design strategies, and surface roughness cannot be applied to the structures.

ASLI/QASLI [102] is an open-source software tool to design strut and sheet-based TPMS structures into objects. It can create uniform and hybrid TPMS structures. Additionally, maps can be imported to define the relative density or unit cell size, which ultimately can be used to create, for example, graded structures. It is also possible to upload custom unit cells. However, this tool is limited as it relies on maps that need to be created through an external tool, making functional grading or applying stochastic design strategies difficult.

Manipulator is a software tool to create cellular materials developed at the University of Liverpool over several years [61, 191, 40, 192]. The software tool can design a cellular material unit cell wireframe in a cylinder, cuboid, or loaded object. The useable cellular materials are an Octahedral, an Octahedral with pillars, a Truss, and a Truss with pillars cellular material. The cellular materials can be designed in various ways, which include regular tesselation of a unit cell, random design based on a uniform RNG, and a regular or polar mapping of unit cells to an object [192]. The software tool can also create support structures and import customary strut-based unit cells [192]. The uniform randomness within a range is applied to the vertices of the strut-based cellular materials, which allows for defining a range of the random movement and the specification of Isotropic and Anisotropic Randomness [61, 191, 40, 192]. However, the authors remain vague about utilising Anisotropic Randomness, and it is unclear if they use it. This could be addressed as it is a crucial design strategy. Furthermore, a patent was published describing the design process [193] and another patent [194] describes how roughness is applied by randomising only the near-surface cellular material unit cells and letting the struts overlap with the surface of an object for a defined length to create roughness. The cellular materials created with this software are finally sliced by the Manipulator software for use in an SLM machine [192]. It is unclear if the unit cells developed by Song [195] are part of the Manipulator software. Hence, Song's work is discussed in Chapter 2.2.7.

Metastruct [196] is a Python script-based open-source software tool that can create strut-based, strut, and sheet-based TPMS and stochastic cellular materials. The stochastic cellular materials include Voronoi structures, random lattices, and Delaunay structures. The random lattice tool creates a point cloud in space and randomly connects the points with defined connectivity. Additionally, the code includes Noise and Perlin Noise, but the usage of these is not well documented. It seems that both Noises are used to create a cellular material and not to create surface roughness. Primitive structures can also be created, which can be used to design the cellular materials into these. These Python scripts are limited by their capability to use design strategies. Grading and stochastic design strategies were not found.

Gibbon [30] is a Matlab toolbox with an extensive compendium of research-related packages. These packages include CAD, FEA, Meshing, Lattice Design, Visualisation, and Image Separation. The Lattice Design package offers to design cellular materials in objects and provides various cellular materials. The cellular materials range from strut-based, strut- and sheet-based TPMS to spinodal structures. The spinodal structures can be designed isotropic, cubic, lamellar, and columnar. The limitations of this package are that the cellular materials can not be graded (not found in the documentation) and that, apart from spinodal and Voronoi structures, stochastic design strategies are not available.

The Porous Media Generator (PMG) [197], based on MATLAB, can create various porous structures. The porous structures that can be designed include fibers, cloth, lattices, foams, branching structures, overlapping and non-overlapping spherical structures, percolated structures, and non-spherical structures. It offers the ability to design lattices in an object. Rules can be applied to spherical cellular materials to avoid overlaps. Though randomness can be applied to the structures, there is no explanation if the applied randomness can be controlled. Thus, it is assumed that controlled stochasticity cannot be used. In the 'non-spherical section', 'particle options', "Randomness Isotropic", and "Randomness Anisotropic" are mentioned, but there is no control over the randomness. Thus, this software tool falls short in applying stochastic design strategies, such as Isotropic or Anisotropic Randomness etc.

MiniSurf [198] is a MATLAB-based design tool to create TPMS-based cellular materials. It allows the input of implicit equations, which broadens the design flexibility, but the implicit equations are evaluated at zero. Hence, only surface-based topologies without thickness can be created, which limits this software tool, and stochastic design strategies are not implemented.

Scaffolder [189] is a Python-based cellular material design tool that also offers a Plug-In for Blender. It can design strut-based cellular materials and strut-based TPMS structures into objects. However, this software is limited to uniform designs and does not include stochastic design strategies.

Lattice _Karak [199] is a MATLAB-based software tool to create TPMS structures. It can design sheet and strut-based TPMS structures. These structures can be designed uniformly, graded (relative density and cell size), and hybridised. Additionally, a hierarchical design strategy is available. However, this design tool does not include stochastic design strategies for TPMS structures.

TPMS Designer [200] is based on MATLAB and can create several strut and sheet-based TPMS structures as well as strut-based structures. This software tool can visualise properties related to the geometry, such as Gaussian or Mean Curvature, or manufacturing, such as quality issues due to an LPBF manufacturing process. The TPMS Designer is limited by its functionality to manipulate and design the cellular material. Stochastic design strategies are not available.

The described commercial, open-source, and open- and non-opensource research software tools functionalities are analysed and tabulated in Table 2.2. Table 2.2 shows that most investigated software offers a GUI for users to interact with the functionalities. Primitive Elements such as the design with cylinders, cuboids, and spheroids were available in the advanced CAD packages. Cellular materials formed from primitive elements, such as spheroids, were only found in the PMG [197]. Strut-based cellular materials and strut and sheet-based TPMS structures were available in various software tools, while spinodal structures were only found in Gibbon [30]. Various software tools include functional grading. The ability to create Voronoi structures is also available in several of the investigated software tools. Designing a cellular material into an object seems to be a standard design feature available in most software packages. When it comes to stochastic design strategies, the authors are currently not found in established software packages. Only the software Manipulator was identified to create a stochastic cellular material by randomly offsetting the vertices of a cellular material using a uniform RNG and allowing to control the level of stochasticity. The use of controlled stochasticity was not observed for TPMS structures, primitive elements, and cellular materials designed from primitive elements. However, only Altair Sulis [173] can design stochastic TPMS structures, but the level of stochasticity cannot be controlled, and the underlying algorithm is not explained. Autodesk Within, Crystallon (In conjunction with Rhinoceros 3D), Manipulator, and nToplogy can apply Stochastic Surface Roughness. Converge Control and Gap Control were not identified in any tool. However, PMG [197] allows creating a non-overlapping sphere but gives no control over the gap. Hence, there is a need to develop GUI-based software tool that enables stochastic design strategies for primitive objects, complex objects, primitive-based and TPMS-based cellular materials. It is also necessary to have a user-friendly way to add surface-roughness to the cellular materials based on a field-based strategy such as Perlin noise [116] and to use the same generation of stochasticity for all structures.

Table 2.2: Cellular material design functionality comparison of various software tools. PE (Primitive Element), PS (Primitive Strut), ST (Strut), TPMS-S (Strut-based TPMS), TPMS-SH (sheet-based TPMS), SP (Spinodal), G (Grading), V (Voronoi), OB (Design in object), IR (Isotropic Randomness), AR (Anisotropic Randomness), G (Graded Randomness), LR (Layered Randomness), SR (Surface Roughness), SECC (Surface Element Converge Control), SEGC (Surface Element Gap Control)

Software	GUI	PE	PS	ST	TPMS-S	TPMS-SH	SP	G	V	OB	IR	AR	GR	LR	SR	SECC	SEGC
Altair Inspire	X	X	-	X	-	-	-	-	-	X	-	-	-	-	-	-	-
Altair Sulis	X	X	-	X	X	X	-	X	X	X	-	-	-	-	-	-	-
ASLI	X	-	-	-	X	X	-	-	-	X	-	-	-	-	-	-	-
Autodesk Within	X			X			-	-	-	X	-	-	-	-	X	-	-
Blender	X	X	-	-	-	-	-	-	-	X	-	-	-	-	-	-	-
Carbon Design Engine	X		-	X	-	-	-	X	X	X	-	-	-	-	-	-	-
Crystallon	X	X	-	X	-	-	-	X	X	X	-	-	-	-	X	-	-
Fabpilot	X	-	-	X	-	-	-	X	X	X	-	-	-	-	-	-	-
FLattPack	X	-	-	X	X	X	-	X	-	X	-	-	-	-	-	-	-
FreeCAD	X	X	-	-	-	-	-	-	X	X	-	-	-	-	-	-	-
Fusion 360	X	X	-	X	X	-	-	X	-	X	-	-	-	-	-	-	-
Gibbon	-	X	-	X	X	X	X	-	X	X	-	-	-	-	-	-	-
Lattice _Karak	X	-	-	-	X	X	-	X	-	-	-	-	-	-	-	-	-
Manipulator	X		-	X	-	-	-	-	-	X	X	X	-	-	X	-	-
Metafold3D	X	X	-	X	X	X	-	X	X	X	-	-	-	-	-	-	-
Metastruct	-	X	-	X	X	X	-	-	X	X	-	-	-	-	-	-	-
Minisurf	X	-	-	-	-	X	-	-	-	-	-	-	-	-	-	-	-
Netfabb 2024	X	X	-	X	-	X	-	X	X	X	-	-	-	-	-	-	-
MSLattice	X	-	-	-	X	X	-	X	-	-	-	-	-	-	-	-	-
nTopology	X	X	-	X	X	X	-	X	X	X	-	-	-	-	X	-	-
PMG	X	-	X	X	-	-	-	-	-	X	-	-	-	-	-	-	-
Scaffolder	X	-	-	-	-	-	-	-	-	-	-	-	-	-	-	-	-
TPMS designer	X	-	-	X	X	X	-	-	-	X	-	-	-	-	-	-	-
Ultrasim	X	-	-	X	-	X	-	X	-	X	-	-	-	-	-	-	-

2.2.7 Applications

Cellular materials have a wide range of properties due to the flexibility in choosing their constituent shape, material, manufacturing process, post-processing, etc. The consequence is a wide range of applications. Typical applications for cellular materials include [26, 27, 37]: Lightweight Structures, Implants, Energy Absorbers, Vibration Absorbers, Thermal Management, Carriers, Buoyancy, Electrical Management, Acoustic Absorbers, and Filtration. Implant and lightweight structures will be briefly reviewed, the characteristic selection criteria stated, more in-depth reviews suggested, and, if applicable, the implication of stochastic cellular materials mentioned.

Implants

The design and manufacture of implants using cellular materials manufactured by AM has been the topic of many reviews [37, 201, 202, 203, 204, 205]. A well-designed implant using a cellular material must follow specific design criteria to achieve a long service life [37]. To ensure a long service life, it is advised to design the elastic properties of the cellular material similar to those of bone, providing a large surface area and good permeability [37, 201]. Similar elastic properties will prevent stress shielding [206], a large surface area provides interaction surface for cell-growth [207], and enough permeability ensures that nutrients can be transported to the growing cells [208]. Additionally, it is advised to manufacture implants from Ti6Al4V rather than from stainless steel or cobalt-chromium alloys because Ti6Al4V excels in biocompatibility and corrosion resistance and has a lower Young's modulus than the latter [209]. It is also recommended to design a cellular material for bone implants using pore sizes within a range of approximately 300 to 600 μm [201], which results in a good compromise between the mentioned criteria. Implants were proposed to be manufactured by SLM both using regular and stochastic cellular materials [191, 40] and typically presented implants or demonstrator implants based on cellular materials, including hip [191, 210], craniofacial [211], pelvic [212], or dental implants [213] among others. The majority of reviews focused on the utilisation of regular cellular materials [37, 201], while the research on the use of stochastic cellular materials is only a little elaborated on [202], studies on stochastic cellular materials on implants with a focus on AM will be presented. The review by Chen et al. [202] points out that more stochastic design strategies and stochastic cellular materials based on unit cells different from Voronoi structures should be investigated.

Stamp proposed the first orthopaedic structures based on cellular materials manufactured using SLM [61]. The proposed structures included Orthopedic Screws, a Mitch Acetabular Cup, an Acetabular Augment, a Tibial Knee Tray, and a Sinter Cap made from cp-Ti. The applied stochastic octahedral-based cellular materials were created using an in-house software called Manipulator, described in Chapter 2.2.6. For the selected stochastic cellular material, a 30% stochastic level was determined based on customer preference and improved compression strength, which was approximately 25% higher than the regular structure. Cell in-growth was shown to be successful. However, the structures did not have the desired mechanical parameters, and further mechanical tests were necessary. Additionally, the cell in-growth test was carried out externally. Thus, little information is given on the testing procedure and if different levels of stochasticity were investigated for cell growth.

To overcome the limited knowledge of manufacturability and mechanical properties, Mullen et al. [191, 40] investigated the regular and stochastic octahedral-based unit cell. First, the manufacturability of octahedral regular unit cells and their compression strength [191] and then fatigue and compression strength of the stochastic octahedral-based structure [40] was experimentally investigated. The process windows to manufacture titanium octahedron-based unit cells in the range of 0.6 to 1.4 mm with defined porosity, compression strength, and pore size were established [191]. It was demonstrated that a regular octahedron-based cellular material could fulfil the requirements regarding compression strength, unit cell size, and porosity for a medical implant such as a Hip Augment. This was the foundation for selecting manufacturing parameters for a stochastic cellular material, which was investigated in a follow-up study [40]. The influence of 30% stochasticity on the tensile properties and the fatigue behaviour was evaluated, as well as the level of stochasticity on the compression strength for sintered and unsintered specimens mullen2010selective. A 0.6 mm unit cell and cp-Ti were used. It was shown that sintering significantly increases the cellular material's mechanical properties and that the octahedral cellular materials fulfil the mechanical requirements for a bone implant at 30% stochasticity. It was observed that the compression strength follows a distinct curve when the level of stochasticity is varied. First, the compression strength drops between 0 to 15% stochasticity, then increases within a range of 15 to 35% to then remain almost constant for larger levels of stochasticity, which ultimately leads to a 20% (35% stochasticity) higher compression strength for the sintered structure. It was mentioned that the elastic modulus was in an acceptable range for bone implants; however, it would be interesting to see how the elastic modulus evolves regarding the level of stochasticity.

To improve the strength of the studied stochastic cellular materials, Stamp [61] proposed and demonstrated stronger stochastic cellular materials by adding gridded walled substructures. A better version of this substructure is a platelet cellular material as proposed by [195]. The platelet structures were developed for implant design and comprise plates arranged in a rectangular, hexagonal, or triangular grid in which holes can be selectively designed to form vaulted cellular materials. The plates can also be designed with different aspect ratios. Different stochasticity levels can be applied to these structures (Isotropic and Anisotropic Randomness). Compression tests of the stochastic structure have shown a decrease to a minimum to then increase to a compression strength similar to the regular structure. This behaviour differs from the increase of the compression strength in stochastic octahedral structures [40]. For these structures, no bone-ingrowth tests were performed [195].

The previous study's [40] mechanical properties of octahedral are not directly applicable to the mechanical properties of other stochastic cellular materials, and the elastic properties for different levels of stochasticity were not reported. Thus, Wang et al. [135] investigated the printability and compression properties of SLM Ti6Al4V Voronoi structures on which different levels of stochasticity were imposed. The manufactured specimens' geometry deviated approximately 4% from the CAD model, and pore sizes of 200 to 1200 μm and porosities of 60 to 95% were reached, making them suitable for implants. The elastic modulus and compression strength were evaluated for the different porosity levels, showing acceptable implant values. Changing the stochasticity from a low to a high stochasticity level correlated negatively with elastic modulus. At the same time, the compression strength first decreased from regular to around 0.3 stochasticity and then increased again to levels of the regular structure of around 33 MPa at approximately 83% porosity. This study shows that stochastic Voronoi structures can be used for implant design regarding available pore sizes, porosity, elastic modulus, and compression strength. Additionally, at a given porosity level, the right amount of stochasticity can decrease the stiffness and increase the strength within a given stochasticity range of 0.2-0.5. It is important to note that a regular structure was not tested. It could be possible that the overall strength is lower than the strength of a regular Voronoi structure (this is what [214] indicates). Additionally, in-vitro and in-vivo tests were not performed to provide evidence for using different levels of stochasticity in implants.

Hence, in-vivo experiments were performed by Liang et al. [214]. The authors investigated the mechanical properties and the in-vitro cell growth of Ti6Al4V Vornoi cellular materials manufactured by SLM. The Voronoi structures were designed with different levels of stochasticity, and discrepancies were observed between the

designed and manufactured specimens. For stochastic Voronoi structures ranging from stochastic levels of 0.06, 0.25 to 0.5, they showed that the elastic modulus decreases from 3.8 GPa to 3.25 GPa. Similar behaviour also occurred in heat-treated specimens of the same level of stochasticity. Contrary to that, the strength dropped from 180 MPa to 110 MPa, then increased again to 120 MPa at the given stochastic levels. Significantly higher cell growth rates were observed on days 1 and 3 in the sample comprising the highest stochasticity level. This study showed a similar mechanical behaviour of the stochastic structures investigated by [135] but different to [40], who demonstrate an increase in octahedral stochastic cellular materials with higher stochasticity. Additionally, Liang et al. present faster growth rates in the structure, which gives a first indication that a stochastic Voronoi structure shows advantageous growth rates and mechanical suitability for implants.

While previous research studies have shown the mechanical compatibility of Voronoi structures with different levels of stochasticity as a bone implant and performed in-vitro studies, Lu et al. [41], conducted a 21-week in-vivo experiment in two beagle dogs by inserting three specimens in the left and right tibia. The specimens were manufactured from SLM Ti6Al4V with pore diameters of 800 μm, a porosity of 70%, and three levels of stochasticity termed Irregularity Parameter (IPM) of 0.15, 0.3, and 0.45 were used, where the level of stochasticity is indicated by higher numbers. The osteogenesis efficiency was evaluated by removing the specimens and relating the bone volume grown into the cellular material to the original bone. Osteogenesis efficiency of approximately 43%, 69%, and 55% were reported for the IPM 0.15, 0.3, and 0.45. It is indicated that a higher osteogenesis efficiency is reached at IPM 0.3.

The previously mentioned studies focus on strut-based unit cells such as octahedral and Voronoi structures and vaulted structures for implant design. However, stochastic TPMS structures also gained attention for implant design. Kanwar et al. [107] showed that in-vitro cell growth was possible on SS316L SLM strut-based Gyroid structures at approximately 70% porosity. Unfortunately, growth values were not compared to a regular structure, and it still has to be answered if different levels of stochasticity show a similar growth-promoting response in TPMS structures as shown for Voronoi structures [214, 41] and if the stochastic TPMS structures may outperform Voronoi or strut-based structures.

In summary, stochastic cellular materials have proven suitable for implants and are used in implants manufactured by Stryker [215]. However, to enable further research into stochastic cellular materials for implants, a software tool that includes

various design strategies to investigate Isotropic and Anisotropic for various cellular materials is necessary. This research field could be advanced by enabling other cellular materials with controlled stochasticity and using design strategies such as Graded Randomness or Layered Randomness.

Lightweight Structures

Lightweight structures are valuable for the automotive and aerospace industries to reduce the amount of transported mass to save on fuel. The criteria to select cellular materials for lightweight applications are a high specific stiffness and strength ratio [27, 37]. To design a lightweight structure, the property relation (Eq. 2.3) has to be evaluated for appropriate unit cells and relative densities [26, 27, 37]. This was done, for example, by Al-Ketan et al. [216], who determined the coefficients for strut-based and TPMS structures. The authors studied the Toughness, Plateau Stress, Peak stress and Young's Modulus of strut-based Kelvin, Gibson-Ashby and Octett-Truss, and TPMS-based Gyroid (Sheet, Strut), Diamond (Sheet, Strut), IWP (Sheet, Strut), and Schwarz-P (Strut) made from maragin steel and manufactured on an SLM machine. The quality was checked through SEM, and the relative density was measured through weighting. The authors reported the scaling laws for the Toughness, Plateau Stress, Peak Stress, and Young's Modulus. This evaluation showed that the best-performing cellular materials category for each property were the sheet-based TPMS structures, followed by the strut-based and strut-based TPMS structures. The Gyroid sheet-based TPMS structures achieved the best overall performance. The data reported in this study can be used to design lightweight structures, though it has to be noted that the scaling laws vary as shown in the review [35]. A summary [35] of different studies shows for strut and sheet-based TPMS structures across various TPMS unit cells [35], relative density ranges, materials [35] and manufacturing processes [35] that the scaling laws are not the same. This indicates that the scaling laws must be evaluated carefully for each application to ensure a fair and reasonable comparison. In terms of stochastic cellular materials with different levels of stochasticity, it can be concluded the following according to Fig. 2.11, 2.12 and Table 2.1. For 2D-Voronoi structures, the relative stiffness can decrease, increase, or stay almost the same as the regular structure. The stiffness decreases in general, thus making 2D-Voronoi structures of higher levels of stochasticity are not viable for lightweight applications. Regarding sheet and strut-based 3D-Voronoi structures, it can be noted that the relative strength was generally lower. In contrast, the relative Young's modulus showed both an increase and decrease with increased stochasticity, making the use as a lightweight structure inconclusive. Contrary to the observed decline of the relative strength in 2D and 3D-Voronoi structures, a study on titanium octahdral SLM cellular materials

with different levels of stochasticity [40] has shown that the strength increases from approximately 38 to 45 MPa (Normalised compression strength, unsintered), rendering the strength increase as useful for lightweight purposes. Unfortunately, elastic properties are not mentioned for given levels of stochasticity, which makes it impossible to give a final answer on the suitability of octahedral cellular materials for lightweight structures. Additionally, Al-Ketan [91] presents stiffness and strength results for a stochastic and regular SS316L SLM TPMS sheet-based Gyroid. The stiffness and strength of the stochastic structures were lower than those of the regular structure. However, it has to be noted that different levels of stochasticity were not investigated, which makes it impossible to judge the suitability of stochastic TPMS structures comprising different levels of stochasticity for lightweight purposes. Hence, it is advised to study the strength and stiffness regarding varying levels of stochasticity for TPMS and strut-based cellular materials, including various materials and manufacturing processes to arrive at a more conclusive picture.

To solve this, a strategy to create TPMS-based structures utilising controlled stochasticity should be developed to allow various stochastic design strategies to enable researchers to study their potential use as a lightweight structure.

2.3 Research Gaps

The literature review presented the different design strategies to create cellular materials and their classification. A particular emphasis was put on stochastic cellular materials, where the classification offers a template for their creation and description through various stochasticity parameters. Introducing stochasticity influences the mechanical and osseointegration response, which makes them candidates for energy absorption applications, lightweight structures, and implants, though more research is necessary. Some currently available software tools provide the means to create a structure with randomness though different levels of stochasticity are currently limited to strut-based cellular materials. These complex structures are well suited for AM. AM can also manufacture thermal devices such as heat exchangers and heat sinks using cellular materials or surface elements such as cylinders, shark-inspired structures, etc. To further drive research into stochastic design, the following gaps must be addressed to improve this field. The explained research gaps are the basis for each Result Chapter. Four research gaps in the research field of stochastic design were identified.

1. The predominant methodology of creating stochastic cellular materials is to apply stochasticity to the seed points of Voronoi structures or vertices of strut-based structures. Additionally, in some cases, controlled stochasticity is applied. Only a few studies include directional stochasticity, and most studies use a uniform RNG or Poisson Disc sampling process. The methodology to create stochastic cellular materials from primitive elements (Ellipsoids) combined with a Gaussian Distribution and stochastic design strategies has not been presented.

2. The creation of stochastic TPMS structures was reviewed in the Literature Review. Current methodologies start by creating randomly distributed discretisers filled with randomly created TPMS structures [92, 93, 91]. This prevents control over each unit cell, and it is possible that two discretisers could be sampled in too close proximity. Additionally, randomisation is not applied to all parameters, such as the relative density, which reduces the flexibility of the approach. It can also be observed that these structures are not combined with stochastic design strategies such as Graded Randomness and Layered Randomness. A methodology to add Stochastic Surface Roughness to this type of structure is also not presented.

3. Randomness has been applied to primitive surface elements [127, 47, 51]. The Gaussian Distribution was also used to design primitive surface elements [127, 49] and overlaps were prevented [49]. However, the Gaussian Distribution was not used to create stochastic arrays using complex shapes and design rules regarding manufacturing, and the application of controlled randomness was not explained.

4. In the Literature Review, various software tools were reviewed. Their capability to create cellular materials and their use of stochastic design strategies are presented in Table 2.2. Currently, no software tool is available that combines the stochastic design strategies of Isotropic, Anisotropic, Graded, and Layered Randomness (based on a Gaussian Distribution) with TPMS, primitive element-based cellular materials and primitive/complex elements. Additionally, Converge Control and Gap Control for stochastic arrays of primitive/complex elements are not implemented.

Chapter 3

Materials and Methods

3.1 Introduction

This Chapter describes the methodology that was used in this thesis. It introduces the software, shapes, equations, algorithms, statistical tests, hardware, materials and characterisation methods.

3.2 Software

Table 3.1 refers to the software packages used in this work and briefly describes their functionality. The software packages will be mentioned when used.

Table 3.1: Software Packages used in this work.

Software	Description
Blender	Blender (Blender Foundation, the Netherlands) is a software to create and render animations and 3D objects. It offers a wide range of tools to manipulate meshes, and its Python API allows for designing custom Plug-Ins.
Fiji	Fiji is based on the software ImageJ and includes tools and Plug-Ins to analyse images.
Fusion 360	Fusion 360 (Autodesk, Inc. USA) is a software that provides CAD, CAM, and simulation tools. It offers a Python API, which allows to build custom tools.
GrabCAD	GrabCAD (Stratasys Ltd., USA) is a slicing tool to set up print jobs for Stratasys PolyJet printers.
Helicon Focus	Helicon Focus (Helicon Soft Ltd., Ukraine) is an image processing tool that can create a focused image from a stack of images.
MATLAB	MATLAB (The MathWorks, Inc., USA) is a software to program with the high-level programming language MATLAB. This tool can be used to perform mathematical operations, data visualisations, or write automatisation scripts.
Materialise Magics	Materialise Magics (Materialise NV, Belgium) offers a wide range of tools to manipulate meshes and set up build jobs for various AM processes.
Paraview	Paraview is a tool that visualises data from, for example, a CFD analysis and colour codes the data on the mesh.
PreForm	PreForm (Formlabs, USA) is a slicing tool to set up builds for Formlab's SL and SLS 3D printers.
PyCharm CE	The PyCharm Community Edition is a Python interpreter.
SliView	SliView (EOS GmbH, Germany) is a slicer that prepares and sends a build job to an EOS 3D printer.
Spyder	Spyder is a Python interpreter with a GUI similar to MATLAB.

In Table 3.2 software libraries relevant to this work are listed and briefly explained. The software libraries will be mentioned when used.

Table 3.2: Software Libraries.

Libraries	Description
NumPy	NumPy is a library in Python that provides various mathematical operations and functions such as matrix calculations or the creation of normally distributed random numbers.
Vedo	Vedo is a Python library that offers a substantial amount of functions to manipulate, generate, and analyse 3D meshes.
SciPy	SciPy is a Python library that provides various scientific analysis tools, among these statistical tests for populations.
Matplotlib	Python library that is specialised in visualising data.
Pandas	Pandas is similar to Matplotlib, with the difference that Pandas uses data frames.
Sympy	A Python library that uses symbolic math to solve equations.
Noise	Noise [217] is a Python library that provides the implementation of the Perlin noise algorithm.
STL Write	STL write is a function for MATLAB to produce an stl file from a mesh [218].

3.3 Shapes

This Section describes the shapes used in this work, which include various primitive shapes, a shark skin denticle, primitive-based cellular material structures, and the design of TPMS structures.

3.3.1 Primitive Shapes

Four primitive shapes are used in this work, which are depicted in Fig. 3.1: a cylinder, sphere, cube, and cone. These structures are part of Blender. The cylinder a) is defined by a height H and a diameter D. The sphere b) can be described by the diameter D. The cube c) is described by its width W, and the cone d) is described by a lower diameter D, an upper diameter D_T or a height H. (The diameters can also be represented by their radii).

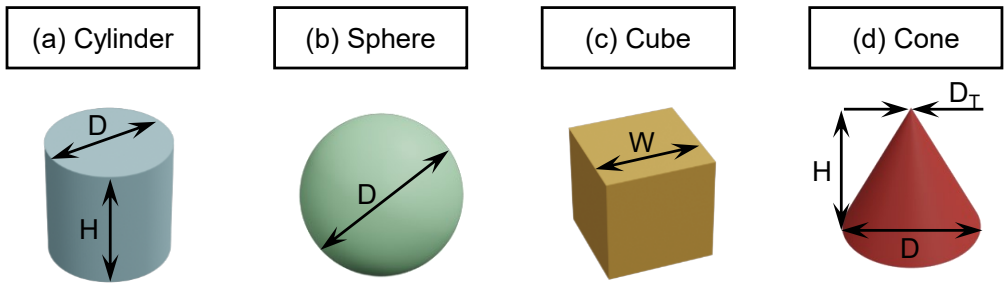

Figure 3.1: Utilised primitive shapes. a) a cylinder, b) a sphere, c) a cube, d) a cone

3.3.2 Shark skin shape

In this Subchapter, a complex demonstrator shape is described. Figure 3.2 illustrates the shark skin denticle used in this work. Twenty-two parameters describe the shark skin denticle. The parameters are defined so that most depend on the shark denticle width w_s. The angle β is an independent parameter. The parameters that are now described depend on the width, and the dependencies are described in Subchapter 3.5.1. In Fig. 3.2 a) the denticles centre position is illustrated by (x_c, z_c) and the ridge heights $hr0 - 2$ and the height of each level slice is described by $level1$ to 5 (level5 = 0). These are shown relative to the centre coordinates. The side view in b) shows the angle β to tilt the unit cell head while the socket remains in its position. The parameters $rh2$ to 5 describe the height ratio of each $level2$ to 5, which scales the $level1$ down to $level2$ to 5. The ridges are also described by a length parameter $lr0$ to $lr2$ and y position corresponding to the ridges maximum height $hr0$ to $hr2$. The ridges x position can be described by an angle a_s, b_s and the width w_s. Finally, Fig. 3.2 d) shows the iso-view of the shark denticle where the socket, the ridge, and the ridge valley are shown.

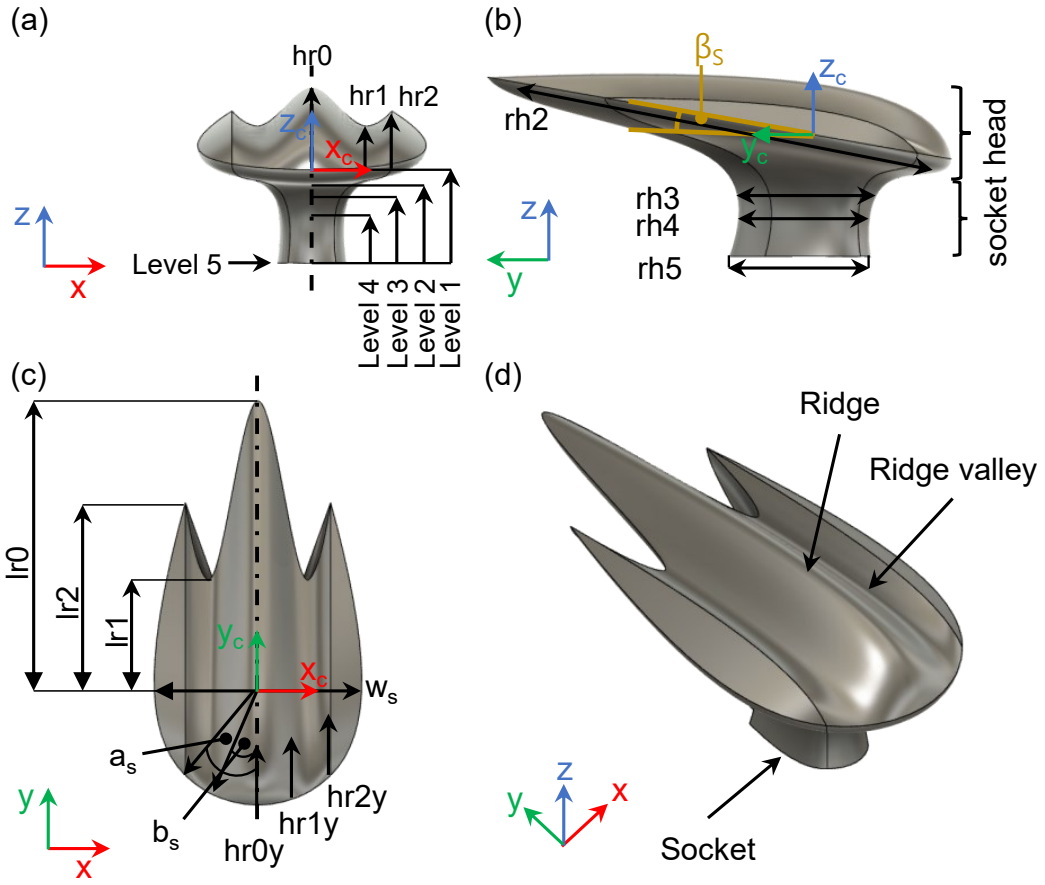

Figure 3.2: Complex shark denticle shape. a) front view, b) side view, c) top view, and d) iso view.

These described 22 parameters can be translated to a matrix 3.1 comprising 18 parameters that describe the shape of the shark denticle (vertices from which the geometry is formed). x_n, y_n, z_n are Cartesian coordinates while ϕ_n, ξ_n, r are the polar coordinates of the width, the ridges, and the centre x_c, y_c, z_c. The polar coordinates describe the rotation around the axis x_c. Other rotations could be added by extending this for y_c and z_c axis rotation.

$$\begin{bmatrix} x_1 & y_1 & z_1 & \theta_1 & \xi_1 & r_1 \\ \vdots & \vdots & \vdots & \vdots & \vdots & \vdots \\ x_{18} & y_{18} & z_{18} & \theta_{18} & \xi_{18} & r_{18} \end{bmatrix} \tag{3.1}$$

The matrix 3.1 stores the coordinates for the first level ($level1$) by using the introduced height ratios for each level $rh2$ to 5, the $level1$ can be scaled down to each level and positioned at each level's height ($level1$ 5). This matrix is then used through the Python API in Fusion 360 [219] combined with standard Fusion 360 [169] functions to create the described solid model of a shark denticle.

3.3.3 Primitive-based cellular material shapes

Strut-based cellular materials are created by defining a cube with the unit cell expansions u_x, u_y, u_z as illustrated in Fig. 3.3 a) from which crystal arrangements are subtracted through a boolean operation with ellipsoids. These crystal arrangements include a Cubic b), a Body Centred Cubic (BCC) c), a Face Centred Cubic (FCC) d) and a Face Centred Cubic (FCC+) arrangement with an additional ellipsoid in the centre e).

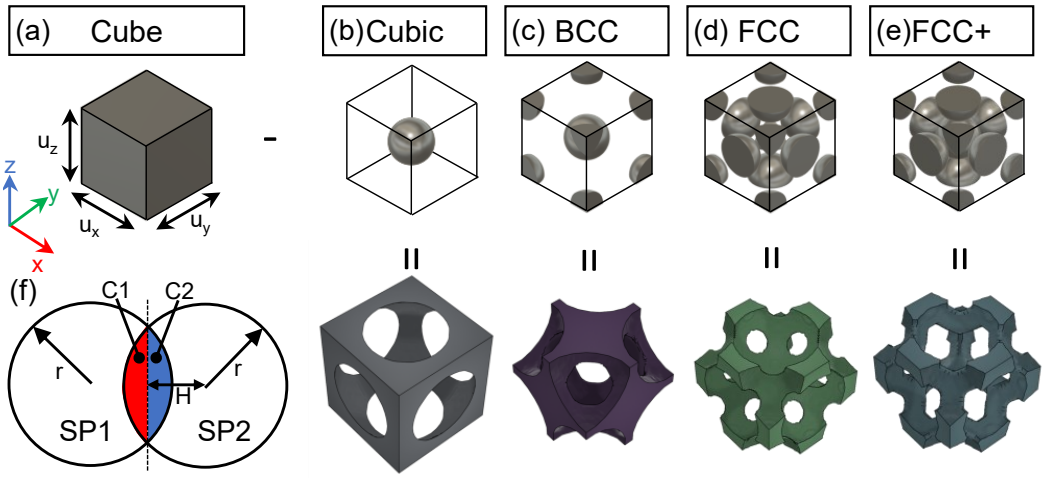

Figure 3.3: The creation of strut-based cellular materials is illustrated. a) A cube. A b) Cubic b), BCC c), FCC d) and FCC+ e). f) Intersection of two circles.

The ellipsoids can be described by Eq. 3.2. In this equation x, y, and z are the grid coordinates in a Cartesian system $\mathbb{R}^3$ and r_x, r_y and r_z are the focal points which are geometrically the radii in the directions x, y and z, respectively. In the special case where $r_x = r_y = r_z$, this results in a sphere which is the regular case in this work.

$$\phi_{ellipsoid} = \frac{x^2}{r_x^2} + \frac{y^2}{r_y^2} + \frac{z^2}{r_z^2} = 1 \tag{3.2}$$

The volume of a cellular material V_{CM} can be determined from the relative density ρ_{rel} and the cellular material bounding box volume V_{Box}.

$$V_{CM} = \rho_{rel} \cdot V_{Box} \tag{3.3}$$

V_{CM} can be defined by the volume of spheres cut from the initial volume V_{Box} according to the specified crystal structure configuration. Here, two cases have to be considered: first, the spheres are not intersecting each other, and second, the spheres intersect each other. The first case results in a closed-cell cellular material, and the

second one gives an open-cell cellular material. These cases can be determined from a limiting relative density ρ_{lim} at which at least two spheres start to become tangential. The first case is represented by $\rho_{rel} \geq \rho_{lim}$, and the second case is $\rho_{rel} < \rho_{lim}$. Thus, V_c can be determined from Eq.3.5, where V_{sphere} is the volume of a sphere and V_{cap} is the volume of a cap, which is the volume of a sphere $SP1$ intersecting with a sphere $SP1$, forming two caps $C1$ and $C2$. A cap of two intersecting spheres can be calculated from Eq.3.4, where r is the sphere's radius, and H is the height of the cap. This is illustrated in Fig. 3.3 f).

$$V_{cap} = \frac{\pi}{3} \cdot (r - H)^2 \cdot (2r + H) \tag{3.4}$$

Here, i describes the number of potential spheres occurring for a specific crystal structure configuration, and j is the number of overlapping caps.

$$V_{CM} = \begin{cases} V_{Box} - i \cdot V_{sphere} & if\, \rho_{rel} \geq \rho_{lim} \\ V_{Box} - i \cdot V_{sphere} + j \cdot V_{cap} & if\, \rho_{rel} < \rho_{lim} \end{cases} \tag{3.5}$$

The values of i, j and ρ_{lim} for specific crystal structure configuration is shown in Table 3.3

Table 3.3: Unit cell parameter to determine the volume of a cellular material. i is the number of spheres. j is the number of caps and ρ_{lim} is the limiting case for a closed-cell cellular material.

Unit cell	i	j	ρ_{lim}
Cubic	1	6	$1 - \frac{\pi}{6}$
BCC	2	16	$1 - \frac{\sqrt{2}\pi}{8}$
FCC	4	48	$1 - \frac{\sqrt{2}\pi}{6}$
FCC+	5	12	$1 - \frac{5\pi}{48}$

3.3.4 TPMS Shapes

This study utilises TPMS unit cells commonly used in AM. These unit cells are presented in Table 3.4. These unit cells are the Schoen-Gyroid (Gyroid), the Schwarz-Primitive (Schwarz-P), and the Schwarz-Diamond (Schwarz-D) unit cell. An illustration of these unit cells as a sheet-based TPMS cellular material is shown in the 'Unit Cell' column of Table 3.4. A TPMS unit cell can be represented by a level-set equation $\phi(X, Y, Z)$ [63] [65]. X can be described by Eq. 3.6, where p is the period scaling factor, x is the grid on which the level-set equation is evaluated, and u_{cx} is the

relevant unit cell size in the specified direct. For Y and Z, the same equation applies. These level-set equations are based on trigonometric equations and approximate the TPMS with sufficient accuracy [220].

$$X = \frac{p\pi x}{u_{cx}} \tag{3.6}$$

Table 3.4: Level-set equations of common TPMS unit cells

Unit Cell	Name	$\phi(X,Y,Z)$	Ref.
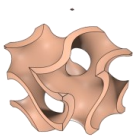	Gyroid	$sin(X) \cdot cos(Y) + sin(Y) \cdot cos(Z) + cos(X) \cdot sin(Z)$	[63], [65]
	Schwarz-Primitive	$cos(X) + cos(Y) + cos(Z)$	[63], [65]
	Schwarz-Diamond	$cos(X - Y) \cdot cos(Z) + sin(X + Y) \cdot sin(Z)$	[63]

TPMS rotation

Any geometry in $\mathbb{R}^3$ can be rotated in the Cartesian coordinate system by rotating the nodes of a geometry around the x, y or z axis. Thus, the nodes with the coordinates (x, y, z) can be transformed to new coordinates (x', y', z') by a rotation matrix M_{rot} as shown in Eq. 3.7, [91, 81].

$$\begin{bmatrix} x' \\ y' \\ z' \end{bmatrix} = M_{rot} \cdot \begin{bmatrix} x \\ y \\ z \end{bmatrix} \tag{3.7}$$

The rotation matrix M_{rot} can be expressed by a rotation around the x, y and z axis. The rotation matrices represent these axis rotations X_{rot}, Y_{rot} and Z_{rot} Eq. 3.8.

$$M_{rot} = Z_{rot} \cdot Y_{rot} \cdot X_{rot} \tag{3.8}$$

The single matrices X_{rot}, Y_{rot} and Z_{rot}, can be described by the matrices 3.9, 3.10 and 3.11, respectively. The parameters α, β, and γ are the axis-specific rotation

angles.

$$Z_{rot} = \begin{bmatrix} \cos(\alpha) & -\sin(\alpha) & 0 \\ \sin(\alpha) & \cos(\alpha) & 0 \\ 0 & 0 & 1 \end{bmatrix} \tag{3.9}$$

$$Y_{rot} = \begin{bmatrix} \cos(\beta) & 0 & \sin(\beta) \\ 0 & 1 & 0 \\ -\sin(\beta) & 0 & \cos(\beta) \end{bmatrix} \tag{3.10}$$

$$X_{rot} = \begin{bmatrix} 1 & 0 & 0 \\ 0 & \cos(\gamma) & -\sin(\gamma) \\ 0 & \sin(\gamma) & \cos(\gamma) \end{bmatrix} \tag{3.11}$$

TPMS hybridisation

TPMS cellular materials such as the one described in Subchapter 3.3.4 can be blended into each other by using a blending function. Here, a blending function was used as described by several authors like Yang et al. [79], [221] and Al-Ketan et al. [65]. Their approach involves a blending function Eq. 3.12 where weights w_i that corresponds to a substructure $\phi_i(X,Y,Z)$ are multiplied by the $i-th$ substructure $\phi_i(X,Y,Z)$ to form an overall structure ϕ_c, where the weight is a Sigmoid function.

$$\phi_{CM} = \sum_{i=1}^{N} w_i \cdot \phi_i \tag{3.12}$$

The weight w_i Eq. 3.13 is expressed by a Sigmoid function in the nominator q_u Eq. 3.14 and denominator q_l Eq. 3.15.

$$w_i = \frac{q_u}{q_l} \tag{3.13}$$

In the Sigmoid function Eq. 3.14 and Eq. 3.15 the parameter k_s is a shape factor set to 8 and the d_i and d_j are a elliptical scalar distance fields, Eq.3.16, where i and j are the $i-th$ or $j-th$ control point.

$$q_u = \frac{1}{1+e^{k_s * d_i}} \tag{3.14}$$

$$q_l = \sum_{j=1}^{m} \frac{1}{1+e^{k_s * d_j}} \tag{3.15}$$

$$d = \sqrt{\left(\frac{x_i - x_j}{u_{cx}}\right)^2 + \left(\frac{y_i - y_j}{u_{cy}}\right)^2 + \left(\frac{z_i - z_j}{u_{cz}}\right)^2} \tag{3.16}$$

This approach is also used for determining the relative density scalar field, where ϕ_{CM} would be substituted by c' and ϕ_i with c_i, where c_i is the $i-th$ control parameter of the relative density. (c is the offset parameter)

TPMS thickening

To thicken a cellular material, it is necessary to determine which relative density ρ_{rel} is required. The relative density can be described as the division of the cellular material volume V_{CM} by the bounding box volume V_{Box} (Eq. 3.17) [26, 27].

$$\rho_{rel} = \frac{V_{CM}}{V_{Box}} \tag{3.17}$$

The cellular material is thickened by Eq. 3.18 as described by Maskery et al. [66]. n is either one for strut-based TPMS lattices and two for sheet-based TPMS lattices. c is a value that correlates with ρ_{rel}.

$$\phi_c = \phi_{CM}^n - c^n \tag{3.18}$$

3.4 Equations

This Section describes the Equations that are used to create the stochastic design strategies Isotropic, Anisotropic, Graded, and Layered Randomness, and Stochastic Surface Roughness.

3.4.1 Gaussian Distribution

In this study, pseudo-randomness is introduced through the utilisation of the Gaussian probability density function Eq. 3.19. Here, σ is the standard deviation, a parameter that controls the spread of the population. The parameter μ is the mean value around which the spread occurs, and x is the parameter sampled by a RNG. The parameter x can be sampled by integrating Eq. 3.19 to receive the cumulative density function (CDF). Utilising the Inverse CDF method then yields pseudo-random numbers

distributed according to Eq. 3.19, see [222]. It is worth mentioning that the Gaussian distribution and the Weibull distribution are used as examples and could be replaced by other known distributions.

$$f(x,\sigma,\mu) = \frac{1}{\sqrt{2\pi}\cdot\sigma}\cdot e^{-0.5\cdot(\frac{\mu-x}{\sigma})^2} \tag{3.19}$$

The standard deviation σ is described by Eq.3.20, where x_i describes each population parameter. N is the population size. Hence, the standard deviation describes the average distance of all observations to the mean.

$$\sigma = \sqrt{\frac{\sum(x_i-\mu)^2}{N}} \tag{3.20}$$

A plot of the Gaussian distribution is demonstrated in Fig. 3.4. It can be seen that increasing the standard deviation σ leads to an increasingly flatter curve. In this example, the mean value μ is 0. A change of the mean value will lead to a shift of the Gaussian distribution either in the right direction (positive values) or in the left direction (negative values).

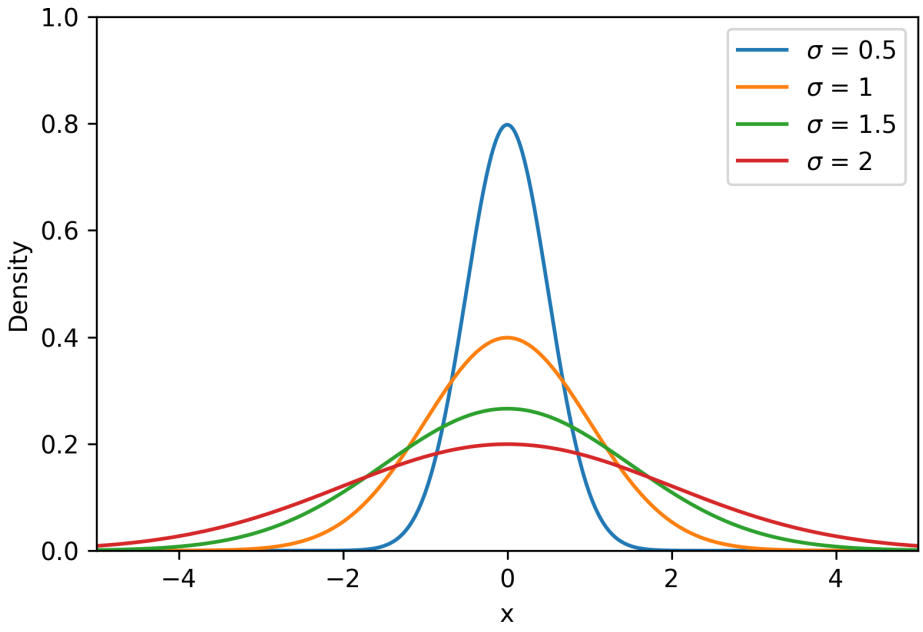

Figure 3.4: Gaussian distributions. The manipulation of the standard deviation σ changes the flatness of the distribution.

The CDF of the Gaussian distribution is expressed by Eq. 3.21, where erf is an error function. As all parameters are known, Eq. 3.21 has to be rearranged to state $x = ...$ to get the x values. As this is complicated and not part of this work, an existing implementation is used, which is readily available in NumPy [222].

$$F(\frac{x-\mu}{\sigma}) = 0.5\left[1 + erf\left(\frac{x-\mu}{\sigma}\right)\right] \tag{3.21}$$

The value computed by the RNG combined with the Gaussian distribution can be understood as an offset value Δx, which perturbes the original value x to arrive at x', see Eq. 3.22. This is the same for other parameters.

$$x' = x + \Delta x \tag{3.22}$$

In nature, various patterns occur as a summation of multiple sequential random and not random processes, which can be described by distributions such as the Poisson Distribution, Uniform Distribution, Exponential, Gamma, Power Law, or Gaussian Distribution, among others [223]. According to [223], the Poisson Distribution is commonly used to describe spatial or temporal processes, while the Exponential and Gamma Distribution are usually applied for dependent and independent waiting time occurrences, respectively. A Uniform Distribution is generally used in reverse engineering strategies where no information about the pattern is at hand [223]. At the same time, a Gaussian Distribution is well suited if the mean μ should be preserved and the standard deviation is known. The rationale for using the Gaussian Distribution is:

- ▷ The design process starts from a regular design, and the mean should be preserved.
- ▷ Assuming that nature arrives at a design influenced by several subsequent independent random or not random processes, the distribution should converge to the Gaussian Distribution according to the Central Limiting Theorem [223].

3.4.2 Weibull Distribution

The Weibull distribution, Eq. 3.23, is another continuous distribution that can be utilised with a RNG, where k_w is a shape factor, see [224].

$$f(x, k_w) = (k_w \cdot x^{k_w - 1} \cdot e^{-x^{k_w}}) \tag{3.23}$$

A plot of the Weibull distribution is presented in Fig. 3.5 where it can be seen how manipulating the shape factor k_w lets the Weibull distribution transition from a hyperbola-like shape to a skewed bell like shape.

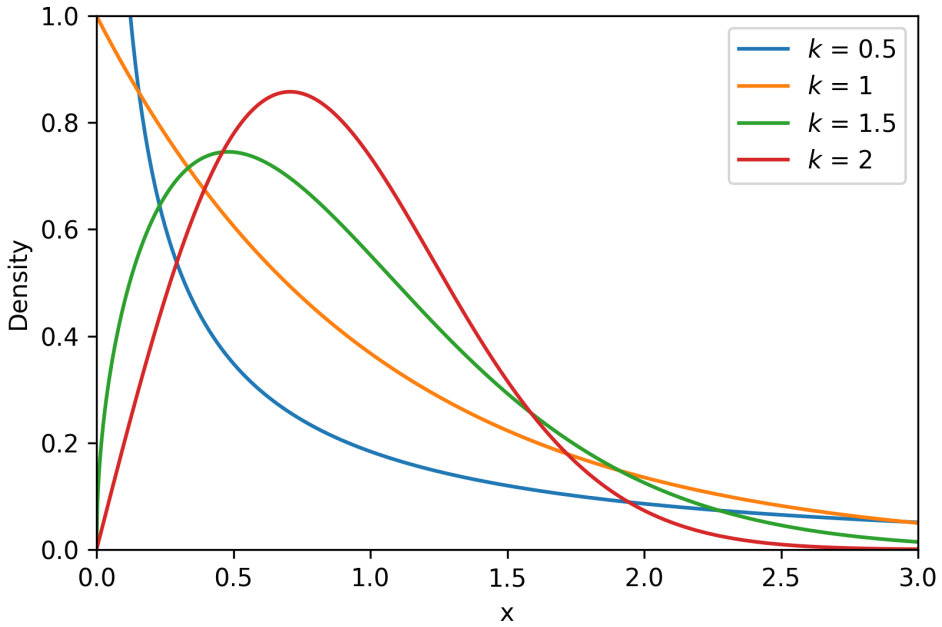

Figure 3.5: Weibull distributions. The shape factor k_w changes the appearance of the Weibull distribution from a hyperbola-like shape to a shape that resembles a skewed bell-like shape.

The scaling λ is necessary to tune the sampled values x to the desired positional parameters because the Weibull distribution is not bound to a mean value, unlike the Gaussian distribution. The result is the modified X values as demonstrated in Eq. 3.24. This is the same for y coordinates.

$$X = \lambda \cdot x \tag{3.24}$$

The Gaussian Distribution samples symmetrically around a mean, see Fig. 3.4. If directional perturbation is the intention of the design, this could be achieved using the Weibull distribution.

3.4.3 Graded Randomness

As previously stated, the standard deviation σ of the Gaussian distribution Eq. 3.19 determines the flatness or the steepness of the curve. By using a linear equation

Eq. 3.25 or radial equation Eq. 3.26 grading function, it is possible to express the standard deviation as a function of positional parameters. The linear grading, as shown in Eq. 3.25 allows for grading the standard deviation from a minimum value σ_{min} to a maximum value σ_{max}, from a start point l_0 to an end point l_x. The direction x as shown here, can be changed to y, or z, or the graded randomness can be applied to all three directions at the same time.

$$\sigma(x) = \frac{\sigma_{max} - \sigma_{min}}{l_x - l_0} \cdot x + \sigma_{min} \tag{3.25}$$

The linearly graded randomness is illustrated in Fig.3.6, where the standard deviation increases from left to right with increasing x.

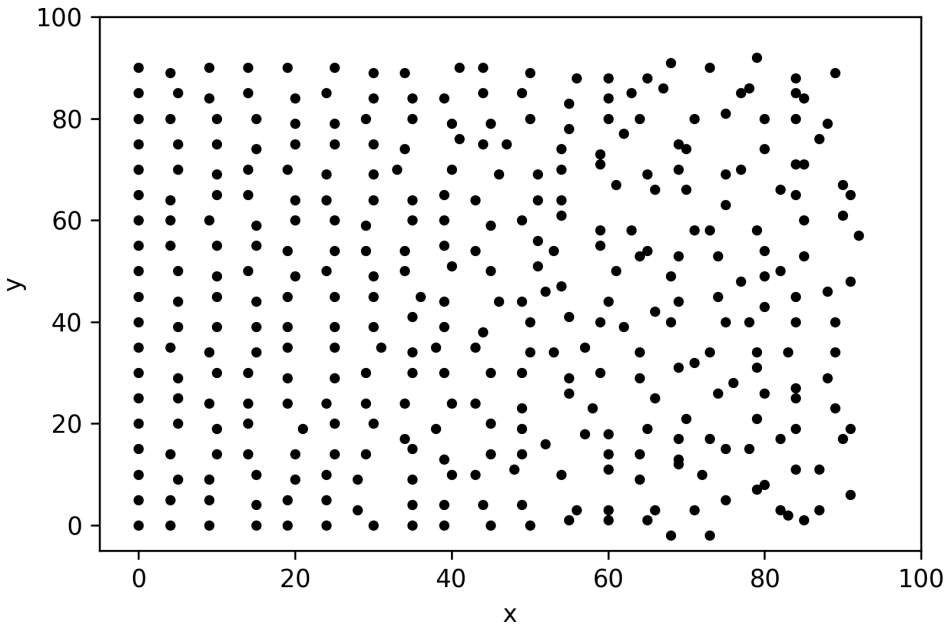

Figure 3.6: Graded Randomness. The stochasticity increases in the x-direction. This varies the location of the dots spatially.

Compared to that, the radial randomness Eq. 3.26 linearly grades the standard deviation from σ_{min} to σ_{max} in the x,y-plane. Where x_c and y_c are the centre coordinates around which the standard deviation expands radially according to the focal points/ radii r_x and r_y.

$$\sigma(x,y) = (\sigma_{max} - \sigma_{min}) \cdot \sqrt{\left(\frac{x - x_c}{r_x}\right)^2 + \left(\frac{y - y_c}{r_y}\right)^2} + \sigma_{min} \tag{3.26}$$

3.4.4 Layered Randomness

Layered randomness is created from a sine function, as shown in Eq. 3.27, which allows the creation of either a flat layer of randomness or sine curve at height H with an amplitude ym and a period of p_e.

$$f(x) = ym \cdot sin(p_e \cdot x) + H \tag{3.27}$$

However, this would only give the locations of a line. Thus, positional values from $-t_s$ to t_s as presented in Eq. 3.28 are selected to create a layer thickness that ranges from $-t_s$ to t_s.

$$-t_s < f(x) < t_s \tag{3.28}$$

A schematic of the stochastic layer can be found in Fig. 3.7 a).

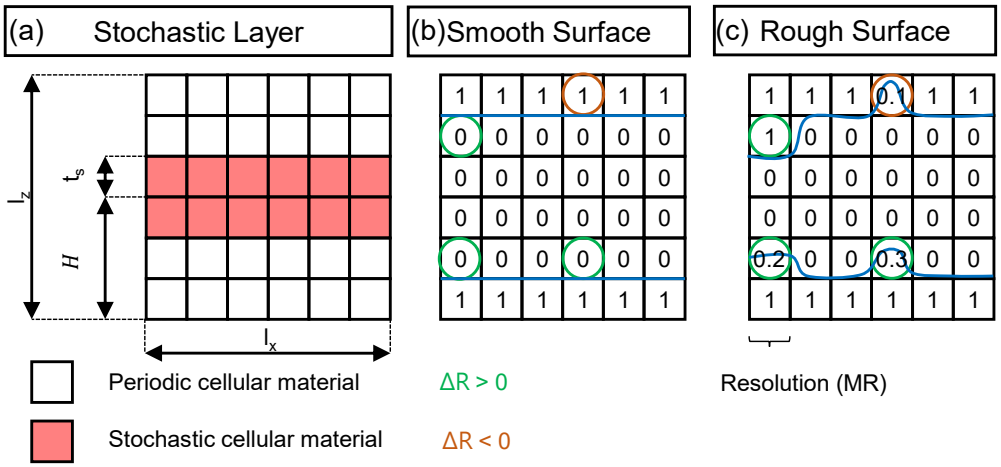

Figure 3.7: Layered randomness and stochastic surface roughness. a) Stochastic layer. b) smooth surface with values selected for $\Delta R < 0$ and $\Delta R > 0$. The blue line symbolises the resulting surface. c) Roughened surface, where ΔR was applied to.

3.4.5 Binary surface roughness

The first applied randomness procedure is used for binary matrices, representing a volume by 1 and a void by 0. Surface randomness can now be used by finding the boundary between 1 and 0 and then generating a random value from the Gaussian distribution Eq. 3.19 according to Eq. 3.29. The principle of roughening the surface is exemplified in Fig. 3.7 b-c). If the pseudo-randomly generated value ΔR is negative then ΔR is added to the 1 of the matrix $M_{i,j,k}$. On the contrary, if ΔR is positive it is added to the 0 value. Thus, the boundary (blue line) can be shifted positively and

negatively. However, to allow for some smoothness, every third value is randomised.

$$M_{i,j,k} = \begin{cases} 1 + \Delta R & if\ \Delta R < 0 \\ 0 + \Delta R & if\ \Delta R > 0 \end{cases} \tag{3.29}$$

3.4.6 Perlin Noise surface roughness

The second applied randomness procedure for volumetric distance fields is called Perlin Noise [116], [124]. This noise generator was implemented into the Python 'noise' library by Casey [217]. The output noise ϕ_{PN} generated is within a range where $\{\phi_{PN} \in \mathbb{R} | -1 \leq \phi_{PN} \leq 1\}$. Upon observing the distance field of the implicit surface functions of the TPMS cellular material, Table 3.4, it is obvious to rescale these values to control the roughness amplitude. Thus, a transfer function ϕ'_{PN} is introduced.

$$\phi'_{PN} = m_{PN} \cdot \phi_{PN} + k_{PN} \tag{3.30}$$

ϕ'_{PN} is a linear transformation which takes the input from the noise generator ϕ_{PN}, where m_{PN}, Eq. 3.31, is the slope and k_{PN} is the offset, Eq. 3.32. $High$ is the new upper bound set, and Low is the lower bound set.

$$m_{PN} = \frac{High - Low}{2} \tag{3.31}$$

$$k_{PN} = \frac{High + Low}{2} \tag{3.32}$$

3.4.7 Parametrising Stochasticity

Zhu et al. [121] described a parameter to describe the introduced randomness for Voronoi foams based on the beam length. This work uses a Gaussian distribution coupled with an RNG. Thus, an appropriate way to describe the level of stochasticity is based on the standard deviation σ and the mean value μ as demonstrated by Eq.3.33. (See Literature Review 2.2.3). This parameter was also used by [133, 129]

$$\delta_{SDP} = \frac{\sigma}{\mu} \tag{3.33}$$

To describe the combined stochastic level δ_{tot} of the whole system, the levels of stochasticity δ_{SDP} are added similar to a Gaussian error propagation as seen in

Eq. 3.34.

$$\delta_{tot} = \sqrt{\sum_{i=1}^{N} (\delta_{SDP}^2)_i} \tag{3.34}$$

3.5 Algorithms

The Algorithm section describes the workflows to create the structures described in this thesis.

3.5.1 Procedure to create a generic surface element-based array

A shark's skin comprises a plurality of denticles and is used as a demonstrator to explain the approach. To create a shark skin, the following program flow as illustrated in Fig. 3.8 a) is used. At first, the input parameters that define the size of the shark skin, l_x and l_y, the grid spacings x_{sg} and y_{sg} and the average angle β_s is defined b). The standard deviations $\sigma_{\beta s}$, σ_{xs}, σ_{ys} for the angle and grid coordinates is defined. The standard deviation changes the flatness of the Gaussian distribution, Fig. 3.8 c), allowing tuning the distribution for the design purpose. After defining all the input parameters, the regular coordinates x_s and y_s are determined, and the desired Gaussian distribution is added. Similarly, β_s with superimposed Gaussian distribution is calculated for each denticle. Then, the distance between the randomised denticle coordinates i and j is calculated, and the minimum distance is used as the width w_s of $i-th$ denticles. This prevents any collision. After all necessary parameters for a shark denticle are determined, each is created at the (0,0) position and then moved to its final position. Finally, the design and property metrics of the shark skin are exported. These include the positions x_s, y_s, the widths w_s, angles β_s, the surface area A_s and the volume V_s. This program flow was implemented in Python, and the script was executed with Autodesk Fusion 360 API's [219] standard operations.

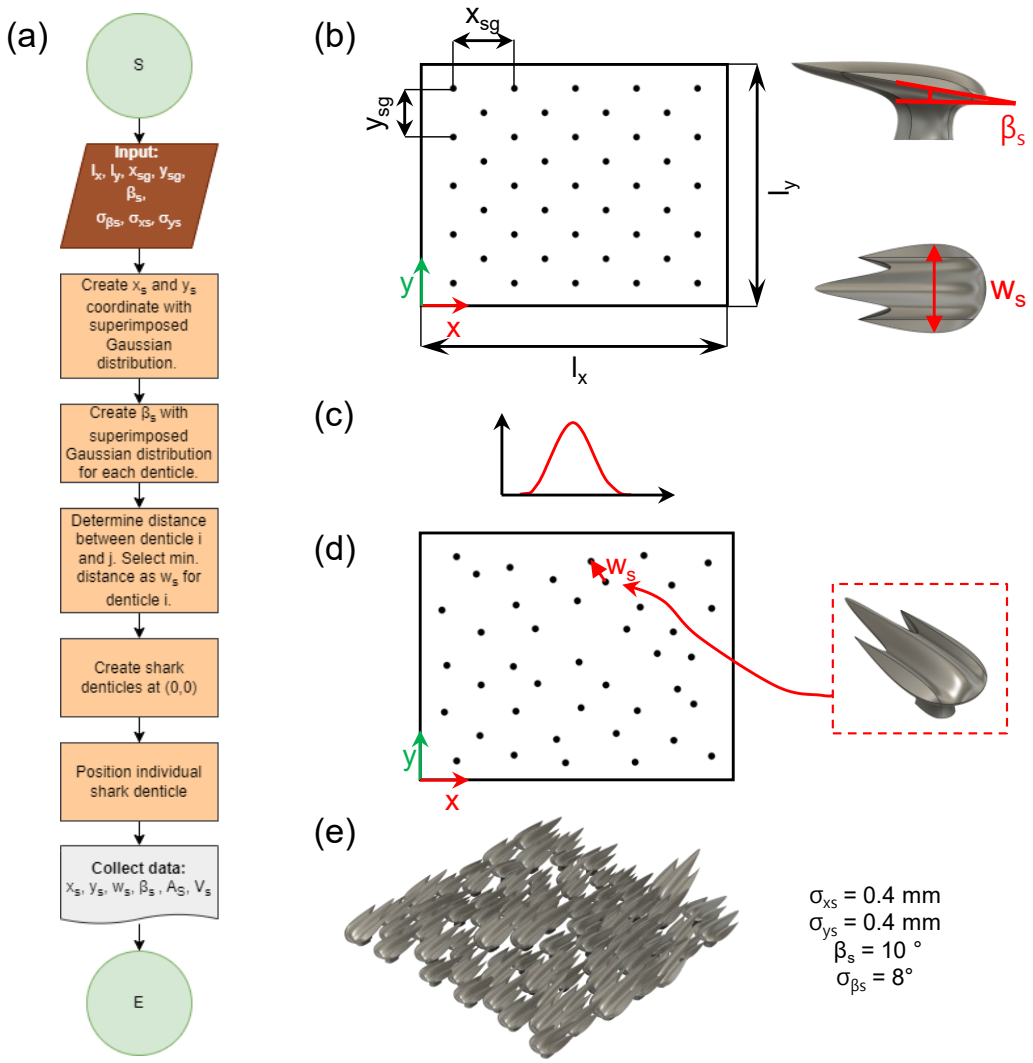

Figure 3.8: Stochastic surface pattern design tool. a) Program flow. b) Grid and denticle set-up. c) Gaussian distribution is added. d) Positioning of shark denticle. e) Final shark skin.

Following the described workflow (Fig. 3.8), the parameters to create the shark skin arrays are shown in Table 3.5. Samples of the shark skin arrays are manufactured on a Formlabs Form 2 SLA 3D printer from Formlabs Clear Resin V4.

Table 3.5: The parameters that were used to describe the shark denticle array.. Orange: Calculated parameters. White parameters are constants. Green parameters randomisation values. Yellow parameters are dependent.

No.	Parameter	Value	No.	Parameter	Value
1	w_S	Calculated	15	hr0y	$0.25 \cdot w_S$
2	l_x	30 mm	16	hr1y	$0.25 \cdot w_S$
3	l_y	30 mm	17	hr2y	$0.25 \cdot w_S$
4	x_{sg}	5 mm	18	lr0	$1.50 \cdot w_S$
5	y_{sg}	4 mm	19	lr1	$0.70 \cdot lr0$
6	beta (β)	20°	20	lr2	$0.90 \cdot lr0$
7	a_s	30°	21	level4	$0.50 \cdot level1$
8	b_s	40°	22	level3	$0.25 \cdot level1$
9	σ_x (mm)	0.0/0.4/0.8	23	level2	$0.125 \cdot level1$
10	σ_y (mm)	0.0/0.4/0.8	24	level1	$0.50 \cdot w_S$
11	σ_β	3°	25	rh2	0.90
12	hr0	$0.20 \cdot w_S$	26	rh3	0.50
13	hr1	$0.30 \cdot hr0$	27	rh4	0.30
14	hr2	$0.50 \cdot hr0$	28	rh5	0.30

3.5.2 Procedure to create a cellular material from a primitive structure

The program flow to create a stochastic strut-based cellular material is described in Fig. 3.9. First, a cellular material unit cell such as the Cubic, BCC, FCC or FCC+ unit cell is chosen. Second, the unit cell size is set in the x, y, z direction as denoted by u_x, u_y and u_z. The size of the cellular structure is defined by defining the length l_x, l_y and l_z. The relative density is also defined for this unit cell size and structural size. Third, one out of five tools is chosen to design the cellular material; this could be Isotropic Randomness, Anisotropic Randomness, Graded Randomness, a Sine Layer or Stochastic Surface Roughness. Stochastic Surface Roughness can be applied separately or in conjunction with the other four stochastic design tools. For each of the design tools, the characteristic stochastic levels are defined. Fourth, after applying the stochastic design tool, the overall relative density is adjusted to meet the desired relative density. Fifth, the cellular material is created and saved as an STL file for further use. This tool was designed in MATLAB, and the STL saved using the following library [218]. Python offers a higher versatility than MATLAB and

is free, so the code was transferred to Python using the Vedo, NumPy, and SimPy libraries.

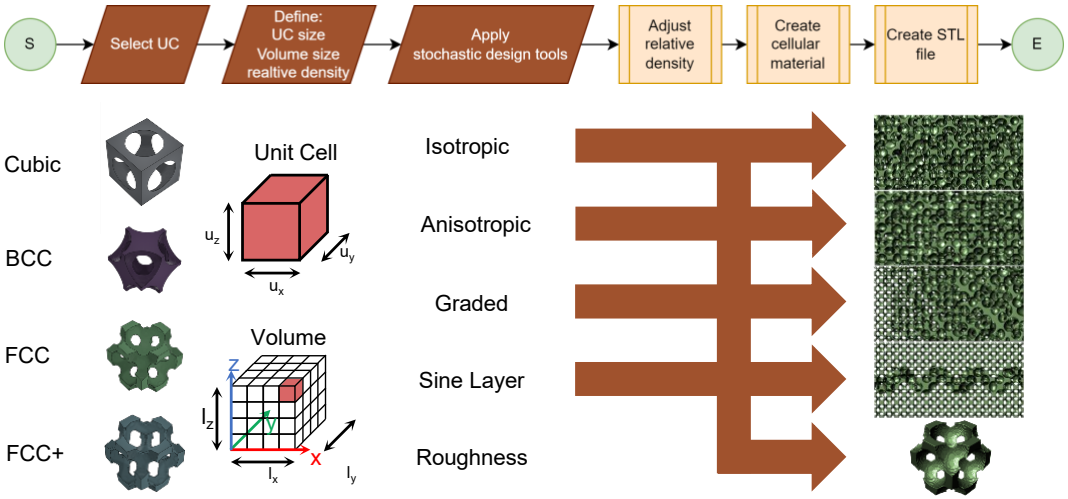

Figure 3.9: Program flow to create stochastic strut-based cellular materials from different stochastic design strategies.

Design parameters

Several strut-based cellular materials are designed according to the parameters shown in Table 3.6.

Table 3.6: Cellular material design parameters for strut-based stochastic structures.

Function	$u_{x,y,z}$	l_x / l_y / l_z	ρ_{rel}	MR	d	t_s	p_e
Isotropic	5	25/25/25	0.2	0.2	-	-	-
Anisotropic	5	25/25/25	0.2	0.2	-	-	-
Grading	5	50/25/25	0.2	0.2	-	-	-
Sine 0	5	25/25/25	0.2	0.2	2	4	1
Sine I	5	25/25/25	0.2	0.2	2	4	0.25
Sine II	5	25/25/25	0.2	0.2	2	4	0.5
Roughness	10	60/30/30	0.2	0.2	-	-	-
Heat Sink	10	50/50/10	0.2	0.2	-	-	-

3.5.3 Procedure to create Stochastic TPMS Structures

In this Subchapter, the workflow to design a stochastic TPMS-based cellular material is described as shown in Fig. 3.10 a). First, one out of five tools is chosen. Fig. 3.10 b) shows these five tools. The tools include Isotropic Randomness, Anisotropic Randomness, Layered Randomness, and Stochastic Surface Roughness. Stochastic

surface roughness can be applied in parallel to the other four tools. Third, a specific unit cell is selected, such as a Gyroid, a Schwarz-P or Schwarz-D unit cell, and the unit cell defining parameters are set as shown in Fig.3.10. Fourth, according to the chosen tool, the stochastic level is defined. Fifth, the size of the whole cellular material structure is computed, and at the centre of each unit cell, a discretiser is placed, as shown in Fig. 3.10. The discretiser is a location that is used to apply an interpolation method to create a smooth transition between parameters. Sixth, the stochastic distribution for each of the parameter sets is computed (Fig. 3.10 e) and seventh, the relative density is evaluated for each unit cell (Fig. 3.10 f). After all parameters are determined, the initial cellular material is created in the eighth step. If stochastic surface roughness should be added to the cellular material, it is added in the ninth step. If not, the final cellular material is computed in the tenth step. The relative density is corrected in the eleventh step, and the file is saved. The created cellular material Fig. 3.10 g) can be further processed by a slicer software and then manufactured through additive manufacturing. The parameters used to create the various stochastic TPMS-based cellular materials are shown in Appendix A.1. A Stratasys J750 Polyjet AM machine was used to manufacture the coloured specimen. Table A.1 describes the cellular material design parameters. The reference values for calculating the stochasticity parameter are shown in Table A.2. This workflow was implemented using Python and the libraries Vedo, NumPy, and noise [217].

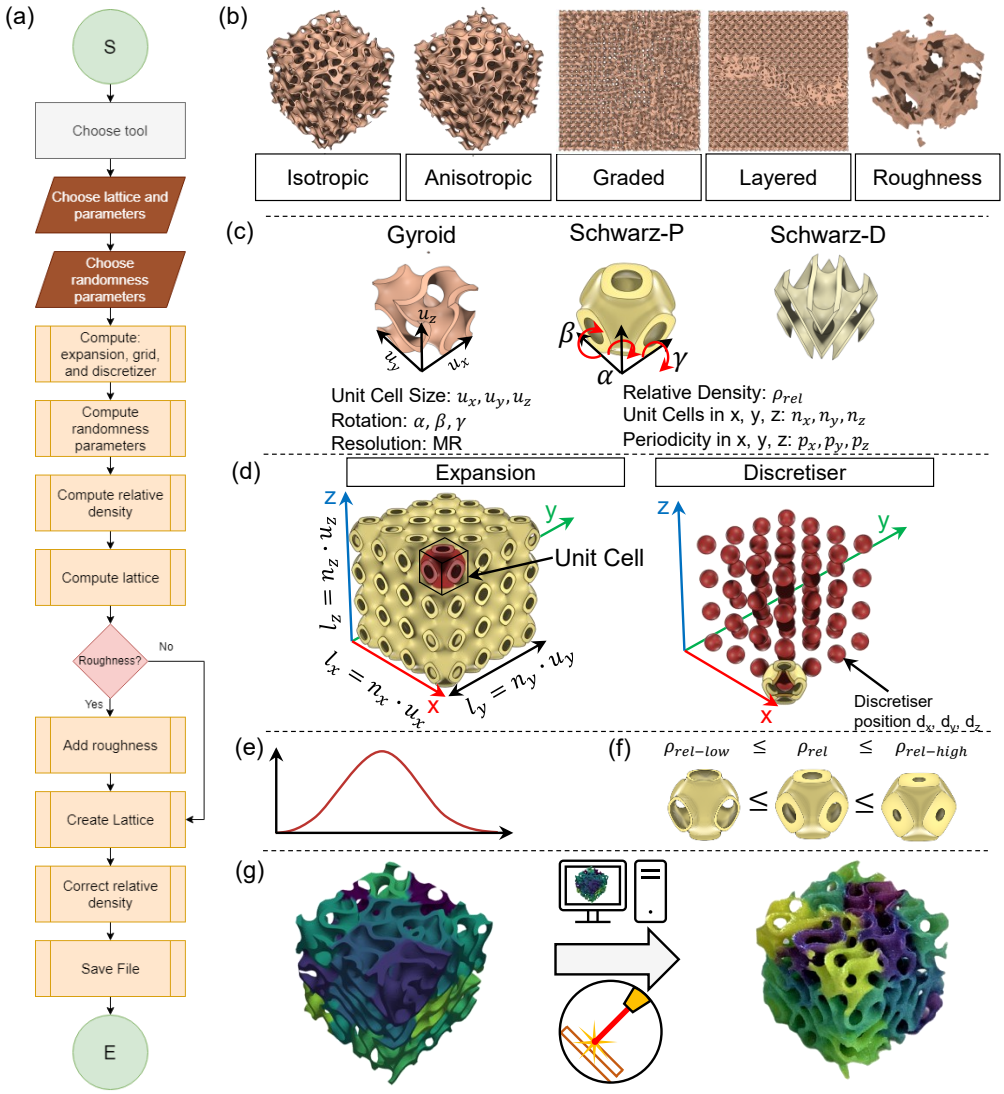

Figure 3.10: Steps to create a stochastic cellular material based on TPMS structures.

3.5.4 Procedure to create a stochastic array

This section describes the workflow flow to create a staggered pin fin array with superimposed stochasticity (Fig. 3.11 a), Converge Control and Gap Control. This workflow is not limited to the pin fin array and is the same for the sphere, cube, cone primitive shape and shark denticle (input parameters vary). This workflow is also the same for inline arrays. First, the geometrical properties of the pin fin array are defined. The main parameters are shown in Fig. 3.11 b) such as the radius r, height H, the lateral spacing in x-direction X and the transverse spacing in the y-direction, Y. Additionally, a level of stochasticity is defined for the parameters r, H and the x and y location. The levels of stochasticity for these parameters are defined by the standard deviations σ_r, σ_H, σ_x, and σ_y, respectively (The definition of this parameters depends

on the stochastic design strategies, Isotropic, Anisotropic, Graded, and Layered Randomness. Depending on these design strategies, the stochasticity levels can be chosen, and the stochastic level regarding its spatial distribution is calculated). Additionally, a minimum length m between two cylinders is defined. The number of pins n in the n_x and n_y direction, n_x and n_y define the size of the array. Second, the positions and radii with superimposed stochasticity (Fig. 3.11 b), and height are calculated. Third, the program checks that the surface area A, the average radius r, average height H and the defined standard deviation σ of these parameters match the input parameters of a regular staggered pin fin array to ensure comparability. If not, a new stochastic pin fin array is sampled (Converge Control). Fourth, if the parameters are within a given tolerance, then the Euclidean distance $d_{i,j}$ between the pin position i and j is determined to find the nearest neighbour. Fifth, if the distance $d_{i,j}$ between two cylinders is larger than d_m, then the staggered pin fin array is accepted, else the sampling process starts again (Gap control). Sixth, the staggered pin array is created. An example of a final staggered pin fin array is shown in Fig. 3.11 d) where a plate of thickness 1 mm was added manually.

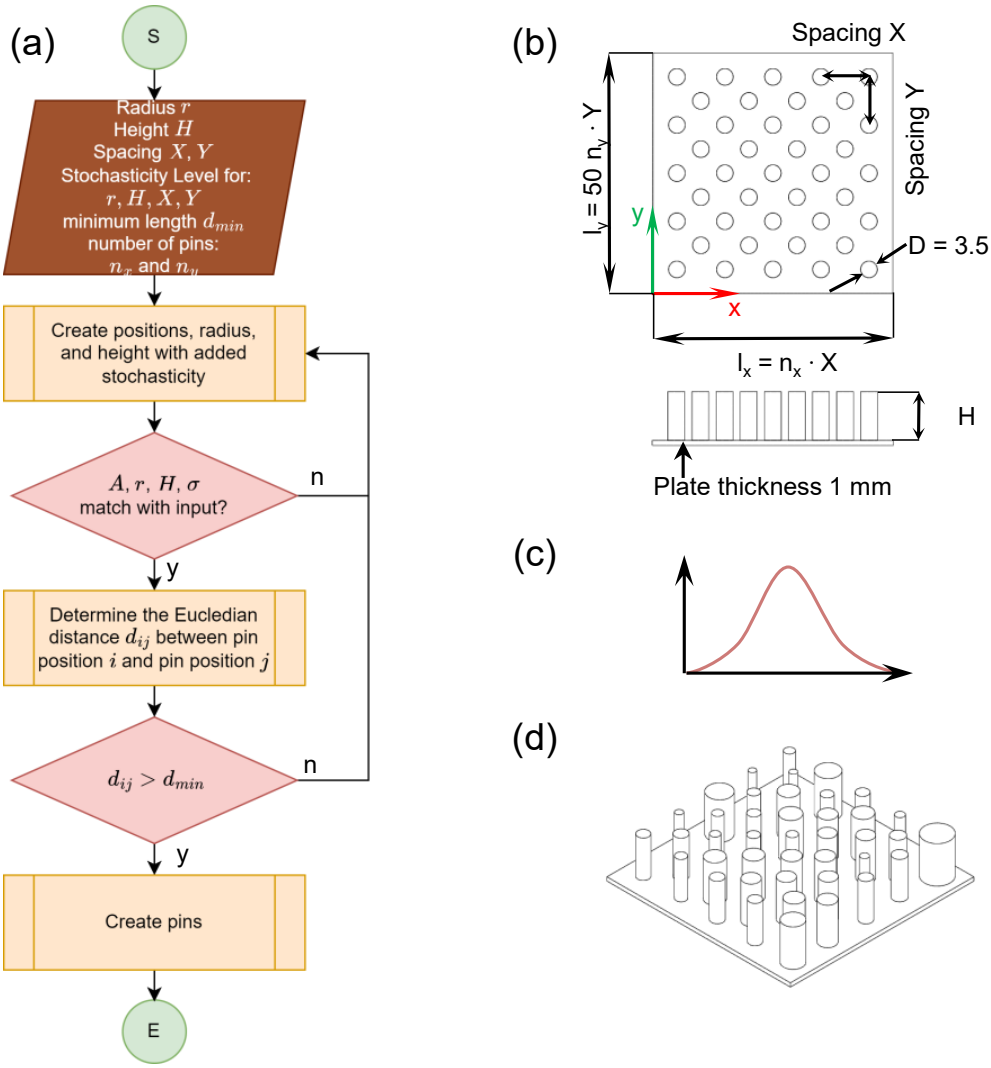

Figure 3.11: Program flow to create stochastic pin fin arrays.

3.6 Shapiro-Wilk test

The Shapiro-Wilk Test [225] is used as a statistical test to either accept or reject the Null Hypotheses that a distribution is distributed normally. The Null Hypothesis (H0) and Alternative Hypothesis (H1) of this work are:

- ▷ H0: The Gaussian distribution sampled from a RNG is normally distributed.
- ▷ H1: The Gaussian distribution sampled from a RNG is not normally distributed.

Apart from the Shapiro-Wilk Test [225], other tests in use are the Anderson-Darling, Kolmogorov-Smirnov and Lilliefors Test [226]. These tests for normality were investigated by Razali et al. [226], and their power was ranked over significance

levels of $\alpha = 5\%$ and $\alpha = 10\%$ for sample sizes ranging from 10 to 2000. They found out that the Shapiro-Wilk test has a higher power than the other normality tests, which makes it better. As such the Shapiro-Wilk Test was selected as the method of choice. The Shapiro-Wilk Test is conducted using Python and the SciPy and NumPy libraries. An implementation of the Shapiro-Wilk Test is available in the SciPy library [227]; the Shapiro-Wilk implementation is based on the Algorithm AS R94 published by Royston [228]. The Shapiro-Wilk Tests in SciPy takes as an input the distribution that should be tested and outputs two statistical values, W and the p-value for the Hypothesis test [227].

The test statistic W is calculated according to Eq. 3.35 [225], where N is the number of observations, μ the average of the distribution and y_i is a value of and ordered sample y_1, y_2, y_N, which is tested for normality.

$$W = \frac{(\sum_{i=1}^{N} a_i x_i)^2}{\sum_{i=1}^{N}(x_i - \mu)^2} \tag{3.35}$$

The factor 'a' can be calculated according to Eq. 3.36 [225], where m is a vector, which includes the expected values, and V is the covariance matrix of the expected values. The expected values are computed from the standard normal distribution.

$$a_i = \frac{m' V^{-1}}{\sqrt{m' V^{-1} V^{-1} m}} \tag{3.36}$$

The p-value is based on W, and its calculation is based on the standard normal integral, which is explained in detail by Royston [229, 230], who uses an implementation of the standard normal integral by Hill [231].

The Hypothesis test is conducted based on the W and p-value. A significance level of $\alpha = 5\%$ is chosen. H0 will be accepted if $p > 5\%$; otherwise, it will be rejected.

3.7 Hardware

This Section describes the Additive Manufacturing hardware used to produce the objects demonstrated in this thesis. The described hardware includes Stereolithography (SL), Selective Laser Sintering (SLS), and Material Jetting.

3.7.1 Stereolithography

An SL AM machine has three critical features: a build platform, a mirror, and a UV laser, as shown in Fig. 3.12. The UV laser beam is redirected through a mirror towards the build platform to follow a sliced part's inner and outer contours to cure photopolymer resin in contact with the build platform selectively. After one layer of the component has been cured, the build platform moves one layer height of usually 25 to 200 μm down or up (depending on the used machine) to cure the next layer. This process is repeated until the entire component has been manufactured. Depending on the component orientation and shape, overhangs have to be supported through support material. The advantage of SL is the good surface quality compared to other AM processes, such as SLS, which makes this technology well-suited for applications requiring a reasonably smooth surface. As SL deals with photo-curable polymers, the negative implications of this process are that the properties of the cured material are not stable and that the resin is toxic. Additionally, the need for a support structure can result in rough surfaces, which could be undesired for some applications. [1]

This work used a Formlabs Form 2 (Farmlabs, USA) SL AM machine to produce components. Each build is set up with the slicing tool PreForm (Farmlabs, USA). The Formlabs Form 2 is specified to reach layer heights of 25, 50 and 100 μm and has a laser spot size of 140 μm [232]. This limits the Formlabs Form 2's feature size; therefore, the features must be at least greater than the reported 140 μm. Diegel et al. [1] recommends for SL manufacturing the following design considerations; hole diameters should be greater than 0.5 mm and walls should have a thickness of at least 0.4 mm. In general, tolerances highly depend on the geometry of the manufactured object and therefore, tolerances within at least $\pm$ 0.1 mm have to be expected [233].

After the component has been manufactured through SL, the component is removed from the build platform and placed in a Formlabs Form Wash unit (Farmlabs, USA) filled with Isopropyl Alcohol. In the washing unit, the component is cleaned from uncured photopolymer resin. After the cleaning process, the component is cured in the Formlabs Form Cure unit (Farmlabs, USA), where the component is situated on a platform and rotates while cured through UV light from all sides. Removal of support structures follows the curing process.

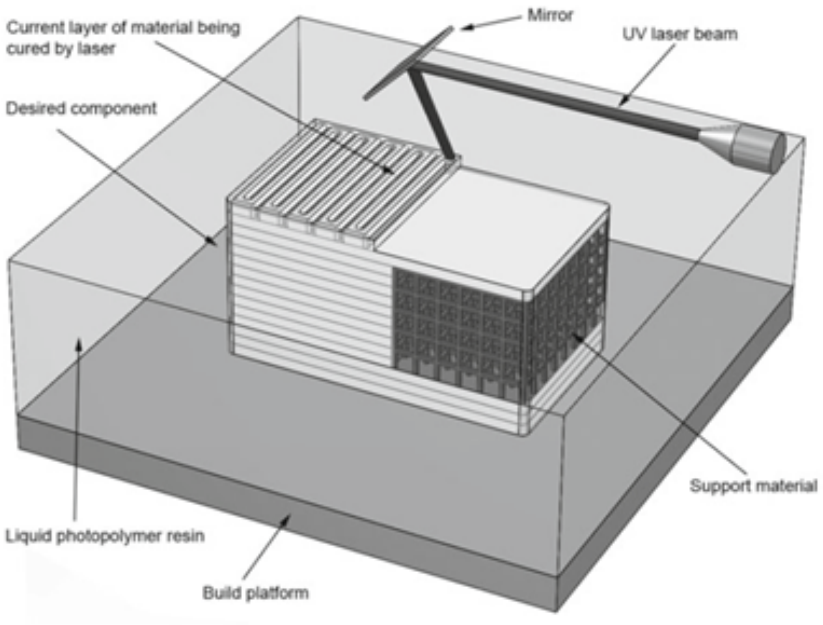

Figure 3.12: Schematic of a Stereolithography Additive Manufacturing process, reproduced from [1].

3.7.2 Selective laser sintering

Selective Laser Sintering (SLS) is a polymer-based AM process, which is also termed polymer-based PBF. The machine consists of five essential components, as shown in Fig. 3.13: a fresh powder supply chamber, a moveable build plate, an excess powder chamber, a roller to distribute the powder, and a laser whose beam is directed by a mirror on a build plate. First, a fine layer of powder is spread by a roller from the fresh powder chamber over the build plate. The excess powder is collected in the excess powder chamber. Then, the powder on the build platform is selectively melted through the laser beam following the computationally generated laser path of the sliced component. After that, the build plate moves down by a layer height of 100 μm, and a new polymer powder layer is distributed over the build plate, covering up the previous layer and the component slice. When this layer is distributed, the laser selectively melts the next layer, which merges with the previous layer. Repeating this process creates a part. [1]

In this work, the used SLS machine to manufacture samples is the EOS EOSINT Formiga P100 (EOS GmbH, Germany). The build job is prepared in Materialise Magics (Materialise NV, Belgium). Then, it was sliced in SliView (EOS GmbH, Germany) and sent to the EOS machine. After manufacturing, the build platform, including the powder cake and the manufactured component, is removed. The

excess powder is removed and recycled. The components are then transferred to a sandblasting chamber, where they are cleaned from any powder dust that adheres to the surface. This process is followed by water jet cleaning and an ultrasonic bath. The material is then dried in an oven.

SLS machines usually achieve tolerances of ±0.25 mm. For larger parts, it is usually recommended to have a length-specific tolerance, which is ±0.0015 mm/mm. It is also recommended not to use feature sizes smaller than 0.5 mm. The advantages of SLS are that supports are unnecessary and that engineering polymers such as PA12 are used, making it well-suitable for industrial applications. A downside of this process is the introduced Anisotropy in the build direction and the surface roughness. [1]

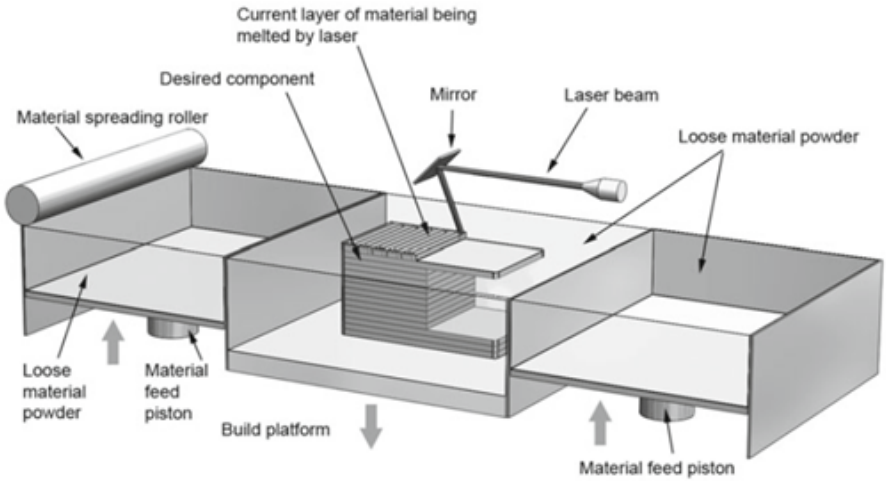

Figure 3.13: Schematic of a Powder Bed Fusion Additive Manufacturing process, reproduced from [1].

3.7.3 Material jetting

Material Jetting is an AM process that uses an Inkjet printhead to distribute finely dispersed drops of a photopolymer resin as per the layer-wise computer-generated path of a component (See Fig.3.14). The ejected photopolymer resin drop attached to the surface of the previous layer or the build platform is cured by a UV light attached to the printhead. Necessary support material can be printed through an extra nozzle in the printhead. The main advantages of Material Jetting are that the surface is smoother than other AM processes, such as SLS or Filament Deposition Moulding, and that it can produce coloured parts and parts utilising various materials. This makes it especially useful for creating prototypes. However, there are also

disadvantages associated with Material Jetting. As this is a photopolymer resin-based manufacturing process, it faces similar disadvantages as SL, primarily related to the use of resin. The post-curing mechanical part properties are unstable, and the work with toxic resin could cause safety issues. Further disadvantages are that support is necessary. [1]

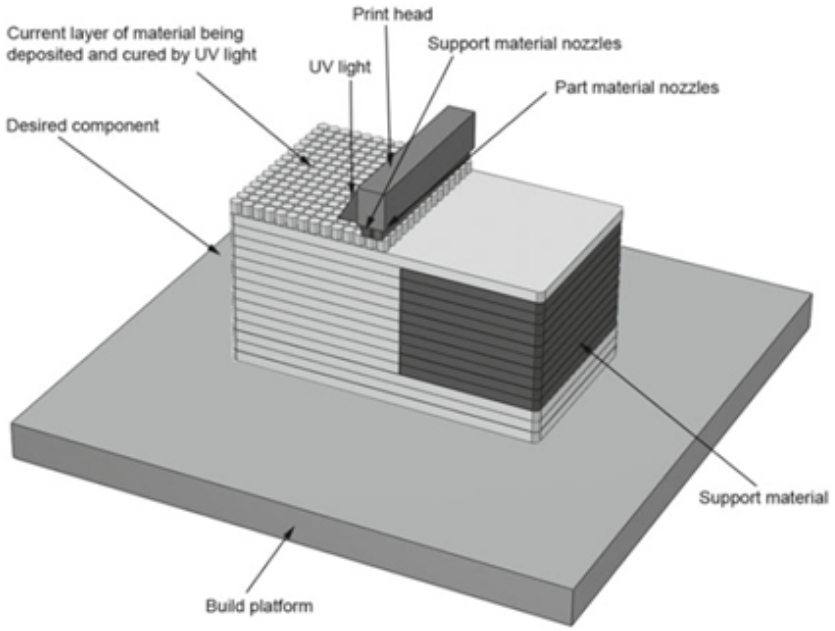

Figure 3.14: Schematic of a Material Jetting process, reproduced from [1].

This work manufactures multi-colour cellular material demonstrators on the Stratasys J750 3D Printer (Stratasys, Israel). For this machine series, Stratasys recommends designing parts with at least a wall thickness of 0.6 mm and features of 0.2 mm and greater for a successful print [234]. The slicer and print preparation software GrabCAD Print is used to set up the printer.

3.8 Materials

The Materials used to manufacture the demonstrators in this work are described in this Section. The included materials are the Stereolithography Resin, the Selective Laser Sintering Powder, and the Material Jetting Resin.

3.8.1 Stereolithography resin

The Formlabs resin Clear V4 (Farmlabs, USA) is used for samples manufactured through SL. After the samples are manufactured, the uncured samples are washed for 10 min in Isopropyl Alcohol and then cured for 15 min at 60°C. The chosen layer height for this material is 50 μm.

3.8.2 Selective laser sintering powder

White Nylon PA12 (PA2200), manufactured by EOS GmbH, Germany, is used with standard process parameters (Table 3.7) as described in [235] on the EOS EOSINT P100 Formiga SLS printer. After the build process, the powder cake was removed from the machine, and excess powder was removed. Then, the samples were sandblasted, followed by a subsequent water-jet cleaning. After the water-jet cleaning, the samples were cleaned in an ultrasonic bath for a total of 60 min with a resting period of 15 min after every 30 min at 40°C. Finally, the samples were dried in an oven for 120 min at 80°C.

Table 3.7: EOS EOSINT Formiga P100 SLS PA12 process parameters [235].

Laser Power	Layer Thickness	Scan Speed	Hatch Spacing	Chamber Temperature
21 W	100 μm	2500 mm/s	250 μm	173 °C

3.8.3 Material jetting resin

The coloured samples were manufactured on the Stratasys J750 3D Printer from VergoMagentaV, VeroCyanV, and VeroYellowV (Strarsys, Israel). The support structures were manufactured from SUP706. For these materials, the layer height is 14 μm [236]. After printing, the samples were washed in an Alkaline Solution (Water mixed with 2% sodium hydroxide and 1% sodium metasilicate) [237] for approximately 24h.

3.9 Pin characterisation method

Two staggered pin fin arrays were manufactured using SL from Clear Resin V4 at an angle of 45° to the Build Plate (Fig. 3.15), then washed, cured, and the support

structure was removed. The pin height is 1 mm, the diameter is 3.5 mm, and the distance between the pins is 10 mm, see Fig. 3.15. A minimum distance of 1 mm between pins is set to prevent overlaps. The pins are situated on a 50x50x2 mm^3 plate. This is the regular staggered pin fin array. 10% Stochasticity was applied to the stochastic pin fin array's diameter and x and y position. The top of the pins was painted with a Matt Grey colour (Revell Enamel Matt 76). Images of two-pin fin arrays were taken using an Alicona Infinite Focus G4 and the Objective IFM G4 2-5x. The optics were focused on the pin surface, Focus-Variation was not applied, and the measurement process was controlled through the software MeasurementSuite (Due to the transparency of the Clear V4 resin, a white sheet of paper was put under the sample for a better contrast). The Field Of View is 286.65 Pixels per mm^2. The post-processing of the images was conducted using Fiji. The images were converted to a 16-bit greyscale image. Then, a Threshold was applied using the automatic Minimum algorithm, which is implemented in Fiji. The Minimum Algorithm smoothes the binarised 16-bit grey scale image and selects the local minimum between two local maxima as Threshold [238]. The Minimum Algorithm was chosen because of the strong contrast between the coloured top pin surfaces and the transparent base on a white paper sheet. After applying the threshold to the image, a Particle Analysis was conducted utilising Fiji. The particle size was set to 0.5-∞ mm^2, and the Circularity was set to 0.1-1.0. The Particle Analysis Algorithm then measured the pins' Area and Centroid position. From this, the average diameter and its Standard Deviation were evaluated. The Centroid position was used to determine the distance between pins (Euclidean Distance) within rows in the x and y direction; an example is presented in Fig. 3.15. One row in the x direction is exemplified by a red line, and one row in the y direction by a green line. This process is repeated for each line.

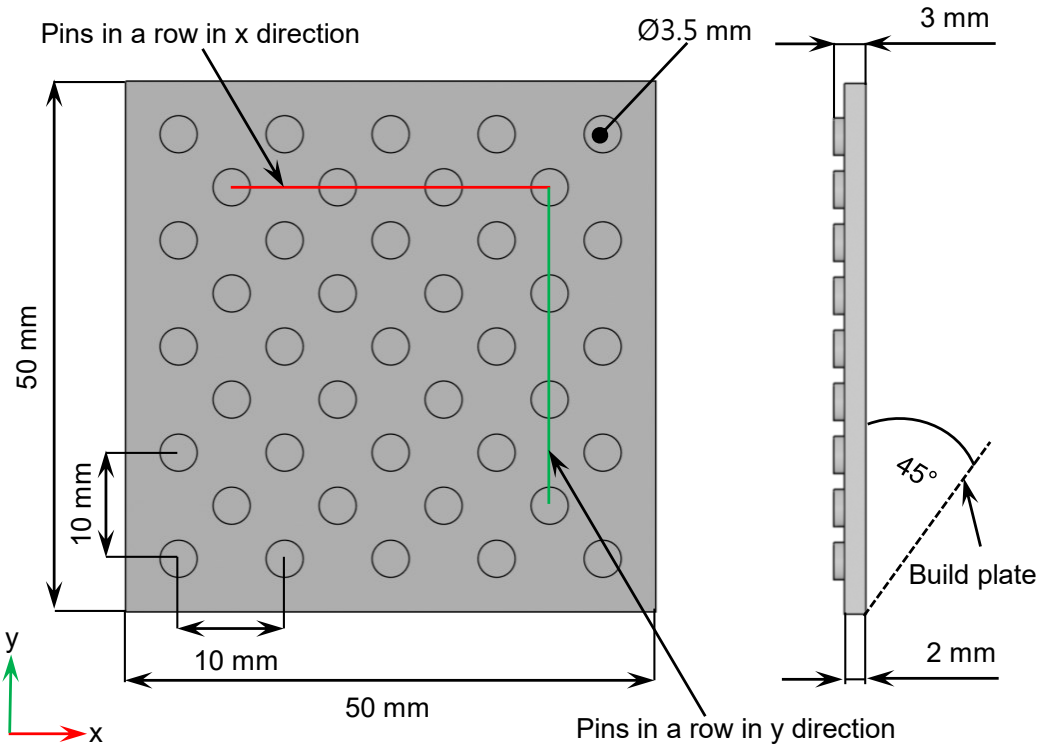

Figure 3.15: Regular SL pin sample.

Chapter 4

Stochastic design for strut-based cellular materials

4.1 Introduction

This Chapter solves Research Gap No.1 to develop novel design strategies for strut-based cellular materials based on primitive objects. The randomised unit cells are a Cubic, a Body-Centred Cubic (BCC), a Face Centred Cubic (FCC) and a Face Centred Cubic structure with an extra void in the centre (FCC+). First, the Gaussian RNG is checked using a Shapiro-Wilk test to determine if the Gaussian RNG output follows a Gaussian distribution. Second, a regular and stochastic array of cylinders is manufactured using SL. The distance between the cylinders and the diameter is then analysed and compared to evaluate the manufacturability of the introduced stochasticity. Third, Isotropic Randomness will be applied, using a single stochasticity parameter for the parameters from which the unit cell is constructed. Fourth, Anisotropic Randomness is illustrated, which allows the application of different stochasticity parameters on each available set of unit cell-defining parameters. Fifth, a linear gradient is combined with the stochasticity parameters controlling the x, y, and z locations and the x, y, and z radii of an ellipsoid to apply Graded Randomness to the FCC cellular material. Sixth, the stochasticity parameter is combined with a sine function, resulting in localised randomness in the shape of a sine function. Fifth, the Gaussian randomisation method is used to alter the surface topology of the cellular material. Finally, a heat sink is illustrated as a demonstrator for a possible application.

Further information: This chapter is based on the publication “Five simple tools for stochastic lattice creation”, of which the author of the thesis is the first author.

Caelan Anderson, a former MEng student at the University of Nottingham, did his final year project, which the author of this thesis co-supervised, concerning this research project. Caelan Anderson contributed to the code implementation, which the author of this thesis improved and corrected to create this content to demonstrate stochastic cellular materials according to the design intent.

4.2 Results

This section presents the validation of the Gaussian distribution sampled from an RNG, the manufacturability of a stochastic array, and stochastic design strategies for strut-based cellular materials based on primitive shapes.

4.2.1 Validating the Gaussian Distribution from an RNG using the Shapiro-Wilk Test

A Shapiro-Wilk Test is performed on three Gaussian Distributions sampled from an RNG based on the PCG64 [111] and MT19937 [109] algorithm. The PCG64 is by default used in NumPy [239] while the MT19937 is the default algorithm used in MATLAB [240]. The Shapiro-Wilk Test is done to have evidence that the values are drawn from Gaussian Distribution. The test is conducted using Python and the libraries NumPy and SciPy. For each RNG, three different Seeds are used, presented in Table 4.1. For each distribution, a sample of $N = 5000$ random values from a Gaussian Distribution is drawn using a mean value $\mu = 0$ and a Standard Deviation of $\sigma = 0.1$. The resulting test statistic W and the p-value are rounded to two digits. The significance level is $\alpha = 0.05$. The distributions are accepted as drawn from a Gaussian Distribution if $p > 0.05$, and W is close to 1. For $p < 0.05$, the distributions are not accepted as being drawn from a Gaussian Distribution. The results of the Shapiro-Wilk Test are reported in Table 4.1. The rounded W values are 1.00, and all reported p-values are greater than 0.05. Hence, it can be concluded that the distributions are drawn from a Gaussian Distribution.

Table 4.1: Shapiro-Wilk Test Statistics.

Generator	Seed	N	μ	σ	W	p
PCG64	250	5000	0	0.1	1.00	0.88
PCG64	579	5000	0	0.1	1.00	0.19
PCG64	1564	5000	0	0.1	1.00	0.62
MT19937	250	5000	0	0.1	1.00	0.37
MT19937	579	5000	0	0.1	1.00	0.58
MT19937	1564	5000	0	0.1	1.00	0.57

4.2.2 A Comparison of the Manufacturing Tolerance and the introduced Level of Stochasticity

Figure 4.1 illustrates the two investigated samples of a regular staggered pin fin array a) and a staggered pin fin array that includes 10% Stochasticity superimposed on the diameter and the x and y position. The samples were manufactured using SL.

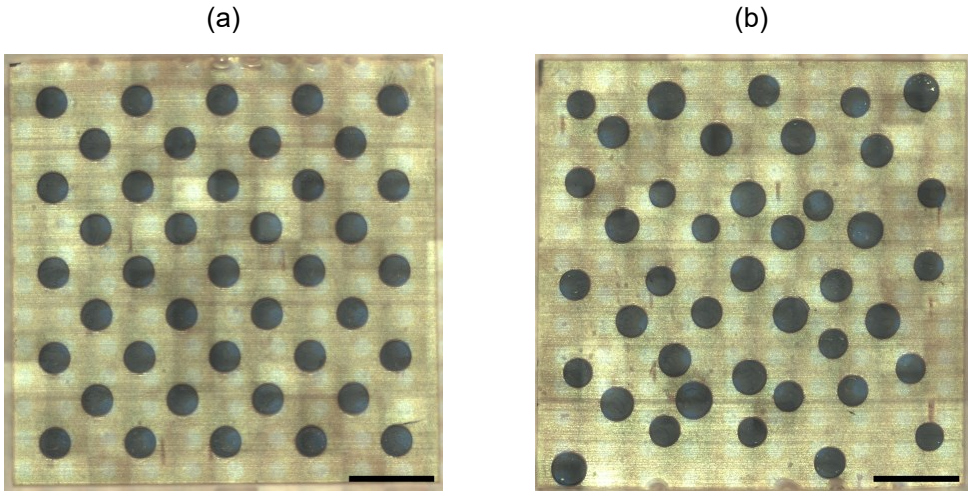

Figure 4.1: Images of an SL regular and random pin fin array. Scale bar 10 mm

The evaluation of the average diameter, the average row-wise spacing distance in the x and y direction, and the associated standard deviation are tabulated in Table 4.2. The Regular CAD sample has a diameter of 3.5 mm and a row-wise spacing in x and y of 10 mm. The Standard Deviation is 0 in all three cases. The Regular CAD sample manufactured by SL exhibits an average diameter of 3.78$\pm$0.05 mm. It shows that the diameter is approximately 0.3 mm larger than the design intent of 3.5 mm. The row-wise spacing in x and y direction of 10.00$\pm$0.03 mm and 9.99$\pm$0.04 mm

agree with the design intent. The 10% Stochasticity CAD sample has a diameter of 3.51±0.31 mm. Ideally, this should be 3.50±0.35 mm at 10% Stochasticity. However, differences are expected due to the population size of 41 pins and the nature of the RNG that can also have some variance in the sampled data. The row-wise spacing in x and y direction is 10.12±1.26 mm and 10.18±1.66, respectively. This is consistent with the values measured from the manufactured 10% Stochasticity SL sample where the row-wise spacing in x and y is 10.10±1.27 and 10.20±1.67. Similar to the Regular samples, the 10% Stochasticity SL sample has a 0.3 mm higher average diameter value of 3.81±0.33. As all evaluated standard deviations of the 10% Stochasticity SL sample were larger than the standard deviations of the Regular SL samples; it can be concluded that Stochasticity can be successfully included as long as it is larger than the manufacturing tolerance.

Table 4.2: Characteristic measurements of CAD and SL samples.

Sample	D [mm]	X-Row [mm]	Y-Row [mm]
Regular CAD	3.50±0	10.00±0	10.00±0
Regular SL	3.78±0.05	10.00±0.03	09.99±0.04
10% Stochasticity CAD	3.51±0.31	10.12±1.26	10.18±1.66
10% Stochasticity SL	3.81±0.33	10.10±1.27	10.20±1.67

4.2.3 Isotropic Randomness

In Figure 4.2, the design of Isotropic Randomness is exemplified on four different unit cells: Cubic a), BCC b), FCC+ c) and FCC d). On these structures, different levels of stochasticity are applied. Starting from a regular structure (0% stochasticity), the level of stochasticity is increased to 3% and 6%. The reference parameter for the stochastic level is the unit cell size for all parameters. The increase in stochasticity results in a more perturbed stochastic structure. The stochastic cellular materials displayed in d) were manufactured by a PBF AM process and illustrated in e).

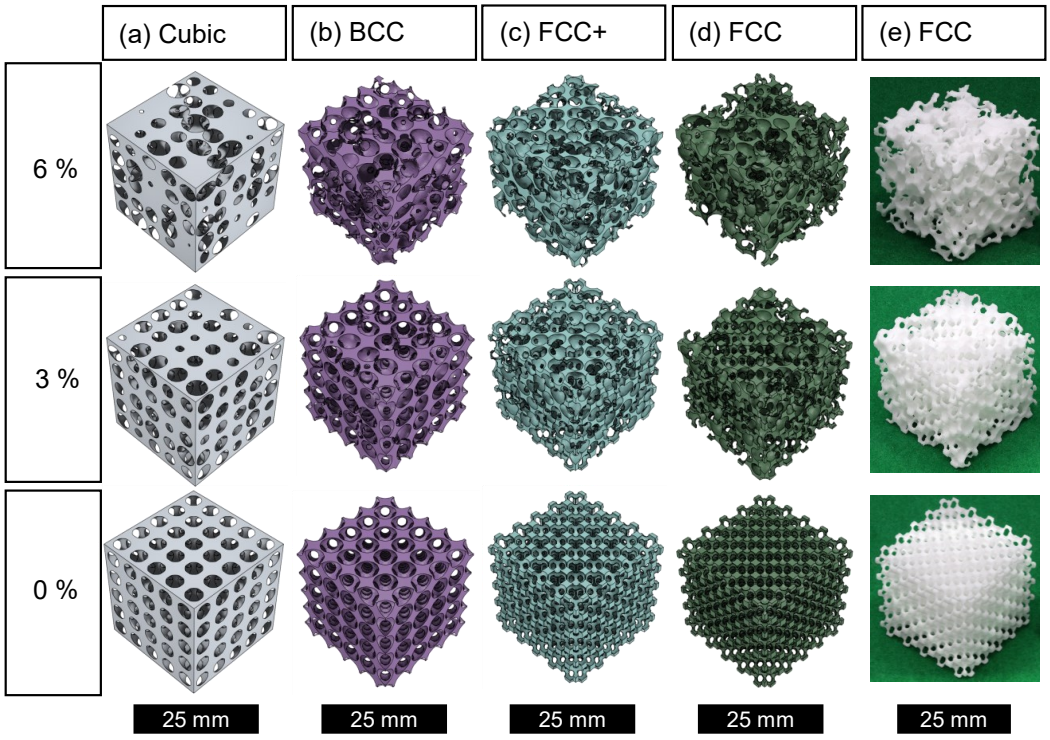

Figure 4.2: Effect of different levels of isotropic randomness. a) Cubic, b) BCC, c) FCC+ and d) FCC cellular material configuration. e) FCC cellular manufactured by a PBF process.

The randomness intended by design can be checked by examining the distribution of each randomised parameter. These parameters are associated with the ellipsoid from which the unit cell is formed and as such Fig. 4.3 illustrates the Gaussian distribution of the parameters that randomise the x, y, and z positional values a) to c) and the radii in x, y, z direction as shown in d) to f). The graphs were produced by introducing 3% Isotropic Randomness, equivalent to a standard deviation of $\sigma = 0.15$ mm. The introduced stochastic level is within the expected ranges, which is a result of the population size. The highest deviation from the reported standard deviation is 0.014 mm, and the lowest deviation from the standard deviation is 0.001 mm.

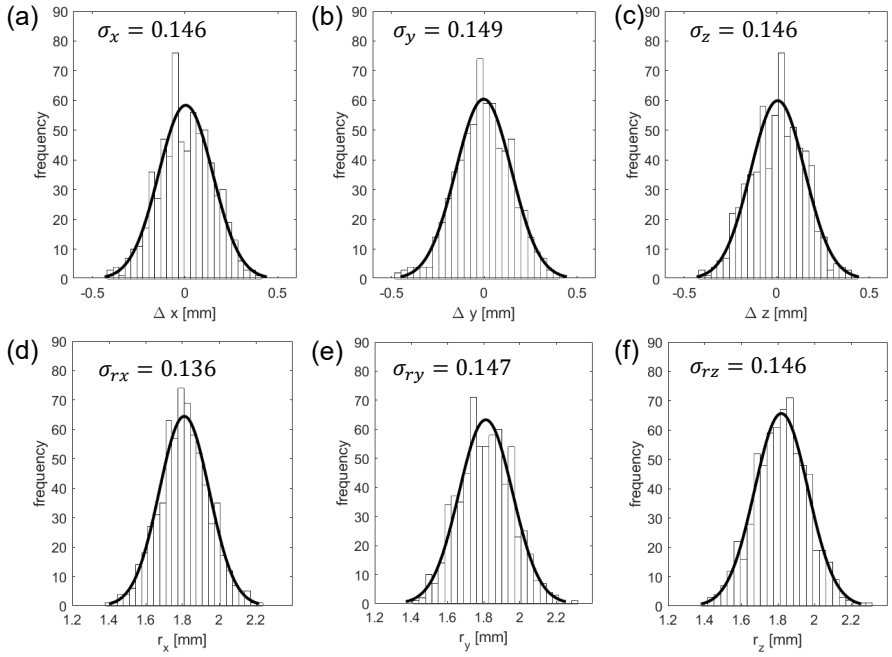

Figure 4.3: Gaussian parameter distributions of the unit cell defining parameters of the isotropic randomness applied to the FCC unit cell. a-c) positional parameters. d-f) radii.

4.2.4 Anisotropic Randomness

After introducing Isotropic Randomness, with only one randomisation parameter, Anisotropic Randomness follows. Here, a different level of stochasticity is chosen for each FCC unit cell defining parameter. As shown in Fig. 4.4 a) to c) that stochasticity is applied separately to the radii of the cellular structure. In a) 8% stochasticity is applied to radii pointing in the x-direction, in b) 5% stochasticity is introduced to the y-direction radius, and in c) it can be seen that 3.5% stochasticity was applied to the radius in the z-direction. As illustrated, the ellipsoids are more likely to deform in the direction where the stochasticity is applied. Stochasticity was added to the x, y, and z positional parameter with amplitudes of 4%, 3%, and 6%, respectively. However, in the examples from a) to f), stochasticity was only applied to one parameter to demonstrate the principle. g) shows two cellular structure materials where the previously described stochasticity was applied to all parameters simultaneously. The upper cellular material is rendered, while the lower one is manufactured by SLS.

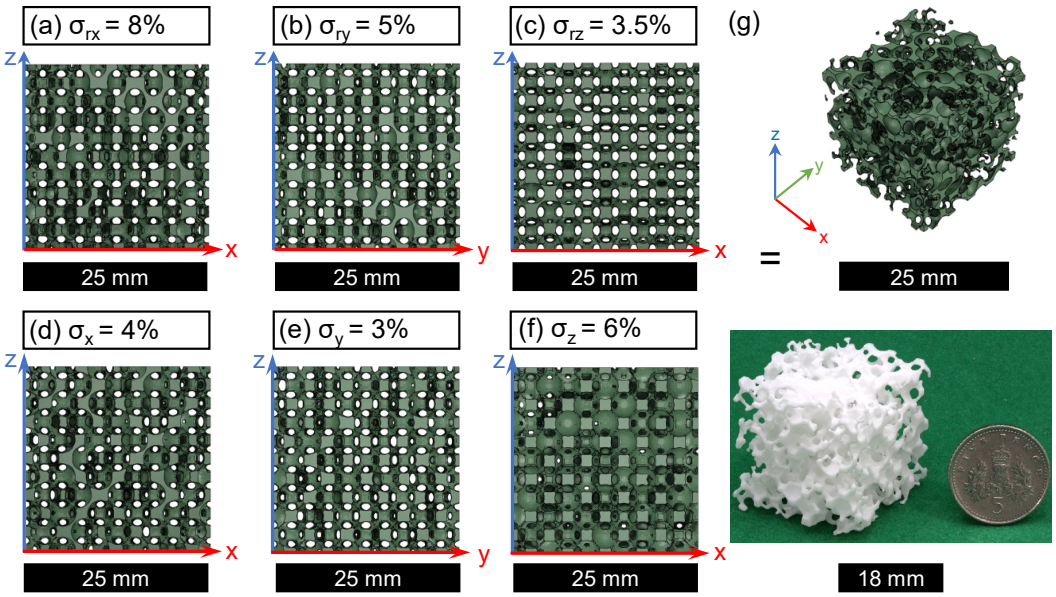

Figure 4.4: Anisotropic randomness applied to the cellular material defining parameters of a FCC cellular structure. Stochasticity applied to radii parameter a-c) and location parameter d-f). g) Stochasticity of a-f) combined and example manufactured by SLS.

4.2.5 Graded Randomness

After having introduced Isotropic and Anisotropic Randomness, Graded Randomness is presented. In Graded Randomness, the standard deviation that governs the Gaussian distribution is linearly graded from a low level to a high level of stochasticity as a function of a chosen direction. Taking the FCC unit cell as an example, the location and radius parameter in the x-direction can be graded from $0 - 6\%$, which results in Fig. 4.5 a) where a rendered and additively manufactured example is shown. A rendered and SLS sample is illustrated for the position and radii's y and z direction, as demonstrated in b) and c). b) present a stochastic gradient reaching from $0 - 5\%$ and c) illustrates a gradient from $0 - 4\%$. As these examples show, the stochasticity expands from a periodic cellular material to a stochastic one with increasing perturbation. It is also possible to overlay the stochastic cellular structures described in a-c) and create the stochastic cellular structure in d), simultaneously graded in the x, y, and z-direction. As can be seen in the cellular structure in the lower left corner, the periodic cellular material can still be identified and with increasing distance away from the lower left corner, the structure becomes more stochastic.

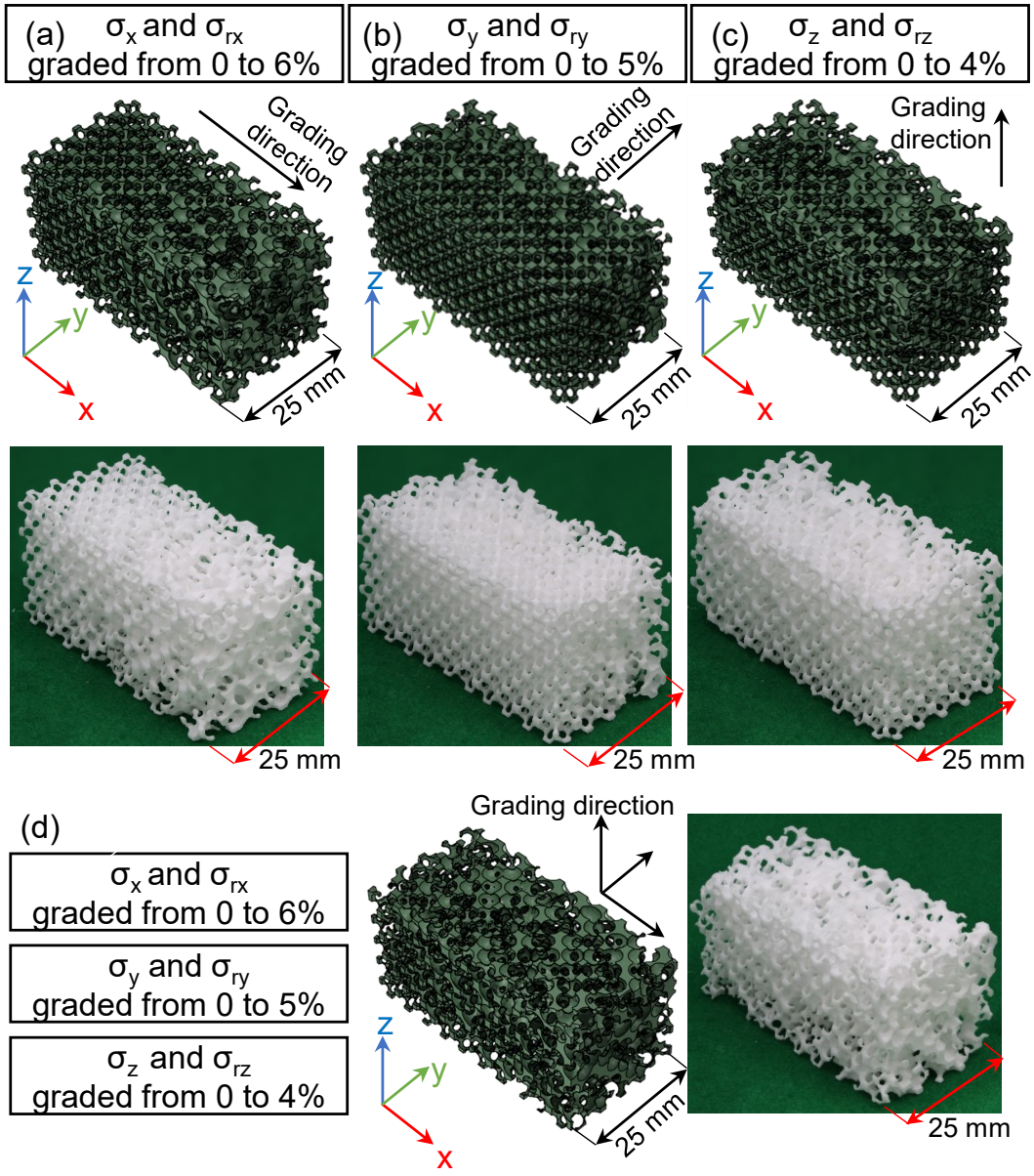

Figure 4.5: Graded Randomness is illustrated for a FCC cellular structure. Grading in a) x-, b) y- c) z-direction, and d) in the x, y, z-direction.

4.2.6 Layered Randomness

The Layered Randomness tool creates a stochastic layer within a defined cellular structure. In this case, the Layered Randomness tool is exemplified by a FCC unit cell that forms a cellular structure in which the layer is designed. The designed stochastic layers and their AM parts are shown in Fig. 4.6 a-c). a) shows a flat layer where the amplitude of the sine function is zero. In b), an amplitude and a period are applied to the sine function, and as such, a sine layer with a period of the length of

the cellular structure can be seen. In c), the period of the sine layer is shortened, and the result is the illustrated cellular structure. Judging by the sample, manufactured by SLS.

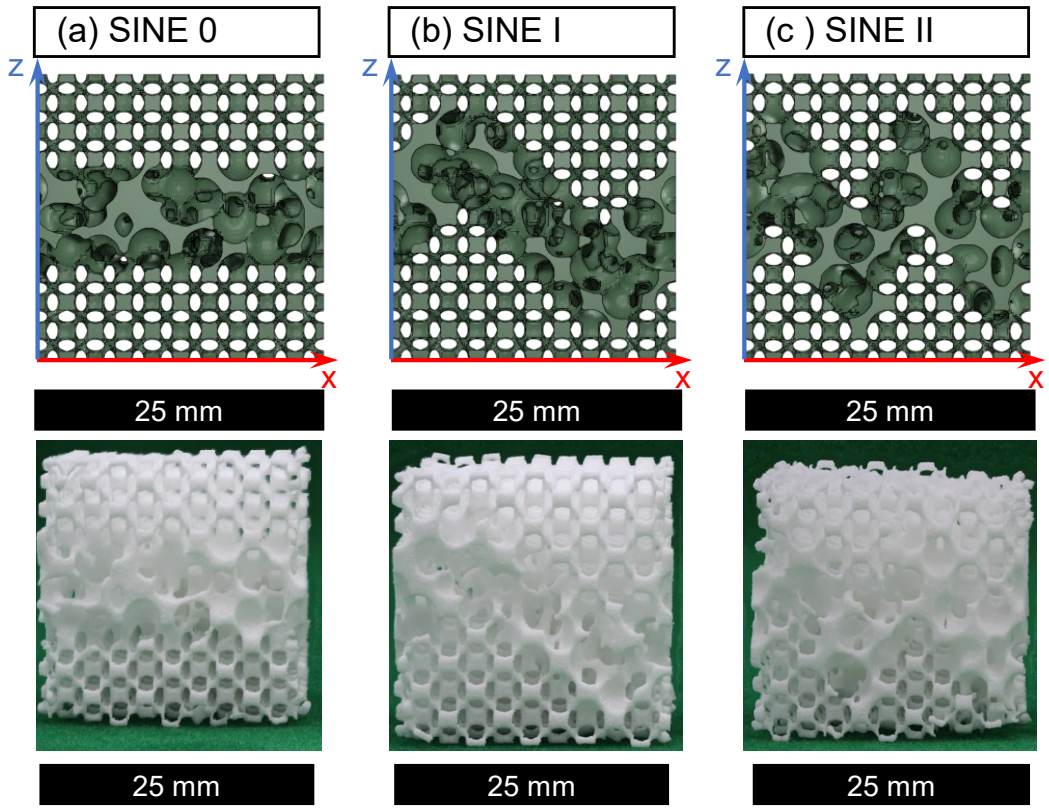

Figure 4.6: A sine function used to create different types of stochastic layers. a) a flat layer, b) and c) sine layers.

4.2.7 Surface Roughness

The fifth and final tool is the Stochastic Surface Roughness tool. Normally, when a cellular structure is designed, such as the rendered and additively manufactured regular FCC cellular structure in Fig. 4.7 a). The rendering presents a smooth surface, while the AM part exhibits a surface roughness related to the AM process. Here, stochastic surface roughness is introduced by using the described Gaussian randomisation process, which detects the near-surface area of the binary field and then randomises it. This results in a rough surface, as shown in b). Here, μ_{rough} is the amplitude of the roughness which should be applied, and σ_{rough} is its randomisation parameter. When looking at the SLS sample, it can be seen that some surface bumps are reproduced, but not the whole surface roughness is captured, which is linked to the rough surface roughness of the chosen SLS process.

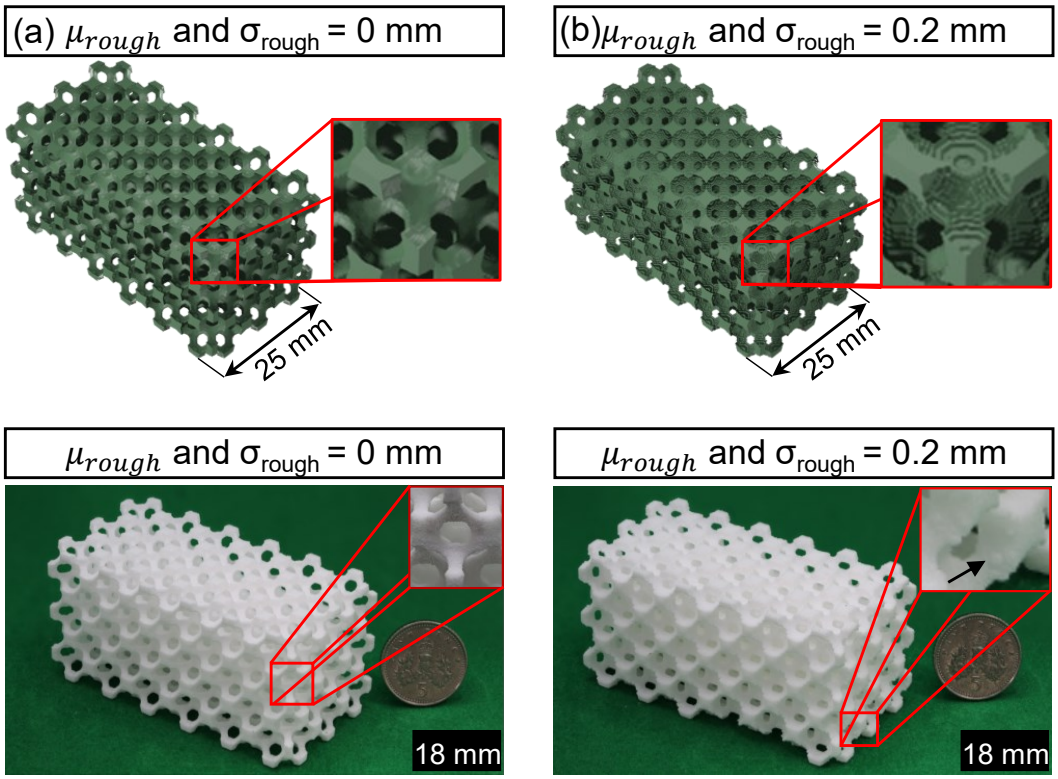

Figure 4.7: Application of stochastic surface roughness. a) presents a smooth FCC structure, including a SLS sample and b) illustrates a roughened structure where, in the magnification, a roughened surface can be seen.

4.2.8 Example Application

The FCC structure demonstrates a possible application such as a heat sink. Figure 4.8 illustrates a heat sink where a volume of 50x50x10 mm^3 is populated with the FCC shape to create a regular heat sink a) and b) a novel heat sink, which includes 2.5% stochasticity.

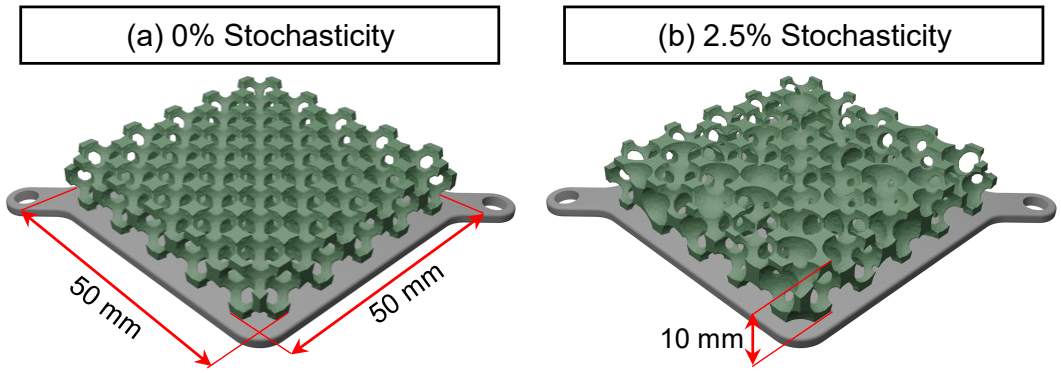

Figure 4.8: Regular and stochastic FCC-based heat sink.

4.3 Conclusions

This Chapter exemplifies five design strategies for stochastic design. It was shown that a Gaussian distribution is successfully drawn from an RNG and that stochasticity can be used in a design as long as the level of stochasticity is greater than the manufacturing tolerance. The design strategies were developed for strut-based cellular materials such as the Cubic, BCC, FCC, and FCC+ unit cells created by subtracting ellipsoids from a defined solid. The ellipsoid offers six parameters to be randomised, such as the radii and the x, y, and z positions. The first presented randomisation strategy is Isotropic Randomness, where all six randomisable parameters are controlled by one stochasticity parameter. This was followed by the second design tool, Anisotropic Randomness, where the parameters are individually randomised. The third tool introduced is Graded Randomness, where a parameter can be linearly varied in one direction from a low to a high level of stochasticity. This results in a linear gradient where the stochasticity parameter changes with the position. The fourth tool is a stochastic layer, where, according to a sine function, unit cells can be selected in the overall structure and stochasticity applied to form a layer with a distinct thickness, period, and amplitude, resulting in a stochastic layer. The fifth tool introduced is the Stochastic Surface Roughness tool, which can be applied to the previously discussed tools. Here, the binary field is randomised with an amplitude and stochasticity value that results in a rough surface.

These tools play an important role because they allow mimicking nature's variation and help make stochastic design available for the research community. This will help engineers across different research domains explore their acoustic properties, mechanical properties, or suitability for implant design, to name a few research fields.

However, these tools are currently limited to strut-based unit cells based on using ellipsoids for cellular material creation. The introduced stochasticity relies on the accuracy of the AM process. As designed in this Chapter, the Stochastic Surface Roughness could only be partly captured by the SLS process as the implicit manufacturing tolerance and the surface quality are imperfect. Nevertheless, other AM processes have better manufacturing tolerance and better surface quality, such as SL. In addition, because the surface roughness tool relies on a binary field, it is not a suitable method for structures based on signed distance or scalar fields.

As these tools were developed for one type of category of cellular material, the so-called strut-based cellular materials, there is also a need to use these design tools for TPMS structures to give more flexibility to the designer. The user feedback

could be improved by developing a user interface and integrating these design tools into easy-to-use software to make it usable and research-friendly. Finally, there is also a need to enhance the Stochastic Surface Roughness. The creation of surface roughness relied on noise, but continuous noise exists, such as Perlin noise [116], which would be better for creating a continuous surface roughness.
In summary, five stochastic design tools were presented for strut-based cellular materials. These include Isotropic, Anisotropic, Graded, Layered Randomness, and Stochastic Surface Roughness. This gives new opportunities to study the properties of these stochastic cellular materials for different engineering fields. However, this does not exist for TPMS structures and is described in the next Chapter.

Chapter 5

Stochastic design for sheet-based cellular materials

5.1 Introduction

The tool in the previous Chapter allows the application of different stochastic levels on cellular structures created from ellipsoids cut from a solid according to a crystal structure. This Chapter demonstrates a software tool that applies different levels of stochasticity and the previously described stochastic design strategies (Chapter 4) on TPMS-based cellular materials. This will enable other researchers to study the influence of different levels of stochasticity on the mechanical, acoustic, and other properties of TPMS cellular materials. Hence, this Chapter solves Research Gap No.2, combining the previously developed five stochastic design strategies with TPMS structures.

This Chapter is structured as follows. First, this section begins by illustrating Isotropic Randomness applied to common TPMS cellular structures such as the Gyroid, the Schwarz-D, and Schwarz-P structures. Isotropic Randomness means that only one stochasticity parameter controls all unit cell-defining parameters. Common errors associated with an increasing stochasticity level are described, and the introduced stochasticity at 5% is inspected to ensure the application of the intended Gaussian distributed values. Second, Anisotropic Randomness is shown. Anisotropic Randomness allows the application of controlled stochasticity of each unit cell, defining parameters separately, thus giving more control over the whole structure. It will be illustrated that increasing the stochasticity of the discretiser position while keeping the other parameter's stochasticity values constant increases the surface area and creates a more evenly distributed mass. Third, Graded Randomness is described where the stochasticity is linearly graded in different directions. However, a linear

gradient can also be used to grade stochasticity from a low to a high level in a radial manner. Fourth, using a sine function allows one to select cells according to this function and only randomise these values to form a layer. Fifth, using Perlin Noise to roughen the surface topology of the introduced TPMS structures allows for creating Stochastic Surface Roughness with increased surface area.

Further information: The figures used in this Chapter are part of the intended publication "Five simple tools for stochastic triply periodic minimal surface-based lattice creation", of which the author of the Ph.D. is the first author. For this research project, Oraib Al-Ketan (New York University Abu Dhabi) manufactured the cellular materials, provided the images of the additively manufactured objects, edited the intended publication, and wrote the part on the manufacturability in the intended publication. In a discussion, the author and Oraib Al-Ketan decided to use Perlin Noise to create the Stochastic Surface Roughness instead of the method described in the previous section. The author implemented the code.

5.2 Results

The following subsections present the application of different stochastic design strategies to TPMS structures.

5.2.1 Isotropic Randomness

In Figure 5.1, periodic cellular structures composed of a Gyroid TPMS a), a Schwarz-P TPMS b) and Schwarz-D TPMS c) are illustrated at the bottom (0% stochasticity level). The Schwarz-D TPMS structure is also shown as an AM structure in d). On the regular cellular structures, Isotropic Randomness levels of 2.5%, 5%, and 10% are introduced, producing noticeable defects. At 2.5% stochasticity, it can be seen that knots are formed at the intersection of different unit cells. These knots can become mass agglomerations at a stochastic level of 5% and 10%. At a stochastic level of 5% and 10%, low and high periods can be identified, which can, combined with a considerable variation in the relative density, form 'missing cells' at a stochastic level of 10%. At a stochastic level of 10%, these 'missing cells' are the result of low relative density levels combined with low periods which, when smaller than the resolution of the AM process, cannot be captured in the manufactured object.

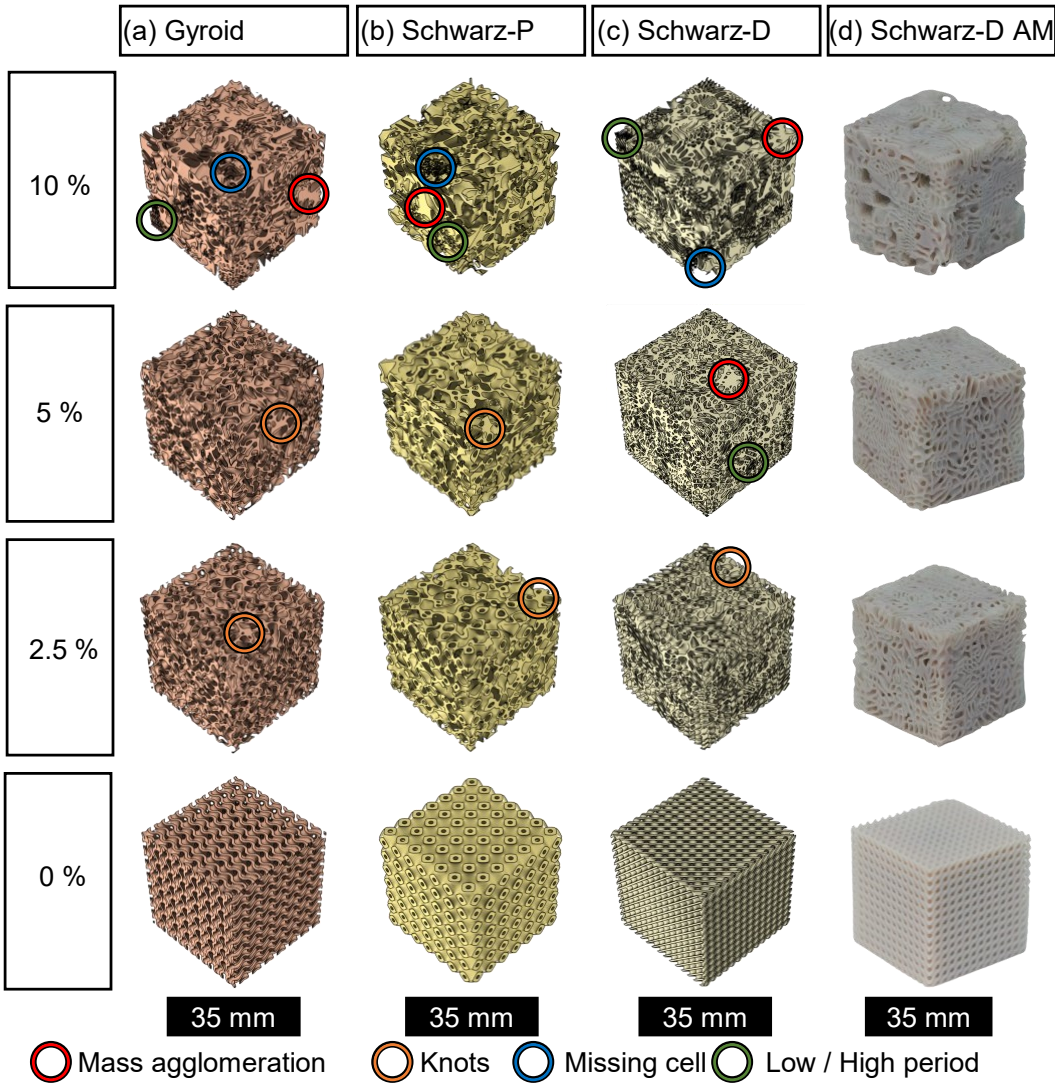

Figure 5.1: $0 - 10\%$ **isotropic randomness applied to different unit cells.** Rendered a) Gyroid, b) Schwarz-P, and c) Schwarz-D-based cellular material. d) additively manufactured Schwarz-D cellular material.

The defects mentioned in the Isotropic Randomness structures are magnified in Fig. 5.2. The presented defects originate from the Gyroid-based structure. In a) a knot is shown that formed at a stochastic level of 2.5%. This knot occurs when at least two different walls of a unit cell intersect each other. With increasing levels of stochasticity, for example, at 10%, the knots can become larger and form mass agglomerations (see b). A local increase in the relative density potentially causes this. The mass agglomerations can be identified when the knots grow to a size of at least half a unit cell. Another observable defect is illustrated in c), the missing cell. As evident from the illustration, a void appears in the cellular material. This void appears when the relative density is too low or the period becomes shorter. The early stage of a void is presented in d); the unit cell is formed with a low period, which

causes thin walls. The walls can still be noticed in the model. However, the AM process might not be able to manufacture this. These defects depend on the level of introduced stochasticity.

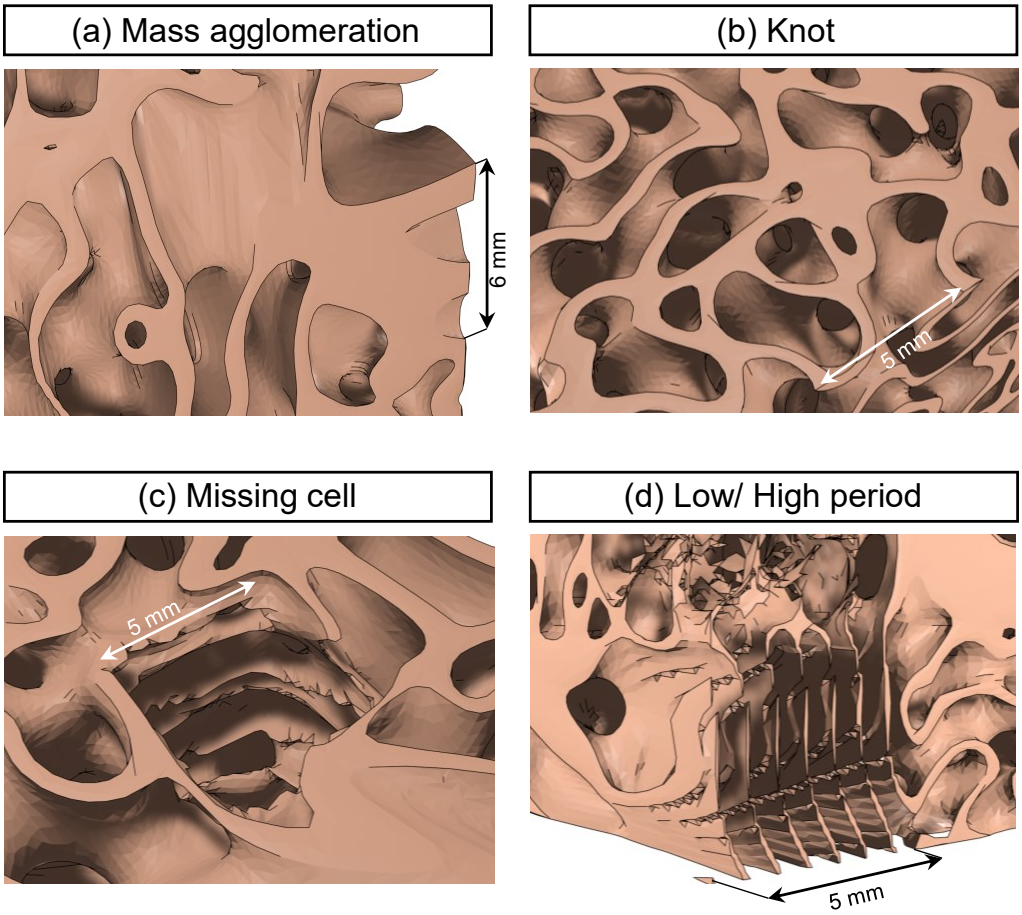

Figure 5.2: Magnified defects that occur after the application of stochasticity. a) Knot. b) Mass agglomeration. c) Missing cell. d) Low/ High period

If stochasticity is applied to a cellular structure, each unit cell's defining parameter is associated with a unique value resulting from a distribution from which the stochasticity is sampled. In this case, each parameter set is distributed according to a Gaussian distribution. The distribution of each of the ten defining TPMS unit cell parameters are illustrated for a Gyroid-based TPMS cellular structure in Fig. 5.3, where 5% Isotropic Randomness was applied to the overall structure. This structure is illustrated in k). The randomisation of the rotation α, β and γ is demonstrated in a-c), resembling the bell shape of a Gaussian distribution around the mean 0. In d-f), the period scaling factor is illustrated, showing a Gaussian distribution around the designed value of 1, and g-i) shows the distribution of the offset that is applied to the different discretiser positions in the x, y, and z direction. Finally, the relative density

and its distribution are shown in j), which, too, follows the shape of a Gaussian distribution.

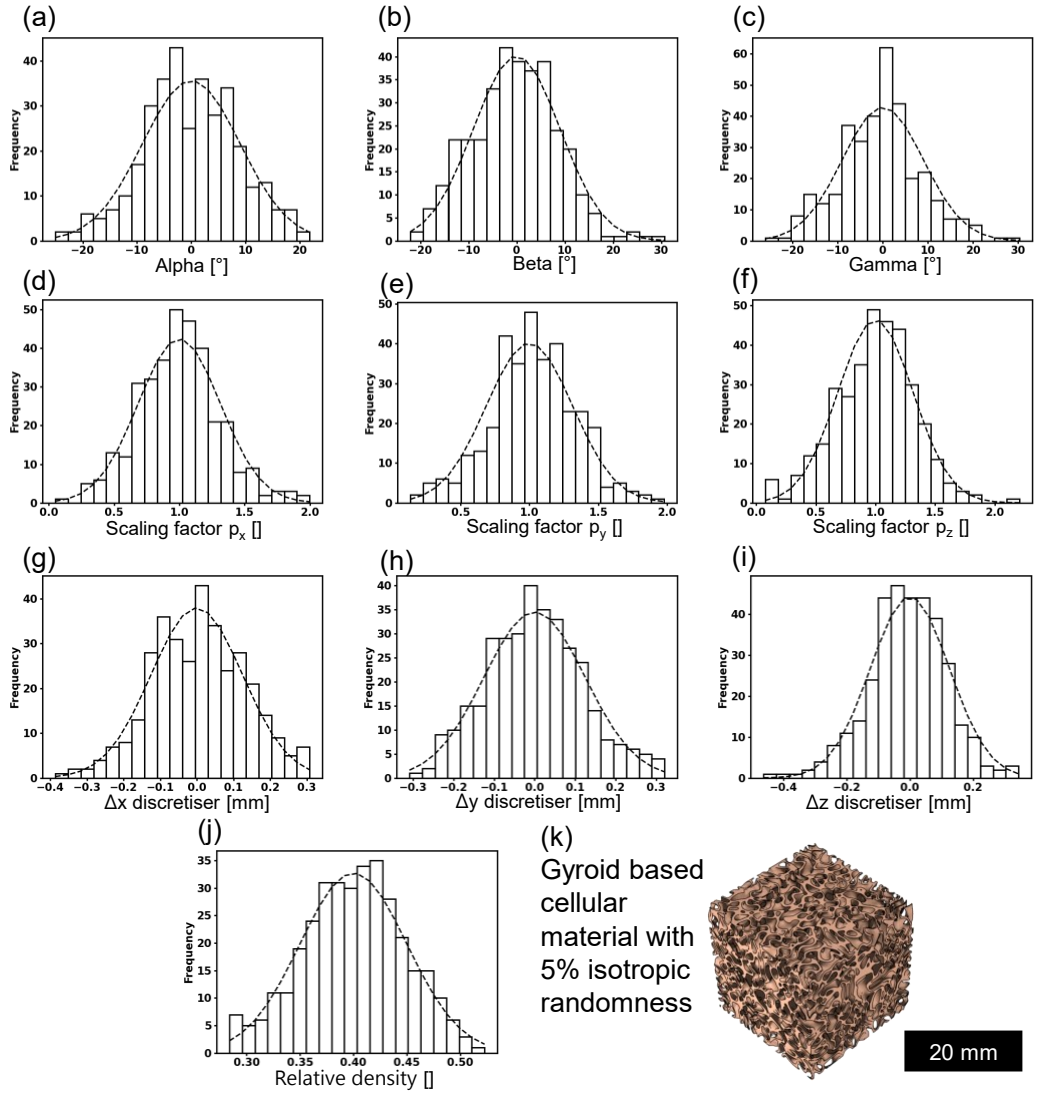

Figure 5.3: Gaussian parameter distributions of 5% isotropic randomness applied to a cellular structure composed of a Gyroid TPMS unit cells. a-c) α, β, and γ rotation. d-f) period scaling factor p_x, p_y, and p_z, g-i) Δx, Δy, and Δz discretiser, j) relative density, k) example stochastic cellular structure based on a Gyroid TPMS unit cell.

5.2.2 Anisotropic Randomness

In this section, the application of Anisotropic Randomness is demonstrated on a Gyroid-based cellular structure. Anisotropic Randomness allows control of the stochasticity of each parameter separately. Figure 5.4 shows how the Gyroid unit cell elements react to the stochasticity of the different unit cell defining parameters. The different colours show the various parameter values. Applying a stochastic

level of 5% to the α, β, and γ rotation results in many different angles, as shown in a-c). This is similar to the relative density where, through the randomisation process, a different relative density is applied to each single unit cell, and then interpolated to create a smooth transition from one unit cell to the other. e)-g) shows the randomisation of the period scaling factor in the x-direction e), y-direction f) and z-direction g). The result is that the period of unit cells can vary from a low period to a high period. A short and a long period are demonstrated in the magnification. In h) to j), an application of 25% stochasticity to the x, y, and z-position is presented. The magnification illustrates that this changes the bounding box of the randomised unit cell.

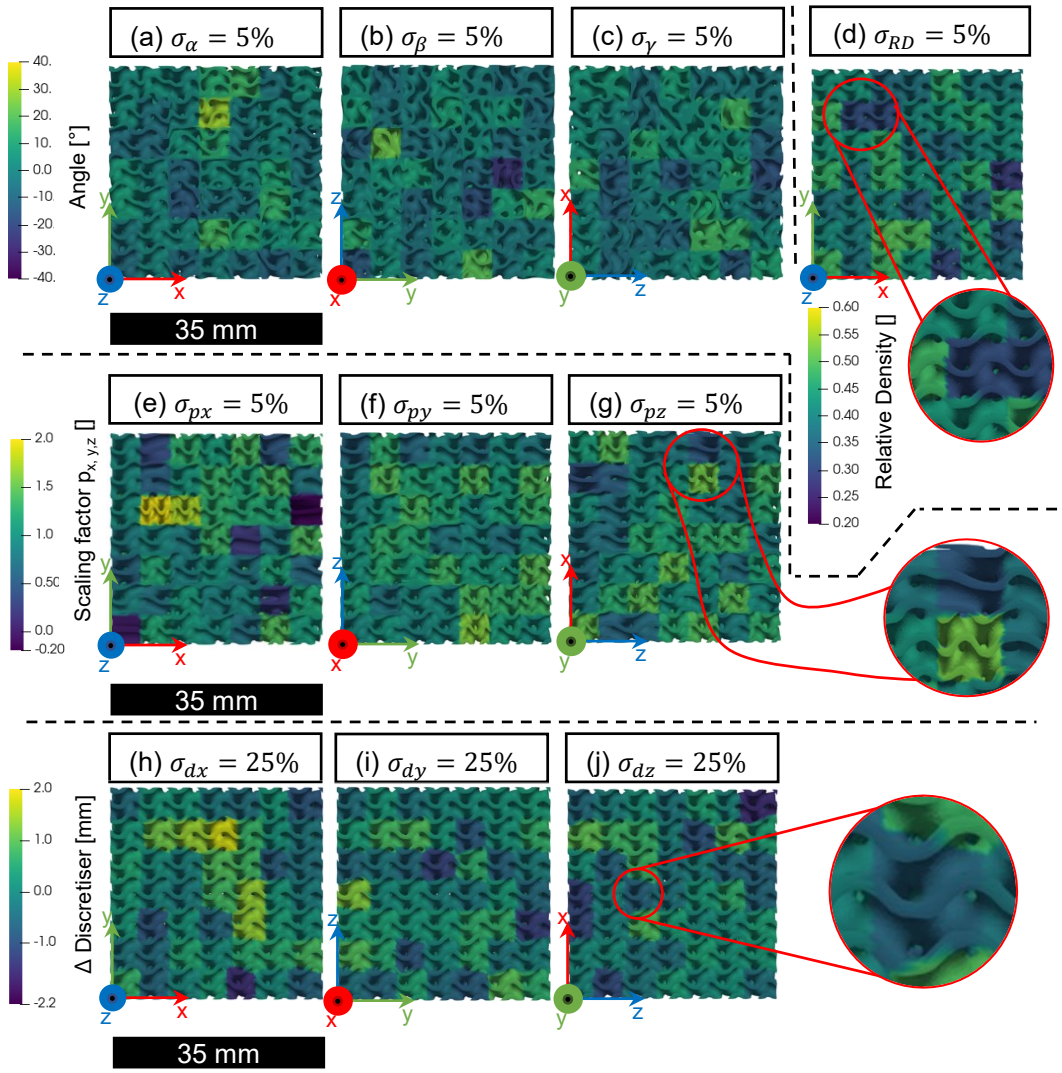

Figure 5.4: 5% **randomness applied to a single parameter of a cellular structure made up of Gyroid TPMS structures resulting in Anisotropic Randomness.** a-c) Rotation, d) Relative Density, e-g) Period Scaling Factor, h-j) Discretiser

The randomisation process influences the cellular material's properties, such as the relative density distribution or the surface area to volume ratio, as shown in Fig. 5.5. The cellular structure shown in b) is sliced at increments of 0.15 mm in the $x-y$ and z-direction. At each interval, the relative density is evaluated. In a), the standard deviation of the overall relative density distribution and the normalised surface area to volume ratio (A/V) is evaluated concerning the applied stochasticity levels ranging from 0% to 120% at distinct intervals. The discretiser stochasticity was altered, and the remaining parameters were kept at a constant stochastic parameter. Stochastic cellular structures based on a Gyroid TPMS structure are shown from c-g) where the discretiser stochasticity and, therefore, the different offset values of the applied stochasticity on the discretiser are represented by a colour map. The immediate effect of applying stochasticity is that the surface area increases by approximately 10% and stays nearly constant over the whole applied stochasticity range greater than 0% as illustrated in a). However, at a low level of stochasticity of roughly 2.5% x-discretiser stochasticity, a maximum level of heterogeneity of the relative density is reached. As seen in h), the increased heterogeneity directly results from an aggregation of mass at the interface between two adjacent unit cells. However, with increasing stochasticity, the heterogeneity decreases, and at around $25-30\%$ x-discretiser stochasticity, it falls below the relative density standard deviation of the periodic cellular material. The higher heterogeneity is shown by the green area, while the red area indicates a heterogeneity lower than the periodic cellular structure. With increasing x-discretiser randomness, precisely in the range of $80-120\%$ stochasticity, the standard deviation of the relative density drops to a value which is approximately half the standard deviation of the regular structure. This decrease in the heterogeneity of the relative density can be seen in h), where the peaks smooth out, thus indicating the less heterogeneous distribution of mass in the cellular structure.

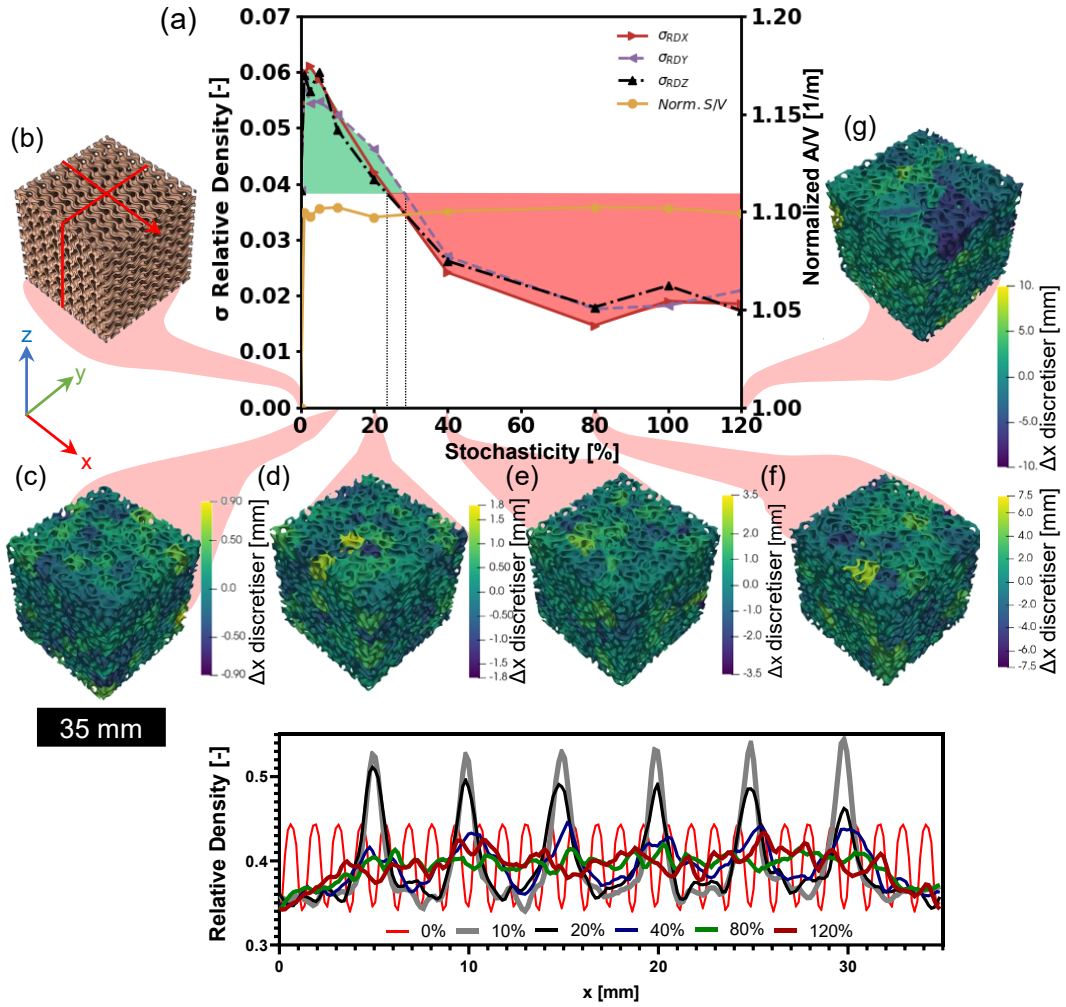

Figure 5.5: Influence of the level of stochasticity on the standard deviation of the relative density and the normalised surface area to volume ratio.

5.2.3 Graded Randomness

The random sampling process can be coupled with a gradient where the standard deviation is used to randomise the structure from low to high levels of spatial stochasticity. This is demonstrated for different TPMS structures in Fig. 5.6 where the stochasticity is linearly graded from 0% to 1.4% for a specific parameter in a particular direction. In a) the α rotation stochasticity is graded in the x-direction, in b) the stochastic grading in the y-direction of the β rotation is illustrated, and in c) the grading of the γ rotation is presented. Additionally, in d), the superposition of parameter-specific directional stochastic grading of a-c) is shown. From a) to d), graded randomness was shown based on Gyroid unit cells. However, the same method can be applied to the α rotation with Graded Randomness in the x-direction for a Schwarz-P e) and Schwarz-D f) unit cell.

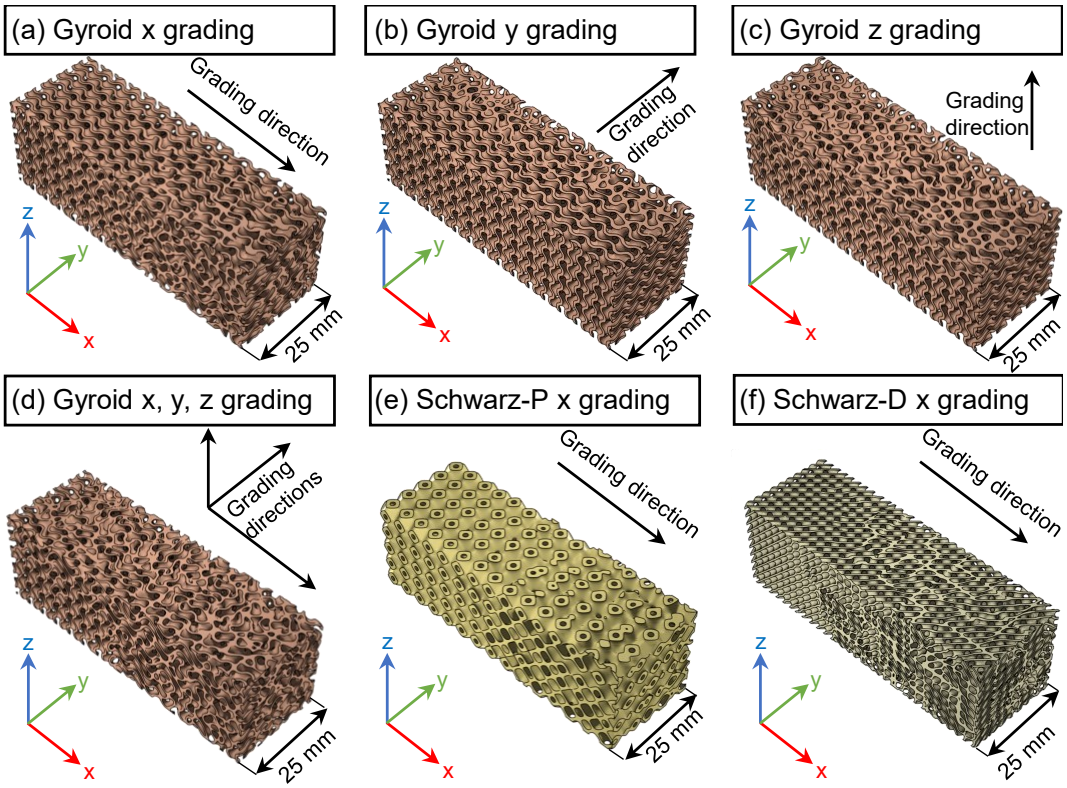

Figure 5.6: Graded randomness from a low level to a high level of stochasticity applied in different directions and to different TPMS unit cells. Graded randomness applied to the x-direction a), e), f), y-direction b), z-direction c).

5.2.4 Radial Randomness

Figure 5.7 illustrates the use of Radial Randomness, where the stochasticity linearly expands from a centre from a low level to a high level. In a), this can be seen for a Gyroid-based TPMS structure, in b) for a Schwarz-P-based TPMS structure and in c) Schwarz-D TPMS structure.

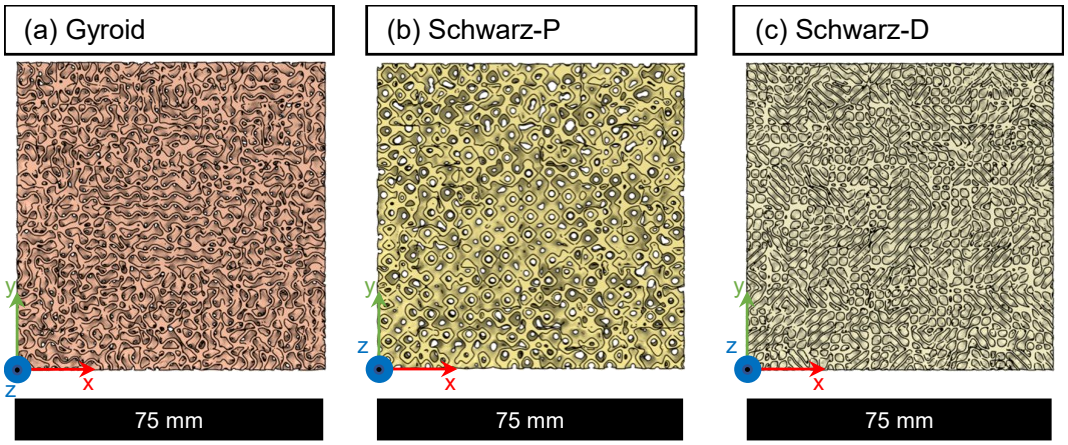

Figure 5.7: Radial randomness expanding from the centre of the stochastic cellular structure from a low level to a high level of stochasticity. The radial randomness is demonstrated in a) a Gyroid, b) Schwarz-P and c) Schwarz-D unit cell-based cellular structure.

5.2.5 Layered Randomness

Figure 5.8 demonstrates several examples of applying a stochastic layer based on a sine function. Applying a sine function with a zero amplitude allows a flat stochastic layer a) to be constructed within a periodic Gyroid-based cellular structure. By setting the period of the sine curve to the length of the Gyroid-based cellular structure, a sine curve as shown in b) can be designed, and if the period is doubled, a structure such as described in c) is the result. The stochastic sine layer, as shown in b), can be employed to a Schwarz-P d) or Schwarz-D e) based cellular structure, which could be then manufactured by an AM process as shown in f).

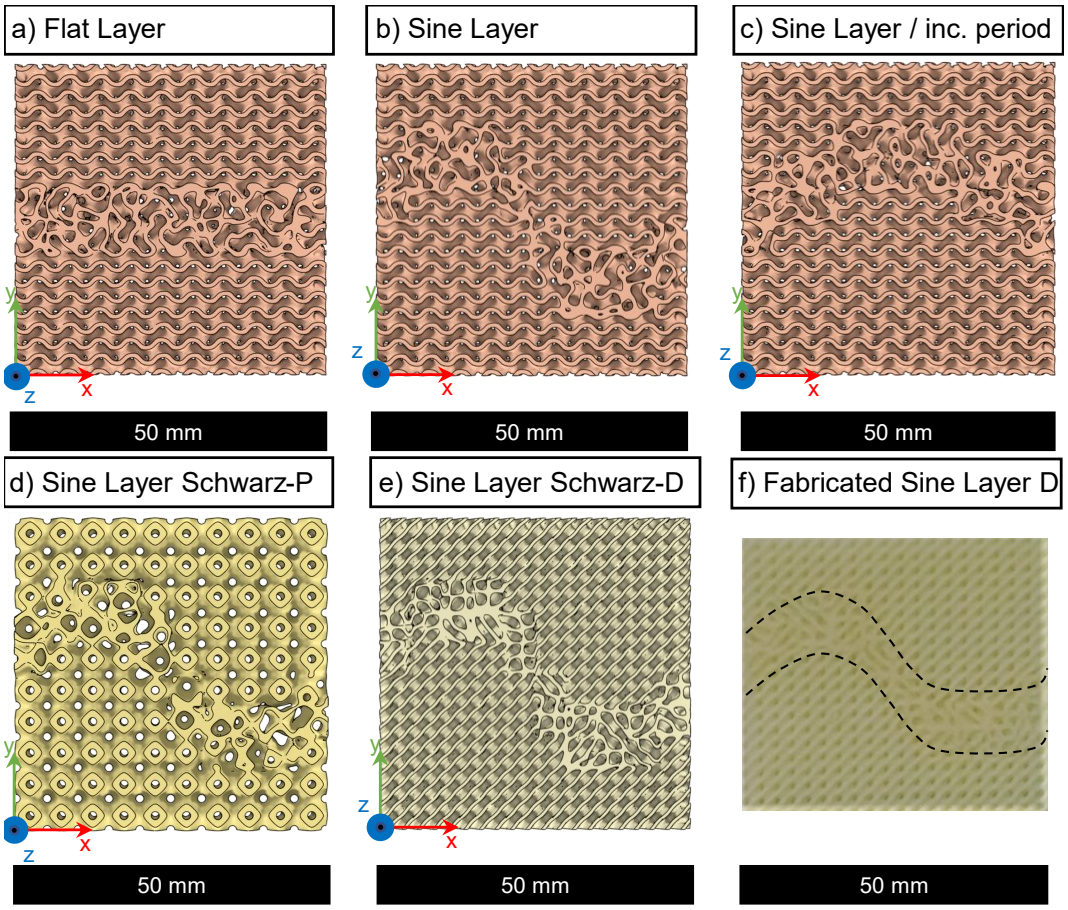

Figure 5.8: Stochastic sine layer applied to different TPMS unit cell types. a-c) Gyroid, d) Schwarz-P, e-f) Schwarz-D.

5.2.6 Surface Roughness

Figure 5.9 and 5.10 illustrate using Perlin Noise to create a rough surface topology on TPMS-based cellular structures. Perlin Noise can be adjusted for a TPMS-based cellular material in many different ways as presented in Fig. 5.9. As a comparison, a) shows a smooth and periodic Gyroid-based cellular structure on which the different Perlin Noise operations are performed. The standard Perlin Noise, ranging from [-1, 1] is applied to the Gyroid structure; the result is shown in b). In the highlighted area, a bump can be seen. (The Perlin Noise is a scalar field and thus has to be adjusted to the scalar field of the different TPMS structures to create roughness.) This bump's height can be adjusted by transforming the Perlin Noise scalar field to a new range, as shown in c) to e). Here, the scalar field range is scaled down to [-0.75, 0.75], [-0.5, 0.5], and [-0.25, 0.25], respectively, resulting in smaller bumps. However, the Perlin Noise can also be applied with different layers, persistence, and lacunarity. With each applied layer, the persistence (amplitude) and lacunarity (frequency) change;

this means that at a persistence of 0.5 and a lacunarity of 2, the bump size halves but is more frequent, f). However, setting the persistence to 0.25 will result in even smaller bumps as shown in g), and changing the lacunarity to 4 results in more frequent smaller bumps, as illustrated in h).

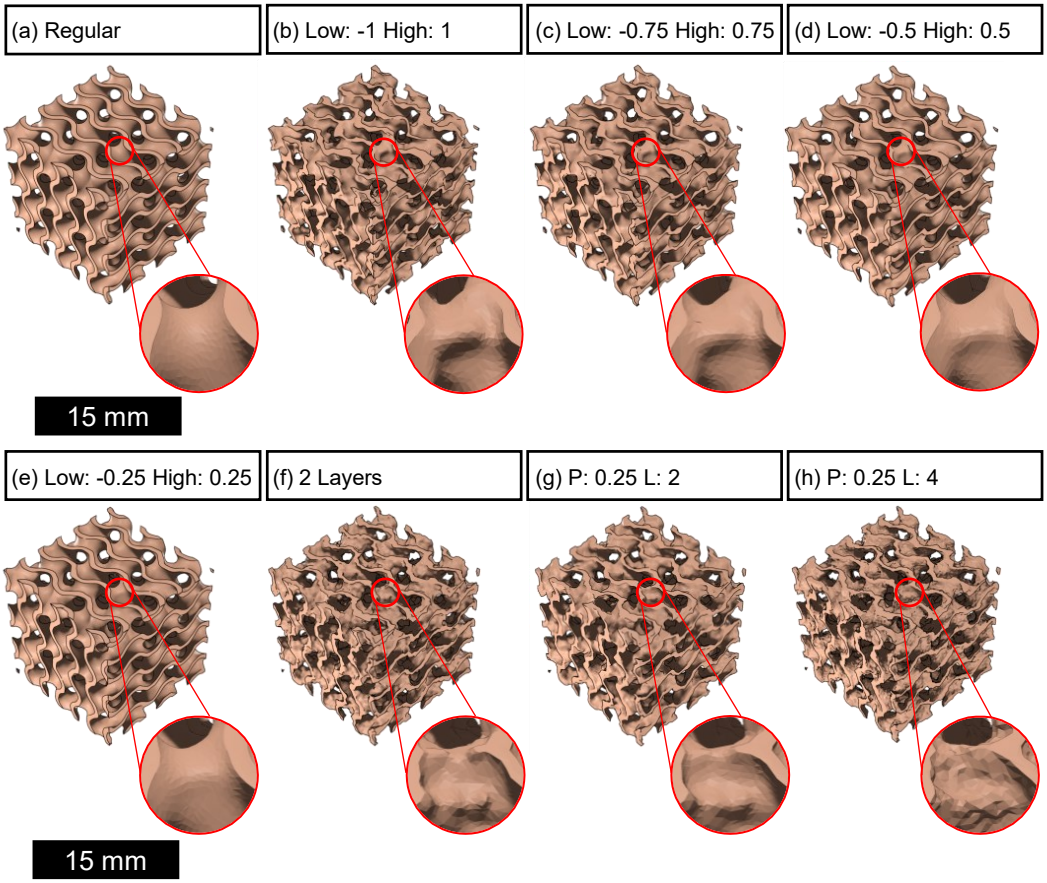

Figure 5.9: Perlin Noise applied to a periodic Gyroid cellular material changing the surface topology of the cellular structure. Persistence: P, Lacunarity: L

The application of Perlin Noise is not limited to the sheet-based Gyroid TPMS structure and can be applied to the strut-based Gyroid structure as shown in Fig. 5.10 a). It can be used on already randomised TPMS structures b) and on different unit cells such as the Schwarz-P c) and Schwarz-D d) unit cells. The cellular structures on which Perlin Noise was applied can also be additively manufactured as shown in e-h).

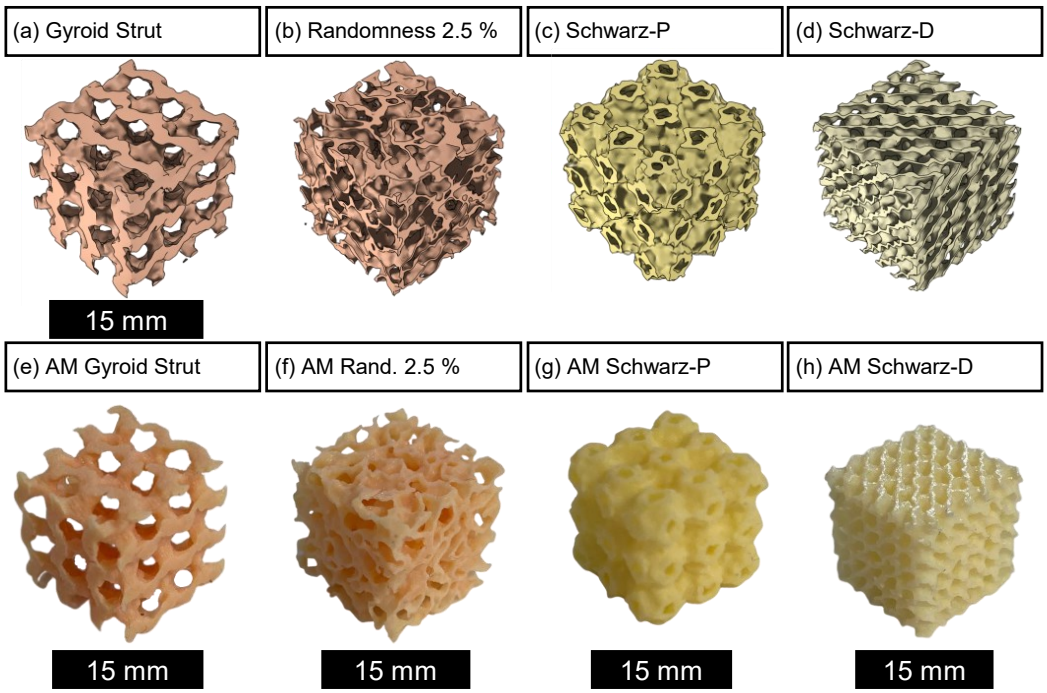

Figure 5.10: Perlin Noise introduced to different types of cellular structures. L: Lacunarity, P: Persistence.

As presented, the utilisation of surface roughness for cellular materials lead to a perturbed surface topology. Adding Perlin Noise to the Gyroid, Schwarz-D, and Schwarz-P cellular material unit cells where the Amplitude is scaled from zero to one, increases the surface area to volume ratio of the cellular structures. At an Amplitude of one, the surface area to volume ratio of the Gyroid and Schwarz-D cellular material increased by approximately 13% and the Schwarz-P by around 17% when compared to the periodic cellular material, indicating that the surface area increased. The results are presented in Fig. 5.11.

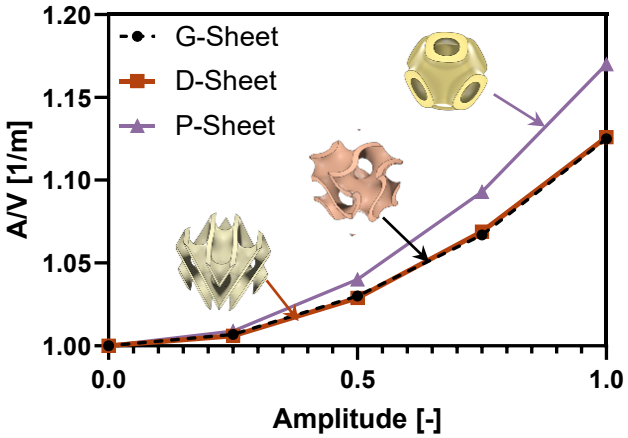

Figure 5.11: Influence of the Perlin Noise amplitude on the normalised surface area to volume ratio $A\backslash V$.

5.2.7 Example Application

Similar to the previous Chapter 4, the same volume of 50x50x10 mm^3 is populated with the traditional regular Gyroid cellular structure with a unit cell size of 10x10x10 mm^3, as illustrated in Fig. 5.12 a). In b) the novel heat sink comprises a stochastic Gyroid-based structure with 2.5% introduced stochasticity.

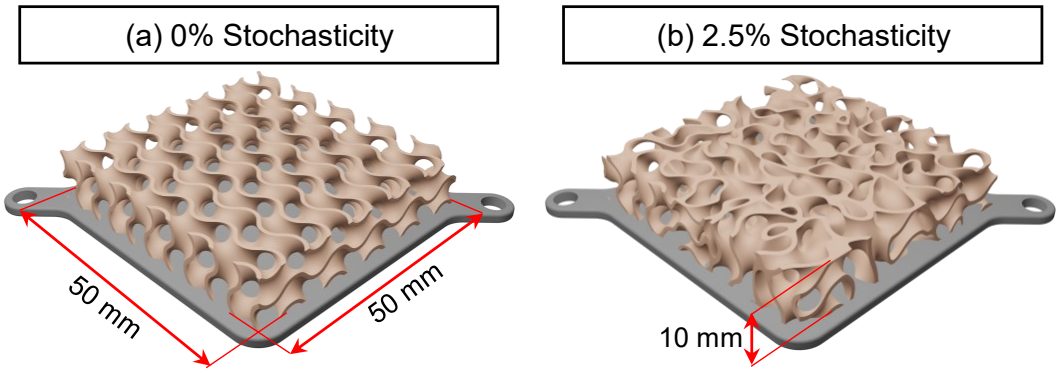

Figure 5.12: Regular and stochastic Gyroid-based heat sink.

5.3 Conclusions

This Chapter introduced five tools to design stochastic cellular structures based on TPMS cellular materials. The five demonstrated tools include Isotropic Randomness (randomisation with a single stochasticity parameter). Increased stochasticity led to

voids at a stochastic level of 10%, visible in the AM process. Anisotropic Randomness uses a randomisation parameter for every defined parameter of a TPMS unit cell. Increasing the stochasticity of the discretiser position affected the distribution of the relative density, resulting in an increase in heterogeneity for stochasticity values lower than $25-30\%$ and a decrease of heterogeneity for greater stochasticity values than the relative density distribution of the periodic structure. Graded Randomness was illustrated by combining the applied stochasticity with a linear function to linearly grade the stochasticity parameters in the x, y, and z directions or different directions. Additionally, a radially linear graded randomness can be achieved in the x and y plane. Layered Randomness was demonstrated where a layer of randomised unit cells was created by a sine function where the amplitude, period, thickness, and position in the cellular structure could be altered. This resulted in either a flat layer or a layer with an amplitude and different period. Finally, Perlin Noise was used to modify the surface topology of a cellular structure, which causes a rough surface. Adding roughness led to an increased surface area; depending on the chosen Perlin Noise amplitude and the unit cell, the surface area can be up to 17% higher. The proposed design tools for stochastic cellular structures have some limitations. This includes the formation of voids or fine details at higher stochastic levels, such as at 10% in the Isotropic Randomness tool. Choosing an appropriate stochasticity level for AM can avoid this.

The proposed tools are script-based design tools, so developing a user-friendly GUI is necessary to make these tools readily available for researchers. Furthermore, it is helpful to adapt the scripts for surface elements.

In summary, five randomisation tools for the creation of TPMS-based stochastic cellular materials were introduced, which allow the application of Isotropic Randomness, Anisotropic Randomness, Graded Randomness, Layered Randomness, and Stochastic Surface Roughness to the desired TPMS structure. These tools are well suited for AM and should be used to drive research to explore the influence of different levels of stochasticity on, for example, the heat transfer or mechanical properties of the described structures.

Chapter 6

Stochastic design

6.1 Introduction

This Chapter will introduce the concept of stochastic design and solve Research Gap No.3, introducing design rules and strategies. This Chapter is separated into two sections. The results and the conclusions. The result section first demonstrates what must be considered to set up a stochastic system using the Gaussian distribution. This will involve how the standard deviation can be defined within a minimum and maximum level. Second, the terms Isotropic and Anisotropic Randomness are defined and exemplified to introduce the first two stochastic design strategies (Inspired by [51]). Third, the discussed setup and design strategies are exemplified on a surface element array where stochasticity is added to the positional parameters. It is important to clarify that this approach is not limited to surface elements; the shark-skin surface element is chosen as an example and could be replaced by other surface elements or cellular materials. If the width of an object is tied to the distance to the nearest neighbour, the appearance of an array changes. The stochasticity of the width of a shark denticle can be designed within a range that nature intended. Finally, it is demonstrated that other distributions can also be used to design stochastic structures. Additionally, important design rules are summarised.

Further information: This Chapter is based on the publication “Stochastic design for additive manufacture of true biomimetic populations” of which the author of this thesis is the first author.

6.2 Results

The result section is separated into five parts. At first, the necessary design considerations to choose an appropriate stochasticity level is discussed. Subsequently, the design strategies Isotropic Randomness and Anisotropic Randomness are introduced. These two design strategies are then exemplified using a shark skin unit cell (The shark skin unit cell is a demonstrator). The results from this subsection are then used to present a linear model to design a shark skin with a natural distribution. Finally, the utilisation of the Weibull distribution is shown to demonstrate that other distributions could be potentially used, too.

6.2.1 Stochastic design level consideration

The concept of stochastic design relies on adding variation to a uniform array that comprises unit cells. Naturally occurring unit cells are cellular material unit cells or surface-related elements such as denticles, cones, or cylinders. A biological shark skin unit cell is chosen as a demonstrator to demonstrate the principle, shown in Fig. 6.1. A shark skin unit cell can be described by a location x, y, width w_s, angle β_S, and a unique surface topology. A plurality of these unit cells will form an array. An array without variation is considered a uniform array, and an array that includes variation is considered a stochastic array. The question is: What are the limitations of stochasticity? Hence, a lower limit of stochasticity σ_{min} and a maximum limit σ_{max} exist. The lower limit of stochasticity depends on the implicit manufacturing tolerance (Fig.6.1 black line). Thus, the introduced stochasticity must be greater than the implicit manufacturing tolerance to be recognised as different. Furthermore, the maximum limit of stochasticity is where the system collapses (Fig.6.1 red line). 'System collapse' means that a condition occurs that limits the performance of the designed array. The engineered stochasticity is the stochastic level between the manufacturing tolerance and the system collapse (Fig.6.1 green line).

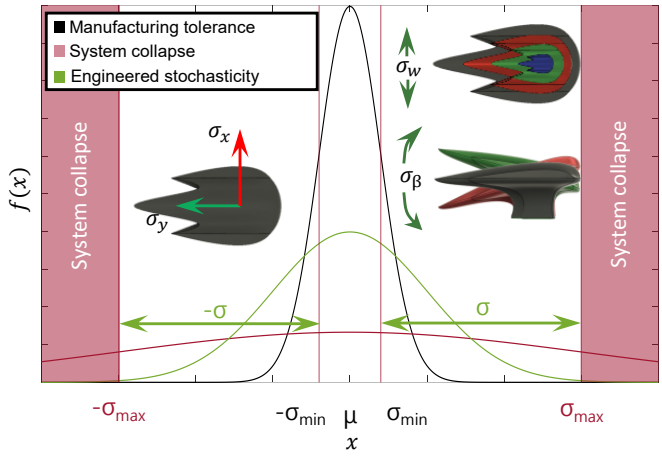

Figure 6.1: Stochastic design level consideration chart. The introduced stochasticity level σ is between the manufacturing tolerance σ_{min} and the system collapse σ_{max}.

6.2.2 Concept of isotropic and anisotropic randomness

After introducing the maximum and minimum stochasticity levels, the first two design strategies are presented. For example, a uniform 2D array Fig. 6.2 a) of dots is chosen for simplicity. On each of the dots with a positional value x and y, an offset can be added, sampled from a Gaussian pseudo-RNG, where the standard deviation allows tuning the variation of the system. If the same standard deviation is used for the x and y location, as illustrated in Fig. 6.2, an array is created where the positional stochasticity is the same in both directions. This is called Isotropic Randomness. However, if the standard deviations differ, as shown in Fig. 6.2, the stochasticity is more pronounced in one direction than in the other. Here, e.g. the irregularity in the y direction is more potent than in the x direction. This design strategy is referred to as Anisotropic Randomness.

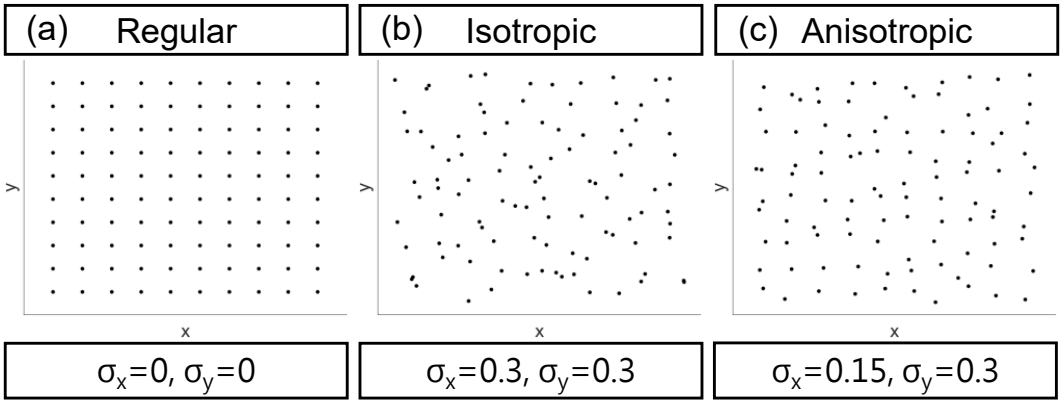

Figure 6.2: Introduction of a different level of stochasticity to the positional parameter. a) illustrates a regular array composed of dots. b) shows a perturbed array where the same standard deviation is introduced to the positional parameter called Isotropic Randomness. c) shows two different standard deviations resulting in a more pronounced disorder in the y direction compared to the x direction. This is termed Anisotropic Randomness.

The concept of Anisotropic Randomness can be used for any pair of at least two parameters such as location parameters, rotational parameters, periodic functions, etc., which define the shape and position of a geometry.

6.2.3 Application of different stochastic design levels to shark skin

Isotropic and Anisotropic Randomness is introduced to the x and y location parameters of an array of an example geometry. As an example geometry, a shark skin unit cell is used, where the width results from a nearest-neighbour approach; thus, overlaps are prevented. Three sets with 9 shark skin arrays are created as illustrated in Fig. 6.3 a) to c). A stochasticity level of 0, 0.4, and 0.8 mm is introduced to the x and y locations. The uniform array can be found in the lower left corner of a-c). Increasing the stochasticity independently in the x or y direction leads to Anisotropic Randomness. On the diagonal, Isotropic Randomness shark skin arrays can be identified. Increasing the stochasticity increases the distance between the shark skin denticles, indicated by the larger gaps. It can be seen that the difference between the largest and smallest shark denticles increases with increasing stochasticity. This observation can be confirmed by the violin plots, as shown in Fig. 6.4 d). The lower left corner of the violin plots shows that all shark denticles have the same width in the uniform array. According to the introduced Gaussian distribution, the spread is also expected to increase with increasing stochasticity. The upper right corner demonstrates this. The spread of the three arrays is large. Thus, the violin plots

flatten, and extreme width in the lower and upper range occurs. This can be seen in the shark denticle arrays exhibiting 0.8 mm variation. In the literature, it was mentioned that the aspect ratio of shark skin and the shark skin length ranges approximately from $1-9\%$ [44] (Fig. 1.4 a)). Taking this into consideration and linking the introduced stochasticity of 0.4 and 0.8 mm to x_{sg}, the stochasticity parameter for the x direction would lead to 8% and 16%, respectively. Thus, the expected natural reproductions of shark skin could be assumed between an introduced standard deviation of 0 to 0.4 mm. That shows that variation is included. However, extremes with large discrepancies in the width between the largest and smallest denticles with resulting large gaps might not be favoured to design within this *natural range*. It is reasonable to assume that large stochasticity values are not favoured in nature because a small unit cell behind a large unit cell (see Fig.6.2 a) 0.8/0.8) will have a limited effect on, for example, drag reduction because it is over-dominated by the larger unit cell. This essentially makes the too-small unit cell redundant. To design the width requires some additional analysis, which will be done after the demonstration of printability of some of the previously shown examples.

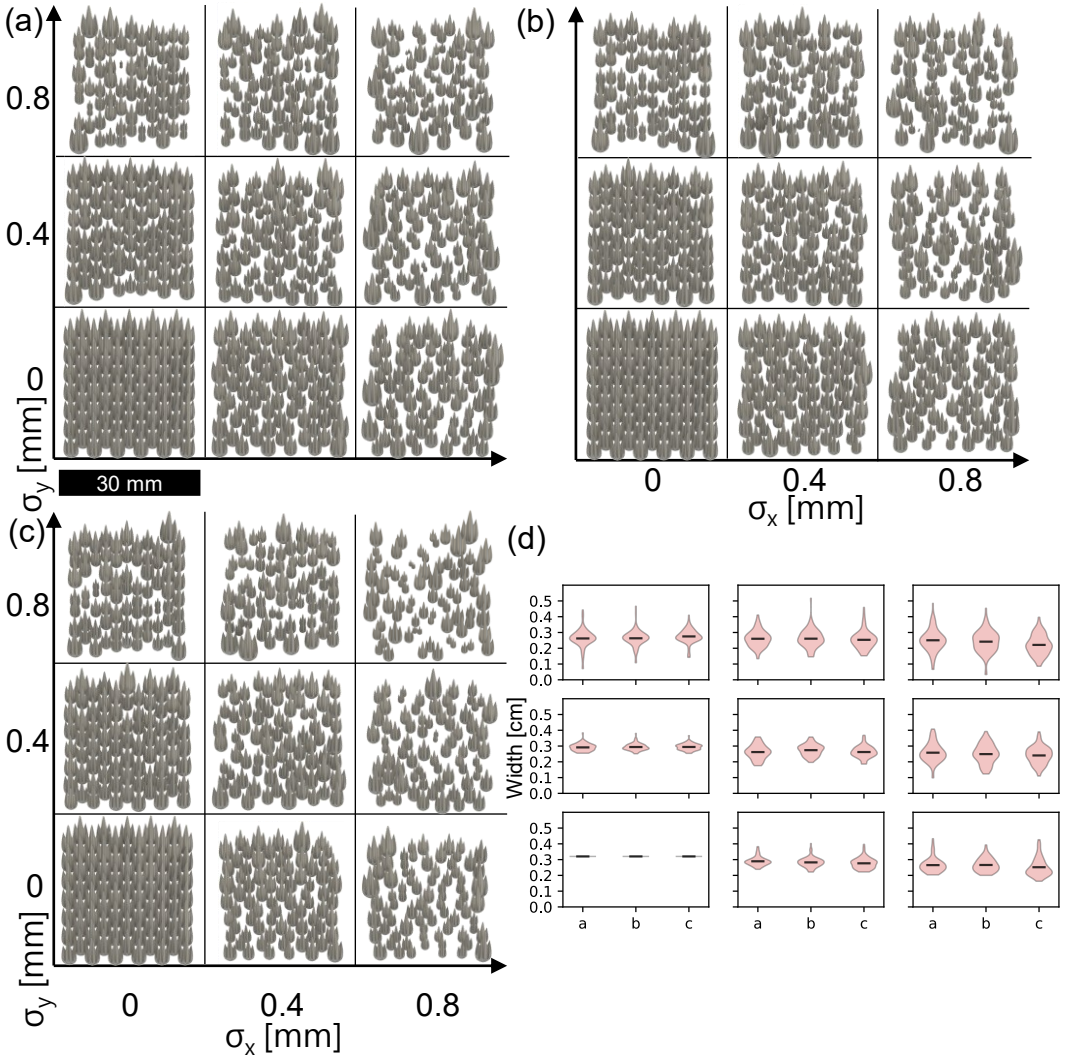

Figure 6.3: Several shark denticle arrays and their width distribution. a)-c) three sets of nine shark denticle arrays illustrating isotropic and anisotropic randomness. d) shows violin graphs of the width distribution of each array of the arrays shown in a) to c).

The arrays, including Isotropic Randomness, Fig. 6.3 a), with a stochasticity level of 0, 0.4 and 0.8 mm are used to demonstrate manufacturability through a generic AM process. A SL process is used to manufacture these samples, as shown in Fig. 6.4. The stochasticity in these arrays increases from 0 a), 0.4 b) to 0.8 mm c). In b) and c), the magnification shows that the manufacturing process can capture details of the ridges.

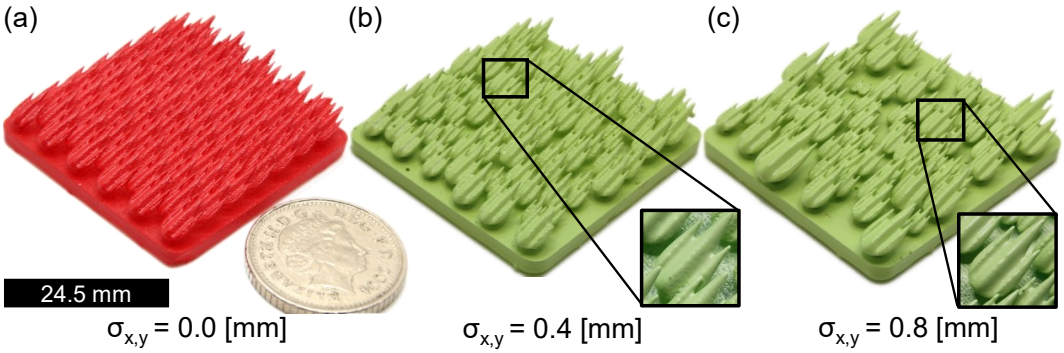

Figure 6.4: Shark skin arrays with different values of Isotropic Randomness.

To better design with stochasticity, such as replicating nature in a more accurate way, it is necessary to understand the effect of the positional stochasticity on the width and its distribution. Figure 6.5 shows the effect of different stochasticity levels on the width, standard deviation of the width, and the stochasticity level. In a), it can be seen that the average width reduces with increasing variation from approximately 3 mm to 2 mm. After reaching a minimum, it increases to the initial average width. This is because if increased variation is added to the uniform array, variation below 4 mm (smaller than the defined unit cell) causes the objects to be closer to one another. Thus, smaller denticles appear. Beyond a variation of 4 mm (larger than the defined unit cell), the objects can step out of the designated unit cell, resulting in more space between objects, thus increasing the width. If only a fraction of the stochasticity level is considered between 0 and 1 mm, as shown in b), it is apparent that the behaviour of the average width is approximately linear. This information can be used to derive a design equation (see Section 6.2.4). The shark denticle width decreases from approximately 3 mm to 2 mm. The introduction of variation into the system affects the average width and influences the width's standard deviation c), d). As illustrated, the width variation increases with increasing introduced variation. The average width and standard deviation indicate stochasticity; therefore, combining them into a single parameter is reasonable. This single parameter is the stochasticity parameter that combines the standard deviation with its design parameter (average width). The combination of the width's standard deviation and the average width can be seen in e) and f). e) demonstrates that the stochasticity increases steeply to a positional variation of around 2 mm. In f), the relative randomness increases from 0 to 40% within a range from $0 - 1$ mm.

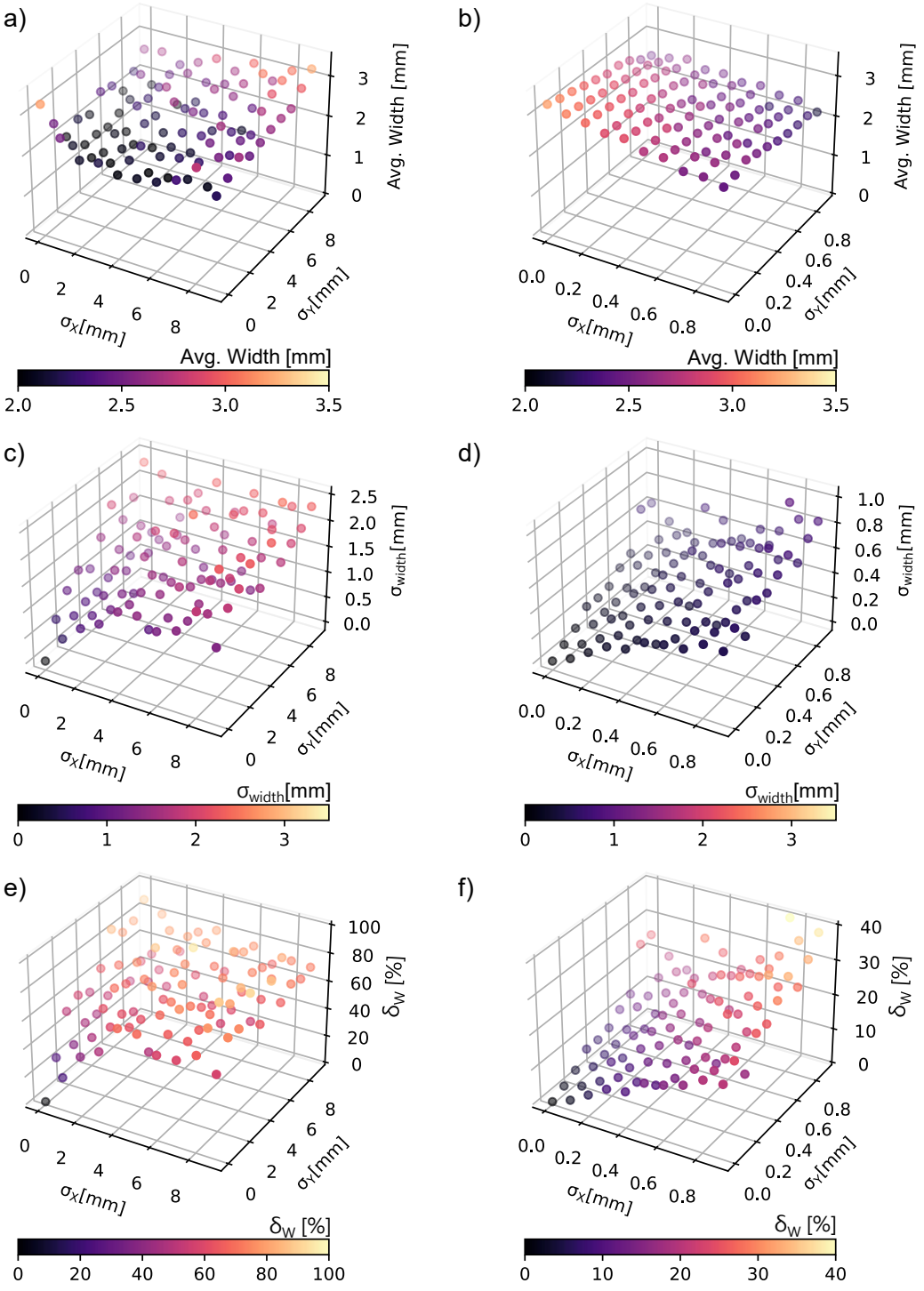

Figure 6.5: Influence of the stochasticity level of the positional parameters x and y on array parameters. Influence on the average width a) and b), the standard deviation of the width c) and d), and the stochasticity level of the width e) and f).

6.2.4 Designing a shark skin with nature-like variation

From the parameter evaluation, as shown in Fig. 6.5 f), a simple linear equation Eq.6.1 ($R^2 = 0.98$) can be derived to design a shark denticle array that includes variation as found in nature.

$$\sigma_W(\sigma_x, \sigma_y) = 18.32\sigma_x + 21.32\sigma_y \tag{6.1}$$

Depending on the location of denticles on a shark, Ankhelyi et al.'s [44] data suggests that stochasticity of the shark denticle's width ranges approximately from 1% to 8%. Here, a stochasticity level of 5% is chosen, which yields to $\sigma_x = \sigma_y = 0.13$. The resulting shark denticle array is demonstrated in Fig. 6.6 a) and b). a) shows through utilising Voronoi tesselation and colour codes, the distribution of the width. The same array can be observed in b) as an iso-view where the final evaluated width stochasticity level is 4.8%. The feasibility of introducing stochasticity into a system can be shown by examining the design parameter values, as illustrated in c) to f). c) and d) demonstrate the introduction of variation to the x and y location, respectively, while e) and f) show the β_S angles and width.

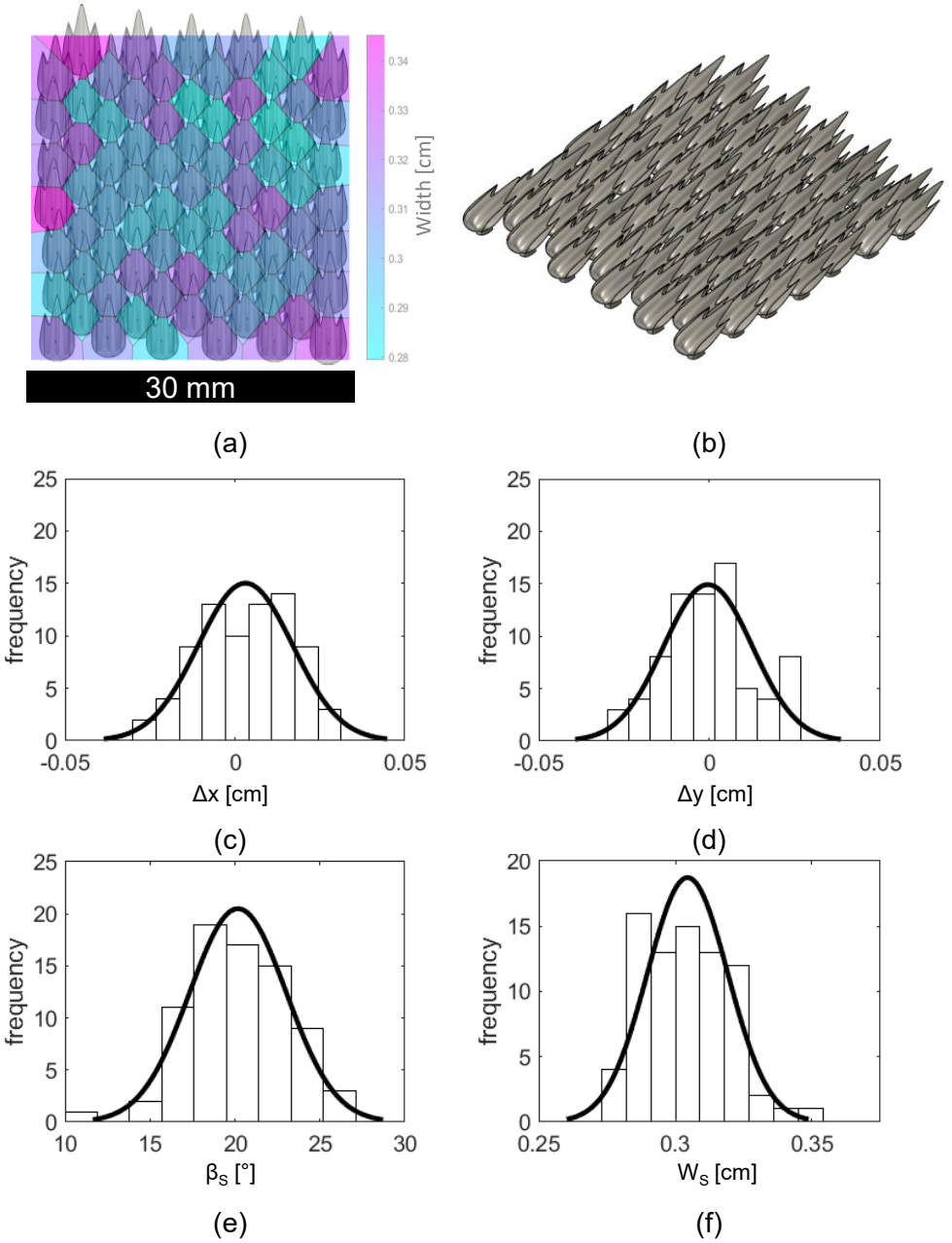

Figure 6.6: Parameter distribution within a shark denticle array. a) illustrates a shark-skin array where the width distribution is highlighted through Voronoi cells. b) Iso-view of the shark skin array. The distribution of the offset value of the positional parameters x and y is shown in c) and d), while e) and f) present the distribution of the β_S angle and the width, respectively.

6.2.5 Application of different probabilistic functions

Here, the Gaussian distribution is used as a probabilistic function combined with a pseudo-RNG. In Fig. 6.7 a), the distribution of the x location parameter utilising a Gaussian distribution is shown. The used array is the same as shown in Fig.6.3. On

the contrary, b) shows the utilisation of a Weibull distribution. The values are not symmetrically distributed around a mean value, as shown in b).

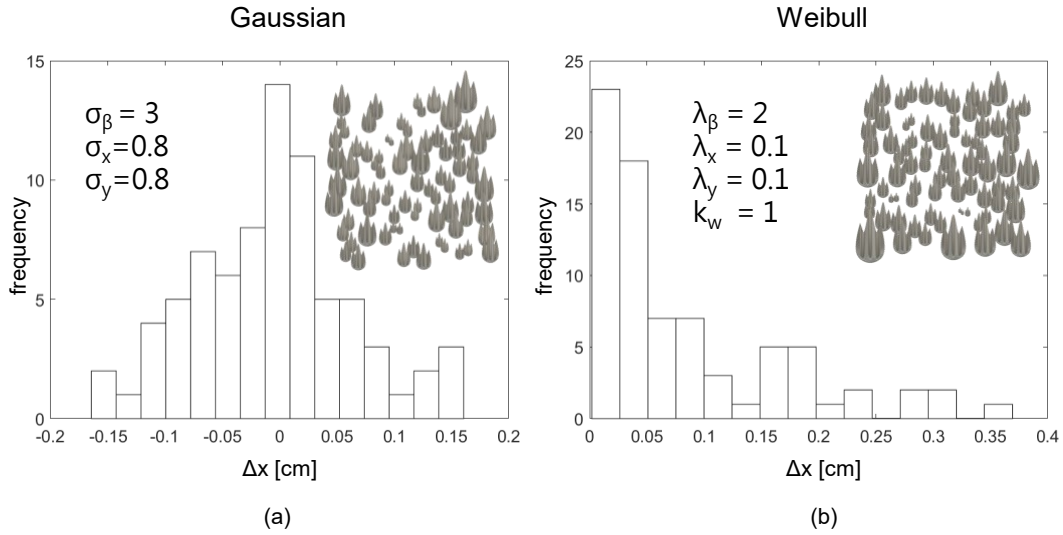

Figure 6.7: Illustration of different distribution introduced to shark-skin. a) Gaussian distribution and b) Weibull distribution

6.3 Conclusions

This Chapter introduced the concept of Isotropic and Anisotropic Randomness as design strategies for stochastic design of complex shapes. It exemplified that increasing the positional stochasticity affects the width. Hence, a linear model was created that considers the positional stochasticity to design the width' stochasticity. To introduce stochasticity, different probabilistic models can be used. However, the Gaussian model is advantageous because the parameters vary symmetrically around a mean, which the Weibull model cannot offer. From the design process, the following design rules (Fig.6.8) can be established:

- ▷ The volumetric design rule a) implies that a body needs to have a volume greater than zero. Negative parameters should be avoided, resulting in a standard deviation $0 < \sigma \leq D/3$. This ensures that at least 99.85% of the values are greater than zero. (Still, negative values could be filtered.)
- ▷ As long as no boundaries exist, the rotation b) can have a standard deviation of $0 < \sigma \leq n \cdot \pi$. If a limit blocks the rotation, it follows $0 < \sigma \leq \alpha/3$ where α is the rotation to the next boundary.

▷ Coordinates c) can be placed everywhere, and every standard deviation is allowed $0 < \sigma \leq +\infty$. However, if boundaries are present, the limit of the standard deviation is $0 < \sigma \leq D/3$, where D is the distance to the nearest boundary.

To achieve a feasible design where only the coordinates of circular objects are moved can be seen in d). Three pins exist, and a wall. If stochasticity is added, the probable new locations can be represented by a circle in the case of isotropic randomness. If the circles overlap with one another or the wall, zones are the result where the pins should not appear. As such, the stochasticity must be altered in different directions according to the established design rules, which results in ellipses that describe the probable location. As can be seen, overlaps are prohibited.

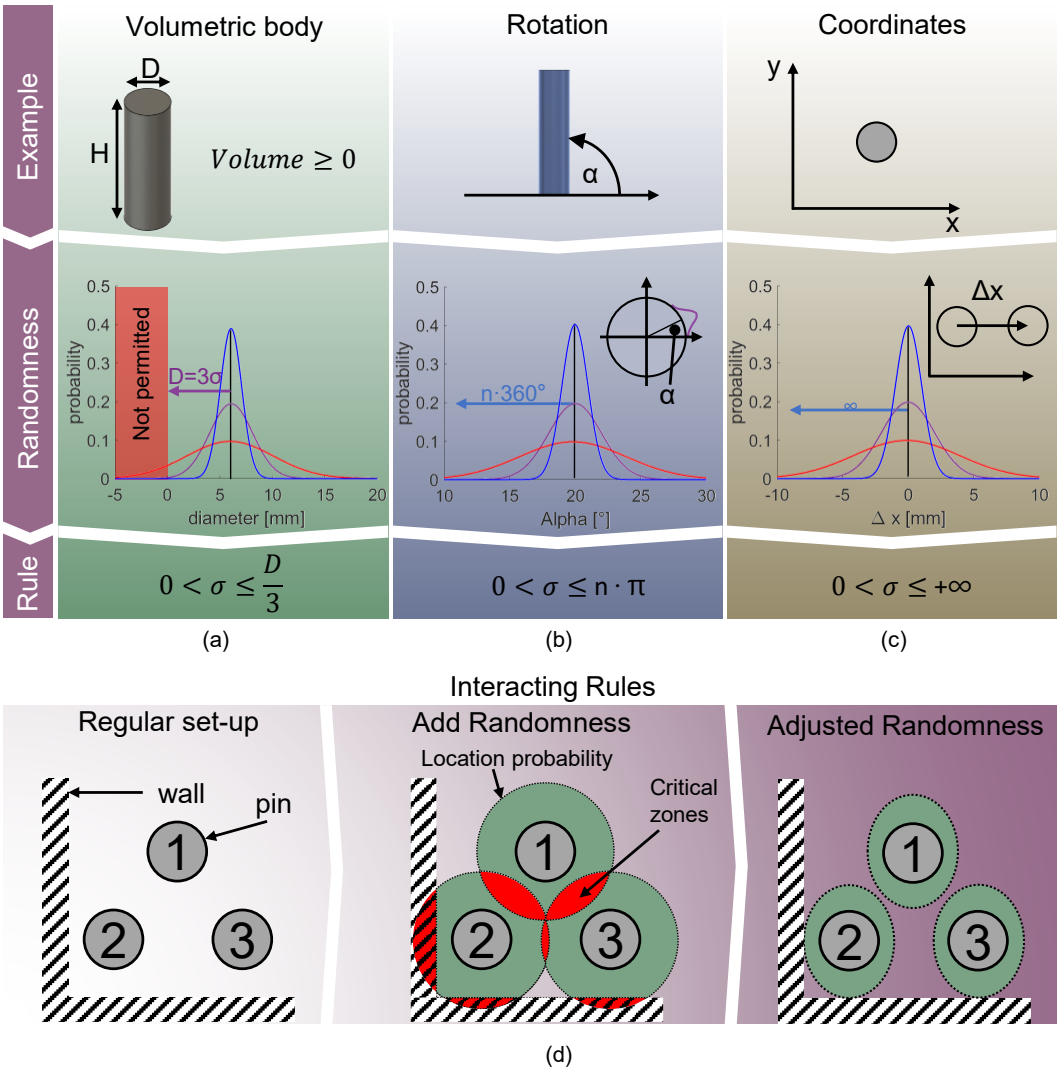

Figure 6.8: Stochastic design rules. Design rules established for a volumetric body a), a rotation b) and coordinates c). These rules help to adjust the stochasticity for a feasible design, d).

In this Chapter, overlaps were prohibited by combining the Euclidean distance with the nearest neighbour approach, resulting in the worst case in unit cells touching each other. However, in nature, overlaps exist, but how much overlap is beneficial cannot be answered without extensive experimentation. Different degrees of overlap are shown in Fig. 6.9.

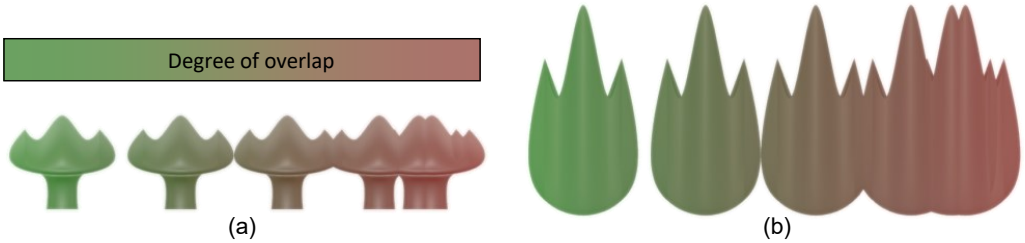

Figure 6.9: Different degrees of overlap. In nature, surface elements can overlap as presented by a front view a) and a top view b).

Another critical measure is how many design parameters should be included in the stochastic design process; "n-order randomness". Some parameters have a more significant effect than other parameters. Depending on their influence, these parameters could be termed first, second, and third-order randomness. This is different from Al-Ketan [91], who refers to each parameter as "first level of randomization" and "second level of randomization" without ranking them by their influence. Choosing a large enough population size to converge to an actual biomimetic design is also essential. The impact of overlaps, n-order randomness, and population size should be studied in the future for a plurality of designs.

Chapter 7

Stochastic design Plug-In for Blender

7.1 Introduction

This Chapter solves Research Gap No.4, which states that no Plug-In or software tool exists to create stochastic primitive and TPMS-based cellular materials and surface elements with different stochasticity levels and stochastic design strategies. The 'tools' described in the previous Chapters to create the described stochastic structures were separate scripts. As such, these tools do not have a GUI, making them difficult to access by academic and industrial researchers. Consequently, the described stochastic design strategies must be combined into one design tool. Therefore, a Plug-In is developed and accessed through the design software Blender and is called 'stodelas' (**Sto**chastic **De**sign toolbox for **la**ttices and **s**urface elements). This Plug-In simplifies stochastic design and allows the adjustment of the disorder combined with different stochastic design strategies. The designed stochastic structure can be created in space, into objects (cellular materials), and on objects (surface elements). This will allow the use of stochastic design for a multitude of applications.
In this Chapter, the 'stodelas' app is introduced, the stochastic design Plug-In for Blender for lattices and surface elements (The design features are implemented in the "Stochastic Python" StoPy library). First, the stochastic design toolbox for lattices is illustrated, and then the introduction of the stochastic design toolbox for surface elements follows. Both sections are structured as follows. First, the user interface is described. Second, the elements that can be used are introduced with the associated design parameters. Third, the population strategies are illustrated. These show how to design the elements in an open space or into/onto an object. Fourth, the design

strategies are described, and fifth, examples of how the software tool could be used to create novel designs for future research or applications are provided.

7.2 Stochastic design toolbox for lattices

This section describes the functionality of the stochastic design toolbox for lattices.

7.2.1 User interface

The GUI, Fig. 7.1, located in the Blender 'viewport,' comprises four tiles. The first tile, a) is used to select the desired unit cell and its associated geometrical and mesh parameters. The second tile, b) the 'Population Strategies,' allows selecting the creation of the cellular structure either as a cuboid or in the shape of a selected object. In the 'Stochastic Design Tools' tab, the third tile c) one out of five design strategies can be chosen. However, 'Stochastic Surface Roughness' can be applied in parallel to any other design strategy. In the fourth tile, d), the cellular structure can be created by pressing the button 'Create'; if required, the metrics, set in the GUI, can be saved as a 'CSV' file.

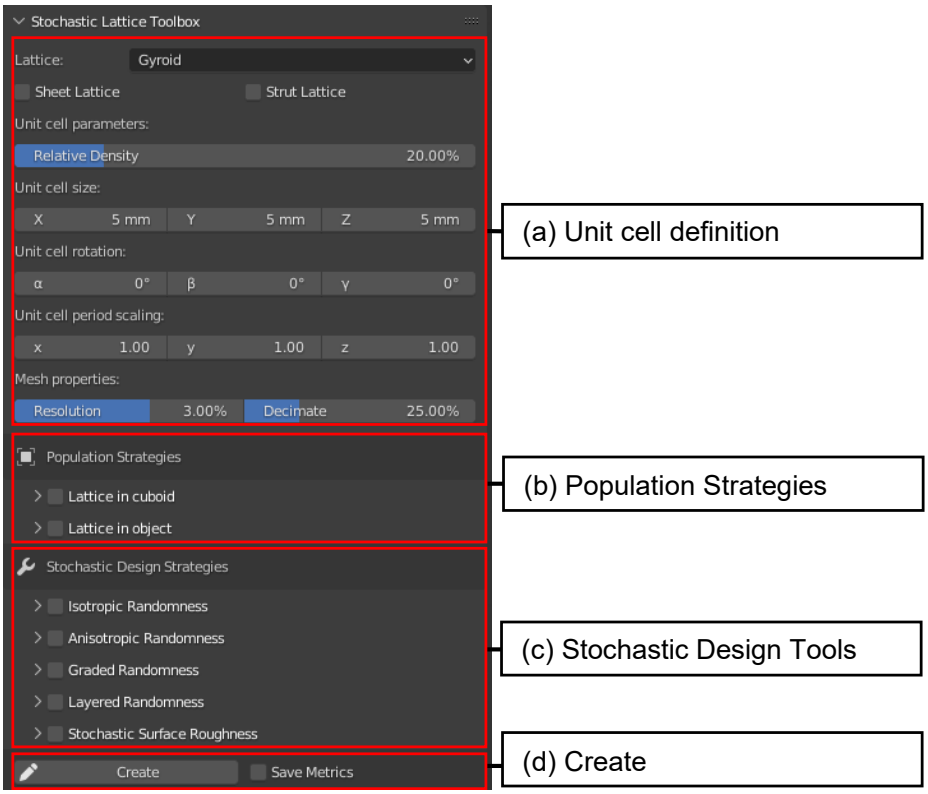

Figure 7.1: GUI of the stochastic lattice toolbox in Blender. a) Unit cell definition. b) Population strategies. c) Stochastic Design tools d) Create button.

7.2.2 Design workflow

The Plug-In is operated through the described GUI. The Design Workflow follows eight steps as shown in Fig. 7.5 and 7.6. The User selects an appropriate cellular material, such as a TPMS or a crystal-based structure. The selectable TPMS and crystal-based cellular materials are illustrated in Fig. 7.2 a).

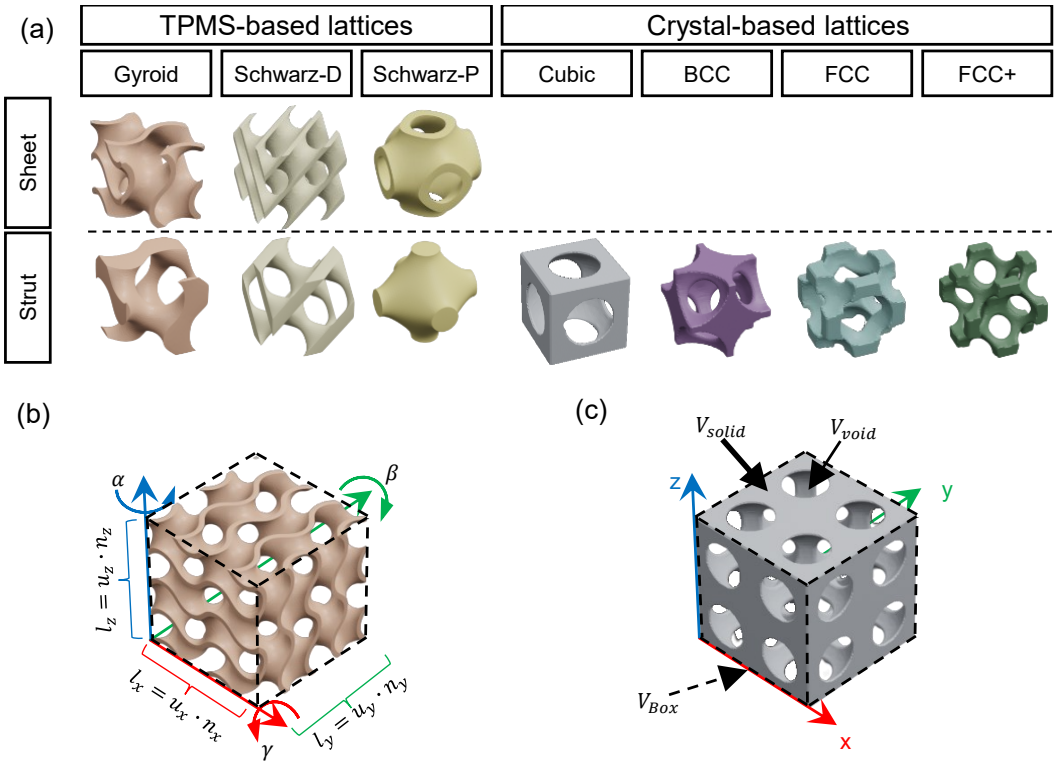

Figure 7.2: Stochastic design lattice toolbox design parameters. a) Available shapes. b) Parameters to design TPMS shape. c) Representation of Relative Density.

Three TPMS and four Crystal-based structures are offered. The TPMS shapes are the Gyroid, The Schwarz-P, and the Schwarz-D, and the Crystal-based shapes include the Cubic, BCC, FCC, and FCC+ structures. As shown in Step 2 (Fig. 7.5) the TPMS shapes can be designed as a sheet or strut-based cellular material, while the dcrystal-based structure can only be designed as a strut-based structure. After defining the cellular material, the Plug-In displays the parameters that describe the shape of the cellular material, which the User can define in Step 3. Five different parameters define the shape of the TPMS structure. The Unit Cell Size specifies the expansion of a Unit Cell in which the TPMS shape is evaluated in the x, y, and z direction as u_x, u_y, and u_z (Fig. 7.2 b) (see Eq. refeq.design-parameter-x). The Relative Density can be chosen from 0-100%, where 0% represents no volume (void) and 100% presents a solid (solid) (Fig. 7.2 c). Hence, it describes the ratio of a cellular material's solid fraction to a solid bounding box (see Eq. 3.17). The Period Scaling factors p_x, p_y, and p_z, are multiple of π and control the frequency of the TPMS structure in the x, y, and z direction (see Eq. 3.6). The Rotation Angles α, β and γ control the orientation of the TPMS structure around the z, y, and x-axis (see Eq. 3.8). The Mesh Resolution (MR) describes the set-up grid (GS) discretisation to calculate the TPMS structure. The value is in %, and from this value, the grid

size is calculated by multiplying the Mesh Resolution by the minimum of u_x, u_y, and u_z: $GS = MR \cdot min(u_x, u_y, u_z)$. The Decimation factor is a value between $0 - 100\%$ and describes to which percentage of the Mesh calculated from the Vedo 'isosurface function' is decimated by the Vedo function 'decimate'. Similarly, the available design parameters for the crystal-based structure are the Relative Density, the Unit Cell Size, the Mesh Resolution, and the Decimation. Once the shape of the Cellular Material and the Mesh Parameters are defined, the User can choose whether to design the Cellular Material in the shape of a Cuboid or an arbitrarily shaped object. If a Cuboid is selected, the number of Unit Cells n_x, n_y, and n_z is defined from which the size l_xxl_yxl_z is calculated (Fig. 7.2 b). A cuboid is illustrated in Fig 7.3 a).

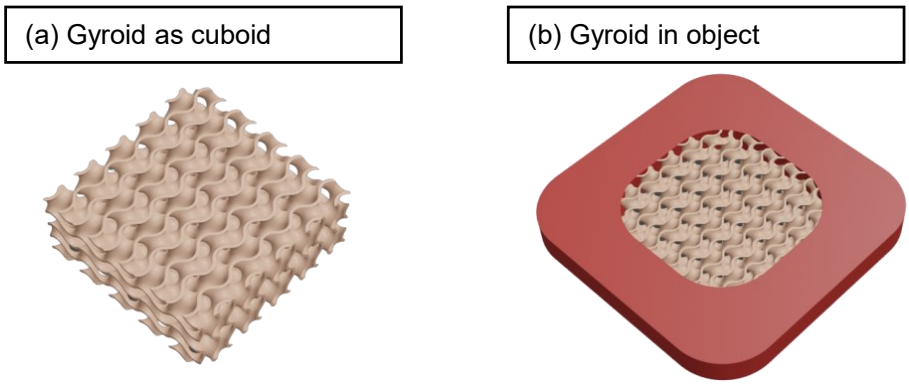

Figure 7.3: Two Gyroid cellular material designs. a) as a cuboid, and b) in an object.

However, an arbitrary mesh object can be loaded into Blender, and a stochastic cellular material can be designed into the loaded object. In this case, the tool determines the necessary expansion from the bounding box of the arbitrary object, creates the cellular structure, and performs a boolean operation with the object selected by the 'eyedropper'[1] tool. (See Fig 7.3 b). In Step 5, the User selects the Design Strategy and can choose between Isotropic Randomness, Anisotropic Randomness, Graded Randomness, and Layered Randomness. For each Design Strategy, the User defines the Level of Stochasticity. The Isotropic Randomness is defined by one parameter δ. Choosing Anisotropic Randomness gives the User the option to select a Stochasticity parameter δ for the defined design parameter (Step 3). Grading Randomness offers to design the level of Stochasticity from a low level δ_{min} to a high level δ_{max} for each cellular material design parameter. Layered Randomness defines a layer in the Cellular Material, where the layer's

[1]The 'eyedropper' tool is a concept in Blender that allows loading an entity with a programming script.

Height, Amplitude, Period Scaling, and Thickness are defined. Additionally, for each cellular material parameter, a a Stochastic Level δ can be set (See Chapter 3.4.4). The Stochastic Levels of all Stochastic Design Strategies can be adjusted between 0-100% Stochasticity. In Step 6, Stochastic Surface Roughness can be applied. To do so, the User defines a Seed, Amplitude, and Frequency with which the Perlin Noise is applied (See Chapter 3.4.6 and 5.2.6). The output data with which the Perlin Noise is added can be scaled up and down by defining a Min and Max value. Each Stochastic Design Tool is demonstrated in Fig. 7.4.

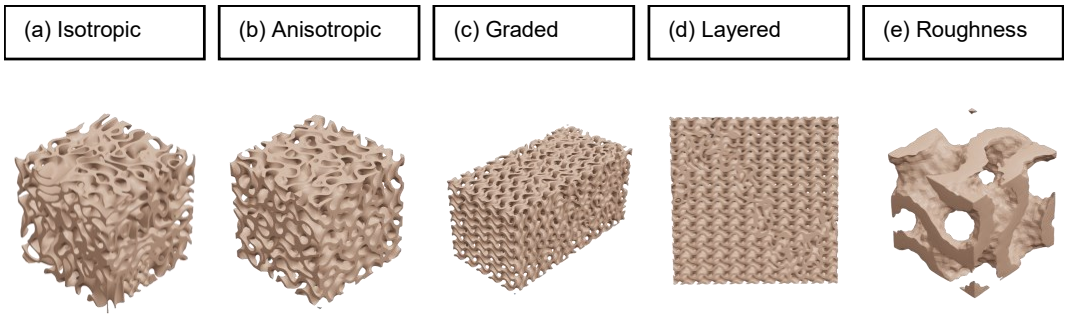

Figure 7.4: Five stochastic design strategies exemplified by a Gyroid cellular structure. a) Isotropic Randomness $\sigma_{iso} = 5\%$, b) Anisotropic Randomness $\sigma_{RD} = 2\%$, $\sigma_{\alpha,\beta,\gamma} = (2,3,4)\%$, $\sigma_{dx,dy,dz} = (2,3,4)\%$ c) Graded Randomness $\sigma_{\alpha min,\alpha max} = (0,5)\%$, d) Layered Randomness $\sigma_{\alpha} = 5\%$, period scaling = 2, e) Roughness $Low = 0$, $High = 0.45$.

In Step 7, the part is calculated, and the design metrics are saved on the Desktop in the stochastic-design folder as a csv file. The calculation method follows Chapter 3.5.2 and 3.5.3. The result of the calculation is a Matrix from which Faces and Vertices are determined using Vedo's isosurface algorithm. Finally, the Faces and Vertices are visualised using Blender API functions, and the cellular material appears in Blender. Blender can then export the cellular material as an STL or OBJ file, which stores the faces and vertices. The resulting STL or OBJ file can be imported into a slicing software, such as PreForm, and then manufactured with the desired AM process, for example, SL. After all the design parameters are defined, the part is calculated

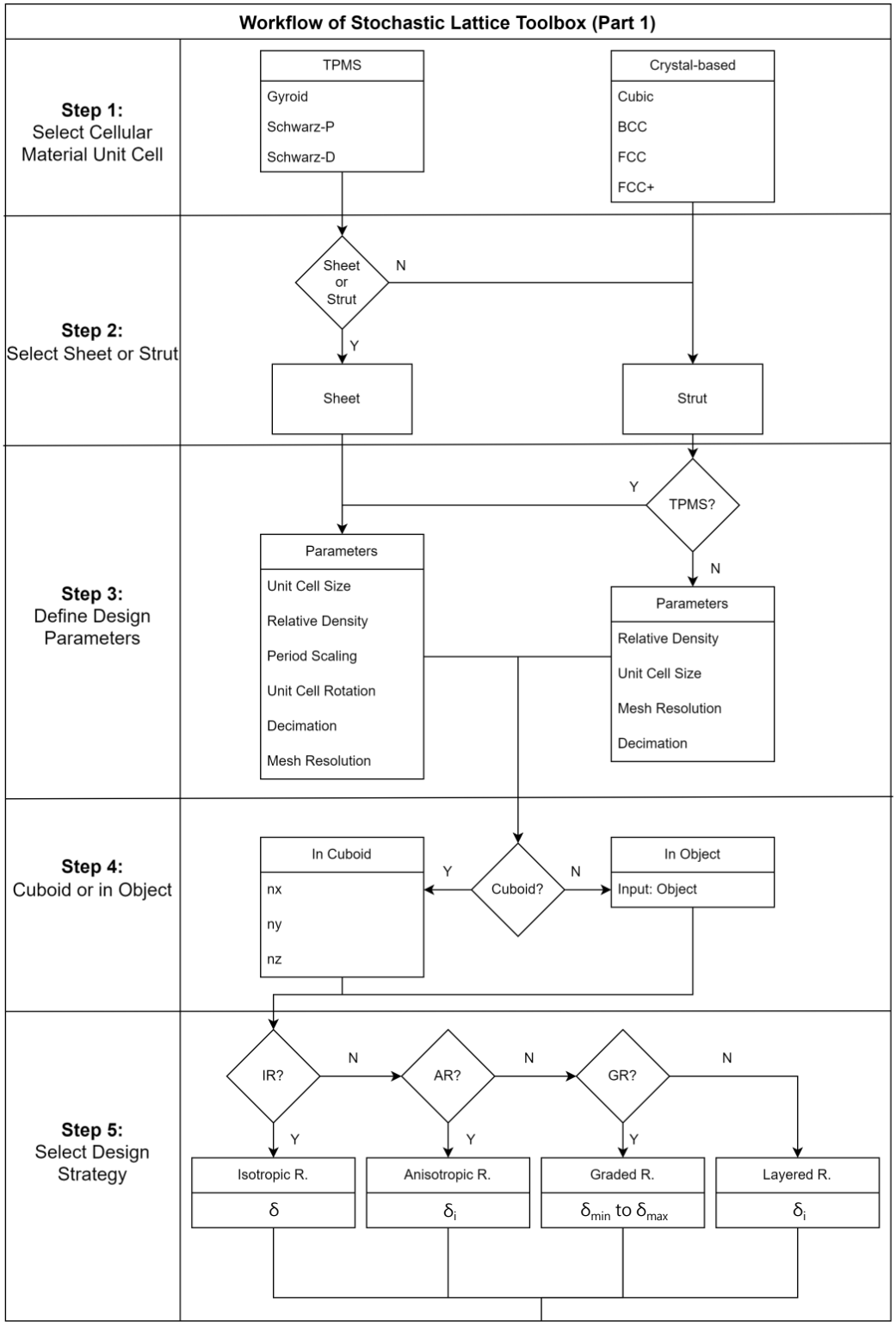

Figure 7.5: Stochastic Lattice Toolbox Workflow (Part 1).

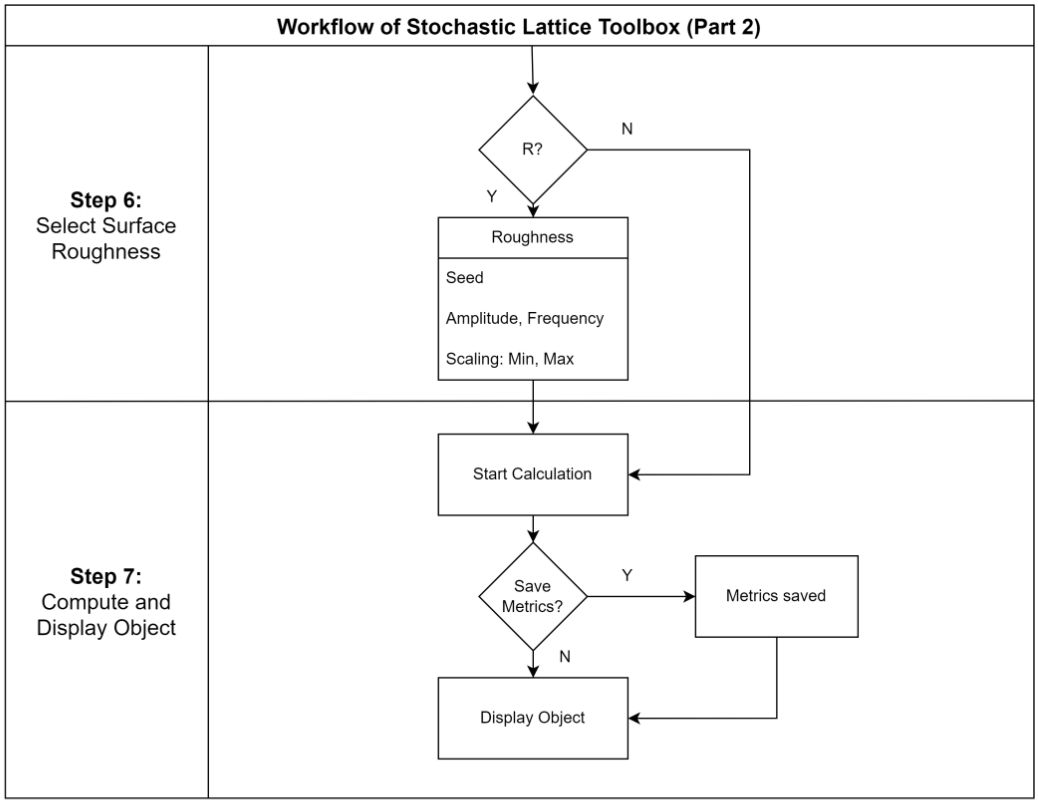

Figure 7.6: Stochastic Lattice Toolbox Workflow (Part 2).

7.2.3 Possible Applications

This software tool simplifies the design with different levels of stochasticity. TPMS structures exhibit anisotropic properties, and as such, they are not suitable for any application [241]. However, composing a cellular material from randomly oriented TPMS unit cells leads to isotropic mechanical properties [91]. For this reason, the developed randomisation tool allows the use of cellular materials for applications requiring isotropic mechanical properties. Hence, some possible applications are proposed in Fig. 7.7. To design applications using stochasticity, the first step is to choose an object. This object is then separated into smaller components in the second step. The separation process intends to define the geometry in which the final stochastic cellular material should be designed. After separating and identifying the parts to be populated with a cellular structure, step three follows: The stochastic structure is designed into one or more parts of the separated object. The fourth and final step is to assemble the separated parts to form the completed design. The design proposals that follow these design steps are not intended to be application-ready

designs.
The first proposal for using stochastic cellular materials is an airless tyre, Fig. 7.7 a) (inspired by [242]). A traditional tyre design model created by [243] comprises a tread, a sidewall, and a rim. This model can be separated into three parts: the rim, the tread, and the air chamber, including the sidewall. The stochastic cellular structure based on a Gyroid is designed into this air chamber and combined with the tread and rim in the last step. Here, the stochastic cellular materials property of having isotropic mechanical properties should allow the tire to behave the same at the point of contact. This should not be achievable with a regular cellular structure with anisotropic mechanical properties. The second proposed field of application is to substitute bone with a stochastic cellular material to build implants. In Fig. 7.7 b) a Femur model made by [244] CC-BY-4.0 was selected as an object. This bone is separated into three parts: a lower part that includes the connection to the knee, an upper part that reaches the hip joint, and an extracted middle part. The middle part is filled with a stochastic cellular material and assembled with the upper and lower parts.
Another field of application is to use stochastic cellular materials in heat exchangers to increase the heat transfer performance by applying a stochastic gradient in the direction of flow to promote flow mixing and hopefully converge to an average Nusselt number faster. This could result in a smaller heat exchanger. A possible design workflow for the heat exchanger is demonstrated in Fig. 7.7 c). A traditional heat exchanger model by Sinan [245] was used, and the heat exchanger's air volume was separated. The separated air volume was then used to design a stochastic cellular structure with a stochastic gradient. This results in a heat exchanger with a stochastic gradient cellular material between the metal plates.
Stochastic cellular structures are also well-suited for frequency-damping applications. Regular structures can filter a typical frequency bandgap [246]; this could be enhanced through the use of stochastic cellular materials by maybe broadening the frequency bandgap and thus filtering more frequencies by a plurality of different unit cell sizes, relative densities, etc., across the overall structure. An application where frequencies occur due to the machining process is milling. Hence, it is important how the machined part is fixed for the subtraction process. Hence, conformal fixtures were developed and proposed by Craig et al. [247], Fig. 7.7 d). Their proposed fixture was taken as an inspiration and adopted. It was separated into a base, fixture beams, and conformal pads. Stochastic cellular materials were designed into the beams, and the whole fixture was assembled, ready to be additively manufactured.

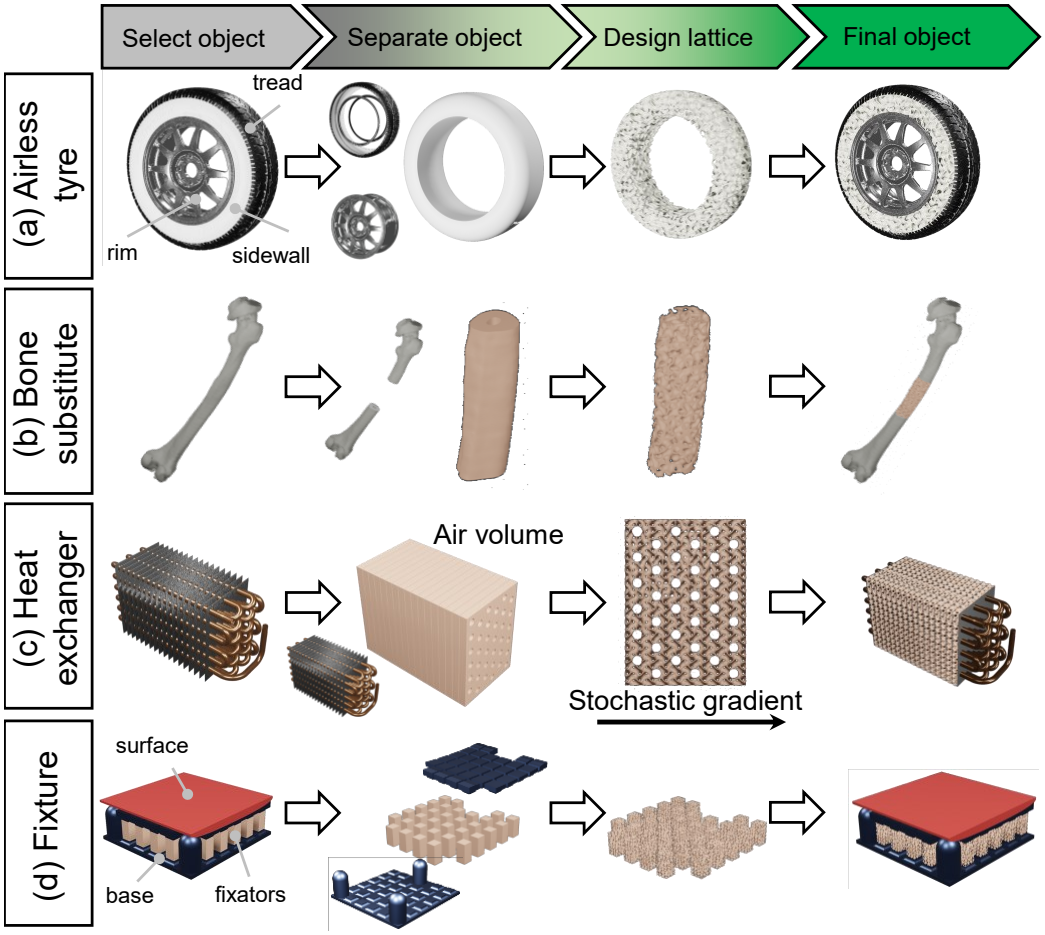

Figure 7.7: Possible applications for stochastic cellular materials. a) an airless tyre (Tyre model made from Fedor Karasev [243]), inspired by [242]. b) cellular material substituting bone in a femur (Bone model geometry by mvrohan [244] CC-BY-4.0). c) stochastically graded cellular material to promote heat transfer (Heat exchanger base model adapted from Sinan [245]). d) Stochastic cellular material for broadening the frequency damping response in a fixture. (Fixture model inspired by Craig et al. [247])

7.3 Stochastic design toolbox for surface elements

The stochastic design toolbox for surface elements allows the use of different surface elements and combines them with different stochastic design strategies.

7.3.1 User interface

The GUI of the stochastic design toolbox is separated into four parts, as shown in Fig. 7.8: a) a section where the unit cell is chosen and their basic unit cell parameters are set. An inline and staggered grid and its X and Y spacing can be defined. In the next tile, the 'Population Strategies' b) are defined. This means the surface elements

can be populated flat in space or on an object. If populated in the design space, the number of unit cells in the x and y direction is set, or the surface elements are populated on an object. The population of a surface element on an object is done by creating a 'lattice' with zero thickness and shrink-wrapping it on an object. Then, the 'eyedrop' tool can select the 'lattice', and the surface elements are populated on the object. (If this is not giving the wanted results due to too curvy surfaces, one can use Blender's 'snap' function on a 'joined' surface element array). In the 'Element design space', one can select 'Gap Control' or 'Converge Control'. 'Gap Control' ensures a minimum distance between two surface elements. If negative, the elements can overlap to a certain level; if positive, a minimum distance is maintained between the elements. To use this effectively, it is advised to keep the array spacing and object size in mind. In addition, the 'Stochastic Design Strategies' can be selected, c). Isotropic Randomness uses one stochasticity parameter to randomise all array parameters. Anisotropic Randomness uses a single stochasticity parameter for each array parameter. Graded randomness is a stochastic linear gradient that allows grading the stochasticity for each array parameter from a low to a high level. The strategy Band Randomness allows the creation of a band in the shape of a sine curve through the surface element array where only the elements in that band are randomised.

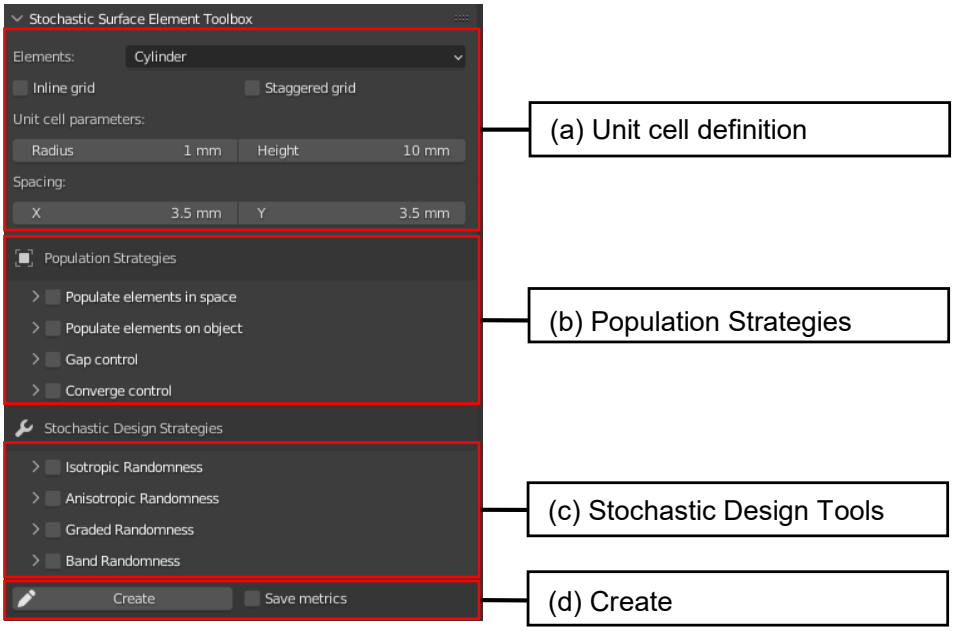

Figure 7.8: GUI of the stochastic surface element toolbox, which is separated into four tiles.

7.3.2 Design workflow

This Subchapter describes the Design Workflow. The Design Workflow is illustrated in the Figures 7.10, 7.11, 7.12, and consists of ten design steps. In the first design step, the User chooses one of five shapes: the Cylinder, Sphere, Cube, Cone, or Shark Denticle. In Step 2, the arrangement of the shapes in space is selected, either an inline or staggered arrangement. Step 3, the relevant design parameters appear depending on the selected shape. The design parameters are listed in the Appendix Table B.3. The Radius can be defined for the Cylinder, Sphere, and Cone shape. The Height appears for the Cylinder and Cone. The Width is available for the Cube and the Shark Denticle. The Radius Top is available for the Cone and Angle for the Shark Denticle. In Step 4, the spacing between the shapes for the inline or staggered arrangement is defined by setting a value for x-spacing (X) and y-spacing (Y). In Step 5, the User can opt for the population of a shape in space or on an object. For the first, the number of elements in the x and y directions is set as n_x and n_y. This enables to calculate the array length l_x or l_y to determine the expansion of the array. The latter works as follows: An object is created or loaded into Blender. Then, the User creates a 'lattice' and positions it where needed over the object. 'lattice' is a concept used in Blender to create a cuboid mesh. Setting one of the Axis to one, it becomes a flat squared mesh. This flat mesh can be wrapped through a 'Shrinkwrap modifier' on an appropriate object. The 'lattice' wrapped on an object's surface can be selected by the User using the 'eyedropper' tool in the GUI. An 'eyedropper' is a tool that allows selecting an object from the 'viewport'. Utilising the 'eyedropper', the object can be used by the Python script designed for the GUI. The Python script collects the position relative to the Blender coordinate system and each side's length (l_x and l_y) of the positioned 'lattice'. This allows calculating n_x and n_y. In Step 7, a 'Gap Control' can be selected, allowing setting a minimum distance d. d describes the distance of an object to its nearest neighbour, excluding the objects' expansion. In Step 8, the User can select the 'Converge Control', which checks that the parameters and properties of a designed array are within a defined Tolerance. The Tolerance (T) is a percentage so that the actual parameter or property is within a Tolerance of the designed parameter P (See Eq. 7.1).

$$(1 + T/100) \cdot P \leq P \leq (1 - T/100) \cdot P \tag{7.1}$$

The parameters and properties include each parameter's (shape parameters, spacing) designed Stochastic Level (Standard Deviation) and the surface area. In Step 9, the desired stochastic design strategy is chosen. The demonstration of the design

strategies is presented in Fig. 7.9: Isotropic Randomness a), Anisotropic Randomness b), Graded Randomness c) or Branded Randomness d).

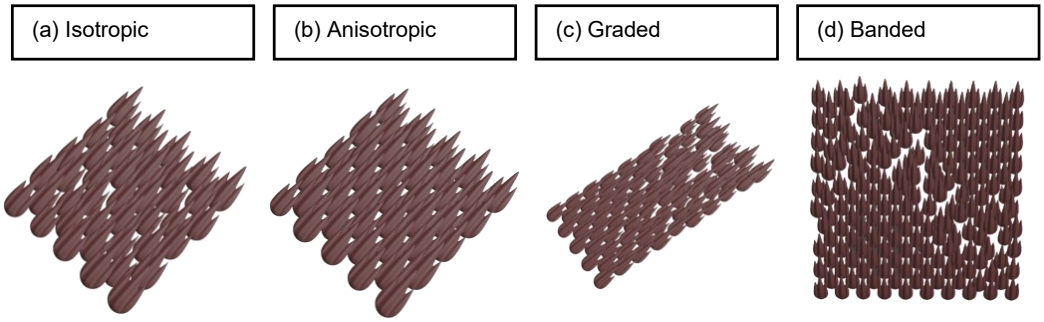

Figure 7.9: Four design strategies included in the stochastic surface element toolbox.

In Step 10, the calculation is started. The stochastic values are sampled using a Gaussian distribution from an RNG according to the selected shape, set parameters, population strategies, and stochastic design strategies. Each shape's stochastic coordinates are determined, and each shape is created and positioned. The design metrics, individual positional values, and design parameters can be saved if needed. Finally, the array occurs in Blender. The array can be selected and exported to a file used in AM, such as OBJ or STL. The OBJ or STL file can then be imported into a slicer software and prepared for a selected AM process.

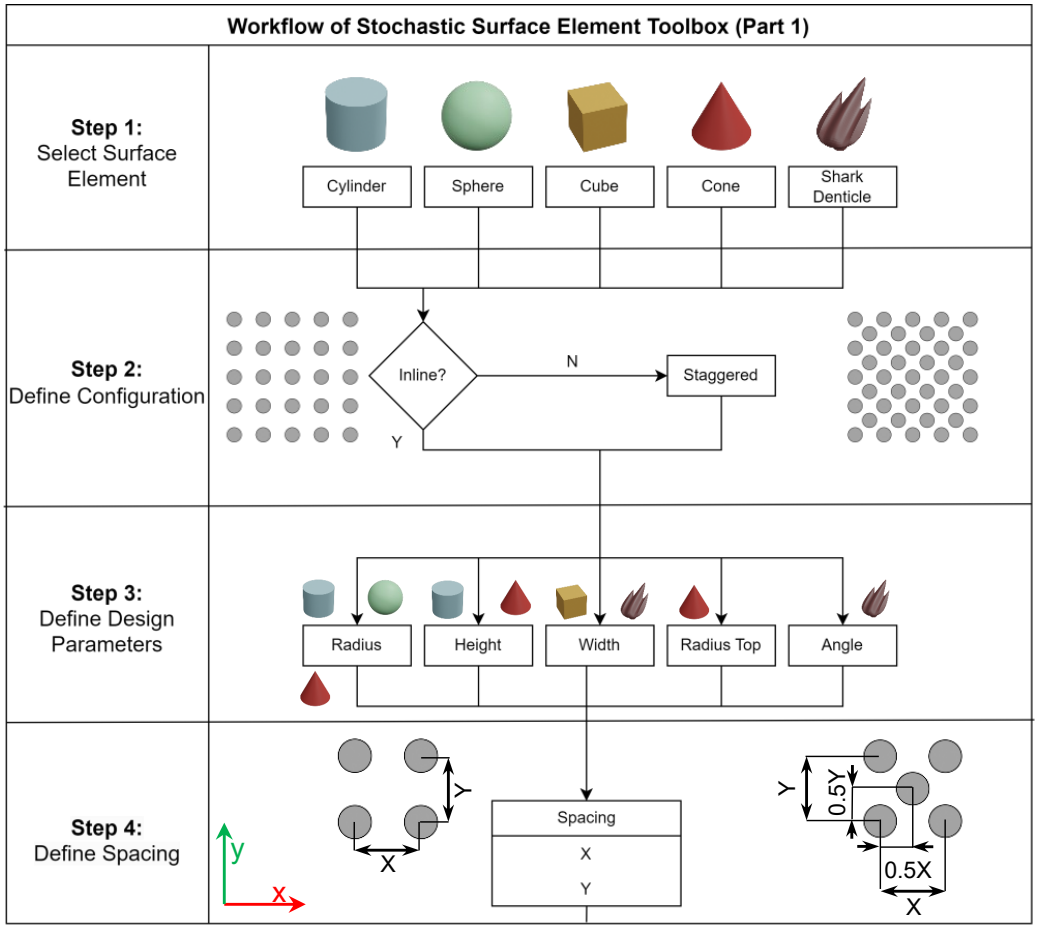

Figure 7.10: Stochastic Surface Element Toolbox Workflow (Part 1).

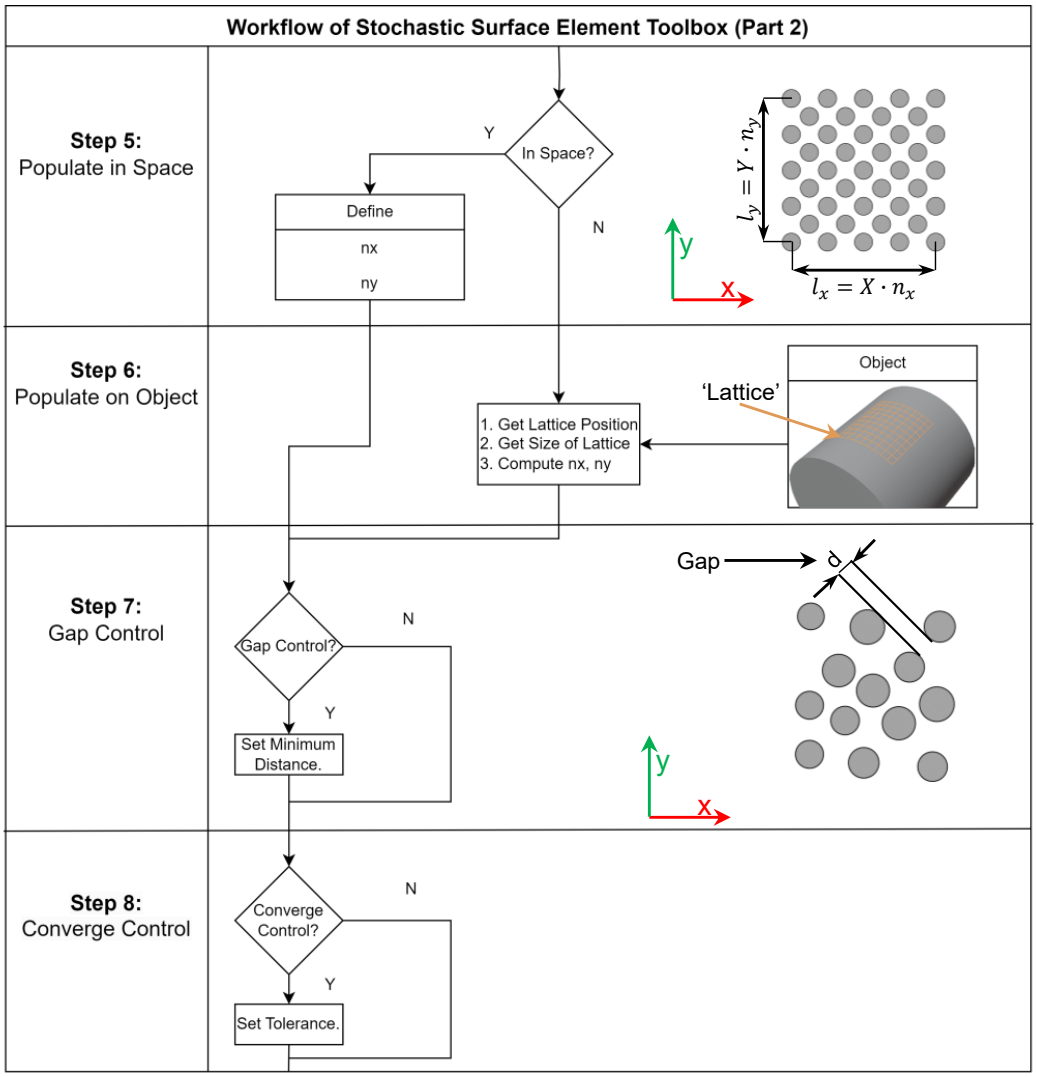

Figure 7.11: Stochastic Surface Element Toolbox Workflow (Part 2).

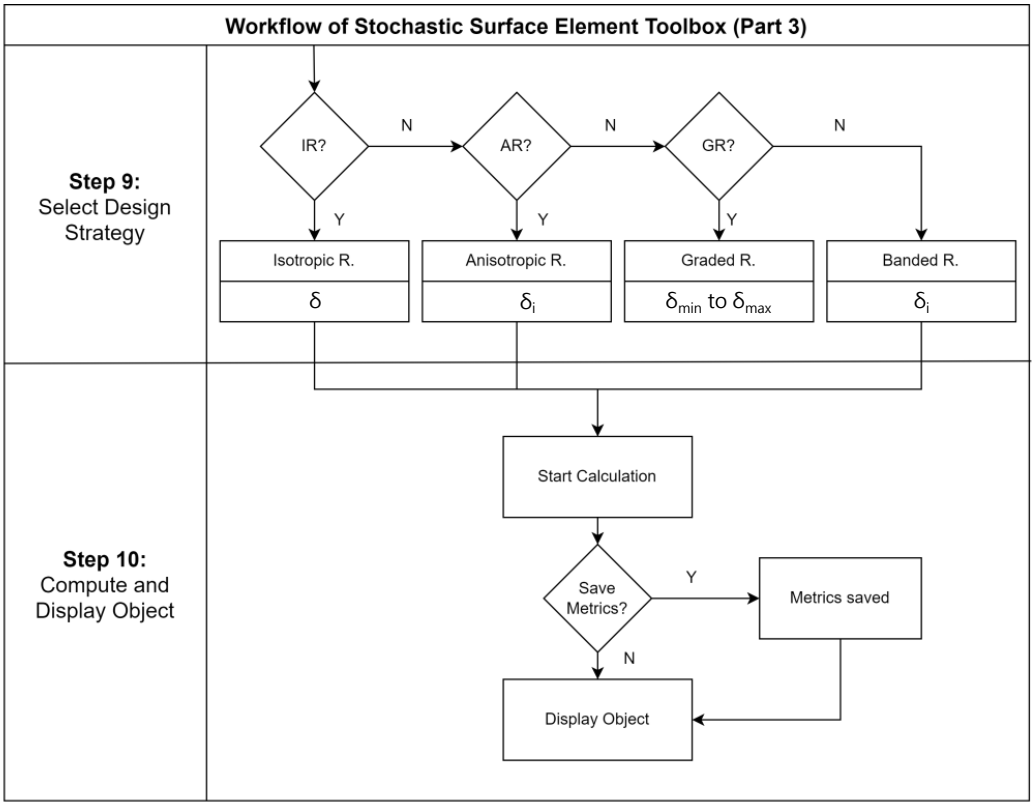

Figure 7.12: Stochastic Surface Element Toolbox Workflow (Part 3).

7.3.3 Possible Applications

The stochastic surface design toolbox offers five geometries, which can be used for endless applications. In Fig. 7.13, the typical design process is exemplified for four applications. These designs are not application-ready designs and need further improvements to be employed. The design process is separated into three steps. The first step is to select an object for which the application of stochasticity could be beneficial. Second, the stochastic array is designed. Third, the design is employed for the selected object to arrive at a final solution. To demonstrate this design process, four designs are presented. a) shows a traditional heat sink based on circular pin fins that cool central processing units (CPUs). The regular pin fin array is substituted with a stochastic array to increase the heat transfer potentially. b) presents the use of the cone structure to create a lotus-like surface (water and dirt-repellent). The cone array could be positioned on a car body (Car CAD model adapted from [248]). This can be done by defining where the cones should be populated to produce a stochastic cone array to be allocated on the car body. The result is a car body fully covered by a hydrophobic surface. This could be beneficial in reducing drag and preventing

dirt from accumulating. Another application for stochastic surfaces could be using stochastic dimples on cutting tools c). The use of regularly positioned dimples on a cutting tool has been shown to decrease friction during the cutting process [249]. Thus, taking a generic cutting tool by Sandvik [250], an array of stochastic dimples could be designed on the surface. In d), the use of stochastic shark skin on the hull of a Yacht (CAD model adapted from [251]) is demonstrated. An area is defined where the stochastic shark skin could be arranged; the stochastic shark skin is created and placed on the hull. This will potentially result in a boat hull with reduced drag and a stochastic shark skin texture that mimics nature better.

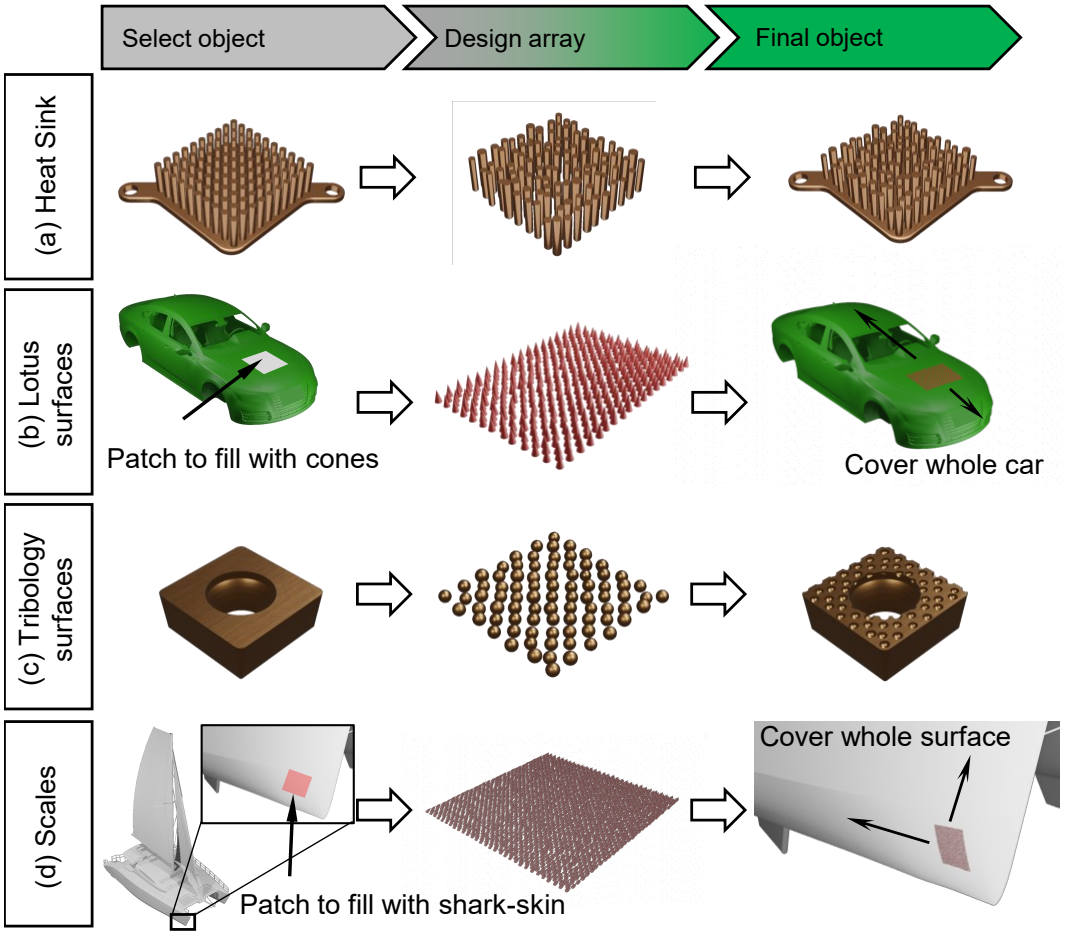

Figure 7.13: A selection of recommended applications for the stochastic surface toolbox. a) A heat sink. b) A car body (CAD Model adapted from [248]) on which cones are placed. c) A cutting tool by Sandvik [250] on which Dimples are randomly positioned. d) A Catamaran (CAD Model adapted from [251]) where a set of stochastic shark skin is situated on the hull.

7.4 Conclusions

In this Chapter, the Plug-In 'stodelas' for Blender was presented. The Plug-In features a toolbox for stochastic cellular materials and stochastic surface elements. Seven different cellular materials from the crystal structure and TPMS-based cellular materials can be chosen, and five different surface elements can be selected for various design purposes. Five design strategies can be applied to the cellular materials and four to the surface elements. The design strategies are Isotropic Randomness, which chooses one single stochastic parameter for the overall structure. Anisotropic Randomness is where, for each parameter, a stochastic parameter can be defined. Graded Randomness describes stochasticity increasing from low to high in a specified direction. Layered Randomness is a localised randomness process where a specific layer in a cellular material or band in a surface element structure is randomised. Stochastic Surface Roughness can be applied to the cellular structures only. Finally, examples of where the Plug-In could be utilised to create novel designs, such as in thermal devices, fixtures, implants, or tribological, hydrophobic, or drag-reduction surfaces, were provided. The software tool's limitations, manoeuvrability, and novel design features are as follows:

Limitations

- ▷ The cellular materials are created by evaluating the ellipsoid function or a level-set equation over a defined design space. The summation of these (including the interpolation function for the level-set equations) creates the cellular material. For each summation, a volumetric matrix is created to represent the shape. Thus, the memory consumption scales volumetric (cubic), increasing calculation times exponentially. This could be solved by only calculating the necessary cellular material near its unit cell.
- ▷ The design capability of the tool is limited to stochastic design strategies; in the future, more design strategies such as grading, hybridization, interpenetration, or topology optimisation could be added.
- ▷ Python is limited by the Global Interpreter Lock (GIL) to execute the calculation on only one core in sequence. This limits the calculation speed. Hence, essential parts of the software could be improved by starting calculations in parallel using appropriate libraries.

Maneuverability

- ▷ Inputs such as the number of unit cells or relative density are restricted to 100, and 0 to 100 %, respectively, to prevent the creation of matrix arrays that are too large to handle for the computer. Large matrix arrays could cause the computer to crash.
- ▷ Hovering over an input field, button, or selection field opens a box that explains its purpose, making the software tool easy to use.
- ▷ The Gap Control and Converge control are limited to 1000 iterations to find a solution. This prevents a calculation process lasting from an hour to multiple days. Thus, an unresponsive Blender is prevented.
- ▷ A GUI allows interacting with the Python script without using Python, making creating stochastic cellular material simpler.
- ▷ As the code is open-source for a restricted audience, a proficient Python user could add more design strategies, cellular materials, and surface elements.

Novel design features

A list of software tool and their functionality regarding stochastic design strategies is presented in Table 2.2. Comparing ‘Stodelas’ to the described software tools reveals the following novel design characteristics:

- ▷ The application of Isotropic, Anisotropic, Graded, and Layered Randomness to TPMS, primitive element-based cellular materials, and surface elements using a Gaussian Distribution.
- ▷ The availability of Gap Control and Converge Control for surface-based elements combined with the described stochastic design strategies.

Chapter 8

Thesis Conclusions

The aim of this thesis, as described in Chapter 1, was to develop design frameworks for using controlled stochasticity for various shapes. In Chapter 2, the Literature Review provides extensive insights into the design and classification of cellular materials. It highlights the various design methods that can be used to enhance the properties of cellular materials. A classification of the various stochastic design methods was provided, which shows that six different stochastic design strategies exist to create cellular materials. Additionally, a myriad of stochastic design parameters were identified, and the influence of the level of stochasticity was discussed, which shows that there is evidence to support that the right level of stochasticity can, e.g., increase the compression strength [40] (octahedral), or lower the elastic modulus and compression strength (Voronoi structure) [135] and the application of randomness without any control lead in stochastic TPMS-based structures to lower mechanical properties [91]. However, the comparability of these studies is limited by not being able to control the level of stochasticity, and using different stochasticity parameters and approaches. It was also observed that design strategies such as Grading or locally applying Stochasticity was not applied, and the application of stochasticity is usually limited to only a few parameters and unit cell types. These are the reasons why, in Chapter 4, primitive shapes are combined with stochastic design strategies to provide further unit cells and stochastic cellular materials with spatially varying stochasticity. In Chapter 5 the existing design framework of TPMS-based stochastic structures is improved by giving complete control over each unit cell, which allows the application of controlled stochasticity and stochastic design strategies. The set-up of stochastic structures using a Gaussian RNG can be tedious, and overlaps can occur. That is why in Chapter 6, an existing approach was enhanced by including an overlap prevention. The understanding of applying stochasticity lead to the formulation of stochastic design rules. In Chapter 7, the enhanced design frameworks are combined into a single design framework to form a Python library called ‘Stochastic Python’

(StoPy), which can be accessed through the 'stodelas' GUI in Blender. 'stodelas' enables the use of stochastic cellular materials and surface elements. It is the first Plug-In that enables various stochastic design strategies for cellular materials and surface elements. Additionally, it enhances overlap prevention to overlap control and ensures that surface elements converge to the same geometrical and stochastic properties for better comparability in forthcoming studies.

Thus, the original key contributions of this thesis are:

- ▷ The existing compendium of unit cells that include controlled stochasticity, such as strut-based, Voronoi and vaulted structures were advanced to primitive-based cellular materials and the existing design frameworks were advanced with spatially varying stochasticity, namely Graded Randomness and Layered Randomness. A stochastic array produced with this approach was in good agreement with the created file and provided evidence that the stochasticity level can be controlled.
- ▷ Existing stochastic TPMS-based design frameworks start from randomly positioned subdomains, which (a) gives no control over each unit cell and (b) is error-prone to create subdomains of too close proximity, and (c) makes it difficult to apply stochastic design strategies purposefully. The enhanced design framework starts from a regular subdomain grid on which different levels of stochasticity are applied, giving control over each unit cell and preventing errors if the stochasticity level is selected correctly. This approach makes it possible to use stochastic design strategies such as Isotropic, Anisotropic, Graded and Layered Randomness as well as Stochastic Surface Roughness for stochastic TPMS-based structures.
- ▷ A problem encountered with stochastic arrays is that overlaps can occur when stochasticity is applied, especially at higher levels of stochasticity. As such, the design of stochastic arrays was enhanced using a "Euclidean Distance" approach to determine the object size, which fully prevents overlaps. Through understanding this approach, the 3σ rule was established to determine the maximum introduceable level of stochasticity to prevent collisions or unwanted parameter values for any stochastic design.
- ▷ The reviewed design software tools (Table 2.2) were limited by (a) not providing stochastic design strategies for surface-based objects, and primitive and TPMS-based cellular materials, and (b) not providing a gap control or converge control for surface elements. Hence, the enhanced design frameworks were combined into a single Python library accessible through Blender, and

a gap control and converge control was established for the surface elements. Additionally, the design strategies Isotropic, Anisotropic, Graded and Layered Randomness are made accessible for both cellular materials and surface elements, and Stochastic Surface Roughness only for cellular materials.

Chapter 9

Future work

In this work, different aspects of stochastic design for AM were explored. Several design strategies were introduced for cellular materials and surface elements, which are combined in a design Plug-In for Blender. Future work is proposed to enhance the research field of stochastic design. The future work is based on the research conducted in this work. The Chapters 4, 5, 6, and 7 build upon each other. Starting from introducing Isotropic, Anisotropic, Graded, Layered Randomness and Stochastic Surface Roughness to strut- and TPMS-based cellular materials and the development of design rules exemplified on Isotropic and Anisotropic complex shapes. The different unit cells and strategies were combined into a single Plug-In for Blender called 'Stodelas'. This tool offers the design of the initial surface or cellular-based unit cells combined with four stochastic design strategies for the surface elements and five stochastic design strategies for the cellular unit cells. However, as this software tool allows for many combinations, the research field to explore is large. Consequently, future work regarding the software tool is divided into three parts. First, how can the usability and research functionality be improved? Second, what can be done to improve the software? Finally, research studies are proposed to determine the advantages or disadvantages of stochastic design and improve its understanding.

- Usability improvements: The usability of the Blender Plug-In could be advanced by adding more cellular material and surface element unit cells. This would increase the number of investigable unit cells. Currently, the surface elements can converge on average unit cell properties. In the future, this could be added to the cellular material unit cells. Adding an AM check procedure would be advisable. The check procedure could reject stochastic geometries composed of isolated struts that cannot be manufactured or wrongly orientated structures that need support structures, which cannot be removed when in the centre of the cellular structure.

- ▷ Software improvements: Currently, the Blender Plug-In is based on Python. Python is a high-level programming language, while C is a low-level programming language. The difference is that Python is easier to use to build a prototype where speed is not the main goal, while C is more complicated but offers advantages in speed. To develop a widely used product, it is advisable to integrate this Plug-In into a proprietary computer-aided (CAD) design suite or develop a stand-alone stochastic design tool.
- ▷ Research studies: The goal for future research studies is to link the stochastic level and population size of a given stochastic design strategy with structural properties such as yield strength, energy absorption, heat transfer, and thermal conductivity. This will allow the establishment of the necessary design recommendations and identify fields of applications. Potential fields of applications are Stochastic cellular materials as a matrix material for heat exchangers or as an impact-absorbing structure. Further applications could also involve stochastically distributed dimples applied to the cutting tool rake. Only regularly distributed dimples were investigated, reducing friction compared to a smooth surface [249].

In the following decades, humanity might experience a shift from uniformly dominated designs to heterogeneous ones in all engineering fields. In these engineering fields, heterogenic designs will establish its space. The shift towards this heterogeneous design will be aided by stochastic design as proposed in this work. However, it is also important to mention that other tools, such as Topology Optimisation or Artificial Intelligence, will gain more importance, with implications that cannot be foreseen today.

Acronyms

AI Artificial Intelligence. 8

AM Additive Manufacturing. 6, 8, 12, 15, 24, 36, 38, 43, 44, 46, 48, 50, 51, 58, 63, 71, 85, 90–92, 100, 104, 105, 107, 110, 112, 118, 123, 129, 142, 149, 159

API Application Programming Interface. 52, 69, 142

A-R Accept Reject Method. 31, 32, 37–39

BCC Body Centred Cubic. 23, 52, 70, 83, 97, 100, 107, 140

CAD Computer Aided Design. 8, 15, 19, 49–52, 55, 56, 60, 99, 100, 152, 153, 160

CAM Computer Aided Manufacturing. 49, 52

CDF Comulative Distribution Function. 74, 76

CPU Central Processing Unit. 152

csv Comma-separated value file. 142

CT Computer Tomography. 25

CV Covariance. 35

DfAM Design for Additive Manufacturing. 6

FCC Face Centred Cubic. 52, 70, 83, 97, 100, 102–107, 140

FEM Finite Element Modeling. 37, 38, 41, 42, 44, 45, 49

GIL Global Interpreter Locker. 154

GUI Graphical User Interface. 56, 123, 137–139, 146, 148, 155, 157

IPC Interpenetrating Phase Composites. 24, 46, 47

IPM Irregularity Parameter. 61

NN Neural Networks. 8

OBJ Rapid Prototyping File Format. 142, 149

PBF Powder Bed Fusion. 8, 42, 43, 46, 56, 91, 100

PMG Porous Microstructure Generator. 55, 56

RBF Radial Basis Function. 27, 28

RM Random Movement. 39

RNG Random Number Generator. 12, 29, 30, 54, 56, 64, 74, 76, 80, 88, 97, 98, 100, 107, 126, 133, 149, 156

SDF Signed Distance Field. 19

SEM Scanning Electron Microscopy. 62

SL Stereolithography. 6, 8, 89, 90, 93, 94, 97, 99, 100, 107, 129, 142

SLM Selective Laser Melting. 8, 19, 48, 54, 58–63

SLS Selective Laser Sintering. 8, 48, 89–92, 94, 102, 103, 105, 107

SSI Simple Sequential Inhibition. 31, 32

STL Rapid Prototyping File Format. 83, 142, 149

StoPy Stochastic Python. 137, 157

TM Traditional Manufacturing. 6

TO Topology Optimisation. 6, 9, 25

TPMS Triply Periodic Minimal Surfaces. 7, 9, 12, 13, 19–21, 24–26, 28, 36, 45–47, 50–56, 61, 63, 64, 67, 71–74, 80, 84, 85, 110, 112, 115–117, 119, 120, 122, 123, 137, 139, 140, 144, 154, 156, 159

VC Voronoi Structure Closed Cell. 44, 45

VO Voronoi Structure Open Cell. 42–44

VS Voronoi Structure. 37, 38, 40, 41

References

[1] Olaf Diegel, Axel Nordin, and Damien Motte. *A practical guide to design for additive manufacturing*. Springer, 2019.

[2] Hideo Kodama. "Automatic method for fabricating a three-dimensional plastic model with photo-hardening polymer". In: *Review of scientific instruments* 52.11 (1981), pp. 1770–1773.

[3] Anton Du Plessis et al. "Beautiful and functional: a review of biomimetic design in additive manufacturing". In: *Additive Manufacturing* 27 (2019), pp. 408–427.

[4] Chris Broeckhoven and Anton du Plessis. "Escaping the labyrinth of bioinspiration: biodiversity as key to successful product innovation". In: *Advanced Functional Materials* 32.18 (2022), p. 2110235.

[5] Li Wen, James C Weaver, and George V Lauder. "Biomimetic shark skin: design, fabrication and hydrodynamic function". In: *Journal of Experimental Biology* 217.10 (2014), pp. 1656–1666.

[6] August G Domel et al. "Shark skin-inspired designs that improve aerodynamic performance". In: *Journal of the Royal Society Interface* 15.139 (2018), p. 20170828.

[7] Kerstin Koch, Bharat Bhushan, and Wilhelm Barthlott. "Diversity of structure, morphology and wetting of plant surfaces". In: *Soft Matter* 4.10 (2008), pp. 1943–1963.

[8] Lufthansa Technik. *AEROSHARK*. `https://www.lufthansa-technik.com/en/aeroshark`. Last accessed: 30/05/2023. n.d.

[9] Ping Li, Dingzhang Guo, and Xinyue Huang. "Heat transfer enhancement, entropy generation and temperature uniformity analyses of shark-skin bionic modified microchannel heat sink". In: *International Journal of Heat and Mass Transfer* 146 (2020), p. 118846.

[10] Steven E Naleway et al. "Structural design elements in biological materials: application to bioinspiration". In: *Advanced materials* 27.37 (2015), pp. 5455–5476.

[11] Ian Maskery et al. “A mechanical property evaluation of graded density Al-Si10-Mg lattice structures manufactured by selective laser melting”. In: *Materials Science and Engineering: A* 670 (2016), pp. 264–274.

[12] Lei Zhang et al. “Hierarchical sheet triply periodic minimal surface lattices: design, geometric and mechanical performance”. In: *Materials & Design* 209 (2021), p. 109931.

[13] Neil W Ashcroft and N David Mermin. *Solid state physics*. Hartcourt Inc., 1976.

[14] Hermann Amandus Schwarz. *Gesammelte mathematische abhandlungen*. Vol. 1. Verlag von Julius Springer, 1890.

[15] Edvard Rudolf Neovius. *Bestimmung zweier speciellen periodischen Minimalflächen, auf welchen unendlich viele gerade Linien und unendlich viele ebene geodätische Linien liegen*. J.C. Frenckell & Sohn (Helsingfors), 1883.

[16] Georges Voronoi. “Nouvelles applications des paramètres continus à la théorie des formes quadratiques. Deuxième mémoire. Recherches sur les parallélloèdres primitifs.” In: *Journal für die reine und angewandte Mathematik (Crelles Journal)* 1908.134 (1908), pp. 198–287.

[17] Franz Aurenhammer. “Voronoi diagrams—a survey of a fundamental geometric data structure”. In: *ACM Computing Surveys (CSUR)* 23.3 (1991), pp. 345–405.

[18] Hugo Junkers. *Abdeckung für Flugzeugtragflächen u. dgl*. DE Patent 310040. 1915.

[19] Rudolf Höfler. *Plattenförmiger Baukörper*. DE Patent 355056. 1914.

[20] MA De Meller. “Produit métallique pour l’obtention d’objets laminés, moulés ou autres, et procédés pour sa fabrication”. In: *French Patent* 615.147 (1925), p. 1926.

[21] John W Cahn. “On spinodal decomposition”. In: *Acta metallurgica* 9.9 (1961), pp. 795–801.

[22] Alan H Schoen. *Infinite periodic minimal surfaces without self-intersections*. Tech. rep. 1970.

[23] S Scott Crump. *Apparatus and method for creating three-dimensional objects*. US Patent 5,121,329. 1989.

[24] Carl R. Deckard. *Method and apparatus for producing parts by selective sintering*. US Patent 4,863,538. 1986.

[25] Wilhelm Meiners, Konrad Wissenbach, and Anres Gasser. *Selective laser sintering at melting temperature*. European Patent 0 946 325 B1. 1993.

[26] Lorna J. Gibson and Michael F. Ashby. *Cellular Solids: Structure and Properties*. 2nd ed. Cambridge Solid State Science Series. Cambridge University Press, 1997. DOI: 10.1017/CBO9781139878326.

[27] Michael F Ashby et al. "Metal foams: a design guide". In: *Appl. Mech. Rev.* 54.6 (2001), B105–B106.

[28] Zhuo Wang et al. "Machine learning unifies flexibility and efficiency of spinodal structure generation for stochastic biomaterial design". In: *Scientific Reports* 13.1 (2023), p. 5414.

[29] ETH-Bibliothek Zürich, Bildarchiv. *Portr _16191-146-AL-FL*. Ed. by Fotograf: Nyblin, Daniel. Public Domain Mark. n.d. DOI: http://doi.org/10.3932/ethz-a-000090391.

[30] Kevin M Moerman. "GIBBON: the geometry and image-based bioengineering add-on". In: *Journal of Open Source Software* 3.22 (2018), p. 506.

[31] Asliah Seharing, Abdul Hadi Azman, and Shahrum Abdullah. "A review on integration of lightweight gradient lattice structures in additive manufacturing parts". In: *Advances in Mechanical Engineering* 12.6 (2020), p. 1687814020916951.

[32] Shakib Hyder Siddique et al. "Lessons from nature: 3D printed bio-inspired porous structures for impact energy absorption–A review". In: *Additive Manufacturing* (2022), p. 103051.

[33] M Benedetti et al. "Architected cellular materials: A review on their mechanical properties towards fatigue-tolerant design and fabrication". In: *Materials Science and Engineering: R: Reports* 144 (2021), p. 100606.

[34] Inderjot Kaur and Prashant Singh. "Critical evaluation of additively manufactured metal lattices for viability in advanced heat exchangers". In: *International Journal of Heat and Mass Transfer* 168 (2021), p. 120858.

[35] Oraib Al-Ketan and Rashid K Abu Al-Rub. "Multifunctional mechanical metamaterials based on triply periodic minimal surface lattices". In: *Advanced Engineering Materials* 21.10 (2019), p. 1900524.

[36] Meisam Askari et al. "Additive manufacturing of metamaterials: A review". In: *Additive Manufacturing* 36 (2020), p. 101562.

[37] Anton Du Plessis et al. “Properties and applications of additively manufactured metallic cellular materials: A review”. In: *Progress in Materials Science* 125 (2022), p. 100918.

[38] Francis Galton. *Natural inheritance*. Vol. 42. Macmillan, 1889.

[39] Adrian Bejan and Sylvie Lorente. “The constructal law and the evolution of design in nature”. In: *Physics of life Reviews* 8.3 (2011), pp. 209–240.

[40] Lewis Mullen et al. “Selective laser melting: A unit cell approach for the manufacture of porous, titanium, bone in-growth constructs, suitable for orthopedic applications. II. Randomized structures”. In: *Journal of Biomedical Materials Research Part B: Applied Biomaterials: An Official Journal of The Society for Biomaterials, The Japanese Society for Biomaterials, and The Australian Society for Biomaterials and the Korean Society for Biomaterials* 92.1 (2010), pp. 178–188.

[41] Teng Lu et al. “Roles of irregularity of pore morphology in osteogenesis of Voronoi scaffolds: from the perspectives of MSC adhesion and mechano-regulated osteoblast differentiation”. In: *Journal of Biomechanics* (2023), p. 111542.

[42] Derek Aranguren van Egmond et al. “The benefits of structural disorder in natural cellular solids”. In: *arXiv preprint arXiv:2110.04607* (2021).

[43] Ina C Meier and Christoph Leuschner. “Leaf size and leaf area index in Fagus sylvatica forests: competing effects of precipitation, temperature, and nitrogen availability”. In: *Ecosystems* 11 (2008), pp. 655–669.

[44] Madeleine V Ankhelyi, Dylan K Wainwright, and George V Lauder. “Diversity of dermal denticle structure in sharks: Skin surface roughness and three-dimensional morphology”. In: *Journal of morphology* 279.8 (2018), pp. 1132–1154.

[45] Robert W Corkery and Eric C Tyrode. “On the colour of wing scales in butterflies: iridescence and preferred orientation of single gyroid photonic crystals”. In: *Interface focus* 7.4 (2017), p. 20160154.

[46] David Halbützel. *n.t.* `https://pixabay.com/photos/honey-beehive-honeycomb-beeswax-3216984/`. Last accessed: 09/07/2023. n.d.

[47] Matthew J Dalby et al. “The control of human mesenchymal cell differentiation using nanoscale symmetry and disorder”. In: *Nature materials* 6.12 (2007), pp. 997–1003.

[48] R Rosli, KA Mohd Annuar, and FS Ismail. “Optimal pin fin heat sink arrangement for solving thermal distribution problem”. In: *Journal of Advanced Research in Fluid Mechanics and Thermal Sciences* 11.1 (2015), pp. 1–18.

[49] Mohammad Zargartalebi and Jalel Azaiez. “Effects of nanoparticle adsorption on heat transfer in random pin-based microchannel heat sinks”. In: *International Journal of Heat and Mass Transfer* 130 (2019), pp. 420–430.

[50] Minh-Son Pham et al. “Damage-tolerant architected materials inspired by crystal microstructure”. In: *Nature* 565.7739 (2019), pp. 305–311.

[51] Sunkyu Yu et al. “Engineered disorder in photonics”. In: *Nature Reviews Materials* (2020), pp. 1–18.

[52] Thomas S Lumpe and Tino Stankovic. “Exploring the property space of periodic cellular structures based on crystal networks”. In: *Proceedings of the National Academy of Sciences* 118.7 (2021), e2003504118.

[53] Dhruv Bhate et al. “Classification and selection of cellular materials in mechanical design: Engineering and biomimetic approaches”. In: *Designs* 3.1 (2019), p. 19.

[54] Irving E Ramirez-Chavez et al. “A Classification of Aperiodic Architected Cellular Materials”. In: *Designs* 6.4 (2022), p. 63.

[55] Michael F Ashby. “The properties of foams and lattices”. In: *Philosophical Transactions of the Royal Society A: Mathematical, Physical and Engineering Sciences* 364.1838 (2006), pp. 15–30.

[56] J Clerk Maxwell. “L. on the calculation of the equilibrium and stiffness of frames”. In: *The London, Edinburgh, and Dublin Philosophical Magazine and Journal of Science* 27.182 (1864), pp. 294–299.

[57] Mark W Jones, J Andreas Baerentzen, and Milos Sramek. “3D distance fields: A survey of techniques and applications”. In: *IEEE Transactions on visualization and Computer Graphics* 12.4 (2006), pp. 581–599.

[58] Sarah F Frisken and Ronald N Perry. “Designing with distance fields”. In: *ACM SIGGRAPH 2006 Courses* (2006), pp. 60–66.

[59] Yan Liang et al. “Design of conformal lattice structures using the volumetric distance field based on parametric solid models”. In: *Rapid Prototyping Journal* 26.6 (2020), pp. 1005–1017.

[60] William E Lorensen and Harvey E Cline. “Marching cubes: A high resolution 3D surface construction algorithm”. In: *ACM siggraph computer graphics* 21.4 (1987), pp. 163–169.

[61] Robin Charles Stamp. "The rapid manufacture of hierarchical structures for orthopaedic applications". PhD thesis. University of Liverpool., 2007.

[62] Manfredo P Do Carmo. *Differential geometry of curves and surfaces: revised and updated second edition*. Dover Publications, 2016.

[63] HG Von Schnering and R Nesper. "Nodal surfaces of Fourier series: fundamental invariants of structured matter". In: *Zeitschrift für Physik B Condensed Matter* 83.3 (1991), pp. 407–412.

[64] Dong J Yoo. "Porous scaffold design using the distance field and triply periodic minimal surface models". In: *Biomaterials* 32.31 (2011), pp. 7741–7754.

[65] Oraib Al-Ketan and Rashid K Abu Al-Rub. "MSLattice: A free software for generating uniform and graded lattices based on triply periodic minimal surfaces". In: *Material Design & Processing Communications* 3.6 (2021), e205.

[66] Ian Maskery et al. "FLatt Pack: A research-focussed lattice design program". In: *Additive Manufacturing* 49 (2022), p. 102510.

[67] Olga Wodo and Baskar Ganapathysubramanian. "Computationally efficient solution to the Cahn–Hilliard equation: Adaptive implicit time schemes, mesh sensitivity analysis and the 3D isoperimetric problem". In: *Journal of Computational Physics* 230.15 (2011), pp. 6037–6060.

[68] Siddhant Kumar et al. "Inverse-designed spinodoid metamaterials". In: *npj Computational Materials* 6.1 (2020), p. 73.

[69] Li Zheng, Siddhant Kumar, and Dennis M Kochmann. "Data-driven topology optimization of spinodoid metamaterials with seamlessly tunable anisotropy". In: *Computer Methods in Applied Mechanics and Engineering* 383 (2021), p. 113894.

[70] Jonàs Martínez, Jérémie Dumas, and Sylvain Lefebvre. "Procedural Voronoi Foams for Additive Manufacturing". In: *ACM Transactions on Graphics (TOG)* 35.4 (2016), pp. 1–12.

[71] Hong-Yuan Lei et al. "Parametric design of Voronoi-based lattice porous structures". In: *Materials & Design* 191 (2020), p. 108607.

[72] Jonàs Martínez et al. "Orthotropic k-nearest foams for additive manufacturing". In: *ACM Transactions on Graphics (TOG)* 36.4 (2017), pp. 1–12.

[73] Matthew McConaha and Sam Anand. “Design of Stochastic Lattice Structures for Additive Manufacturing”. In: *International Manufacturing Science and Engineering Conference*. Vol. 84256. American Society of Mechanical Engineers. 2020, V001T01A036.

[74] Joseph Deering et al. “Selective Voronoi tessellation as a method to design anisotropic and biomimetic implants”. In: *Journal of the Mechanical Behavior of Biomedical Materials* 116 (2021), p. 104361.

[75] Yun Lu Tee et al. “From nature to additive manufacturing: Biomimicry of porcupine quill”. In: *Materials & Design* 210 (2021), p. 110041.

[76] Dong-Jin Yoo. “Heterogeneous porous scaffold design using the continuous transformations of triply periodic minimal surface models”. In: *International Journal of Precision Engineering and Manufacturing* 14.10 (2013), pp. 1743–1753.

[77] Ian Maskery et al. “Effective design and simulation of surface-based lattice structures featuring volume fraction and cell type grading”. In: *Materials & Design* 155 (2018), pp. 220–232.

[78] Oraib Al-Ketan et al. “Functionally graded and multi-morphology sheet TPMS lattices: Design, manufacturing, and mechanical properties”. In: *Journal of the mechanical behavior of biomedical materials* 102 (2020), p. 103520.

[79] Nan Yang et al. “Multi-morphology transition hybridization CAD design of minimal surface porous structures for use in tissue engineering”. In: *Computer-Aided Design* 56 (2014), pp. 11–21.

[80] Dong-Jin Yoo and Kwang-Hyuk Kim. “An advanced multi-morphology porous scaffold design method using volumetric distance field and beta growth function”. In: *International Journal of Precision Engineering and Manufacturing* 16 (2015), pp. 2021–2032.

[81] Nan Yang et al. “Combinational design of heterogeneous lattices with hybrid region stiffness tuning for additive manufacturing”. In: *Materials & Design* 209 (2021), p. 109955.

[82] Benjamin C White et al. “Interpenetrating lattices with enhanced mechanical functionality”. In: *Additive Manufacturing* 38 (2021), p. 101741.

[83] Oraib Al-Ketan, Mhd Adel Assad, and Rashid K Abu Al-Rub. “Mechanical properties of periodic interpenetrating phase composites with novel architected microstructures”. In: *Composite Structures* 176 (2017), pp. 9–19.

[84] Amin Ajdari et al. “Hierarchical honeycombs with tailorable properties”. In: *International Journal of Solids and Structures* 49.11-12 (2012), pp. 1413–1419.

[85] Yuwu Zhang et al. “Dynamic compressive response of additively manufactured AlSi10Mg alloy hierarchical honeycomb structures”. In: *Composite Structures* 195 (2018), pp. 45–59.

[86] Dongjin Yoo. “New paradigms in hierarchical porous scaffold design for tissue engineering”. In: *Materials Science and Engineering: C* 33.3 (2013), pp. 1759–1772.

[87] Bosco Yu et al. “The design of “Grain Boundary Engineered” architected cellular materials: The role of 5-7 defects in hexagonal honeycombs”. In: *Acta Materialia* 243 (2023), p. 118513.

[88] Riccardo Manno, Wei Gao, and Ivano Benedetti. “Engineering the crack path in lattice cellular materials through bio-inspired micro-structural alterations”. In: *Extreme Mechanics Letters* 26 (2019), pp. 8–17.

[89] Irving E Ramirez-Chavez, Christine Lee, and Dhruv Bhate. “Beam Deletion in Square Honeycombs for Improved Energy Absorption Under Quasi-Static In-Plane Compression”. In: *2022 International Solid Freeform Fabrication Symposium*. 2022, pp. 2106–2119.

[90] Lucas Casanova et al. “On the Mechanical Behavior of Additively Manufactured Asymmetric Honeycombs”. In: *2018 International Solid Freeform Fabrication Symposium*. University of Texas at Austin. 2018.

[91] Oraib Al-Ketan, Dong-Wook Lee, and Rashid K Abu Al-Rub. “Mechanical properties of additively-manufactured sheet-based gyroidal stochastic cellular materials”. In: *Additive Manufacturing* 48 (2021), p. 102418.

[92] Nan Yang, Yanling Tian, and Dawei Zhang. “Novel real function based method to construct heterogeneous porous scaffolds and additive manufacturing for use in medical engineering”. In: *Medical engineering & physics* 37.11 (2015), pp. 1037–1046.

[93] Nan Yang, Lilan Gao, and Kuntao Zhou. “Simple method to generate and fabricate stochastic porous scaffolds”. In: *Materials Science and Engineering: C* 56 (2015), pp. 444–450.

[94] Dongjin Yoo. “Heterogeneous minimal surface porous scaffold design using the distance field and radial basis functions”. In: *Medical engineering & physics* 34.5 (2012), pp. 625–639.

[95] Nan Yang et al. “Building implicit-surface-based composite porous architectures”. In: *Composite Structures* 173 (2017), pp. 35–43.

[96] Ole Sigmund and Kurt Maute. “Topology optimization approaches: A comparative review”. In: *Structural and Multidisciplinary Optimization* 48.6 (2013), pp. 1031–1055.

[97] Jun Wu, Ole Sigmund, and Jeroen P Groen. “Topology optimization of multi-scale structures: a review”. In: *Structural and Multidisciplinary Optimization* 63 (2021), pp. 1455–1480.

[98] Dawei Li et al. “Anisotropic design and optimization of conformal gradient lattice structures”. In: *Computer-Aided Design* 119 (2020), p. 102787.

[99] Ajit Panesar et al. “Strategies for functionally graded lattice structures derived using topology optimisation for additive manufacturing”. In: *Additive Manufacturing* 19 (2018), pp. 81–94.

[100] Frank W Zok, Ryan M Latture, and Matthew R Begley. “Periodic truss structures”. In: *Journal of the Mechanics and Physics of Solids* 96 (2016), pp. 184–203.

[101] William H Press et al. *Numerical recipes 3rd edition: The art of scientific computing*. Cambridge university press, 2007.

[102] Fernando Perez-Boerema, Mojtaba Barzegari, and Liesbet Geris. “A flexible and easy-to-use open-source tool for designing functionally graded 3D porous structures”. In: *Virtual and Physical Prototyping* 17.3 (2022), pp. 682–699.

[103] Jiangbei Hu et al. “A lightweight methodology of 3D printed objects utilizing multi-scale porous structures”. In: *The Visual Computer* 35 (2019), pp. 949–959.

[104] Donald Shepard. “A two-dimensional interpolation function for irregularly-spaced data”. In: *Proceedings of the 1968 23rd ACM national conference*. 1968, pp. 517–524.

[105] Jiawei Feng et al. “Porous scaffold design by solid T-splines and triply periodic minimal surfaces”. In: *Computer Methods in Applied Mechanics and Engineering* 336 (2018), pp. 333–352.

[106] JW Feng et al. “Statistical reconstruction of two-phase random media”. In: *Computers & Structures* 137 (2014), pp. 78–92.

[107] Susheem Kanwar, Oraib Al-Ketan, and Sanjairaj Vijayavenkataraman. "A novel method to design biomimetic, 3D printable stochastic scaffolds with controlled porosity for bone tissue engineering". In: *Materials & Design* 220 (2022), p. 110857.

[108] Jan-Hendrik Groth et al. "Five simple tools for stochastic lattice creation". In: *Additive Manufacturing* 49 (2022), p. 102488.

[109] Makoto Matsumoto and Takuji Nishimura. "Mersenne twister: a 623-dimensionally equidistributed uniform pseudo-random number generator". In: *ACM Transactions on Modeling and Computer Simulation (TOMACS)* 8.1 (1998), pp. 3–30.

[110] MathWorks. *RandomStream.list*. `https://uk.mathworks.com/help/matlab/ref/randstream.randstream.list.html`. Last accessed: 15/05/2023. n.d.

[111] Melissa E O'neill. "PCG: A family of simple fast space-efficient statistically good algorithms for random number generation". In: *ACM Transactions on Mathematical Software* (2014).

[112] NumPy Developers. *Random Generator*. `https://numpy.org/doc/stable/reference/random/generator.html`. Last accessed: 15/05/2023. n.d.

[113] Wendy L Martinez and Angel R Martinez. *Computational statistics handbook with MATLAB*. CRC press, 2016.

[114] Ilya S Molchanov and Ilya S Molchanov. *Theory of random sets*. Vol. 19. 2. Springer, 2005.

[115] Davar Khoshnevisan. *Multiparameter Processes: an introduction to random fields*. Springer Science & Business Media, 2002.

[116] Ken Perlin. "An image synthesizer". In: *ACM Siggraph Computer Graphics* 19.3 (1985), pp. 287–296.

[117] Adrian Baddeley and Rolf Turner. "Spatstat: an R package for analyzing spatial point patterns". In: *Journal of statistical software* 12 (2005), pp. 1–42.

[118] Sheldon M Ross. *Simulation*. Academic Press, 2006.

[119] Sahar Choukir et al. "The interplay between constituent material and architectural disorder in bioinspired honeycomb structures". In: *International Journal of Engineering Science* 188 (2023), p. 103863.

[120] Oscar E Sotomayor and Hareesh V Tippur. "Role of cell regularity and relative density on elastoplastic compression response of 3-D open-cell foam core sandwich structure generated using Voronoi diagrams". In: *Acta materialia* 78 (2014), pp. 301–313.

[121] HX Zhu, SM Thorpe, and AH Windle. "The geometrical properties of irregular two-dimensional Voronoi tessellations". In: *Philosophical magazine A* 81.12 (2001), pp. 2765–2783.

[122] AP Roberts and Edward J Garboczi. "Elastic properties of model random three-dimensional open-cell solids". In: *Journal of the Mechanics and Physics of Solids* 50.1 (2002), pp. 33–55.

[123] Meng-Ting Hsieh et al. "The mechanical response of cellular materials with spinodal topologies". In: *Journal of the Mechanics and Physics of Solids* 125 (2019), pp. 401–419.

[124] Ken Perlin. "Improving noise". In: *Proceedings of the 29th annual conference on Computer graphics and interactive techniques*. 2002, pp. 681–682.

[125] Nejc Novak et al. "Impact loading of additively manufactured metallic stochastic sheet-based cellular material". In: *International Journal of Impact Engineering* 174 (2023), p. 104527.

[126] MWD Van der Burg et al. "On the linear elastic properties of regular and random open-cell foam models". In: *Journal of Cellular Plastics* 33.1 (1997), pp. 31–54.

[127] SJ Morris et al. "Complex functional surface design for additive manufacturing". In: *2016 International Solid Freeform Fabrication Symposium*. University of Texas at Austin. 2016.

[128] Jan-Hendrik Groth et al. "Stochastic design for additive manufacture of true biomimetic populations". In: *Additive Manufacturing* 55 (2022), p. 102739.

[129] Satoshi Okubo, Yuki Yamauchi, and Koichi Kitazono. "Effects of Random and Controlled Irregularity in Strut Lattice Structure of PA12 on Compression Anisotropy". In: *Additive Manufacturing* (2023), p. 103385.

[130] MJ Mirzaali et al. "Rational design of soft mechanical metamaterials: Independent tailoring of elastic properties with randomness". In: *Applied Physics Letters* 111.5 (2017), p. 051903.

[131] M Alkhader and M Vural. "Mechanical response of cellular solids: Role of cellular topology and microstructural irregularity". In: *International Journal of Engineering Science* 46.10 (2008), pp. 1035–1051.

[132] Anna Guell Izard et al. “Ultrahigh energy absorption multifunctional spinodal nanoarchitectures”. In: *Small* 15.45 (2019), p. 1903834.

[133] Wenqi Zhu et al. “Micromechanical modeling of effective elastic properties of open-cell foam”. In: *International Journal of Solids and Structures* 115 (2017), pp. 61–72.

[134] Mathias H Luxner, Juergen Stampfl, and Heinz E Pettermann. “Numerical simulations of 3D open cell structures–influence of structural irregularities on elasto-plasticity and deformation localization”. In: *International Journal of Solids and Structures* 44.9 (2007), pp. 2990–3003.

[135] Guanjun Wang et al. “Design and compressive behavior of controllable irregular porous scaffolds: based on voronoi-tessellation and for additive manufacturing”. In: *ACS Biomaterials Science & Engineering* 4.2 (2018), pp. 719–727.

[136] John Çamkıran, Fabian Parsch, and Glenn D Hibbard. “A local orientational order parameter for systems of interacting particles”. In: *The Journal of Chemical Physics* 156.9 (2022), p. 091101.

[137] Yu Duan et al. “The cell regularity effects on the compressive responses of additively manufactured Voronoi foams”. In: *International Journal of Mechanical Sciences* 164 (2019), p. 105151.

[138] HX Zhu, JR Hobdell, and AH Windle. “Effects of cell irregularity on the elastic properties of 2D Voronoi honeycombs”. In: *Journal of the Mechanics and Physics of Solids* 49.4 (2001), pp. 857–870.

[139] HX Zhu, SM Thorpe, and AH Windle. “The effect of cell irregularity on the high strain compression of 2D Voronoi honeycombs”. In: *International Journal of Solids and Structures* 43.5 (2006), pp. 1061–1078.

[140] Oscar E Sotomayor and Hareesh V Tippur. “Role of cell regularity and relative density on elasto-plastic compression response of random honeycombs generated using Voronoi diagrams”. In: *International Journal of Solids and Structures* 51.21-22 (2014), pp. 3776–3786.

[141] Matthew J Silva, Wilson C Hayes, and Lorna J Gibson. “The effects of non-periodic microstructure on the elastic properties of two-dimensional cellular solids”. In: *International Journal of Mechanical Sciences* 37.11 (1995), pp. 1161–1177.

[142] Matthew J Silva and Lorna J Gibson. "The effects of non-periodic microstructure and defects on the compressive strength of two-dimensional cellular solids". In: *International Journal of Mechanical Sciences* 39.5 (1997), pp. 549–563.

[143] K Li, X-L Gao, and G Subhash. "Effects of cell shape and cell wall thickness variations on the elastic properties of two-dimensional cellular solids". In: *International Journal of Solids and Structures* 42.5-6 (2005), pp. 1777–1795.

[144] Ke Li, X-L Gao, and Jun Wang. "Dynamic crushing behavior of honeycomb structures with irregular cell shapes and non-uniform cell wall thickness". In: *International Journal of Solids and Structures* 44.14-15 (2007), pp. 5003–5026.

[145] Hanxing X Zhu, JR Hobdell, and AH Windle. "Effects of cell irregularity on the elastic properties of open-cell foams". In: *Acta materialia* 48.20 (2000), pp. 4893–4900.

[146] HX Zhu and AH Windle. "Effects of cell irregularity on the high strain compression of open-cell foams". In: *Acta Materialia* 50.5 (2002), pp. 1041–1052.

[147] Yue Du et al. "Design and statistical analysis of irregular porous scaffolds for orthopedic reconstruction based on voronoi tessellation and fabricated via selective laser melting (SLM)". In: *Materials Chemistry and Physics* 239 (2020), p. 121968.

[148] Jochen Mueller et al. "Energy absorption properties of periodic and stochastic 3D lattice materials". In: *Advanced Theory and Simulations* 2.10 (2019), p. 1900081.

[149] Yanze Song et al. "Dynamic crushing behavior of 3D closed-cell foams based on Voronoi random model". In: *Materials & Design* 31.9 (2010), pp. 4281–4289.

[150] Zhiqiang Li et al. "On crushing response of the three-dimensional closed-cell foam based on Voronoi model". In: *Mechanics of Materials* 68 (2014), pp. 85–94.

[151] Liqun Tang et al. "Effects of statistics of cell's size and shape irregularity on mechanical properties of 2D and 3D Voronoi foams". In: *Acta Mechanica* 225 (2014), pp. 1361–1372.

[152] Xiaopeng Shi et al. “Study of cell irregularity effects on the compression of closed-cell foams”. In: *International Journal of Mechanical Sciences* 135 (2018), pp. 215–225.

[153] C Chen, TJ Lu, and NA Fleck. “Effect of imperfections on the yielding of two-dimensional foams”. In: *Journal of the Mechanics and Physics of Solids* 47.11 (1999), pp. 2235–2272.

[154] Zhijun Zheng, Jilin Yu, and Jianrong Li. “Dynamic crushing of 2D cellular structures: A finite element study”. In: *International journal of impact engineering* 32.1-4 (2005), pp. 650–664.

[155] Lei Zhu et al. “Design and compressive fatigue properties of irregular porous scaffolds for orthopedics fabricated using selective laser melting”. In: *ACS Biomaterials Science & Engineering* 7.4 (2021), pp. 1663–1672.

[156] Sunil Raghavendra et al. “Quasi-static compression and compression–compression fatigue behavior of regular and irregular cellular biomaterials”. In: *Fatigue & Fracture of Engineering Materials & Structures* 44.5 (2021), pp. 1178–1194.

[157] Stylianos Kechagias et al. “Controlling the mechanical behaviour of stochastic lattice structures: The key role of nodal connectivity”. In: *Additive Manufacturing* 54 (2022), p. 102730.

[158] Georgios Maliaris et al. “Novel additively manufactured bio-inspired 3D structures for impact energy damping”. In: *CIRP Annals* 70.1 (2021), pp. 199–202.

[159] Agyapal Singh, Oraib Al-Ketan, and Nikolaos Karathanasopoulos. “Mechanical performance of solid and sheet network-based stochastic interpenetrating phase composite materials”. In: *Composites Part B: Engineering* 251 (2023), p. 110478.

[160] Ananthan Vidyasagar, Sebastian Krödel, and Dennis M Kochmann. “Microstructural patterns with tunable mechanical anisotropy obtained by simulating anisotropic spinodal decomposition”. In: *Proceedings of the Royal Society A: Mathematical, Physical and Engineering Sciences* 474.2218 (2018), p. 20180535.

[161] Carlos M Portela et al. “Extreme mechanical resilience of self-assembled nanolabyrinthine materials”. In: *Proceedings of the National Academy of Sciences* 117.11 (2020), pp. 5686–5693.

[162] Yunfei Zhang, Meng-Ting Hsieh, and Lorenzo Valdevit. "Mechanical performance of 3D printed interpenetrating phase composites with spinodal topologies". In: *Composite Structures* 263 (2021), p. 113693.

[163] Celal Soyarslan et al. "3D stochastic bicontinuous microstructures: Generation, topology and elasticity". In: *Acta materialia* 149 (2018), pp. 326–340.

[164] KR Mangipudi, E Epler, and CA Volkert. "Topology-dependent scaling laws for the stiffness and strength of nanoporous gold". In: *Acta Materialia* 119 (2016), pp. 115–122.

[165] Celal Soyarslan, Marc Pradas, and Swantje Bargmann. "Effective elastic properties of 3D stochastic bicontinuous composites". In: *Mechanics of Materials* 137 (2019), p. 103098.

[166] Brittany Wojciechowski and Bhisham Sharma. "Acoustical properties of spinodoid porous structures". In: *The Journal of the Acoustical Society of America* 150.4 (2021), A148–A148.

[167] Amin Ajdari, Hamid Nayeb-Hashemi, and Ashkan Vaziri. "Dynamic crushing and energy absorption of regular, irregular and functionally graded cellular structures". In: *International Journal of Solids and Structures* 48.3-4 (2011), pp. 506–516.

[168] Oraib Al-Ketan. "Programmed plastic deformation in mathematically-designed architected cellular materials". In: *Metals* 11.10 (2021), p. 1622.

[169] Autodesk. *Fusion360*. https://www.autodesk.co.uk/products/fusion-360/overview?term=1-YEAR&tab=subscription. Last accessed: 21/09/2023.

[170] nTopology. *nTopology*. https://ntopology.com/. Last accessed: 21/09/2023.

[171] Autodesk. *Netfabb 2024*. https://www.autodesk.co.uk/products/netfabb/features. Last accessed: 20/09/2023.

[172] Altair. *Altair Inspire*. https://altair.com/inspire. Last accessed: 20/09/2023.

[173] Altair. *Altair Sulis*. https://www.altair.com/sulis. Last accessed: 20/09/2023.

[174] Metafold. *Metafold*. https://www.metafold3d.com/. Last accessed: 21/11/2022.

[175] General Lattice. *GL Frontier (beta)*. https://www.generallattice.com/frontier. Last accessed: 21/09/2023.

[176] Sculpteo. *Fabpilot*. https://www.fabpilot.com/features/. Last accessed: 21/09/2023.

[177] Siemens. *NX CAD for product engineering*. https://plm.sw.siemens.com/en-US/nx/cad-online/. Last accessed: 21/09/2023.

[178] William Chanatry. *NX Demonstration: Voronoi Structure creation*. https://blogs.sw.siemens.com/nx-design/nx-demonstration-voronoi-structure-creation/. Last accessed: 21/09/2023. 2021.

[179] William Chanatry. *Design with a Purpose:Introduction into LatticeStructures*. https://blogs.sw.siemens.com/nx-design/design-with-a-purpose-introduction-into-lattice-structures/. Last accessed: 20/09/2023. 2021.

[180] Autodesk. *Autodesk Within*. https://tinyurl.com/autodeskwithin. Last accessed: 20/09/2023.

[181] Carbon. *Latticing Software for Designers of Next-Generation Parts*. https://www.carbon3d.com/products/carbon-design-engine. Last accessed: 21/09/2023.

[182] BASF 3D Printing Solutions. *Ultrasim® 3D Lattice Engine*. https://forward-am.com/service-portfolio/ultrasim-3d-software/ultrasim-3d-lattice-engine/. Last accessed: 21/09/2023.

[183] The FreeCad Team. *FreeCAD - Your own 3D parametric modeler*. https://www.freecad.org/. Last accessed: 21/09/2023.

[184] DeepSOIC. *Lattice2 Workbench*. https://github.com/DeepSOIC/Lattice2/. Last accessed: 21/09/2023.

[185] j8sr0230. *FreeCAD Nodes Workbench*. https://github.com/j8sr0230/Nodes/. Last accessed: 21/09/2023.

[186] The Blender Foundation. *Blender*. https://www.blender.org/. Last accessed: 21/09/2023.

[187] nortikin. *Sverchok*. https://github.com/nortikin/sverchok. Last accessed: 21/09/2023.

[188] nortikin. *Minimal Surface*. https://nortikin.github.io/sverchok/docs/nodes/surface/minimal_surface.html. Last accessed: 21/09/2023.

[189] Jirawat Iamsamang. *Scaffolder*. https://github.com/nodtem66/Scaffolder. Last accessed: 20/09/2023.

[190] Aaron Porterfield. *Crystallon*. https://fequalsf.blogspot.com/p/crystallon.html. Last accessed: 21/09/2022.

[191] Lewis Mullen et al. "Selective Laser Melting: A regular unit cell approach for the manufacture of porous, titanium, bone in-growth constructs, suitable for orthopedic applications". In: *Journal of Biomedical Materials Research Part B: Applied Biomaterials: An Official Journal of The Society for Biomaterials, The Japanese Society for Biomaterials, and The Australian Society for Biomaterials and the Korean Society for Biomaterials* 89.2 (2009), pp. 325–334.

[192] Wesley Brooks. *The creation of lattice structures using selective laser melting*. The University of Liverpool (United Kingdom), 2011.

[193] Eric Jones, Christopher Sutcliffe, and Robin Stamp. *Laser-produced porous surface*. US Patent 11,660,195 B2. 2016.

[194] Eric Jones et al. *Surface modified unit cell lattice structures for optimized secure freeform fabrication*. EP 2 647 453 B1. 2013.

[195] Xiaodong Song. "Titanium vaulted structures for orthopaedic applications". PhD thesis. University of Liverpool, 2013.

[196] Toby Wilkinson. *MetaStruct*. Last accessed: 21/09/2023. URL: https://github.com/wilko339/MetaStruct.

[197] Daniel Niblett et al. "Porous Microstructure Generator". In: (Aug. 2023). DOI: 10.25405/data.ncl.20448471.v7. URL: https://data.ncl.ac.uk/articles/software/Porous_Microstructure_Generator/20448471.

[198] Meng-Ting Hsieh and Lorenzo Valdevit. "Minisurf–A minimal surface generator for finite element modeling and additive manufacturing". In: *Software Impacts* 6 (2020), p. 100026.

[199] S Kamal Krishnam Raju and Prasad S Onkar. "Lattice_Karak: Lattice structure generator for tissue engineering, lightweighting and heat exchanger applications". In: *Software Impacts* 14 (2022), p. 100425.

[200] Alistair Jones et al. “TPMS Designer: A tool for generating and analyzing triply periodic minimal surfaces”. In: *Software Impacts* 10 (2021), p. 100167.

[201] XP Tan et al. “Metallic powder-bed based 3D printing of cellular scaffolds for orthopaedic implants: A state-of-the-art review on manufacturing, topological design, mechanical properties and biocompatibility”. In: *Materials Science and Engineering: C* 76 (2017), pp. 1328–1343.

[202] Hao Chen et al. “Porous scaffold design for additive manufacturing in orthopedics: a review”. In: *Frontiers in Bioengineering and Biotechnology* 8 (2020), p. 609.

[203] Qing Zhou et al. “Additive Manufacturing of Bioceramic Implants for Restoration Bone Engineering: Technologies, Advances, and Future Perspectives”. In: *ACS Biomaterials Science & Engineering* 9.3 (2023), pp. 1164–1189.

[204] Shivank A Tyagi and M Manjaiah. “Additive manufacturing of titanium-based lattice structures for medical applications–A review”. In: *Bioprinting* (2023), e00267.

[205] I Yadroitsava, A Du Plessis, and I Yadroitsev. “Bone regeneration on implants of titanium alloys produced by laser powder bed fusion: A review”. In: *Titanium for Consumer Applications* (2019), pp. 197–233.

[206] Mitsuo Niinomi, M Nakai, et al. “Titanium-based biomaterials for preventing stress shielding between implant devices and bone”. In: *International journal of biomaterials* 2011 (2011).

[207] Fergal J O’Brien et al. “The effect of pore size on cell adhesion in collagen-GAG scaffolds”. In: *Biomaterials* 26.4 (2005), pp. 433–441.

[208] MR Dias et al. “Permeability analysis of scaffolds for bone tissue engineering”. In: *Journal of biomechanics* 45.6 (2012), pp. 938–944.

[209] Marc Long and HJ Rack. “Titanium alloys in total joint replacement—a materials science perspective”. In: *Biomaterials* 19.18 (1998), pp. 1621–1639.

[210] Sajad Arabnejad et al. “Fully porous 3D printed titanium femoral stem to reduce stress-shielding following total hip arthroplasty”. In: *Journal of Orthopaedic Research* 35.8 (2017), pp. 1774–1783.

[211] Khaja Moiduddin et al. “Craniofacial reconstruction with personalized lightweight scaffold fabricated using electron-beam additive manufacturing”. In: *Metals* 12.4 (2022), p. 552.

[212] KC Wong et al. "One-step reconstruction with a 3D-printed, biomechanically evaluated custom implant after complex pelvic tumor resection". In: *Computer Aided Surgery* 20.1 (2015), pp. 14–23.

[213] Jenny Zwei-Chieng Chang et al. "Augmentation of DMLS Biomimetic Dental Implants with Weight-Bearing Strut to Balance of Biologic and Mechanical Demands: From Bench to Animal". In: *Materials* 12.1 (2019), p. 164.

[214] Huixin Liang et al. "Trabecular-like Ti-6Al-4V scaffolds for orthopedic: fabrication by selective laser melting and in vitro biocompatibility". In: *Journal of Materials Science & Technology* 35.7 (2019), pp. 1284–1297.

[215] Stryker. *Implants and disposables*. https://www.stryker.com/us/en/care-settings/asc/implants-and-disposables.html. Last accessed: 15/10/2023.

[216] Oraib Al-Ketan, Reza Rowshan, and Rashid K Abu Al-Rub. "Topology-mechanical property relationship of 3D printed strut, skeletal, and sheet based periodic metallic cellular materials". In: *Additive Manufacturing* 19 (2018), pp. 167–183.

[217] Casey Duncan. *Perlin noise library for Python*. https://github.com/caseman/noise. 2013.

[218] Sven Holcomb. *stlwrite - write ASCII or Binary STL files*. https://www.mathworks.com/matlabcentral/fileexchange/20922-stlwrite-write-ascii-or-binary-stl-files. Last accessed: 01/09/2023. 2018.

[219] Autodesk. *Fusion 360 API User's Manual*. accessed 25.10.2022. 2022. URL: https://help.autodesk.com/view/fusion360/ENU/?guid=GUID-C1545D80-D804-4CF3-886D-9B5C54B2D7A2.

[220] Paul JF Gandy et al. "Nodal surface approximations to the P, G, D and I-WP triply periodic minimal surfaces". In: *Chemical physics letters* 336.3-4 (2001), pp. 187–195.

[221] Nan Yang and Kuntao Zhou. "Effective method for multi-scale gradient porous scaffold design and fabrication". In: *Materials Science and Engineering: C* 43 (2014), pp. 502–505.

[222] NumPy. *Numpy random normal*. https://numpy.org/doc/stable/reference/random/generated/numpy.random.normal.html. Last accessed: 02/06/2023.

[223] Steven A Frank. "The common patterns of nature". In: *Journal of evolutionary biology* 22.8 (2009), pp. 1563–1585.

[224] NumPy. *Numpy random weibull*. https://numpy.org/doc/stable/reference/random/generated/numpy.random.weibull.html. Last accessed: 02/06/2023.

[225] S Shaphiro and MBJB Wilk. "An analysis of variance test for normality". In: *Biometrika* 52.3 (1965), pp. 591–611.

[226] Nornadiah Mohd Razali, Yap Bee Wah, et al. "Power comparisons of shapiro-wilk, kolmogorov-smirnov, lilliefors and anderson-darling tests". In: *Journal of statistical modeling and analytics* 2.1 (2011), pp. 21–33.

[227] SciPy. *scpy.stats.shapiro*. https://docs.scipy.org/doc/scipy/reference/generated/scipy.stats.shapiro.html. Last accessed: 07/09/2023. n.d.

[228] Patrick Royston. "Remark AS R94: A remark on algorithm AS 181: The W-test for normality". In: *Journal of the Royal Statistical Society. Series C (Applied Statistics)* 44.4 (1995), pp. 547–551.

[229] J Patrick Royston. "An extension of Shapiro and Wilk's W test for normality to large samples". In: *Journal of the Royal Statistical Society: Series C (Applied Statistics)* 31.2 (1982), pp. 115–124.

[230] J Patrick Royston. "Algorithm AS 181: the W test for normality". In: *Applied Statistics* (1982), pp. 176–180.

[231] Ian D Hill. "Algorithm AS 66: The normal integral". In: *Journal of the Royal Statistical Society. Series C (Applied Statistics)* 22.3 (1973), pp. 424–427.

[232] Formlabs. *Form 2 Tech Specs*. https://formlabs.com/uk/3d-printers/form-2/tech-specs/. Last accessed: 31/08/2023. n.d.

[233] Formlabs. *Guide to 3D Printing Tolerances, Accuracy, and Precision*. https://formlabs.com/blog/understanding-accuracy-precision-tolerance-in-3d-printing/. Last accessed: 31/08/2023. n.d.

[234] Stratasys. *Design for Additive Manufacturing for PolyJet*. https://tinyurl.com/DfAM-with-PolyJet. Last accessed: 01/09/2023. n.d.

[235] I Maskery and IA Ashcroft. "The deformation and elastic anisotropy of a new gyroid-based honeycomb made by laser sintering". In: *Additive Manufacturing* 36 (2020), p. 101548.

[236] Stratasys. *Data Sheet: Vero*. https://www.stratasys.com/siteassets/materials/materials-catalog/polyjet-materials/verovivid/mds_pj_vero_1020a.pdf. Last accessed: 13/09/2023. n.d.

[237] GrabCad Tutorials. *How to Remove SUP706 Soluble Support on a 3D Printed Part*. https://grabcad.com/tutorials/how-to-remove-sup706-soluble-support-on-a-3d-printed-part. Last accessed: 13/09/2023. 2017.

[238] ImageJ Docs. *Auto Threshold*. https://imagej.net/plugins/auto-threshold. Last accessed: 06/09/2023. n.d.

[239] NumPy. *Random Generator*. https://numpy.org/doc/stable/reference/random/generator.html. Last accessed: 19/06/2022.

[240] MATLAB. *Control Random Number Generator*. https://www.mathworks.com/help/matlab/ref/rng.html. Last accessed: 19/06/2022.

[241] Alistair Jones et al. "Parametric design and evaluation of TPMS-like cellular solids". In: *Materials & Design* 221 (2022), p. 110908.

[242] Michelin. *The VISION Concept*. https://www.michelin.com/en/innovation/vision-concept/. Last accessed: 27/05/2023. n.d.

[243] Fedor Karasev. *Wheel assembly*. https://grabcad.com/library/wheel-assembly-55. accessed: 2022-12-19. 2021.

[244] vmromohan. *Femur*. https://www.embodi3d.com/files/file/50282-single-full-femur-stl-file-processed/. accessed: 2023-01-03. 2021.

[245] Sinan. *Evaporator-condensor-heat exchanger*. https://grabcad.com/library/evaporator-condenser-heat-exchanger-1. accessed: 2023-01-04. 2022.

[246] Waiel Elmadih et al. "Mechanical vibration bandgaps in surface-based lattices". In: *Additive Manufacturing* 25 (2019), pp. 421–429.

[247] Oliver Craig et al. "Conformable fixture systems with flexure pins for improved workpiece damping". In: *Journal of Manufacturing Processes* 50 (2020), pp. 638–652.

[248] Mateusz Zelek. *Audi A7 Sportback*. https://grabcad.com/library/audi-a7-sportback-1. accessed: 2023-01-23. 2022.

[249] Paul Butler-Smith et al. “The influence of femtosecond laser produced periodic surface textures on cutting tool friction”. In: *Procedia CIRP* 95 (2020), pp. 885–890.

[250] Sandvik Coromant UK. *SCMW 12 04 08 H13A*. accessed: 2023-01-06. 2023.

[251] Pariyes Chutipanyaporn. *Catamaran Yacht*. https://grabcad.com/library/catamaran-yacht-3. accessed: 2023-01-23. 2022.

List of Figures

1.1 **Unit cell.** a) Squared unit cells. b) Hexagon unit cells. c) Cubic unit cells. 7

1.2 **Cellular Material timeline.** 1860s: portrait adapted from [29]. The 1910s: image adapted from [18] and [19]. 1920s: image adopted from [20]. The 1960s: Spinodal structure created with Gibbon [30]. 8

1.3 **Performance example of a regular and stochastic design approach.** 10

1.4 **Commonly observed stochastic ranges and examples of natural and artificial cellular materials.** a) Ranges of stochasticity observed in artificial and natural biological entities adapted from [42] (max and min values) and extra values computed from [44] and [43]. b) Honeycomb cells created from bees (image adapted from David Halbützel from Pixabay [46]. c) Sandwich panel utilising a honeycomb structure d) Butterfly wing where the scale is $1\mu m$, adapted from Corkery et al. [45]. e) A pipe surrounded by Gyroid fins for cooling. 11

1.5 **Result Chapter outline.** 14

2.1 **Classification of cellular materials.** Graph adapted, simplified and merged from Bhate et al. [53] and Ramirez-Chavez et al. [54]. . . . 17

2.2 **Characteristic stress-strain curves of cellular materials.** a) Stress-strain curve of a stretch-dominated cellular material that meets the Maxwell stability criterion of $MW \geq 0$ such as the BCC structure [55]. The stretch-dominated structure exhibits an elastic region prior to yielding, after yielding the structure either buckles or crushes in the collapsing zone, after the collapsing zone, it enters the densification zone. b) The stress-strain curve of a bending-dominated cellular material is characterised by a Maxwell criterion of $MW < 0$ and forms a typical stress plateau [55]. A cellular material that has this characteristic is a cubic cellular material. E is the elastic modulus, U is the energy absorption, ϵ_d is the densification stress. σ_N is the stress and ϵ is the strain. Images adapted from [55] 18

2.3 **Strut-based cellular material design process.** a) Definition of vertices for a cubic unit cell. b) Connection of the vertices through edges in the correct order. c) Rendering of the final cubic cellular material unit cell. 20
2.4 **Neovius surfaces**. a) A hand drawing of the Neovius surface, reproduced from [15]. b) A modern rendering of the Neovius surface. 21
2.5 **Spinodal decomposition.** a) Boundary representation of two randomly mixed phases (50 time steps). Decomposition after 100 b), 150 c), and 200 d) time steps. (Code created with ChatGPT). e) Lamellar, f) columnar, g) cubic and h) isotropic spinodal structures (Created with Gibbon [30]). 22
2.6 **Three dimensional Voronoi structure with different levels of stochasticity.** a) Uniform structure. b) Stochasticity level 10%. c) Stochasticity level 20%. 23
2.7 **Main design strategies applied to cellular materials.** a) Uniform, reproduced from [11]. b) Relative density grading, reproduced from [11]. c) Hybridisation, reproduced from [78]. d) Interpenetration, reproduced from [82]. e) Interpenetrating Phase Composites (IPC), reproduced from [83]. f) Hierarchical design, reproduced from [12]. g) Beam deletion, reproduced from [90]. h) Stochastic design, reproduced from [91]. i) CT-based design, reproduced from [94]. j) Conformal design, reproduced from [59]. k) Topology Optimisation, reproduced from [98]. 26
2.8 **A selection of cellular material unit-cells.** a) and b) present sheet- and strut-based TPMS structures, respectively. c) shows the famous honeycomb unit cell, which is a hexagon. d) several different strut-based cellular material unit cells. [26, 52, 100] 27
2.9 **Stochastic design classes.** a) Classification of stochastic design as proposed by Ramirez et al. [54], reproduced. b) Stochastic design methods as mentioned by Feng et al. [106]. c) Stochastic design categories based on Groth et al. [108]. d) Fundamental elements of stochastic design. 31

2.10 **Fundamental stochastic design strategies and examples.** a) Fundamental design strategies. Yellow = Random-Set, and red = Random Field. Examples of b) SSI, reproduced from [131] c) Gaussian noise, reproduced from [122], d) Spinodal structure, reproduced from [132], e) Random positioning and random field, reproduced from [125], f) Random offset and random field, reproduced from [108], and g) Random choice, reproduced from [130]. 33

2.11 **The influence of different levels of stochasticity on the geometry and mechanical parameters.** a) Influence of the stochastic level on the geometry of a 2D Voronoi structure, taken from [42]. b) Affect of the stochastic level on the elastic modulus during compression [140, 138] and during tension [42]. c) Impact of the stochastic level on the plateau stress during compression [140, 120] and the maximum stress during tension [42]. 40

2.12 **Open and closed-cell cellular materials and their mechanical properties** Three 3D open-cell a) (adapted from [129]) and closed-cell b) (adapted from [137]) Voronoi cellular materials with different levels of stochasticity. c) Normalised elastic modulus and normalised plateau stress where 'S' stands for stochastic and 'R' for regular. Data from [134, 145, 150, 137, 120, 149]. Note that the stochastic parameters were adapted to suite the stochastic parameter δ_{MDP}. . 41

3.1 **Utilised primitive shapes.** a) a cylinder, b) a sphere, c) a cube, d) a cone 68

3.2 **Complex shark denticle shape.** a) front view, b) side view, c) top view, and d) iso view. 69

3.3 **The creation of strut-based cellular materials is illustrated.** a) A cube. A b) Cubic b), BCC c), FCC d) and FCC+ e). f) Intersection of two circles. 70

3.4 **Gaussian distributions.** The manipulation of the standard deviation σ changes the flatness of the distribution. 75

3.5 **Weibull distributions.** The shape factor k_w changes the appearance of the Weibull distribution from a hyperbola-like shape to a shape that resembles a skewed bell-like shape. 77

3.6 **Graded Randomness.** The stochasticity increases in the x-direction. This varies the location of the dots spatially. 78

3.7 **Layered randomness and stochastic surface roughness.** a) Stochastic layer. b) smooth surface with values selected for $\Delta R < 0$ and $\Delta R > 0$. The blue line symbolises the resulting surface. c) Roughened surface, where ΔR was applied to. 79
3.8 **Stochastic surface pattern design tool.** a) Program flow. b) Grid and denticle set-up. c) Gaussian distribution is added. d) Positioning of shark denticle. e) Final shark skin. 82
3.9 **Program flow to create stochastic strut-based cellular materials from different stochastic design strategies.** 84
3.10 **Steps to create a stochastic cellular material based on TPMS structures.** 86
3.11 **Program flow to create stochastic pin fin arrays.** 88
3.12 **Schematic of a Stereolithography Additive Manufacturing process, reproduced from [1].** 91
3.13 **Schematic of a Powder Bed Fusion Additive Manufacturing process, reproduced from [1].** 92
3.14 **Schematic of a Material Jetting process, reproduced from [1].** . . 93
3.15 **Regular SL pin sample.** 96

4.1 **Images of an SL regular and random pin fin array.** Scale bar 10 mm 99
4.2 **Effect of different levels of isotropic randomness.** a) Cubic, b) BCC, c) FCC+ and d) FCC cellular material configuration. e) FCC cellular manufactured by a PBF process. 101
4.3 **Gaussian parameter distributions of the unit cell defining parameters of the isotropic randomness applied to the FCC unit cell.** a-c) positional parameters. d-f) radii. 102
4.4 **Anisotropic randomness applied to the cellular material defining parameters of a FCC cellular structure.** Stochasticity applied to radii parameter a-c) and location parameter d-f). g) Stochasticity of a-f) combined and example manufactured by SLS. 103
4.5 **Graded Randomness is illustrated for a FCC cellular structure.** Grading in a) x-, b) y- c) z-direction, and d) in the x, y, z-direction. . 104
4.6 **A sine function used to create different types of stochastic layers.** a) a flat layer, b) and c) sine layers. 105
4.7 **Application of stochastic surface roughness.** a) presents a smooth FCC structure, including a SLS sample and b) illustrates a roughened structure where, in the magnification, a roughened surface can be seen. 106

4.8 **Regular and stochastic FCC-based heat sink.** 106

5.1 $0-10\%$ **isotropic randomness applied to different unit cells.** Rendered a) Gyroid, b) Schwarz-P, and c) Schwarz-D-based cellular material. d) additively manufactured Schwarz-D cellular material. . 111

5.2 **Magnified defects that occur after the application of stochasticity.** a) Knot. b) Mass agglomeration. c) Missing cell. d) Low/ High period 112

5.3 **Gaussian parameter distributions of** 5% **isotropic randomness applied to a cellular structure composed of a Gyroid TPMS unit cells.** a-c) α, β, and γ rotation. d-f) period scaling factor p_x, p_y, and p_z, g-i) Δx, Δy, and Δz discretiser, j) relative density, k) example stochastic cellular structure based on a Gyroid TPMS unit cell. . . . 113

5.4 5% **randomness applied to a single parameter of a cellular structure made up of Gyroid TPMS structures resulting in Anisotropic Randomness.** a-c) Rotation, d) Relative Density, e-g) Period Scaling Factor, h-j) Discretiser 114

5.5 **Influence of the level of stochasticity on the standard deviation of the relative density and the normalised surface area to volume ratio.** 116

5.6 **Graded randomness from a low level to a high level of stochasticity applied in different directions and to different TPMS unit cells.** Graded randomness applied to the x-direction a), e), f), y-direction b), z-direction c). 117

5.7 **Radial randomness expanding from the centre of the stochastic cellular structure from a low level to a high level of stochasticity.** The radial randomness is demonstrated in a) a Gyroid, b) Schwarz-P and c) Schwarz-D unit cell-based cellular structure. 118

5.8 **Stochastic sine layer applied to different TPMS unit cell types.** a-c) Gyroid, d) Schwarz-P, e-f) Schwarz-D. 119

5.9 **Perlin Noise applied to a periodic Gyroid cellular material changing the surface topology of the cellular structure.** Persistence: P, Lacunarity: L 120

5.10 **Perlin Noise introduced to different types of cellular structures.** L: Lacunarity, P: Persistence. 121

5.11 **Influence of the Perlin Noise amplitude on the normalised surface area to volume ratio** $A\backslash V$**.** 122

5.12 **Regular and stochastic Gyroid-based heat sink.** 122

6.1 **Stochastic design level consideration chart.** The introduced stochasticity level σ is between the manufacturing tolerance σ_{min} and the system collapse σ_{max}. 126
6.2 **Introduction of a different level of stochasticity to the positional parameter.** a) illustrates a regular array composed of dots. b) shows a perturbed array where the same standard deviation is introduced to the positional parameter called Isotropic Randomness. c) shows two different standard deviations resulting in a more pronounced disorder in the y direction compared to the x direction. This is termed Anisotropic Randomness. 127
6.3 **Several shark denticle arrays and their width distribution.** a)-c) three sets of nine shark denticle arrays illustrating isotropic and anisotropic randomness. d) shows violin graphs of the width distribution of each array of the arrays shown in a) to c). 129
6.4 **Shark skin arrays with different values of Isotropic Randomness.** 130
6.5 **Influence of the stochasticity level of the positional parameters x and y on array parameters.** Influence on the average width a) and b), the standard deviation of the width c) and d), and the stochasticity level of the width e) and f). 131
6.6 **Parameter distribution within a shark denticle array.** a) illustrates a shark-skin array where the width distribution is highlighted through Voronoi cells. b) Iso-view of the shark skin array. The distribution of the offset value of the positional parameters x and y is shown in c) and d), while e) and f) present the distribution of the β_S angle and the width, respectively. 133
6.7 **Illustration of different distribution introduced to shark-skin.** a) Gaussian distribution and b) Weibull distribution 134
6.8 **Stochastic design rules.** Design rules established for a volumetric body a), a rotation b) and coordinates c). These rules help to adjust the stochasticity for a feasible design, d). 135
6.9 **Different degrees of overlap.** In nature, surface elements can overlap as presented by a front view a) and a top view b). 136

7.1 **GUI of the stochastic lattice toolbox in Blender.** a) Unit cell definition. b) Population strategies. c) Stochastic Design tools d) Create button. 139

7.2 **Stochastic design lattice toolbox design parameters.** a) Available shapes. b) Parameters to design TPMS shape. c) Representation of Relative Density. 140
7.3 **Two Gyroid cellular material designs.** a) as a cuboid, and b) in an object. 141
7.4 **Five stochastic design strategies exemplified by a Gyroid cellular structure.** a) Isotropic Randomness $\sigma_{iso} = 5\%$, b) Anisotropic Randomness $\sigma_{RD} = 2\%$, $\sigma_{\alpha,\beta,\gamma} = (2,3,4)\%$, $\sigma_{dx,dy,dz} = (2,3,4)\%$ c) Graded Randomness $\sigma_{\alpha min,\alpha max} = (0,5)\%$, d) Layered Randomness $\sigma_{\alpha} = 5\%$, period scaling = 2, e) Roughness $Low = 0$, $High = 0.45$. 142
7.5 **Stochastic Lattice Toolbox Workflow (Part 1).** 143
7.6 **Stochastic Lattice Toolbox Workflow (Part 2).** 144
7.7 **Possible applications for stochastic cellular materials.** a) an airless tyre (Tyre model made from Fedor Karasev [243]), inspired by [242]. b) cellular material substituting bone in a femur (Bone model geometry by mvrohan [244] CC-BY-4.0). c) stochastically graded cellular material to promote heat transfer (Heat exchanger base model adapted from Sinan [245]). d) Stochastic cellular material for broadening the frequency damping response in a fixture. (Fixture model inspired by Craig et al. [247]) 146
7.8 **GUI of the stochastic surface element toolbox, which is separated into four tiles.** 147
7.9 **Four design strategies included in the stochastic surface element toolbox.** 149
7.10 **Stochastic Surface Element Toolbox Workflow (Part 1).** 150
7.11 **Stochastic Surface Element Toolbox Workflow (Part 2).** 151
7.12 **Stochastic Surface Element Toolbox Workflow (Part 3).** 152
7.13 **A selection of recommended applications for the stochastic surface toolbox.** a) A heat sink. b) A car body (CAD Model adapted from [248]) on which cones are placed. c) A cutting tool by Sandvik [250] on which Dimples are randomly positioned. d) A Catamaran (CAD Model adapted from [251]) where a set of stochastic shark skin is situated on the hull. 153

List of Tables

2.1 **Influence of the level of stochasticity on mechanical parameters during compression (simplified).** V = Voronoi, TH = Theoretical, A-R = Accept or Reject method, RM = Random movement, σ is either plateau or peak stress. *Depending on the cellular unit cell and plane the force acts on. A shorter version of this table was presented by Duan et al. [137]. 36

2.2 **Cellular material design functionality comparison of various software tools.** PE (Primitive Element), PS (Primitive Strut), ST (Strut), TPMS-S (Strut-based TPMS), TPMS-SH (sheet-based TPMS), SP (Spinodal), G (Grading), V (Voronoi), OB (Design in object), IR (Isotropic Randomness), AR (Anisotropic Randomness), G (Graded Randomness), LR (Layered Randomness), SR (Surface Roughness), SECC (Surface Element Converge Control), SEGC (Surface Element Gap Control) 57

3.1 **Software Packages used in this work.** 66

3.2 **Software Libraries.** 67

3.3 **Unit cell parameter to determine the volume of a cellular material.** i is the number of spheres. j is the number of caps and ρ_{lim} is the limiting case for a closed-cell cellular material. 71

3.4 **Level-set equations of common TPMS unit cells** 72

3.5 **The parameters that were used to describe the shark denticle array.**. Orange: Calculated parameters. White parameters are constants. Green parameters randomisation values. Yellow parameters are dependent. 83

3.6 **Cellular material design parameters for strut-based stochastic structures.** 84

3.7 **EOS EOSINT Formiga P100 SLS PA12 process parameters [235].** 94

4.1 **Shapiro-Wilk Test Statistics.** 99

4.2 **Characteristic measurements of CAD and SL samples.** 100

A.1 **Default cellular material parameters.** 194

A.2 **Reference values for the stochasticity parameter.** 194

A.3 **Stochastic TPMS-based cellular material design parameters for graded randomness.**(l_0 = start position of the lattice, $\sigma_m in$ = lowest level of randomness of the variable, σ_{max} = highest level of randomness of the variable. Abbrevations: Dir. = Direction, Variable = Var.) 194
A.4 **Parameters to design a stochastic TPMS-based cellular material with radially graded randomness.** (ρ_{rel} = relative density, σ_{max} = highest level of randomness of the variable) 195
A.5 **Design parameters for the creation of a stochastic layer in a TPMS-based cellular material.** (H = height in mm, t_s = thickness in mm, ym = amplitude in mm, p = period scaling factor 195
A.6 **Relative randomness values to create a stochastic layer within a TPMS-based cellular structure.** $\sigma_{p_{x,y,z}}$ = period scaling in x, y, z direction, $\sigma_{d_{x,y,z}}$ = discretiser randomisation in x, y, z direction) . . . 195
A.7 **Stochastic surface design parameters for TPMS-based cellular material.** LY = layers, P = persistence, L = lacunarity 195
A.8 **Heat sink cellular material parameters.** 196
A.9 **Design parameters for Gyroid-based heat sinks.** 196

B.1 **Adjustable parameters to design a stochastic cellular structure with the 'Stochastic Lattice Toolbox' in Blender (CS=Crystal structure-based CM) - part 1** 197
B.2 **Adjustable parameters to design a stochastic cellular structure with the 'Stochastic Lattice Toolbox' in Blender (CS=Crystal structure-based CM) - part 2** 198
B.3 **Design parameters associated with different geometries and their description.** 199

Appendix A

Parameters to create cellular materials

A.1 Parameters to design stochastic TPMS-based structures

Table A.1: Default cellular material parameters.

$u_x[mm]$	$u_y[mm]$	$u_z[mm]$	$x_p[rad]$	$y_p[rad]$	$z_p[rad]$	α [°]	β [°]	γ [°]
5	5	5	1	1	1	0	0	0

Table A.2: Reference values for the stochasticity parameter.

σ_{RD}	σ_α	σ_β	σ_γ	σ_{xp}	σ_{yp}	σ_{zp}	σ_{dx}	σ_{dy}	σ_{dz}
ρ_{rel}	180°	180°	180°	2π	2π	2π	$\frac{u_x}{2}$	$\frac{u_y}{2}$	$\frac{u_z}{2}$

Table A.3: Stochastic TPMS-based cellular material design parameters for graded randomness.(l_0 = start position of the lattice, $\sigma_m in$ = lowest level of randomness of the variable, σ_{max} = highest level of randomness of the variable. Abbrevations: Dir. = Direction, Variable = Var.)

Type	nx	ny	nz	ρ_{rel}	σ_{min}	σ_{max}	l_0	Dir.	Var.	Fig.
Gyroid	15	5	5	0.4	0	1.4%	0	x	σ_α	5.6 a)
Gyroid	15	5	5	0.4	0	1.4%	0	y	σ_β	5.6 b)
Gyroid	15	5	5	0.4	0	1.4%	0	z	σ_γ	5.6 c)
Gyroid	15	5	5	0.4	0	1.4%	0	x, y, z	$\sigma_{\alpha,\beta,\gamma}$	5.6 d)
Schwarz-P	15	5	5	0.4	0	1.4%	0	x	σ_α	5.6 e)
Schwarz-D	15	5	5	0.4	0	1.4%	0	x	σ_α	5.6 f)

Table A.4: Parameters to design a stochastic TPMS-based cellular material with radially graded randomness. (ρ_{rel} = relative density, σ_{max} = highest level of randomness of the variable)

Type	nx	ny	nz	ρ_{rel}	σ_{min}	σ_{max}	l_0	Fig.
Gyroid	15	15	1	0.4	0	1.25%	0	5.7 a)
Schwarz-P	15	15	1	0.4	0	1.25%	0	5.7 b)
Schwarz-D	15	15	1	0.4	0	1.25%	0	5.7 c)

Table A.5: Design parameters for the creation of a stochastic layer in a TPMS-based cellular material. (H = height in mm, t_s = thickness in mm, ym = amplitude in mm, p = period scaling factor

Type	nx	ny	nz	ρ_{rel}	p	H	t_s	ym	Fig.
Gyroid	10	10	1	0.4	$2\pi/l_x$	25	5	0	5.8 a)
Gyroid	10	10	1	0.4	$2\pi/l_x$	25	5	10	5.8 b)
Gyroid	10	10	1	0.4	π/l_x	25	5	10	5.8 c)
Schwarz-P	10	10	1	0.4	$2\pi/l_x$	25	5	10	5.8 d)
Schwarz-D	10	10	1	0.4	$2\pi/l_x$	25	5	10	5.8 e)

Table A.6: Relative randomness values to create a stochastic layer within a TPMS-based cellular structure. $\sigma_{p_{x,y,z}}$ = period scaling in x, y, z direction, $\sigma_{d_{x,y,z}}$ = discretiser randomisation in x, y, z direction)

Type	σ_{RD}	σ_α	σ_β	σ_γ	$\sigma_{px,py,pz}$	$\sigma_{dx,dy,dz}$	Fig.
Gyroid	10%	3%	3%	3%	0	0	5.8 a-e)
Schwarz-P	10%	3%	3%	3%	0	0	5.8 d)
Schwarz-D	10%	3%	3%	3%	0	0	5.8 e)

Table A.7: Stochastic surface design parameters for TPMS-based cellular material. LY = layers, P = persistence, L = lacunarity

Type	$n_{x,y,z}$	ρ_{rel}	LOW	HIGH	LY	P	L	$\sigma_{\alpha,\beta,\gamma}$	Fig.
Gyroid	3	0.3	-1	1	1	0.5	2	0	5.9 b)
Gyroid	3	0.3	-0.75	0.75	1	0.5	2	0	5.9 c)
Gyroid	3	0.3	-0.5	-0.5	1	0.5	2	0	5.9 d)
Gyroid	3	0.3	-0.25	0.25	1	0.5	2	0	5.9 e)
Gyroid	3	0.3	-0.5	-0.5	2	0.5	2	0	5.9 f)
Gyroid	3	0.3	-0.5	-0.5	2	0.25	2	0	5.9 g)
Gyroid	3	0.3	-0.5	-0.5	2	0.25	4	0	5.9 h)
Gyroid Strut	3	0.33	-0.25	0.25	1	0.5	2	0	5.10 a)
Gyroid	3	0.3	-0.5	-0.5	1	0.5	2	2.5%	5.10 b)
Schwarz-P	3	0.3	-1	1	1	0.5	2	0	5.10 c)
Schwarz-D	3	0.3	-1	1	1	0.5	2	0	5.10 d)

Table A.8: Heat sink cellular material parameters.

$u_x[mm]$	$u_y[mm]$	$u_z[mm]$	$x_p[rad]$	$y_p[rad]$	$z_p[rad]$	α [°]	β [°]	γ [°]
10	10	10	1	1	1	0	0	0

Table A.9: Design parameters for Gyroid-based heat sinks.

Type	nx	ny	nz	ρ_{rel}	σ_{iso}	Fig.
Gyroid	10	10	1	0.2	0%	5.12 a)
Gyroid	10	10	1	0.2	2.5%	5.12 b)

Appendix B

Stochastic design parameters

B.1 Stochastic cellular structure design parameters

Table B.1: Adjustable parameters to design a stochastic cellular structure with the 'Stochastic Lattice Toolbox' in Blender (CS=Crystal structure-based CM) - part 1

Parameter	Description	TPMS	CS	Randomisable
Sheet	Sheet type lattice	x	-	-
Strut	Strut type lattice	x	x	-
ρ_{rel}	Relative Density	x	x	
u_x	Unit cell size x	x	x	Only TPMS
u_y	Unit cell size y	x	x	Only TPMS
u_z	Unit cell size z	x	x	Only TPMS
α	Yaw	x	-	x
β	Pitch	x	-	x
γ	Gear	x	-	x
p_x	Period scaling x	x	-	x
p_y	Period scaling y	x	-	x
p_z	Period scaling z	x	-	x
Resolution	Mesh resolution	x	x	-
Decimation	Mesh decimation	x	x	-
d_x	Discretiser x	x	x	x
d_y	Discretiser y	x	x	x
d_z	Discretiser z	x	x	x
r_x	Radius x ellipsoid	-	x	x
r_y	Radius y ellipsoid	-	x	x
r_z	Radius z ellipsoid	-	x	x

Table B.2: Adjustable parameters to design a stochastic cellular structure with the 'Stochastic Lattice Toolbox' in Blender (CS=Crystal structure-based CM) - part 2

Parameter	Description	TPMS	CS	Randomisable
Height	Height where the sine function is placed in the cellular structure	x	x	-
Layer Amplitude	Sine amplitude	x	x	-
Thickness	Layer thickness	x	x	-
Period	Sine period scaling factor	x	x	-
Generator	Perlin or simplex noise	x	x	-
Seed	Noise generator start point	x	x	-
Layer	No. of layers added to the noise	x	x	-
Amplitude	Factor to scale down the amplitude with each successive layer	x	x	-
Frequency	Factor to scale down the frequency of the noise with each new layer	x	x	-
LOW	Lower limit of created noise scalar field	x	x	-
HIGH	Upper limit of the created noise scalar field	x	x	-

B.2 Stochastic surface elements design parameters

Table B.3: Design parameters associated with different geometries and their description.

Parameter	Description	Cylinder	Sphere	Cube	Cone	Denticle
Radius	-	x	x	-	-	-
Radius Bottom	-	-	-	-	x	-
Radius Top	-	-	-	-	x	-
Height	-	x	-	-	x	-
Width	-	-	-	x	-	x
Angle	-	-	-	-	-	x
X	x spacing	x	x	x	x	x
Y	y spacing	x	x	x	x	x
n_x	No. of unit cells in x direction	x	x	x	x	x
n_y	No. of unit cells in y direction	x	x	x	x	x
Gap	Min. distance between two objects	x	x	x	x	x
Tolerance	Converge tolerance	x	x	x	x	x
Height	Height of sine curve in array	x	x	x	x	x
Amplitude	Sine amplitude	x	x	x	x	x
Period	Sine period	x	x	x	x	x
Width	$2 * Width$ of the band	x	x	x	x	x